Lehrstuhl für Sensorbasierte Robotersysteme und intelligente Assistenzsysteme
Fakulät für Informatik
Technische Universität München

From robots to brain circuits: learning to harness elasticity for optimal motions

Philipp Stratmann

Vollständiger Abdruck der von der Fakulät für Informatik der Technischen Universität München zur Erlangung des akademischen Grades eines

Doktors der Naturwissenschaften (Dr. rer. nat.)

genehmigten Dissertation.

Vorsitzender:
Prof. Dr.-Ing. Alois Christian Knoll

Prüfende der Dissertation:
1. Prof. Dr.-Ing. Alin Albu-Schäffer
2. Prof. Dr. David Franklin
3. Prof. Gordon Cheng, Ph.D.

Die Dissertation wurde am 27.01.2020 bei der Technischen Universität München eingereicht und durch die Fakulät für Informatik am 08.07.2020 angenommen.

Lehrstuhl für Sensorbasierte Robotersysteme und intelligente Assistenzsysteme
Fakulät für Informatik
Technische Universität München

From robots to brain circuits: learning to harness elasticity for optimal motions

Philipp Stratmann-Funcke

Vollständiger Abdruck der von der Fakulät für Informatik der Technischen Universität München zur Erlangung des akademischen Grades eines

Doktors der Naturwissenschaften (Dr. rer. nat.)

genehmigten Dissertation.

Vorsitzender:
Prof. Dr.-Ing. Alois Christian Knoll

Prüfende der Dissertation:
1. Prof. Dr.-Ing. Alin Albu-Schäffer
2. Prof. Dr. David Franklin
3. Prof. Gordon Cheng, Ph.D.

Die Dissertation wurde am 27.01.2020 bei der Technischen Universität München eingereicht und durch die Fakulät für Informatik am 08.07.2020 angenommen.

Abstract

Whenever a runner strikes the ground, the muscles and tendons deflect like springs and reuse the stored energy to push the athlete off the ground, thereby saving up to 84 % of the muscular energy consumption. In bionic research, roboticists increasingly replicate the elastic properties underlying the human motor performance. But the control of efficient elastic movements in changing environments is largely unknown in both robotics and neuroscience. Bionic approaches to this open question suffer from the difficult identification of functionally distinct circuits within the network of our 86 billion entangled neurons.

The present dissertation fully reverses the bionic approach to explain how the human brain optimizes muscular forces under fast-changing conditions. For this endeavor, the highly interdisciplinary research first answers how the elastic dynamics of robots can be optimally harnessed and then discovers an analogous brain circuit in humans.

Robotic simulations demonstrated that a fast, model-free controller coordinates multiple elastic joints as energy-efficiently as a slow, model-based optimal controller. In robotic experiments, the controller increased the amplitude of jumping by up to 67 %. While an analogous functionality would give the brain a substantial evolutionary benefit, it requires a neuronal mechanism that violates a fundamental neuroscientific consensus: that synapses can only adapt to information that is locally encoded by the pre- or postsynaptic neuron.

Here, the consensus is refuted by a novel, experimentally verified model of a non-local adaptation mechanism. For its development, the robotic controller was used as a blueprint to rigorously unite scattered findings from experimental neuroscience and machine learning. In the resulting model, sensory input triggers the release of serotonin onto motor neurons. The serotonin modulates the output forces according to the same algorithm as the robotic controller. In the simple example of a runner whose knee is blocked by a splint, the model predicts that serotonin specifically suppresses knee muscles, contradicting the generally accepted idea that serotonin affects all limb muscles equally. To test this prediction, human subjects performed fast and strong motions under the precise guidance of a robotic device. The resulting serotonergic effect was quantified and confirmed that serotonin scales the forces of individual muscles to maximize the motion amplitude.

The presented results provide roboticists with a modular controller to boost the energy efficiency of cutting-edge elastic robots. For neuroscientists, the new understanding of serotonergic effects may enhance the rehabilitation of paraplegics. While state-of-the-art therapies substitute serotonin in diffuse ways, the discovered precise effects can be mimicked by electric stimulation and exoskeletons to speed up the gait of patients. These far-reaching implications reveal the large potential of reverse-bionics to predict and explain new neuronal mechanisms. The numerous controllers of biomimetic robots can thereby reduce the frequently raised problem that neuroscience is data rich but theory poor.

Zusammenfassung

Unsere Muskeln und Sehnen wirken wie elastische Federn, die beim Laufen Energie speichern und zum Absprung wiederverwenden, um bis zu 84% ihres Energieverbrauchs einzusparen. Im Bereich der Bionik replizieren Robotiker zunehmend diese elastischen Mechanismen in effizienten Robotern. Die optimale Steuerung elastischer Bewegungen ist jedoch sowohl in der Neurowissenschaft, als auch in der Robotik eine ungelöste Frage. Bionische Antworten scheitern zumeist an der Schwierigkeit, im Gehirns innerhalb der 86 Milliarden verflochtenen Neuronen Schaltkreise mit abgegrenzten Motorfunktionen zu bestimmen.

Die vorliegende Dissertation dreht die bionische Vorgehensweise um und zeigt dadurch, wie das menschliche Gehirn verschiedene Muskelkräfte an veränderliche Bedingungen anpasst. Hierzu wurde nachgewiesen, wie die Dynamik von elastischen Robotern optimal gesteuert werden kann, um mit dem optimalen Regler als Vorlage einen neuronalen Schaltkreis im Gehirn mit gleicher Funktion zu ermitteln.

In Robotersimulationen wurde ein modellfreier Regler aufgezeigt, der aus Sensordaten schnell lernt, gekoppelte elastische Gelenke energieoptimal zu steuern. Auch im Experiment steigerte die Adaption die robotische Sprunghöhe um 67 %. Ein analoger neuronaler Mechanismus wäre für den Menschen evolutionär von Vorteil. Aber er widerspräche einem derzeitigen Grundprinzip der Neurowissenschaft, da er einzelne Synapsen adaptieren müsste an Sensordaten, welche nicht lokal vom prä- oder postsynaptischen Neuron kodiert werden.

Die vorliegende Forschung beweist, dass das menschliche Rückenmark nicht-lokale Adaption beherrscht und Bewegungen algorithmisch wie der robotische Regler an veränderliche Umgebungen adaptiert. Demnach bewirkt sensorischer Input, dass Serotonin an Motorneuronen ausgeschüttet wird und deren Synapsen moduliert. Die Modulation gleicht funktional der robotischen Adaption, wie durch ein mathematisches Modell vorhergesagt und experimentell verifiziert wurde. In den Experimenten gab ein Roboter Probanden präzise vor, welche Trajektorien effiziente elastische Bewegungen ermöglichten. Messungen bestätigten, dass Serotonin – anders als allgemein angenommen – einzelne Muskeln unabhängig modulierte, um deren Zusammenspiel optimimal an die vorgegebenen Trajektorien anzupassen.

Die Ergebnisse zeigen Robotikern einen universellen Regler auf, der die Energieeffizienz modernster elastischer Roboter maximiert. Zudem können Neurowissenschaftler die neue Beschreibung muskelspezifischer serotonerger Effekte nutzen, um nach Rückenmarksverletzungen die verlorenene Wirkung von Serotonin z.B. durch Elektrostimulation oder Exoskelette nachzubilden. Hierdurch kann die Ganggeschwindigkeit von Patienten gegenüber aktuellen Therapien beschleunigt werden. Diese weitreichenden Erkenntnisse belegen das große Potenzial von robotischen Reglern, neuronale Mechanismen vorherzusagen. Zusätzlich erklären die Regler die Funktion neuronaler Schaltkreise und vermindern so das vielgeäußerte Problem, dass die Neurowissenschaft reich an Daten aber arm an Theorien ist.

Acknowledgments

First and foremost, I am deeply grateful to my supervisor Alin Albu-Schäffer for his guidance, support, and encouragement throughout my PhD. His curiosity, sharp mind, and extensive knowledge (not only) of robotics formed the cornerstones of many inspiring discussions. I could not have hoped for a better supervisor.

Special thanks go to Henrik Jörntell for integrating me into his neuroscience group at Lund University. His lab became my second scientific base, in particular in experimental neuroscience. His personal and professional mentorship was essential for me to enter the neuroscientific community. Our discussions led to many exciting projects, and I am looking forward to many further insights along this fruitful journey.

I am also indebted to my former colleague Dominic Lakatos. His work was the starting point for this PhD project, and his mentorship paved my way into the field of robotics.

I was blessed with the opportunity to collaborate with many brilliant researchers, in particular, Patrick van der Smagt, David Franklin, Hannes Höppner, Mehmet Can Özparpucu, Alexander Dietrich, and Florian Röhrbein. I was furthermore fortunate to receive important input during my PhD from Neal Lii, Manuel Keppler, Daniel Seidel, Florian Löffl, Georg Stillfried, Helge Aufderheide, Christoph Richter, Alexander Werner, and Holger Urbanek. I also thank the PhD students Matthias Kohler and Annika Schmidt for their creative ideas and hard work to extend the research presented here, and for their patience as I learned how to advice them.

"A picture is worth a thousand words"—but even a million words are insufficient to express my gratitude to Tilo Wüsthoff, who created the expressive Figure 6.1.

The experiments would not have been possible without Florian Schmidt and Robert Burger, who restructured the electronics of the manipulandum and thus breathed life into it. Thanks also to my colleagues who run the mechanical and electrical workshops at DLR.

Already before my PhD, I had the privilege to have scientific mentors who opened my eyes for the beauty of science. Thus, thanks to Clare Mackay, Paul Goldsmith, Silvia Pani, Martin Arndt, Harald Hiesinger, Jürgen Stockel, Ewald Segna, and Wolfgang Beitl. I am particularly grateful to Tim Vogels, who supervised my master's thesis and inspired me to pursue research in computational neuroscience.

Thanks to Manuela Fischer, Gabriele Beinhofer, Jessica Laskey, and Almut Tresbach, who disentangled administrative regulations that were often as intertwined as brain circuits. I acknowledge the Deutsche Bahn, which typically arrived too late and thus gave me plenty of time to finish many paragraphs of this dissertation on the train.

I am grateful for the advice of those who proofread (parts of) my dissertation, namely, Alin Albu-Schäffer, Alexander Dietrich, Neal Lii, and Lena Funcke.

It is my particular pleasure to thank all those who accompanied me during my time in

Munich. You made it a delight to hike and ski in the Alps, to cycle to work and swim afterwards, to philosophize until late at night or just over a cup of tea.

Above all, I thank my family for their continuous warmth and love. With their constant and selfless support and encouragement, my parents enabled me to find and pursue my passion for science. Thank you to my siblings Anne and Peter for their humor that cheers me up even in stressful times. And to my nephew Alex, who showed me that the brain needs only a year to learn the motor skills that we have tried to implement in robots for decades. My most-heartfelt gratitude goes to my beloved wife Lena. Your curiosity fuels my fascination, your genius inspires my thoughts, and your love gives me a safe haven to anchor my spinning mind.

Munich, January 2020 Philipp Stratmann

Contents

List of abbreviations and symbols

In the present dissertation, scalar quantities are represented by letters in plain type. Vectors and matrices are shown in bold. The letters may appear with different subscripts and superscripts. A dot denotes the total derivative of a quantity with respect to time. An asterix denotes that the quantity has been obtained by optimal control. The following lists summarizes symbols and abbreviations that appear at several places or are of dominant importance.

List of abbreviations

5-HT	Serotonin
ang	Angular
cat	Catabolism
CB	Cone bipolar cells
CNS	Central nervous system
dec	Decay of a synaptic trace
depl	Depletion mechanism of neurotransmitter
DOF	Degrees of freedom
EMG	Electromyography
LIF	Leaky integrate-and-fire
mem	Membrane
mot	Motor
MVC	Maximum voluntary contraction
NM	Neuromodulation
NRO	Nucleus raphe obscurus
NRP	Nucleus raphe pallidus
rad	Radial
rem	Removal of a neurotransmitter by glia or diffusion
scal	Synaptic scaling
SEA	Series elastic actuator
SERT	Serotonin transporter
STD	Short-term synaptic depression
STDP	Spike-timing-dependent plasticity
tar	Target

List of symbols

α	Angle describing a weight vector in polar coordinates
a	Element of an eigenmode / nonlinear normal mode
b	Base of a robot
c	Constant
$\boldsymbol{C}$	Generalized Coriolis and centrifugal matrix
d	Damping
ϵ	Threshold
E	Energy
θ	Angular motor position
f	Friction
F	(Generalized) force
γ	Learning rate
g	Membrane conductance
i, j, l, n, s	Indices used for numbering
$\mathcal{J}$	Cost / error function
$\boldsymbol{J}$	Jacobian
k	Stiffness
K	Michaelis constant
$\boldsymbol{K}$	Diagonal matrix of learning rates
m	Mass (as scalar) or Michaelis Menten kinetics (as index)
$\boldsymbol{M}$	Inertia matrix
ν	Neuronal firing rate
p	Generalized momentum
q	Joint position
r	Friction estimated from sensory signals
S	Spike train
τ	Torque within a joint (when linked with an index) or time constant (with superscripts)
t	Time
V	Depletion velocity of a neurotransmitter
w	Weight of an affine transformation (robotics) or of synapses (neuroscience)
x, X, y, Y	Coordinates
z	Denoting a latent controller space (as subscript) or a synaptic trace (vector with superscript)

List of figures

CHAPTER 1

Introduction

"What I cannot create I do not understand"

– Feyman [1]

1.1 Motivation

Natural selection has equipped us with the central nervous system (CNS) which generates versatile and yet efficient movements in ever-changing environments. The field of bionics replicates the human-like motor performance in robotic systems. In return, neuroscientists have partly reversed the bionic knowledge transfer and have developed the field of *robotics-inspired biology*. The neuroscientists thereby apply tools developed for the analysis of robotic systems to investigate biological motor control and replicate it in biomimetic robotic systems to detect where our understanding is incomplete (cf. Ijspeert [2], Floreano et al. [3], and Gravish et al. [4] for recent reviews). The paradigm can be summarized by a weaker formulation of Feynman's quote: *"What I cannot replicate I do not understand"*. But Feynman's original quote adds an important statement: We understand an approach more thoroughly by its creation than we ever could by its mere replication. And indeed, the highest-performing robotic controllers are traditionally not a result of replication, but are based primarily on considerations about the dynamics of mechanical systems.

This PhD dissertation fully reverses the bionic pathway, which uses biological knowledge to find engineering solutions. Instead, the underlying work uses the powerful engineering solutions created to control robotic movement as blueprints to understand the neuronal motor circuitry. This proposed *enginic* approach is motivated by the common view that all CNS functions have ultimately been shaped by the evolutionary need to control efficient and versatile body movement in order to find food, evade threats, and mate [5, 6].

The enginic research project that led to the present dissertation focused on the scarcely unraveled [7] neuronal control of highly dynamic motions because it is a particularly promising field of research for an enginic knowledge transfer. The underlying circuits are subject to only limited cortical influence in order to react timely to rapid perturbations [8], which narrows down the search for a neuronal counterpart of a given robotic control

algorithm. Furthermore, highly dynamic movements show particularly high energy demands and thus provide a clear benchmark to evaluate if a given robotic controller offers a promising hypothesis for neuronal motor control: its energy efficiency. When a walker starts to run, the energy expenditure required to maintain the gait increases 7-fold [9]. Mechanically, individual muscles and tendons reduce their dissipated energy by up to 84 % [10] as they deflect like springs when the runner strikes the ground and reuse the stored energy to push the foot off the ground [11–13]. Robotic systems increasingly incorporate springs to mimic this beneficial behavior, as illustrated by *Boston Dynamics*' *BigDog* [14], *EPFL*'s *Cheetah-Cub* [15], and *DLR*'s *Bert* [16]. A control algorithm that harnesses the compliance of these biomimetic robots and minimizes their energy consumption is a promising hypothesis to explain also how our CNS controls the locomotor systems.

Specifically, the dissertation demonstrates that a state-of-the-art autoencoder developed to induce energy-efficient motions in such compliant robots links various loose neurophysiological threads into a coherent anatomical and functional description of a neuronal motor circuit. While Lakatos et al. [17, 18] had developed this autoencoder without bionic influence, a comparison revealed that each of its algorithmic components, illustrated in Figure 1.1, is mirrored by a corresponding neuronal circuit or mechanism [19]—with one remarkable exception: As the autoencoder forwards a single motor signal to drive all motors, sensory signals adjust the amplitude of this common signal for specific motors when the mechanical conditions have changed. An equivalent neuronal mechanism would disparately scale the recruitment of individual motorpools that are driven by the same motor signal, a common neuronal circuitry that is known as *motor synergy*. The CNS requires this functionality to reduce, for example, the recruitment of a single muscle from a synergy when the environment blocks its actuated joint (Figure 1.2). But the required proprioceptive information is locally encoded neither within the presynaptic synergy interneurons nor within the postsynaptic motorpools. The adaptation rule would thus violate the fundamental neuroscientific principle that learning depends solely on local information [20–22]. The research summarized here proved that the serotonergic innervation of the spinal cord overcomes this neuroscientific constraint and performs the non-local motor adaptation predicted by the robotic learning algorithm. It demonstrated in human subjects that the serotonergic circuitry receives proprioceptive signals and adapts how individual motorpools react to incoming motor signals. A mathematical analysis demonstrated that the circuitry minimizes a non-local error function by gradient descent, a fundamental technique of machine learning that had not been known in CNS circuitry. According to robotic experiments, this serotonergic motor feedback loop harnesses the compliant properties of muscles and tendons and minimizes the high metabolic demands of fast periodic motions.

1.2 Related work

Robotics engineers have recently started to replicate compliant and other mechanical features that underlie the superior movement performance of animals [23–26].

1.2.1 Compliant control in robotics

For the new biomimetic robots, novel algorithms are required that excite the versatile and energy-efficient natural modes. Their development is a challenging task, since the complex robots comprise multiple degrees of freedom (DOF), are subject to continuously changing environments, and switch between continuous states such as standing and flying.

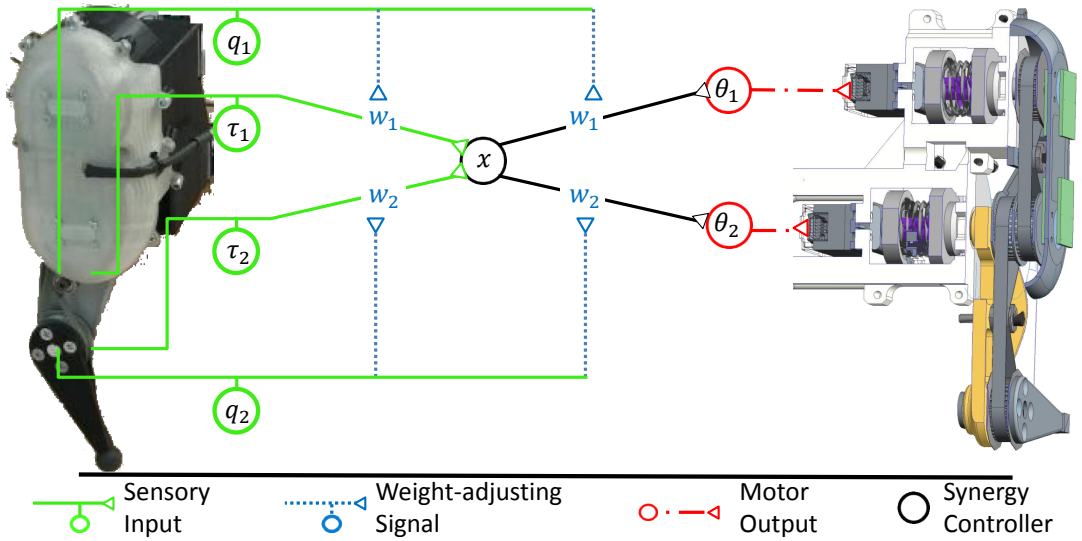

Figure 1.1: Block diagram of the robotic autoencoder that underlies the present research project. Sensory inputs signaling the joint torques $\boldsymbol{\tau}$ are mapped from the joint space onto a one-dimensional sub-manifold along multiplicative weights $\boldsymbol{w}$. The transformed input entrains a timing unit which produces a bang-bang output θ_z, which is reversely transformed into motor signals $\boldsymbol{\theta}$. The input and output weights continuously adapt to sensory information on the joint deflections $\boldsymbol{q}$ to account for changing mechanical conditions. Figure modified, with permission, from Stratmann et al. [27].

Several research groups have developed control algorithms to induce stable and energy-efficient limit cycles in compliant robots based on their dynamics. But these algorithms often suffer from effects which limit their use in robots and make them unsuitable as enginic blueprints of animal motor control. Most approaches rely on a precise dynamic model of the robot and a fixed set of considered initial model parameters [28], such as algorithms based on Poincaré maps [29], transverse linearization [30], or optimal control [31]. They cannot adjust to unexpected conditions and therefore fail to explain how the CNS adapts to fast mechanical changes of the animal body and its environment. In general, the neuronal control of compliant movements is unlikely to rely on precise dynamic models because the compliant properties of musculoskeletal systems critically depend on many complex effects such as nonlinear muscle elasticities, hysteresis effects, and the changing 3D structure of the compliant elements [32]. Algorithms based on *van der Pol* oscillators often use a nonlinear, sign-changing damping term to enforce a pre-defined limit cycle [33]. Imposing van der Pol oscillator dynamics on a multi-body system substantially modifies the intended natural dynamics of the robot and artificially dissipates energy.

The autoencoder considered here has been developed to excite the natural resonance modes of a compliant system instead of to impose artificial dynamics onto the system by control [17, 18]. It simplifies the control of the robot during highly dynamic movements as it empowers a single signal to control several compliant joints. As illustrated in Figure 1.1, the autoencoder is organized in three subsequent stages: The encoder maps sensory input from the multi-dimensional joint space onto a one-dimensional controller manifold by an affine transformation. In this intermediate latent space, the sensory signal entrains a bang-bang unit. The decoder stage reversely maps the latent motor signal onto the joint space where it synchronously drives all actuators involved in the movement. The bang-bang control guarantees that the controlled robotic motion converges to an attractive periodic limit cycle within few oscillation periods because it injects the same energy in each periodic

cycle while the energy dissipated by damping increases with the movement amplitude [17, 19, 34]. Once a movement is excited, sensory signals continuously adapt the transformation weights at the encoder and decoder stage to changing mechanical resonance conditions. For this purpose, Lakatos et al. [17] derived an adaptation rule that aligns the weights with the least-square optimal, linear approximation of the dominant oscillation mode of the mechanical system [35]. The control approach requires only prior knowledge on the DOF of the mechanical system and continuous sensory information on a given movement. But it remained unclear if the autoencoder can excite energy-efficient resonance movements in complex robots or even in biologically plausible mechanical systems.

1.2.2 Compliant control in neuroscience

The robotic autoencoder shows a distinct resemblance to known neuronal structures and functions [19, 36]. In particular, the sensory encoder [37, 38] and the latent control manifold [39, 40] are mirrored by corresponding CNS circuits.

Like the robotic encoder, also the CNS of cats converges sensory signals from different joints to entrain the frequency of all muscles involved in a movement [41, 42]. The robotic controller suggests that the transformation weights adjust according to *Oja's rule*, a mathematical model of Hebbian learning that underlies many forms of synaptic plasticity in the CNS [35, 38]. And indeed, the efficacy of individual nerves to entrain motor signals in the cat changes according to this plasticity rule [37].

The one-dimensional latent layer is the control-theoretic equivalent of a *synergy* [43–45]. Synergies are neuronal structures prevalent throughout the spinal cord [46–48] which solve the problem that the biological locomotor system offers more DOF than required for a specific task [49]. The majority of spinal interneurons receive signals from different modalities and thus form *sensory synergies* [39]. They thereby filter out information which is unnecessary for a specific task. In turn, groups of interneurons elicit synchronous motor signals to a hard-coded group of muscles—the above-mentioned motor synergies [40, 50–54]. A motor synergy chooses among the large number of movement patterns that even a single leg offers due to its more than 50 muscles [43]. Descending commands link the individual synergies into the complex movement patterns observed in humans [55–59].

Given these striking analogies, it is remarkable that there is no known neuronal counterpart for the adaptation rule of the decoder. A neuronal mechanism that adjusts motor synergies in a similar way would provide the CNS with a fundamental function: it can adjust the relative forces of different muscles when their activation is timed by a common ionotropic synergy signal (Figure 1.2). An equivalent neuronal mechanism must receive sensory input and accordingly adjust the synaptic weights between the synergic interneurons and individual motorpools. But the function violates a fundamental principle of neuronal learning: locality. The synaptic weight between two neurons is thought to be shaped exclusively by the local information encoded by the pre- and postsynaptic cell [20]. The proposed new mechanism, in contrast, would perform non-local learning since neither the common interneurons nor the motorpools encode the sensory information which guides the adaptation process. Previous theoretical studies have accordingly focused on properties of synergic motor signals that the CNS can adjust without non-local learning, such as their phase [60, 61] and frequency [62–64], but not on a disparate amplification as the common signal is forwarded to different muscles. This dissertation solves the paradox that the CNS is, according to state-of-the-art knowledge, unable to scale an individual motor signal from a motor synergy despite the large evolutionary benefit of this skill.

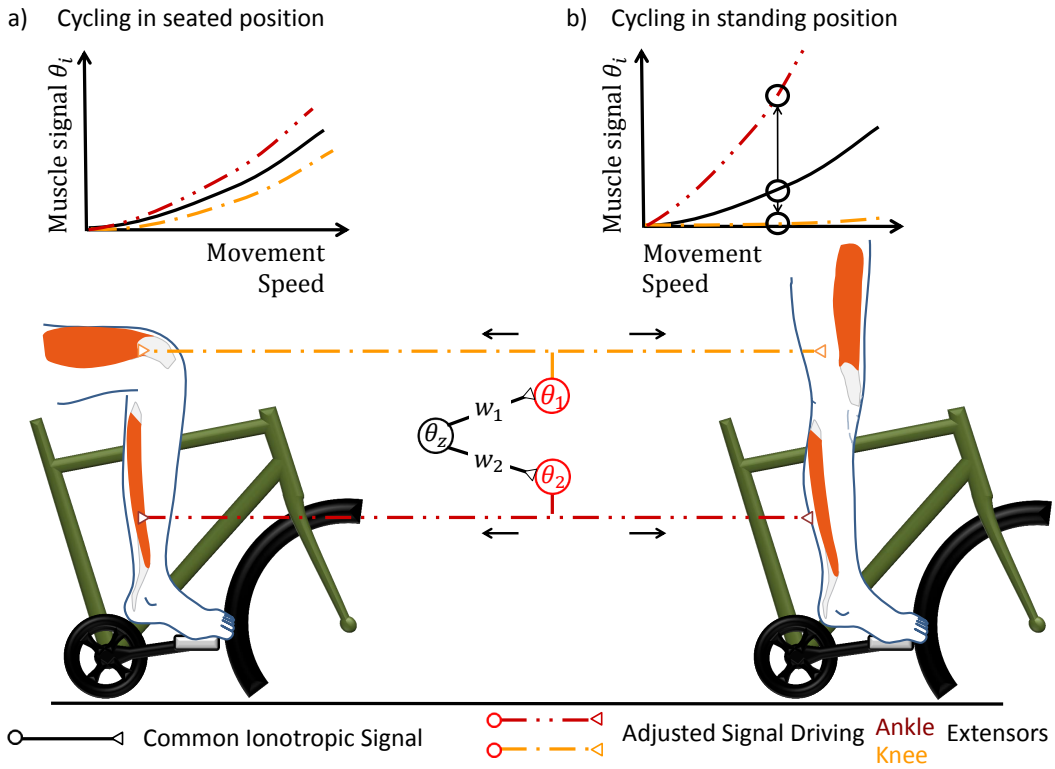

Figure 1.2: Cycling can illustrate why it is essential to disparately scale the forces of different muscles when the mechanical conditions change. For this purpose, assume that cycling is controlled by a pool of M1 neurons that elicit a common motor command θ_z [65]. The synergy signal is transformed along synaptic gains $\boldsymbol{w}$ into signals $\boldsymbol{\theta}$ that drive the spinal motorpools of several muscles [55–57]. (a) When the person sits on the saddle, both knee and ankle extensors need to be actuated. (b) When the subject stands up to accelerate, the knee extensors cannot exert a force along the pedal trajectory and their motor signal should be scaled down. In contrast, the ankle extensors need to receive an amplified signal to maintain the movement speed. Ankle and knee extensors must thus be scaled in opposite directions to adjust to the new mechanical conditions. Also mechanical conditions that restrain the movement less strictly than the pedal show preferred or resonant movement directions that allow excitation of large movement amplitudes with small consumption of metabolic energy. Figure modified, with permission, from Stratmann et al. [27].

1.3 Problem statement

So does the robotic autoencoder explain how the CNS controls compliant movement? This question poses many challenges that justify why the neuroscientific community has not harnessed the diverse control approaches developed for biomimetic robots, yet. As detailed below, the associated enginic knowledge transfer needs to overcome four main problems:

1. It is unclear if the robotic autoencoder shows functional benefits, in particular energy efficiency, which make it a promising hypothesis for neuronal motor control.
2. The CNS seems incapable of the non-local learning predicted by the robotic decoder.
3. Given a predicted functionality, it is difficult to detect a specific neuronal mechanism that performs it due to the complex and intertwined nature of the CNS.
4. The neuronal hypotheses must be verified during fast and strong motions *in vivo*.

In order to solve these four scientific problems, a large range of scientific fields and methods must be mastered, ranging from robotics control theory and experimental robotics, through computational neuroscience, to human-subject experiments. Besides the scien-

tific challenges, the associated interdisciplinary work must also overcome many mental and infrastructural barriers that separate researchers working in these fields.

The quest for control algorithms that achieve the high energy efficiency of animal locomotion is *"one of the biggest challenges in robotics research today"* [66]. While an individual robotic actuator can already outperform the energy efficiency of a mammalian muscle, complex robots require several times more energy for a specific task than their animal counterparts [67]. Mechanical engineers therefore increasingly mimic the mechanical features underlying the mammalian motor performance. A lower-limb exoskeleton is an extreme result of this approach because its dynamics is predominantly determined by the human locomotor system supported by it. These robots are often built to increase the walking efficiency of a human. But exoskeletons controlled by traditional algorithms substantially change the human movement pattern and thus often even increase the human's metabolic energy expenditure [68]. In order to unleash the potential of biomimetic robots, a new controller design is thus needed which harnesses their beneficial intrinsic dynamics. Such a controller needs to continuously adapt online when the robot, for example, steps from solid onto soft ground or lifts a load. While humans can solve this task intuitively, the *Moravec's paradox* states that it is much more challenging for a computer algorithm to learn such a sensorimotor skill than to solve reasoning tasks, such as excelling in chess, that pose severe challenges to the human CNS [69].

The search for a neuronal counterpart of the robotic decoder seems impossible at first sight because its learning rule violates the paradigm of locality that constrains neuronal learning as discussed above. But as illustrated in Figure 1.2, the disparate amplification of different motorpools to non-local information is not only advantageous but even crucial when a motor synergy must control movements that are mechanically constrained, such as pedaling. Also beyond the specific context of motor synergies, the lack of computationally potent non-local learning mechanisms is a key issue for computational neuroscience. For a long time already, this lack has been a *"core objection to the biological plausibility of backpropagation"*, one of the most fundamental learning principles of artificial neural networks [22]. Detecting such a mechanism in the CNS would remove a major barrier between neuroscience and machine learning and open a new path for a mutual knowledge exchange that goes far beyond locomotor control.

If we assume that the CNS performs the non-local learning predicted by the robotic decoder, it will still be challenging to discover the specific underlying neuronal mechanism or circuit due to the sheer complexity of this organ. The CNS consists of roughly 86 billion neurons [70] that are connected to each other via about 100 trillion synapses [71] and exchange far over 100 different neurotransmitters [72]. These billions of cells may in theory calculate a predicted set of equations in myriad different ways.

Even spotting the correct brain counterpart of the robotic controller will only provide a neuronal model. Such a model must be experimentally verified because *"in theory, there is no difference between theory and practice. But, in practice, there is"* [73]. Ajemian and Hogan [74] recently attested that the *"temptation of building elegant models that can never be tested"* is a major problem of motor neuroscience due to the complexity and entanglement of brain circuits. Traditional neuroscientific methods furthermore face specific limitations when analyzing how the CNS controls highly dynamic movements. Invasive recordings that could directly disentangle the underlying low-level motor circuitry are obstructed in animals because the spinal cord shows profound movement within the vertebral column [75]. Well-designed experiments may test neuronal hypotheses non-invasively, but they still require a mechanical test bed that fulfills conflicting requirements.

It must at the same time simulate a desired environment with high precision, allow high forces and velocities, and guarantee the participant's safety.

In addition to the four research challenges, the proposed enginic project poses also communication challenges due to its interdisciplinary nature. Engineers and biologists do not speak the same language—literally: While mathematics lies at the heart of engineering, each additional equation per page reduces the citations a biology paper receives by 28 % [76]. Even between computational and experimental neuroscientists there is a large gap, and experimentalists *"are skeptical of claims based on simulated data, feeling that such efforts are too far removed from biology to be informative"* [77]. An enginic project must overcome these barriers in order to build up an interdisciplinary collaboration team and get its output published to both the robotics and the neuroscience community. Such an endeavor is needed more than ever at the present stage because the cooperation between engineers and neuroscientists have seen a sharp decline during the last years [22].

1.4 Overview and contributions of this dissertation

The research presented in this cumulative dissertation addressed the problems stated in the previous section. Step by step, it transferred the original robotic autoencoder into knowledge on neuronal motor circuitry. The results of the enginic path contribute theoretical and experimental insights to both robotic control and neuroscience. The following four chapters sequentially summarize the obtained four key findings and the methods applied to obtain them:

1. The decoder excites motions in biomimetic robots that are energy optimal under changing conditions. It is therefore a promising blueprint for human motor control.
2. The serotonergic innervation of the spinal cord implements a motor feedback loop, as it receives proprioceptive information and accordingly releases serotonin which modulates the activity of spinal motoneurons. This non-local learning shows close algorithmic resemblance to the learning rule of the robotic decoder.
3. Serotoninergic neuromodulation is the only known substrate for non-local learning in lower motor circuitry, making it a unique basis for the learning rule.
4. In human subjects who perform highly dynamic motions, serotonin modulates motoneuron activity as predicted by the learning rule of our robotic decoder.

For more details, the reader is referred to the four journal articles in the appendix.

Chapter 2 demonstrates that the robotic autoencoder harnesses the compliant elements of a biomimetic robot. It thereby induces periodic movements with minimum energy consumption even in systems subject to hybrid nonlinear dynamics. This result establishes the learning rule proposed by Lakatos et al. [17] as a tool for engineers who can apply it to multi-joint compliant robots. The algorithm will autonomously acquire the resonance frequency of the motor signals and the relative torques of the actuators that increase the overall movement amplitude for constant energy input, in some cases to a value multiple times higher than before adaptation. The rule advances the state of the art in energy-efficient control by an algorithm that features a unique mix of characteristics, as it is highly modular and adapts online to changes of the robot and its environment without prior model knowledge of their dynamics. While the results were obtained by numerical optimization, they were validated in robotic experiments.

Chapter 3 shows that the human CNS may, in theory, perform the same arithmetic operations as the robotic autoencoder to induce fast periodic movement with minimum metabolic requirements. The simulation results show that the high performance of the

robotic autoencoder is thereby determined solely by the decoder, which determines the torque that individual joints contribute to the overall movement. Its adaptation algorithm resembles the effect of neurons in the medullary raphe nuclei, which release the neuromodulator serotonin onto spinal motoneurons. As compared in Figure 6.1, both the robotic adaptation rule and the raphe neurons receive sensory information on an ongoing movement and multiplicatively scale the response, i.e., the excitability, of several actuators to a common motor signal. Analytic reasoning demonstrated that the dynamics of the serotonergic neuromodulation yields the same multiplicative weights as the adaptation rule of the decoder. Previous research has not considered serotonin as basis of neuronal learning because it is presumed to be only a diffuse metabotropic neuromodulator of the topographically precise ionotropic circuitry which dominates CNS functions. In the spinal cord, serotonin is generally accepted to equally scale the response of actuators driving different joints even across limbs [78, 79]. The present model, in contrast, assumes that serotonin predominantly amplifies the actuators of the joints which show particularly large movements in comparison to other joints of the same limb.

The review in chapter 4 attests that previous experimental findings are compatible with the assumption that serotonin disparately multiplies the activity of individual motorpools. While this *precision scaling* could theoretically also originate in ionotropic effects, alternative, non-metabotropic circuits in the spinal cord were found to be computationally limited and show a purely linear processing of sensory signals. The raphe nuclei thus form the only neuronal circuitry that may, according to current data, perform the motor adaptation proposed by the robotic decoder. In a broader context, these findings demonstrate that serotonergic neuromodulation will extend the linear ionotropic circuitry in the spinal cord by the ability to calculate general nonlinear functions if it acts with topographic precision.

Experiments presented in chapter 5 proved that the serotonergic system of human subjects acts with the precision predicted by the robotic output transformation. The CNS specifically increases the excitability of motorpools when their innervated joint, rather than another joint of the same limb, performs highly dynamic movement. As a spin-off of these experiments, a safe controller is developed for a robotic device that guides the arm of human subjects with forces of up to 1.5 kN. This peak force is unrivaled by similar devices [80], prompting that the new controller provides neuroscientists with a tool that shows unmatched acceleration and precision.

In summary, the research presented here has shown that the serotonergic raphe nuclei implement non-local learning and adapt the spinal ionotropic circuitry to sensory input. The serotoninergic system thereby acts not by diffuse neuromodulation as generally assumed. Instead, it forms a topographically precise computational skipping network to the network formed by the ionotropic circuitry. Serotonin thereby adjusts the relative forces of individual joints and harnesses the compliant properties of the whole limb for energy-efficient movement. The functional benefits of this mechanism emphasize it as a versatile and powerful effect that neuroprosthetic systems and exoskeletons can mimic to extend their battery life and the motor performance of injured and healthy people. The results on serotonin in lower motor circuitry furthermore suggest that monoamines may provide topographically precise effects also in other CNS circuits, where their malfunction is tightly linked to neuropsychiatric disorders such as depression, obsessive compulsive disorders, and generalized anxiety disorder [81]. The proposed concept that the underlying monoaminergic systems show topographic precision offers an explanation for the poor and unpredictable treatment outcomes of the psychopharmacological drugs that act on them by diffuse mechanisms. To test its impact for Parkinson's disease, an *in-vivo* study

is currently being prepared at Lund University (Sweden). Besides the new knowledge, the success of the enginic project reveals also a new methodology for neuroscientific research. Accordingly, robotic control algorithms have become an efficient source of well-analyzed models that identify unknown neuronal mechanisms, frame individual known neuronal circuits into an overarching framework, and explain their functions.

1.5 Publications underlying this dissertation

The impact of the present project demonstrates that its research successfully attracted an interdisciplinary project team and overcame the mental barriers between the involved scientific fields. Each of the four key findings presented in the last section resulted in a separate paper which was published in, or in one case is being prepared for, a leading journal in the field of either robotics, computational neuroscience, or experimental neuroscience. To present the findings, a workshop was organized at a major neuroscience conference and a talk was delivered at a major conference in the field of robotics. A patent is currently under review, illustrating also the industrial impact. The results gave rise to two followup doctoral projects that are being carried out at the Technical University of Munich / the German Aerospace Center and an *in vivo* study that is being prepared at Lund University.

1.5.1 Journal publications & patents

Philipp Stratmann, Hannes Höppner, David Franklin, Patrick van der Smagt, and Alin Albu-Schäffer. "Focused neuromodulation of individual motorpools: confirmation of predictions from the efficient control of biomimetic robots". *Nature Communications Biology* (2020, to be submitted).

Philipp Stratmann, Dominic Lakatos, and Alin Albu-Schäffer. "Medizinisches System zur Laufunterstützung durch Muskelstimulation sowie Verfahren zur Regelung eines medizinischen Systems zur Laufunterstützung durch Muskelstimulation". German patent application no. 10 2020 120 164.8 (2020, under review).

Philipp Stratmann, Dominic Lakatos, Annika Schmidt, and Alin Albu-Schäffer. "Medizinisches System zur Laufunterstützung sowie Verfahren zur Regelung eines medizinisches System zur Laufunterstützung". German patent application no. 10 2020 120 161.3 (2020, under review).

Philipp Stratmann and Alexander Dietrich. "Objekt mit variabler Steifigkeit". German patent application no. 10 2018 103 893.3 (2018, under review).

Philipp Stratmann, Alin Albu-Schäffer, and Henrik Jörntell. "Scaling Our World View: How Monoamines Can Put Context Into Brain Circuitry". *Frontiers in Cellular Neuroscience* 12 (2018), p. 506. ISSN: 1662-5102. DOI: 10.3389/fncel.2018.00506.

Philipp Stratmann, Dominic Lakatos, Mehmet Can Özparpucu, and Alin Albu-Schäffer. "Legged Elastic Multibody Systems: Adjusting Limit Cycles to Close-to-Optimal Energy Efficiency". *IEEE Robotics and Automation Letters* 2.2 (Apr. 2017), pp. 436–443. DOI: 10.1109/LRA.2016.2633580.

Philipp Stratmann, Dominic Lakatos, and Alin Albu-Schäffer. "Neuromodulation and Synaptic Plasticity for the Control of Fast Periodic Movement: Energy Efficiency in Coupled Compliant Joints via PCA". *Frontiers in Neurorobotics* 10 (2016), p. 2. ISSN: 1662-5218. DOI: 10.3389/fnbot.2016.00002.

1.5.2 Conference presentations

Philipp Stratmann. *Legged Elastic Multibody Systems: Adjusting Limit Cycles to Close-to-Optimal Energy Efficiency*. Oral presentation and interactive session, *IEEE International Conference on Robotics and Automation (ICRA)*. May 2017.

Philipp Stratmann and Florian Röhrbein. *More for less – Energy Efficiency in Neural Locomotion Control*. Conference workshop, *Bernstein Conference*. Sept. 2016.

CHAPTER 2

A controller for energy optimal motion in biomimetic robots

A robotic control algorithm provides a promising hypothesis for animal motor control if it shows such substantial functional advantages that the neuronal circuitry is likely to have evolved to fulfill an analog functionality. The benefit of control approaches developed for compliant robots can primarily be assessed according to their ability to harness the passive compliant elements for energy-efficient movement because the ability to minimize the muscular energy expenditure is seen as a major—if not the most important—factor underlying the evolution of compliant motor control [5, 6, 11]. Particularly during highly dynamic locomotion, passive compliant elements can substantially lower the high metabolic demands of motion [11], a fact that forms a driving force behind the increasing incorporation of compliant elements in bionic robots [24]. But as summarized in the introduction, previous robotic approaches to compliant control fail as blueprints for brain circuits because they either dissipate energy by artificial damping or require precise models of the mechanical system that can hardly be provided in ever-changing mechanical contexts.

In the present project, numerical optimal control and robotic experiments were applied to check whether the novel modal robotic controller induces energy-optimal movement [82]. "Energy-optimal" hereby means that the control law maximizes the movement amplitude for a pre-defined energy input. The considerations were based on a periodically jumping biomimetic leg, since locomotion bears a particularly high potential for optimization by compliant structures due to its high energy consumption and high occurring impact forces. Its control is challenging, as it shows nonlinear hybrid dynamics.

2.1 The robotic autoencoder

The modal adaptive controller that Lakatos et al. [17, 18] developed for the control of compliant robots is illustrated in Figure 1.1. When considering it in detail, it shows three characteristics that shape the energy efficiency of the resulting movement. The study summarized here subsequently checked the efficiency of each of them.

First, the controller induces periodic movement. It thus converges the ongoing movement of a multi-body system driven by series elastic actuators (SEAs) to a stable limit cycle. The movement can be initiated by deflecting the system from its static equilibrium position and is then iteratively adjusted by the controller.

Second, the controller reduces the control of a robot with n joints to a one-dimensional task by modal transformation weights $\boldsymbol{w} \in \mathbb{R}^n$. These weights remain constant throughout the movement cycle as long as the robot and its environment remain unchanged. The algorithm sets the motor coordinates $\boldsymbol{\theta} \in \mathbb{R}^n$ according to sensory information on the joint coordinates $\boldsymbol{q} \in \mathbb{R}^n$ and the joint torques $\boldsymbol{\tau} \in \mathbb{R}^n$. Since the study considered SEAs, the torques were a function of the difference between joint and motor coordinates,

$$\boldsymbol{\tau} = \boldsymbol{\tau}(\boldsymbol{\theta} - \boldsymbol{q}) \ . \tag{2.1}$$

The controller transforms these torques from the joint space onto a one-dimensional control sub-manifold along the modal weights,

$$\tau_\mathrm{z} = \frac{\boldsymbol{w}^T}{\|\boldsymbol{w}\|}\boldsymbol{\tau} \ . \tag{2.2}$$

When this signal crosses a constant threshold $\epsilon_\tau \in \mathbb{R}_{>0}$, the controller triggers a one-dimensional controller output of constant amplitude $\hat{\theta}_\mathrm{z} \in \mathbb{R}_{>0}$,

$$\theta_\mathrm{z} = \begin{cases} +\hat{\theta}_\mathrm{z} & \text{if } \tau_\mathrm{z} > \epsilon_\tau \\ 0 & \text{if } -\epsilon_\tau \leq \tau_\mathrm{z} \leq \epsilon_\tau \\ -\hat{\theta}_\mathrm{z} & \text{if } \tau_\mathrm{z} < -\epsilon_\tau \end{cases} \ . \tag{2.3}$$

The output is transformed back onto the high-dimensional joint space and the motor torques are accordingly updated to

$$\boldsymbol{\theta} = \theta_\mathrm{z}\frac{\boldsymbol{w}}{\|\boldsymbol{w}\|} \ . \tag{2.4}$$

The following considerations focus on a bionic robot with $n = 2$ joints for reasons detailed below, which implies that the normalized weight can be characterized in polar coordinates by the scalar angle α,

$$\frac{\boldsymbol{w}}{\|\boldsymbol{w}\|} = \begin{pmatrix} \sin(\alpha) \\ \cos(\alpha) \end{pmatrix} \ . \tag{2.5}$$

As a third characteristic, the controller autonomously models the dynamics of a robot and adapts when the robot itself or its mechanical environment changes. For this purpose, the controller observes the joint trajectories $\boldsymbol{q}$ and iteratively adapts the linear transformation weights according to Oja's rule [38],

$$\dot{\boldsymbol{w}} = \gamma(\boldsymbol{w}^T\boldsymbol{q})\left(\boldsymbol{q} - (\boldsymbol{w}^T\boldsymbol{q})\boldsymbol{w}\right) \ . \tag{2.6}$$

The adjustment time constant $1/\gamma = 10\,\mathrm{s}$ is chosen larger than the periodic time of the movement to capture the dynamics of the system during the whole movement cycle. Oja's rule can intuitively be understood as an approach to linearize the mechanical system. If one of the joints shows an extensive movement amplitude q_i, the first term in the squared bracket will increase the associated weight w_i relative to the other weights. The negative second term will not alter the weights relative to each other, but will keep the overall weight vector bounded and will thus prevent its amplitude from infinite growth. In mathematical terms, Oja's rule extracts the dominant principal component of $\boldsymbol{q}$, corresponding to the physical eigenmode that shows the maximum amplitude for simple mechanical systems [35, 83]. In particular, the modal weights allow resonant movement in compliant systems which

show continuous linear dynamics, can be described by a constant diagonal inertia matrix, and are subject to modal damping and white noise. For more realistic nonlinear mechanical systems with hybrid dynamics, as considered here, Oja's rule extracts the least-square-optimal linear approximation to the joint trajectories which describe the dynamics. The robotic experiments focused on the performance of this learning rule due to its importance for the present dissertation, which considers if Oja's rule describes how the CNS adapts motor output to changing mechanical conditions.

The described three characteristics of the control approach formed the research hypotheses tested here: First, an energy-optimal solution is periodic. A control law that optimizes particularly a specific jump in a sequence should thus lead to a periodic trajectory in the preceding jumps. Second, a linear transformation is the optimal transformation between the joint-space and the modal control space without the need to adjust the transformation weights $\boldsymbol{w}$ to different stages of the movement cycle. Third, Oja's rule iteratively extracts the optimal transformation weights from sensory information on an ongoing controlled motion. This study consistently applies a bang-bang unit in the one-dimensional control sub-manifold as this controller type guarantees movement stability [34].

2.2 The compliant biomimetic robot

The robotic test bed for the energy considerations was given by the simulation model of a passive-compliant leg and the original leg, which are illustrated in Figure 2.1a and Figure 2.2a, respectively. The successors of this leg now propel the quadrupedal DLR robot *Bert* [84]. The robotic leg allowed to test the energy efficiency of the overall control algorithm, while the simulation model allowed numerical in-depth answers to the individual research hypotheses raised above.

The robot consists of a trunk that is attached to a two-compartmental leg comprising an upper thigh and a shank. The trunk and the thigh are linked by a hip joint, while the thigh is serially connected to the shank by a knee joint [84]. This robot with $n = 2$ joints was used in order to avoid redundancy during the considered running motions on a flat surface along the sagittal plane. This agrees with animal walking and running, which is mainly powered by two joints, while the third joint is predominantly used for functions that are not considered here, such as modulating the stiffness of the limb [85]. Two SEAs actuated the hip and knee joint, respectively, of the robot by deflecting two torsional springs of constant and equal stiffness by an angle $\boldsymbol{\theta} \in \mathbb{R}^n$. To guarantee that each SEA can independently actuate either of the joints, the second SEA was connected to the knee joint via belt drives. The robot was free to jump vertically, while a boom mounted to the trunk both kept it on a circular horizontal path and prevented rotation of the trunk. The trunk rotation was locked since both animals and advanced robots have a high trunk inertia and can adjust their rotation independently from the jumping motion due to redundant DOF. A sensor at the ground fixation point of the boom recorded the vertical height and circular horizontal position, denoted $x_{\mathrm{b}1} \in \mathbb{R}$ and $x_{\mathrm{b}2} \in \mathbb{R}$, respectively. Sensors in the SEAs filed the joint positions $\boldsymbol{q} \in \mathbb{R}^n$.

For the numerical investigations of the proposed control algorithm, the robotic system was modeled as a floating base with one leg. The floating base was able to freely translate in a vertical plane, described by the coordinates $\boldsymbol{x}_{\mathrm{b}} = (x_{\mathrm{b}1}, x_{\mathrm{b}2})^T \in \mathbb{R}^2$, while its rotation was locked. Joint and floating base coordinates were summarized as $\boldsymbol{x} = (\boldsymbol{x}_{\mathrm{b}}^T, \boldsymbol{q}^T)^T \in \mathbb{R}^{2+n}$. The two SEAs independently actuated either the knee or the hip joint as they deviated their torsional springs of stiffness k and damping c_{d} by angles $\boldsymbol{\theta} \in \mathbb{R}^n$. The overall system

can be modeled by

$$\boldsymbol{M}(\boldsymbol{x})\ddot{\boldsymbol{x}} + \boldsymbol{C}(\boldsymbol{x}, \dot{\boldsymbol{x}})\dot{\boldsymbol{x}} + \boldsymbol{g}(\boldsymbol{x}) = \begin{pmatrix} \mathbf{0} \\ k(\boldsymbol{\theta} - \boldsymbol{q}) - c_{\mathrm{d}}\dot{\boldsymbol{q}} \end{pmatrix} + \boldsymbol{\tau}_{\mathrm{contact}} \tag{2.7}$$

The symmetric, positive definite inertia matrix is denoted by $\boldsymbol{M}(\boldsymbol{x})$, $\boldsymbol{C}(\boldsymbol{x}, \dot{\boldsymbol{x}})$ represents the generalized Coriolis and centrifugal matrix, $\boldsymbol{g}(\boldsymbol{x})$ gravitational forces, and $\boldsymbol{\tau}_{\mathrm{contact}}$ the generalized external force. During the jumping movement, the leg formed a hybrid model and alternatively switched between a standing and flying phase. During the standing phase, the leg was in contact with either a rigid or a more realistic compliant ground model depending on the analysis technique applied for numerical optimization. In order to apply hp-adaptive Gaussian quadrature collocation, the well-tested software package *GPOPS-II* [86] was used whose differential equation solver imposed a rigid ground model that forced a fixed unilateral contact point with the leg. The later Monte Carlo analyses were compatible with a more realistic compliant model that fixed the leg by friction.

2.3 Numerical energy optimization

The following sections summarize the methods applied to test three aspects of energy efficiency as mentioned above:

1. Is each individual jump optimized during a periodic limit cycle?
2. Are the energy-optimal modal transformation weights time-invariant?
3. Does a bang-bang controller in combination with Oja's rule extract the optimal transformation weights from sensory information?

"Optimal" hereby means that the final jumping height, which is used as the objective function in Mayer form, is maximized for a fixed energy input. The energy is inserted into the system by the SEAs, which switch their torque,

$$\boldsymbol{\tau}_0 = k(-\boldsymbol{q}) \;\rightarrow\; \boldsymbol{\tau}_1 = k\left(\frac{\boldsymbol{w}}{\|\boldsymbol{w}\|}\left[\pm\theta_{\mathrm{z}}\right] - \boldsymbol{q}\right) \;,$$

and thereby perform the work (see original paper [82] for derivation)

$$\Delta E = \epsilon_\tau \hat{\theta}_{\mathrm{z}} + \frac{1}{2} k \hat{\theta}_{\mathrm{z}}^2 \;. \tag{2.8}$$

The energy inserted into the mechanical system is therefore determined by the controller threshold ϵ_τ and amplitude $\hat{\theta}_{\mathrm{z}}$. In contrast, the energy input is independent of the polar coordinate α that represents the normalized transformation weights.

2.3.1 Optimality of the periodic limit cycle

The study aims at maximizing all jumps of the robot simultaneously. The goal may be self-contradictory because a high performance of one jump may theoretically induce adverse effects on other jumps of the sequence. It must therefore be tested whether it is sufficient to maximize only the final jumping height and thereby induce a converging limit cycle movement where also all prior jumps are optimal. To answer this question, it is necessary to find the optimal parameter α^* and piece-wise continuous control $\hat{\theta}_{\mathrm{z}}^*(t)$ that maximize the final jumping height after a sequence of eight consecutive jumps. For the analysis, numerical hp-adaptive Gaussian quadrature collocation was applied as implemented in the

software *GPOPS-II* [86]. Accordingly, the state of the mechanical system was described by $(\boldsymbol{x}^T, \dot{\boldsymbol{x}}^T)^T$ and the state equation $\boldsymbol{f} = \left(\dot{\boldsymbol{x}}^T, \ddot{\boldsymbol{x}}^T\right)^T$ was derived from equation (2.7). The software divided the time interval of interest into specific mesh points and discretized the state at these points. The optimal control problem was then transformed into a nonlinear programming problem and solved using the IPOPT software library [87]. States were estimated using Lagrange polynomials, and both the number of mesh points and the degree of the polynomial were dynamically adjusted. The controller was constrained to show bang-bang behavior and the maximum energy inserted into the system was fixed during the eight jumps. The tested hypothesis states that the optimal controller switches after periodic intervals and that the induced leg trajectory showed exponential convergence, which would imply that the optimal movement is compatible with a stable limit cycle.

2.3.2 Optimality of the modal transformation

The focus was then turned to the second hypothesis, namely, that the weights of the mapping from the sensory/actuation space and the one-dimensional control sub-manifold may remain constant throughout the movement cycle. While the calculations repeated the optimization described in the last section, they alleviated the constraint that the weights must be fixed throughout the movement. The algorithm implemented in GPOPS-II therefore searched for the parameters $\hat{\theta}_z^*(t)$ and $\alpha^*(t)$ that maximized the final jumping height.

The obtained optimal weights did vary with time, which raised the question whether this deviation from constant weights is functionally relevant. The question was answered by comparing the improvement gained by allowing time-varying weights $\alpha^*(t)$ to the improvement that can be obtained by optimizing the time-invariant weights α. For this purpose, α was fixed to different equally-spaced values across its full range, GPOPS-II was run for each value, and the maximum achievable jumping height was recorded.

2.3.3 Optimality of the transformation adaptation

Under realistic conditions, the optimal transformation weights of the robot are initially unknown and must be adapted to the ever-changing dynamics of the robot and its environment. The robotic controller extracts an approximation of the optimal weights by applying Oja's rule to the sensory signals. Monte Carlo simulations evaluated whether the learning rule performs this task successfully and reliably given random initial weights and different target jumping heights.

Each simulation trial randomly picked the energy amplitude ΔE and the initial value for α which determine the jumping height and the transformation weights, respectively. It then quantified the performance improvement that the proposed controller gained by applying Oja's rule. Hereby, the mentioned parameters were chosen from an interval of values that we empirically found to induce stable jumping by a prior parameter screening. The simulation modeled how the algorithm controls the movement and adapts the weights according to the sensory feedback. Once the weights and the robotic trajectory had converged to a periodic trajectory, the simulation stopped and recorded the final weights. To quantify the performance improvement induced by Oja's rule, the simulations were repeated with transformation weights that were fixed to either their initial or their adapted values. The jumping height of the converged limit cycle quantified the controller performance. This procedure was repeated 40 times to see if Oja's rule reliably improved the controller performance.

2.4 Confirmation in robotic experiments

Experiments on the robotic leg confirmed that the theoretical results hold under realistic conditions. As mentioned before, the experiments focused on the third hypothesis raised in this chapter, namely, that Oja's rule leads to relative actuator forces that induce energy-optimal movement. If the hypothesis holds, the learning rule must adapt initial transformation weights to values that maximize the jumping height.

The experiments first determined the weights that Oja's rule extracts. For this purpose, the polar coordinate α was screened to detect an interval of possible initial values that allowed persistent leg movement. In two experimental trials, the initial weights were then set first to the lowest and then to the highest value of α in this interval. In each of the two trials, the leg movement was initiated by a standardized delta-stimulus and then controlled by the robotic controller. Oja's rule continuously adapted the transformation weights throughout the movement until convergence was detected and the final weights were recorded.

The experiments next determined if the final weights represented the optimal parameters for the considered robotic system. In subsequent trials, the weights were set to ten different, equally-spaced α values from the full interval of possible values determined above. In two further trial, the weights were initiated as the converged weights obtained by Oja's rule. The weights remained fixed to these values throughout the respective trial. Once the leg movement had converged to a limit cycle, the jumping height was averaged for each value of α to obtain a resonance curve as a point of comparison to assess the weights obtained by Oja's rule.

To exclude perturbing effects, action were taken before, during, and after the experiments. First, the height profile of the ground was characterized at different horizontal positions. The vertical position of the robot measured during the trials were corrected for this bias. Second, the motors were ensured to remain within their normal operating temperature throughout the trials. To heat the motors up, the leg jumped initially using a bang-bang controller with constant weights until the movement had converged. To prevent overheating, trials were subdivided into motion sequences of 45s each, which were interrupted by cooling phases lasting 120s. Third, it was excluded that the mechanics of the robot had changed during the experiments. For this purpose, the motors were set to pre-defined default positions and the resulting standing height of the robot was measured prior to and after the experiments. Furthermore, a reference trial was performed with the same fixed transformation weights after each trial to ensure that the jumping height of the robot remained constant for constant conditions.

2.5 Summary of the Results

The robotic controller considered in this dissertation was developed to induce highly-dynamic resonance movements in realistic compliant robots. These robots have multiple compliant joints with nonlinear coupling and show hybrid dynamics. The controller simplifies their control by three assumptions: First, it should periodically exert the same output at the same point along the jumping cycle and thereby induce a periodic movement. Second, the motor signal can be generated from within a one-dimensional control manifold, and linear transformation weights can transform between the multi-dimensional joint space and the control manifold without the need to adapt these weights during the jumping cycle. Third, Oja's rule can extract the optimal weights for a given robot from

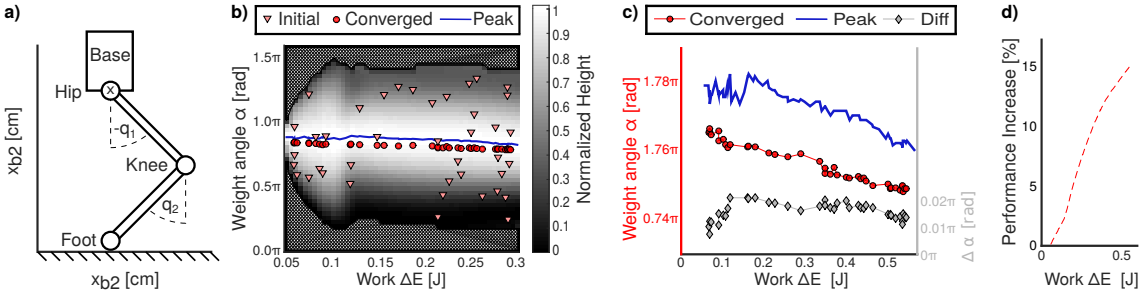

Figure 2.1: Results of the Monte Carlo simulations demonstrate how well Oja's rule approximates the resonance mode of the compliant robot. **a)** The simulations modeled a compliant leg that consisted of a base that was serially connected to two links by a hip and a knee joint. The base coordinates (x_{b1}, x_{b2}) were measured at the middle of the hip joint, as indicated by a x. The joint coordinates (q_1, q_2) were measured clockwise relative to vertically extended links. **b)** A parameter screening shows the jumping height as a function of the two free parameters of the bang-bang controller, namely, the energy ΔE injected into the system in each jump and the polar angle α describing the transformation weight vector. The jumping height was normalized for each value ΔE and the background represents parameter ranges where jumping fell silent. The simulations randomly choose initial tuples of these parameters, initiated jumping of the leg, and waited for Oja's rule to adapt the weights. They converged to values close to the peak line. **c)** A zoom into the parameter space shows that the converged weights differed least from the peak line at particularly low and high energy input. **d)** For each energy input, the graph shows by how much the jumping height can be improved by adjusting the transformation weights from their worst to their optimum values. Hereby, conditions were excluded that caused movement decay.

sensory information without the need for error-prone prior models. The numerical optimization and robotic experiments presented in this chapter show that these assumptions are compatible with energy-optimal resonance movement in compliant robots, as described in detail in the original paper [82] and summarized in the following.

In agreement with the first assumption, the optimal controller switched always at the same point along the 0.41 s long jumping cycle with an uncertainty that was below the numerical resolution of 0.01 s. The optimal controller thus inserts the same maximum possible energy into the system during each jump of the sequence, even though its optimization goal was to optimize only the last jump. The resulting jumping motion was periodic and its peak height converged exponentially. These findings indicate that the optimization of a specific jump requires that each preceding jumps must be driven by the same controller, which results in a periodic limit cycle movement. The proposed periodic controller is thus compatible with optimal control.

In contrast to the second assumption, the optimal transformation weights varied throughout the jumping cycle. Directly after landing and before take-off, the weights were aligned with the eigenmode of the system that can be obtained by linearizing it around its equilibrium position. But when the joints increasingly deviated from their equilibrium position, the optimal weights also deviated from the eigenmode. These deviations increased the final jumping height from 4.8 cm, as obtained for time-invariant weights, by 1.9 % or 0.1 cm. This is more than a magnitude smaller than the performance increase of up to 263 % or 3.0 cm obtained by optimizing the time-invariant transformation weights. It is thus functionally reasonable that the controller ignores any variations of the weights throughout the movement cycle and only adapts them to changing mechanical contexts.

Oja's rule performs this task well according to both the Monte Carlo simulations and the experiment. In the simulated leg illustrated in Figure 2.1a, Oja's rule closely aligned

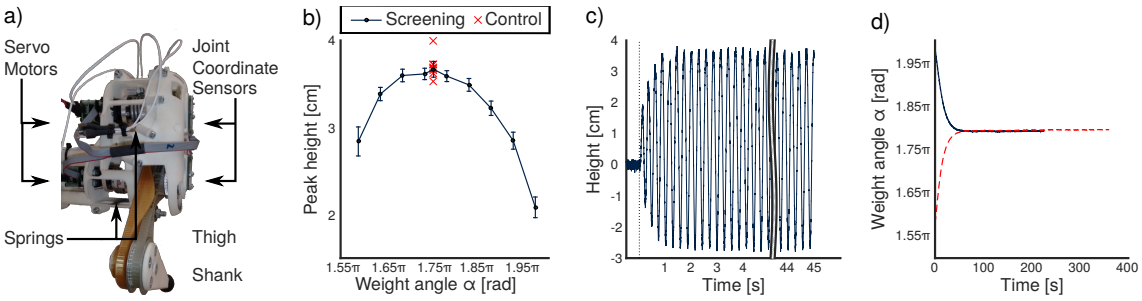

Figure 2.2: Results of the experiment. **a)** The experiments were conducted on a compliant leg that is pictured here. **b)** The robotic controller induced jumping motions with different peak height. The parameter screening found a maximum peak height for values of $\alpha \in [1.68\pi, 1.78\pi]$. Values of α below the illustrated region lead to a movement decay. Each trial was followed by a control trial with $\alpha = 1.75\pi$, which showed highly consistent behavior throughout the experiment. Error bars denote the standard deviation over several jumps. **c)** The standard deviation denoted the fluctuations of the movement amplitude as illustrated here by one exemplary base trajectory. The dotted line indicates the onset of the controller. **d)** Oja's rule aligned the transformation weights with the same value for both initial weights tested here. The converged weights yielded a peak jumping height according to the curve shown in the second panel of this figure.

random initial weights with the optimum weights (Figure 2.1b) and the option that this occurred by chance can be rejected at $p < 10^{-6}$. Upon increasing the energy input and thus the movement speed, Oja's rule approximated the linear resonance weights better and better (Figure 2.1c) because the influence of the nonlinear switching phase decreases with a longer flying phase. At the same time, the performance of badly and perfectly tuned weights monotonously diverged with higher energy input and thus the proper adaptation became increasingly important (Figure 2.1d). In the physical leg illustrated in Figure 2.2a, a small range of weights induced maximum energy efficiency (Figure 2.2b). Within this plateau region, different weights led to jumping heights that mutually differed by less than one standard deviation. Any performance difference within this interval was thus smaller than the inherent fluctuations of the jumping motion exemplified in Figure 2.2c. The weights that Oja's rule extracts from the sensory input lay within this plateau region independently of their initial values (Figure 2.2d). Hereby, Oja's rule increased the jumping height by up to 1.4cm or 67%. The proposed robotic controller thus substantially improves the energy efficiency of compliant movement without the need for error-prone internal models, while the performance difference between the proposed algorithm and an optimal controller are obscured by the inherent noise of the robot. The robotic algorithm can thus effectively induce energy-optimal motion in complex nonlinear compliant robots.

CHAPTER 3

A neuromodulation model resembling the robotic controller

As shown in the last chapter, the robotic autoencoder harnesses the compliant springs of biomimetic robots to induce energy-optimal motion just like animals harness the elastic properties of their tendons and muscles [11, 88, 89]. The modal control algorithm is thus a promising hypothesis for neuronal motor control, because an animal that can minimize the high metabolic demands of highly dynamic periodic motions [9] has a substantial evolutionary advantage [5, 6]. It is indeed known that the spinal cord implements neuronal structures that resemble the proposed autoencoder. In resemblance to the encoder, the proprioceptive information from multiple joints often converge onto a common pool of interneurons within a sensory synergy [39]. Conversely, single pools of interneurons often drive all motorpools involved in a movement with the same phase and frequency and thereby form a motor synergy that resembles the decoder [40, 50–54]. At a first glance, it also seems plausible that the spinal cord adjusts the synaptic weights of sensory synergies as predicted by the robotic encoder [19]. Hebbian learning, a well-known principle of neuronal adaptation, would accordingly adjust how the signals from different joints influence the overall phase of the synergic motor signal. But the decoder adaptation violates the fundamental constraint that neuronal learning is local [20] because it predicts that the gains of the synapses between the synergic interneurons and the motoneurons must be adjusted to proprioceptive information that is not locally encoded within either of these neuron pools. Such a non-local learning mechanism would be required to reduce, for example, the recruitment of a single muscle from a synergy when the environment blocks its actuated joint (Figure 1.2).

This chapter and the underlying paper [36] demonstrates that in theory serotonergic neuromodulation adapts motor synergies as predicted by the non-local learning rule of the robotic decoder. In contrast, realistic forms of Hebbian learning that may operate at a sensory synergy are too slow to react to changing environments as predicted by the robotic encoder. But the results further show that the sensory synergy has in general little influence on the performance of fast periodic motions once a movement has converged, while the decoder, and thus serotonergic neuromodulation, strongly shapes its energy efficiency.

In the following section 3.1, the robotic learning rule links several electrophysiological findings on the spinal serotonergic circuitry into a novel model of a motor feedback loop.

This feedback loop receives proprioceptive information on a movement and metabotropically scales the response of individual motorpools independently of their ionotropic motor signal. This effect was evaluated both analytically (section 3.2.1) and in numerical simulations that model a spiking neuronal equivalent of the proposed robotic autoencoder which controls different locomotor systems (section 3.3). The results, which are briefly summarized in section 3.4, prove that neuromodulation quickly adjusts motor synergies to generate the same relative motor signals as the adaptation rule of the robotic decoder. For sensory synergies, the same simulations showed that biologically realistic forms of Hebbian learning would require hours to react to mechanical changes. But the controlled movement converged already within few step cycle to its final energy-efficient limit cycle. These results emphasize spinal neuromodulation, and in parallel the decoder adaptation of the robotic autoencoder, as the main determinant to minimize the energy requirements of fast compliant movement.

3.1 Qualitative review of serotonergic neuromodulation

In order to adapt the forces of different actuators, the robotic autoencoder applies an adaptation rule that shows a remarkable functional similarity with the serotonergic neuromodulation of spinal motoneurons. About 90% of the spinal serotonin (*5-HT*) originates in the raphe nuclei in the medulla [90]. In the ventral spinal cord, 5-HT is specifically released by the nucleus raphe obscurus (*NRO*) and pallidus (*NRP*), which in turn project almost exclusively to this motor circuitry [91–94]. They thereby implement a metabotropic motor feedback loop that parallels the ionotropic spinal circuitry which drives the muscles. Their function resembles the decoder adaptation as demonstrated by the following comparison and illustrated in Figure 6.1.

As detailed in section 2.1, the decoder learning rule (2.6) receives sensory information $\boldsymbol{q} \in \mathbb{R}^n$ on the deflections of the n joints involved in a movement. Also the serotonergic neurons within the NRO and the NRP receive proprioceptive inputs and increase the firing rate of their serotonergic neurons accordingly [95–97]. These sensory signals are relayed to the NRP and NRO within a short delay of 20 ms [95], which indicates a monosynaptic or a strong oligosynaptic pathway.

Based on its sensory input, the robotic autoencoder adjusts the transformation weights $\boldsymbol{w}$ of its decoder, i.e., the relative force of actuators that drive different joints. Since the sensory information is neither encoded within the latent control signal nor within the final motor output, the CNS cannot rely on the known local learning mechanisms to implement such an algorithm. But the raphe nuclei cause a similar effect when their sensory input triggers them to release 5-HT onto motoneurons [91–94]. Once released, 5-HT stimulates the metabotropic 5-HT_2 receptors, which start a chain of biochemical mechanisms as extensively reviewed previously [98, 99]. As a result, serotonin does not change the baseline excitation of the motoneurons like ionotropic currents, but multiplicatively scales the response of the motoneurons to ionotropic inputs from other neurons [79, 100]. Increasing serotonin concentrations scale up the firing rate of spinal neurons monotonously and multiplicatively by a factor of up to ten [79]. While the ionotropic spinal circuitry can calculate their motor signal without disturbance, the serotonergic motor feedback loop thus scales the effective synaptic weights between the interneurons and the motoneurons according to sensory information that is not encoded by either of them.

The weights of the robotic decoder are adjusted with a time constant of few seconds. This time scale is sufficiently long to collect information on the overall movement cycle and

maintain constant weights under constant conditions. At the same time, it is sufficiently short to quickly react when, for example, the robot steps from a stiff onto a compliant ground. Also the multiplicative effect of serotonergic neuromodulation builds up and returns back to baseline within a few seconds in turtles [101], rats [102], cats [103], and humans [78]. This time scale might impede rapid neuronal calculations within the brain. But it matches the time scale relevant to various motor behaviors.

In summary, the robotic controller links individual experimental findings on the serotonergic innervation of the spinal cord into a coherent motor feedback loop. In agreement with the prediction, the strong activation of proprioceptors can increase the excitability of motoneurons for several seconds [103], an effect that can be enhanced by serotonin agonists and diminished by antagonists [78]. It is plausible that the serotonergic motor loop, like its robotic counterpart, tunes the relative forces of different muscles to harness the compliant properties of the locomotor system.

3.2 Mathematical analysis of serotonergic neuromodulation

For a qualitative comparison between the learning rule (2.6) of the robotic decoder and serotonergic neuromodulation, the serotonergic motor feedback loop can be modeled as illustrated in Figure 3.1 and described in the following. This section also simplifies the model to evaluate it analytically. The subsequent section 3.3 extends this work by numerical simulations that extensively compare the detailed model of the serotonergic circuitry with the behavior of the robotic autoencoder.

3.2.1 Attractive fixed points of neuromodulation

The new model makes one assumptions on the topographic precision of the NRO and NRP. In specific, it requires that their effects are at least joint-specific. For each joint i of the locomotor system, the NRO and NRP accordingly comprise a subgroup of serotonergic neurons that primarily receive proprioceptive input $\nu_{q,i}$ from this joint. Conversely, this subgroup increases the serotonin concentration $[\text{5-HT}]_i$ within the motorpool that innervates the same joint. Apart from this assumption, the mathematical model on the serotonergic motor loop is strictly grounded on previous electrophysiological findings.

The multiplicative gain of the motorpools that innervate a single joint increases proportionally with the serotonin concentration,

$$w_{\text{NM},i} = c_{\text{NM}}[\text{5-HT}]_i \ . \tag{3.1}$$

The serotonin concentration increases with the sensory input $\nu_{q,i}$ to the NRO and the NRP [102, 104]. It's depletion occurs due to reuptake into the cytosol of the cell by the *serotonin transporter* (*SERT*; depletion velocity denoted by V_{SERT}), due to catabolism mainly by monoamine oxidase and aldehyde dehydrogenase (denoted by V_{cat}), or by removal due to glia or diffusion (denoted by V_{rem}) [104]. In summary, the serotonin concentration changes according to

$$\frac{\text{d[5-HT]}}{\text{d}t} = \frac{c_{\text{q}}}{c_{\text{NM}}}\nu_{\text{q}} - V_{\text{SERT}} - V_{\text{cat}} - V_{\text{rem}} \ , \tag{3.2}$$

where c_{q} is a constant. While 5-HT diffusion plays a negligible effect in the spinal cord

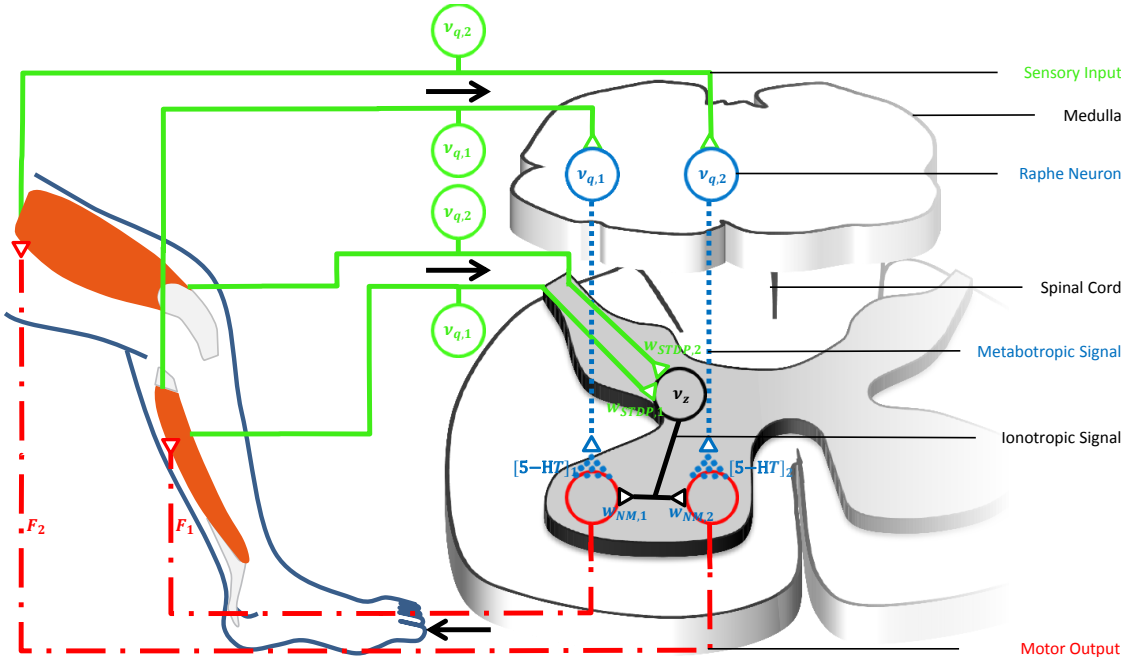

Figure 3.1: Illustrated here is the serotonergic motor feedback loop that is modelled in this chapter. In the medullary raphe nuclei, different pools of neurons receive proprioceptive signals $\nu_{\mathrm{q,i}}$ from the joints i of the animal's locomotor system. Their spikes increase the concentration $[\text{5-HT}]_i$ of serotonin within the spinal motorpools, which acts on metabotropic receptors and increases the motoneuron excitability. These serotonergic raphe projections collectively change the relative multiplicative weights $w_{\mathrm{NM,i}}$, which describe how ionotropic signals are transformed into musculotopic motor force F_{i}. The serotonergic feedback loop acts in parallel to the ionotropic motor circuitry that excites the muscles. This ionotropic circuitry could implement an independent synergy circuit that sends a common motor signal ν_z to all motorpools. Figure modified, with permission, from Stratmann et al. [27, 36].

[105], the other depletion mechanisms follow Michaelis-Menten kinetics [104],

$$V_n = \frac{V_{\max,n}}{\frac{K_{m,n}}{[\text{5-HT}]} + 1} \ . \tag{3.3}$$

The maximum depletion rates $V_{\max,n}$ and the Michaelis-constants $K_{m,n}$ of the depletion mechanisms n are summarized in the original paper [36].

For an analytic chain of thoughts, equation (3.3) can be simplified by the observation that

$$[\text{5-HT}] \ll K_{m,n} \tag{3.4}$$

even after high-frequency stimulation of the NRO and NRP *in vivo* [102]. The simulations described below test this assumption since K_m is set to the smallest literature value [104, 106–108]. A Taylor approximation therefore reduces equation (3.3) to

$$V_{\mathrm{depl}} \approx \frac{V_{\max}^{\mathrm{depl}}}{K_m^{\mathrm{depl}}} [\text{5-HT}] \ . \tag{3.5}$$

All the depletion mechanisms can then be summarized by an effective time constant

$$\tau^{\text{depl}} = \frac{K_m^{\text{SERT}}}{V_{\max}^{\text{SERT}}} + \frac{K_m^{\text{cat}}}{V_{\max}^{\text{cat}}} + \frac{K_m^{\text{rem}}}{V_{\max}^{\text{rem}}} \ . \tag{3.6}$$

With this definition, the time evolution of the motoneuronal gains can be described by a simplified version of equation (3.2),

$$\frac{\mathrm{d}\boldsymbol{w}_{\text{NM}}}{\mathrm{d}t} = c_{\text{q}}\boldsymbol{\nu}_q - \frac{1}{\tau^{\text{depl}}}\boldsymbol{w}_{\text{NM}} \ . \tag{3.7}$$

The simplified model allowed an analytic comparison between the convergence of the motoneuronal gains $w_{\text{NM},i}$ and the output weights w_i of the robotic decoder under the influence of neuromodulation and Oja's rule (2.6), respectively. Their strong qualitative similarity suggests that the two learning rules will lead to aligned weights, $\boldsymbol{w}_{\text{NM}} \parallel \boldsymbol{w}$, if they are provided with the same sensory signals. The amplitude of the weight vectors was thereby neglected because it changes only the overall motor signal and can be counteracted by the latent signal θ_z in the robotic controller or the functionally equivalent synergic ionotropic motor signal ν_z in its neuronal interpretation (Figure 3.1). In order to show that the weight vectors align, Oja's rule was first transformed and the neuromodulation dynamics were simplified into state equations $\dot{w}_1/\dot{w}_2$ and $\dot{w}_{\text{STDP},1}/\dot{w}_{\text{STDP},2}$ that describe how the ratio of weights for the two different joints evolve over time. The chain of thoughts then derived the fixed points of these state equations and proved their stability by linearizing the state equations around these points. According to present hypothesis, the attractive fixed points should be aligned and thus serotonergic neuromodulation should induce the same effect as the learning rule of the robotic decoder.

3.2.2 A gradient descent interpretation of neuromodulation

While the serotonergic effect on motoneurons obtains the same actuator gains as Oja's rule, it has a different mathematical form and will thus converge towards the attractive fixed points along a different path. In particular, the following currently unpublished analysis demonstrates that its convergence behavior can, in contrast to Oja's rule, be interpreted as a gradient descent of errors.

During an ongoing movement, the CNS creates ionotropic training signals and forwards them via the synaptic weights $\boldsymbol{w}_{\text{NM}}$ to all muscle groups involved in the movement. The following derivation will show that serotonergic neuromodulation aims at aligning the synaptic weights with target signals which are represented by the sensory input $\boldsymbol{\nu}_{\text{q}}$ describing the resulting movement. In particular, the claim is that it minimizes the cost function presented by the squared Euclidean norm of the error between the sensory signals and the synaptic weights,

$$\mathcal{J} = \frac{1}{2}\|\boldsymbol{\nu}_{\text{q}} - \frac{1}{c_{\text{q}}\tau^{\text{depl}}}\boldsymbol{w}_{\text{NM}}\|_2^2 \ . \tag{3.8}$$

If the gradient descent hypothesis is true, serotonin will descent along the negative gradient of the cost function with a learning rate γ,

$$\frac{\mathrm{d}\boldsymbol{w}}{\mathrm{d}t} = -\gamma\nabla_{\boldsymbol{w}}\mathcal{J} \tag{3.9}$$

$$= \frac{\gamma}{c_{\text{q}}\tau^{\text{depl}}}\left(\boldsymbol{\nu}_{\text{q}} - \frac{1}{c_{\text{q}}\tau^{\text{depl}}}\boldsymbol{w}_{\text{NM}}\right) \ . \tag{3.10}$$

And indeed, for the particular choice

$$\gamma = c_{\mathrm{q}}^2 \tau^{\mathrm{depl}} \ , \tag{3.11}$$

the gradient descent rule (3.10) is mathematically equivalent to the equation (3.7) which describes the serotonergic effects as derived above. Serotonergic effects therefore adjust motoneuronal gains according to the gradient descent of the error function (3.8).

The fact that the serotonergic neuromodulation can be described as the gradient descent of a cost function forms an important difference to Oja's rule (2.6), which adjusts the robotic decoder. Oja's rule is, in mathematical terms, a non-conservative vector field, because its curl does not vanish,

$$\nabla \times \frac{\mathrm{d}\boldsymbol{w}}{\mathrm{d}t} = \nabla \times \left[\gamma(\boldsymbol{w}^T\boldsymbol{q})\left(\boldsymbol{q} - (\boldsymbol{w}^T\boldsymbol{q})\boldsymbol{w}\right)\right] \tag{3.12}$$

$$\neq 0 \ . \tag{3.13}$$

Non-conservative vector fields like Oja's rule share the property that they cannot be represented in the form of

$$\frac{\mathrm{d}\boldsymbol{w}}{\mathrm{d}t} = -\gamma \nabla_{\boldsymbol{w}} \mathcal{J} \ , \tag{3.14}$$

i.e., as the gradient of any scalar cost function $\mathcal{J}$.

For these reasons, the convergence behavior of serotonergic neuromodulation resembles rather the delta rule, a specific machine learning algorithm [109, 110]. The delta rule works on an artificial neural network such as the robotic decoder, where a single neuron forwards its signal directly to multiple output neurons (Figure 1.1). To adjust the weights of the network, the scalar training input θ_{z} is created and forwarded via synaptic weights $\boldsymbol{w}$. The output $\theta_{\mathrm{z}}\boldsymbol{w}$ of the linear network is compared with a target output $\boldsymbol{\nu}_{\mathrm{q}}$. The quality of the output, or the cost function, is quantified as the squared Euclidean norm of the error,

$$\mathcal{J} = \frac{1}{2}\|\boldsymbol{\nu}_{\mathrm{q}} - \theta_{\mathrm{z}}\boldsymbol{w}\|_2^2 \ , \tag{3.15}$$

and the delta rule descents along the negative gradient of the cost function. When comparing the cost function of the delta rule and of serotonergic neuromodulation (3.8), the only difference is that the neuromodulation compares the target signals with the weight vector and not with the vector of network outputs. But these two quantities differ only by a multiplicative scalar for the present network topology that drives all output neurons by the same input. Therefore, both adaptation mechanisms align the network output with the vector of target signals and perform this task according to the gradient descent method.

3.3 Simulations of the neuronal circuitry

So far, this chapter considered simple models of neuronal learning to evaluate them by analytic methods. The numerical simulations described next examined if more realistic models of Hebbian learning and serotonergic neuromodulation obtain the same weights as the learning rule (2.6) of the robotic encoder and decoder, respectively.

3.3.1 Study design

The simulations modeled a spiking neuronal network that controlled different mechanical systems with two compliant joints i.

The study comprised three sets of simulations which sequentially increased the complexity of their connected mechanical system (section 3.3.2). The three sets analyzed the performance of the neuronal controller, first, as it received feed-forward input from a linear mechanical system, second, as it controlled a linear mechanical system in a closed-loop and, third, in a closed loop with a nonlinear compliant leg.

The simulated neuronal network was formed of spiking neurons (section 3.3.3) and combined a sensory and a motor synergy as illustrated in Figure 3.1 to form the simplest neuronal implementation of the robotic autoencoder. In the sensory synergy, two pools of proprioceptive neurons within the joints sent spikes with a frequency $\nu_{q,i}$ onto a common pool of excitatory interneurons in resemblance to the robotic encoder. In the motor synergy, the output spikes of these interneurons were forwarded to all motorpools in resemblance to the robotic decoder. The synaptic weights $w_{\mathrm{STDP},i}$ of the sensory synergy were subject to *spike-timing-dependent plasticity* (*STDP*; section 3.3.4), which is typically assumed to be the neuronal basis of Hebbian learning [20]. The raphe nuclei adjusted the motoneuronal gains $w_{\mathrm{NM,i}}$ of the motor synergy. For this purpose, the proprioceptors from each joint projected their spikes onto an individual pool of raphe neurons. The resulting spikes of the raphe neurons increased the serotonin concentration $[\text{5-HT}]_i$ within the motorpool that innervated the same joint (section 3.3.5).

To quantify the performance of STDP and neuromodulation, each simulations was run until all the neuromodulatory and the synaptic weights had converged. After convergence, it was tested if the values were aligned with the linearized eigenmode of the controlled mechanical system. The converged weights and their standard deviation were recorded over several movement cycles, varying initial conditions, and different levels of sensory noise to verify the robustness of the results.

3.3.2 Mechanical systems

In the feed-forward simulations, the neuronal network received its proprioceptive signals from two joints that oscillated with both a dominant eigenmode $\boldsymbol{a} \in \mathbb{R}^2$ of unit amplitude and a minor eigenmode. The proprioceptors thus spiked at frequencies of

$$\begin{pmatrix} \nu_{q,1} \\ \nu_{q,2} \end{pmatrix} = 40 \left[\begin{pmatrix} a_1 \\ a_2 \end{pmatrix} \sin(2\pi t) + \begin{pmatrix} 0.05 \\ 0.05 \end{pmatrix} \sin(8\pi t) \right] \text{Hz} \ . \tag{3.16}$$

Negative firing rates were considered as zero. The weights $\boldsymbol{w}_{\mathrm{STDP}}$ and $\boldsymbol{w}_{\mathrm{NM}}$ were supposed to align with the dominant eigenmode of the system. To test this prediction, sequential simulations varied the ratio a_1/a_2. A weighted linear regression compared the ratios $w_{\mathrm{STDP},1}/w_{\mathrm{STDP},2}$ and $w_{\mathrm{NM},1}/w_{\mathrm{NM},2}$ with increasing ratios a_1/a_2.

In the first closed-loop simulation, the output of the neuronal network was fed back to drive a linear mechanical system with analytically known resonance properties. This system consisted of two equal masses that were mutually connected by a spring and each was connected to an individual muscle via a further spring. The muscles excited the system by forces of

$$\boldsymbol{F} = \boldsymbol{w}_{\mathrm{NM}} \nu_z \tag{3.17}$$

that were determined by the firing rate ν_z of the synergic motor signal and by the neu-

romodulatory gains $\boldsymbol{w}_{\mathrm{NM}}$ of the motorpools. In resonance, the two masses oscillate along the two analytic eigenmodes $(\pm 1, 1)^T$. Damping stabilized the system and facilitated the decay of the minor eigenmode. The trajectory of each mass was signaled to the synergy interneurons and the raphe neurons by a separate pool of proprioceptors. Over time, the weights $\boldsymbol{w}_{\mathrm{STDP}}$ and $\boldsymbol{w}_{\mathrm{NM}}$ were predicted to align with the dominant eigenmode of the system. For the given system, both the synaptic weights and the serotonergic concentrations should thus converge to the same value for both DOF.

In the second feedback simulation, the neuronal network controlled a preliminary version of the jumping leg described in chapter 2. This leg comprised two joints i with angular deflections q_i that were driven by series elastic actuators and subject to nonlinear coupling. It periodically jumped and thus switched between a flying phase and a standing phase in contact with a compliant ground [111]. In contrast to the leg described in the last chapter, the present system did not comprise the mechanical decoupling that allowed the actuators to drive each joint separately and therefore had a different linearized eigenmode. The eigenmode was approximated by calculating the dominant principal component of the limit cycle trajectory of the joints. Like the robotic autoencoder, also the synaptic weights and the motorpool gains should align with this dominant principal component under the influence of STDP and neuromodulation, respectively.

3.3.3 Neuron models

The cells that formed the spiking neuronal network were modeled by different neuronal models depending on their role. The proprioceptors that drove the spinal interneurons and the raphe neurons were modeled as Poisson neurons to translate the joint coordinates into neuronal spikes. The post-synaptic synergic interneurons were, in contrast, formed by leaky integrate-and-fire (LIF) neurons. At the output stage, the motorpools low-pass filtered the discrete spikes of the interneurons to combine them with the serotonin concentration and both signals into continuous muscular forces.

At the input stage of the network, Poisson neurons j fired with rates $\nu_{q,i}$ that increased linearly with the coordinate q_i of its associated joint [112–116]. In every simulation time step dt, the neuron spiked by chance according to a Poisson distribution with mean $\nu_{q,i}\mathrm{d}t$. It thus emitted a train S_j of spikes s at time points t_j^s,

$$S_j = \sum_s \delta(t - t_j^s) \ . \tag{3.18}$$

The pool of spinal interneurons were simulated as LIF neurons. While the differential equations were adopted from Zenke et al. [117], the constants for their brain circuitry models were here adjusted to match the *in vivo* conditions observed in spinal circuitry. As a further difference, the present simulated neurons showed an absolute rather than a relative refractory period. While both of these models delay the next spike by a comparable duration, the model applied here fixed the membrane voltage after a spike and thus reduced the required computational power. Over time, the membrane voltage U_l of the LIF neuron l evolved according to

$$\tau^{\mathrm{mem}} \frac{\mathrm{d}U_l}{\mathrm{d}t} = (U^{\mathrm{rest}} - U_l) + g_l(U^{\mathrm{exc}} - U_l) \tag{3.19}$$

with membrane time constant τ^{mem}, resting potential U^{rest}, reversal potential U^{rest} of the excitatory synapses, and membrane conductance g_l. The LIF neurons were driven by

the proprioceptive input S_j, which was relayed via synapses that had a synaptic strength $w_{\mathrm{STDP},jl}$ and which changed the postsynaptic conductance according to

$$g_l = \frac{1}{2}\left(g_l^{\mathrm{ampa}} + g_l^{\mathrm{nmda}}\right) \ , \tag{3.20}$$

$$\frac{\mathrm{d}g_l^{\mathrm{ampa}}}{\mathrm{d}t} = -\frac{g^{\mathrm{ampa}}}{\tau^{\mathrm{ampa}}} + \sum_j w_{\mathrm{STDP},jl} \tag{3.21}$$

$$\frac{\mathrm{d}g_l^{\mathrm{nmda}}}{\mathrm{d}t} = -\frac{g_l^{\mathrm{nmda}}}{\tau^{\mathrm{nmda}}} + \frac{g_l^{\mathrm{ampa}}}{\tau^{\mathrm{nmda}}}. \tag{3.22}$$

The time evolution of conductances thus differentiated between the different time constants τ^{ampa} and τ^{nmda} of the AMPA and NMDA channels, respectively. Once the membrane voltage crossed a threshold, the membrane voltage was reset to its resting value and the neuron outputted a spike to all motoneurons.

The motorpool innervating joint i smoothed the spike train of all interneurons by a low-pass filter to calculate their average firing rate ν_z. The serotonin concentration $[\text{5-HT}]_i$ within the two motorpools multiplicatively increased the resulting muscle force to

$$\boldsymbol{F} = \mathrm{const} \cdot \begin{pmatrix} [\text{5-HT}]_1 \\ [\text{5-HT}]_2 \end{pmatrix} \nu_z \ . \tag{3.23}$$

3.3.4 Synaptic plasticity model

The synapses that linked the proprioceptors j with the synergic interneurons k changed their strength according to a state-of-the-art STDP model developed by Zenke et al. [117] and Pfister and Gerstner [118]. While traditional STDP models adjust synaptic weights according to the time difference between pairs of spikes, the model implemented here considers the overall spike history of the pre- and postsynaptic neuron j and l, respectively. Each spike of a spike train S leaves synaptic traces z^{slow}, z^-, and z^+ that decay over time,

$$\frac{\mathrm{d}z^{\mathrm{n}}}{\mathrm{d}t} = -\frac{z^n}{\tau^n} + S \ , \tag{3.24}$$

with time constants τ^{slow}, τ^-, and τ^+, respectively. The next spike then adapts the synaptic weights by

$$\frac{\mathrm{d}w_{\mathrm{STDP},jl}}{\mathrm{d}t} = A^+ z_l^+ z_j^{\mathrm{slow}} S_j - A^- z^- S_l + \frac{\mathrm{d}w_{\mathrm{scal,jl}}}{\mathrm{d}t} \ . \tag{3.25}$$

Since this STDP rule leads to diverging weights, a homeostatic mechanism was included,

$$\frac{\mathrm{d}w_{\mathrm{scal,jl}}}{\mathrm{d}t} = \frac{1}{\tau^{\mathrm{scal}}\nu_{\mathrm{tar}}}\left(\nu_{\mathrm{tar}} - \left(\frac{\bar{\nu}_n}{\nu_{\mathrm{tar}}^2}\right)\right) \tag{3.26}$$

This synaptic scaling rule is characterized by the time constant τ^{scal}. It pushes the average firing rate ν_l of the postsynaptic neuron, as represented by its low-pass-filtered spike train [117, 119], towards a target firing rate ν_{tar}. The STDP rule used an adjusted learning rate A^+ and A^- of long-term potentiation and long-term depression, respectively, to match the observations in the spinal cord of behaving monkeys [120]. After convergence, the simulation calculated the average synaptic strength $w_{\mathrm{STDP},i}$ of all proprioceptors that

innervated the two joints i. According to the robotic encoder, STDP should align these two average weights with the linearized eigenmode of the controlled mechanical system.

3.3.5 Serotonergic neuromodulation model

The output of the network was modulated by the concentration of serotonin within the motorpools. Each serotonergic raphe neuron r received sensory input from a joint i and as a result outputted a spike train S_r. Each of these spikes released serotonin into the motorpool innervating the same joint and increased its concentration by a fixed amount $[\text{5-HT}]_c$ [102]. The concentration subsequently decayed again according to Michaelis-Menten kinetics as summarized in section 3.2.1. The serotonin concentration within each joint thus evolved according to

$$\frac{\mathrm{d}[\text{5-HT}]_i}{\mathrm{d}t} = [\text{5-HT}]_c \sum_{r \in i} S_r - \frac{V_{\max}}{\frac{K_m}{[\text{5-HT}]_i} + 1} \ . \tag{3.27}$$

Previous experiments determined $[\text{5-HT}]_c$, the maximum rate $V_{\max}$ of serotonin depletion, and the Michaelis constant K_m [102, 104, 106–108]. The serotonin concentration within each of the two motorpools linearly scaled the motoneuronal gain [79, 121],

$$w_{\text{NM,i}} = c_{\text{NM}} \cdot [\text{5-HT}]_i \ . \tag{3.28}$$

According to the robotic decoder, serotonergic neuromodulation should align these two weights with the linearized eigenmode of the controlled mechanical system.

3.4 Summary of the results

The present study tested whether the CNS of animals can in theory adapt fast periodic movements like the robotic autoencoder. For this purpose, it modeled a spiking neuronal network that converged sensory information from all joints onto a common pool of interneurons within a sensory synergy. In return, their synergic motor signal was distributed to all motorpools within a motor synergy. According to the robotic autoencoder, the CNS should align the synaptic weights within the sensory and the motor synergy with the dominant principal component of the controlled mechanical system.

For the sensory synergy, the simulations showed that a state-of-the-art model of STDP adapts the synaptic weights to the expected values. But this adaptation acts too slowly for fast changing mechanical environments and has little functional effect on the performance of a converged motion.

For the motor synergy, the analytic and numerical results suggest a novel motor feedback loop implemented by the raphe nuclei in the medulla. These nuclei receive sensory information and accordingly release serotonin into spinal motorpools to adapt their gains. The adaptation they perform is a neuronal counterpart of a gradient descent algorithm. Due to this mechanism, the relative joint forces align with the normal mode of the locomotor system like the learning rule of the robotic decoder. Upon mechanical changes, the feedback loop quickly adapts these joint torques to the new resonance conditions.

The simulations verified the stated results on a range of different mechanical systems. The neuronal network either only received feed-forward sensory information from the system or was placed in a full feedback loop. The obtained results were stable against a secondary eigenmode, noise, and different initial conditions.

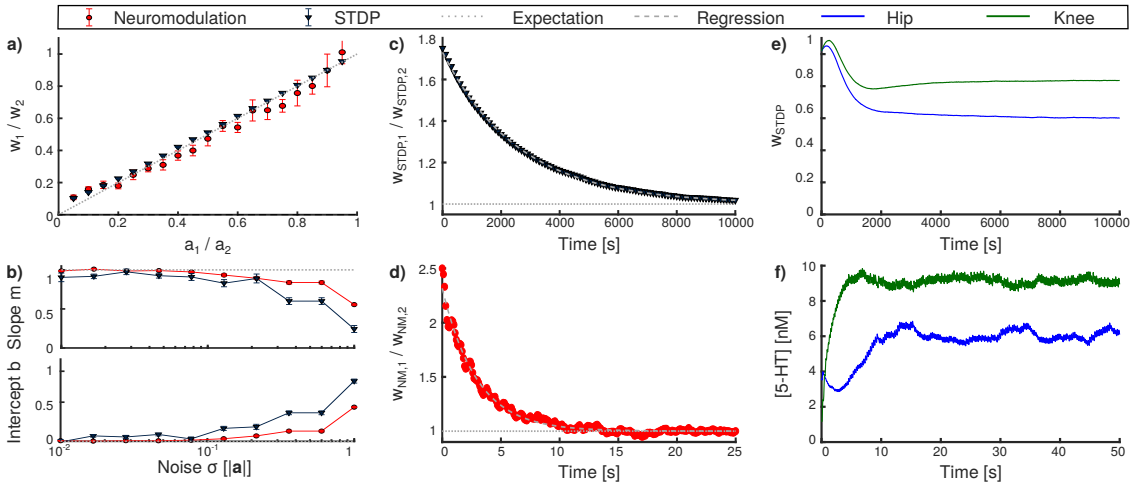

Figure 3.2: The simulations evaluated whether STDP and serotonergic neuromodulation align the synaptic weights $\boldsymbol{w}_{\mathrm{STDP}}$ of a sensory synergy and the gain $\boldsymbol{w}_{\mathrm{NM}}$ of motoneurons, respectively, with the dominant eigenmode $\boldsymbol{a}$ of a given locomotor system. **a)** After convergence, these neuronal weights linearly varied with the changing eigenmode of the mechanical system that provided feedforward input to the neuronal network. **b)** The slope m and the intercept b of a linear regression to the last panel deviated from their expectation value of 1 and 0 , respectively, when noise was added to its sensory input. But this deviation was below 10 % for STDP and neuromodulation even when the standard deviation σ of the noise amounted to 20 % and 13 % of the signal amplitude, respectively. **c,d)** When the neuronal circuit controlled a linear mechanical system in closed loop, both STDP and neuromodulation aligned their relative weights with the eigenmode $\boldsymbol{a} = (1, 1)^T$. STDP and the neuromodulatory effect converged with regressed exponential time constants of 2.9 s and 2.7×10^3 s, respectively. Therefore, only neuromodulation reacted quickly to changing mechanical environments. **e)** In closed-loop with the nonlinear leg, the synaptic weights of the sensory input from the knee and the leg converged to constant values, but also required hours for their convergence. **f)** The neuromodulatory gains converged to the same ration as STDP, but showed its final effect size already after few seconds. Figure modified, with permission, from Stratmann et al. [36].

3.4.1 Synaptic plasticity is too slow to adapt the encoder

In the sensory synergy, STDP consistently aligned the synaptic weights $\boldsymbol{w}_{\mathrm{STDP}}$ between the proprioceptors and the interneurons with the dominant eigenmode $\boldsymbol{a}$ of the considered mechanical systems. The feedforward simulations varied the eigenmode of the mechanical system. The converged synaptic weights adjusted to the varying conditions according to the linear regression illustrated in panel a and b of Figure 3.2,

$$\frac{w_{\mathrm{STDP},1}}{w_{\mathrm{STDP},2}} = m \cdot \frac{a_1}{a_2} + b \ , \tag{3.29}$$

$$m = 0.979 \pm 0.010 \tag{3.30}$$

$$b = 0.016 \pm 0.002 \ . \tag{3.31}$$

When the motor signals of the neuronal circuit was fed back to control a compliant locomotor system, STDP aligned the synaptic weights with the dominant eigenmode of the linear mechanical system and of the nonlinear leg to an accuracy of

$$\frac{w_{\mathrm{STDP},1}}{w_{\mathrm{STDP},2}} - \frac{a_1}{a_2} = 0.005 \pm 0.011 \tag{3.32}$$

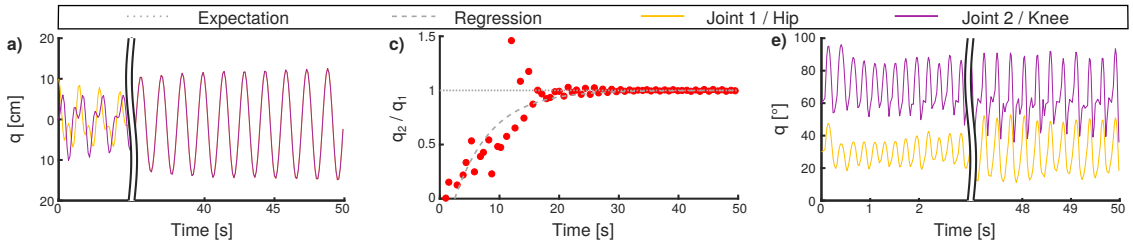

Figure 3.3: The performance of the proposed neuronal motor circuit was evaluated in closed loop with a linear and a nonlinear compliant locomotor system. **a)** The linear system consisted of two masses that were coupled by a spring. An individual series elastic actuator deflected each mass by a distance q from its equilibrium positions. The neuronal network excited only the phasic eigenmode $\boldsymbol{a} = (1, 1)^T$ of the system and thus induced a synchronous resonance motion over time. **b)** The alignment of the masses' trajectories can be illustrated by their deflection ratios. The data set presented here was recorded at peak positions of the first mass and converged with a regressed exponential time constant of 6.2 s. **c)** Also the hip and the knee motion of the nonlinear leg showed a quick convergence to a periodic limit cycle within few seconds. Figure modified, with permission, from Stratmann et al. [36].

as shown in Figure 3.2c and

$$\frac{w_{\mathrm{STDP},1}}{w_{\mathrm{STDP},2}} - \frac{a_1}{a_2} = 0.043 \pm 0.034 \tag{3.33}$$

as shown in Figure 3.2e, respectively.

While STDP successfully extracted the eigenmodes of the mechanical systems, it adjusted the synaptic weights very slowly both in the feed forward and in the feedback simulations. An exponential regression quantified that the ratio $w_{\mathrm{STDP},1}/w_{\mathrm{STDP},2}$ converged towards the eigenmode of the linear mechanical system with an exponential time constant of 2.7×10^3 s (Figure 3.2c). This long time scale agrees with previous measurements in the cat, which determined how the efficacy of proprioceptor pathways to motoneurons changed after the nerve had been cut. Under free behavior, changes in the motoneuronal response to an artificial stimulation occurred only days after a nerve was severed [37]. Plasticity in the spinal cord thus acts substantially slower than the robotic adaptation rule, which adapts to new conditions within few seconds (section 2.1). STDP therefore cannot adapt the sensory synergy to the rapid mechanical changes that the animal's locomotor system faces during fast periodic motion.

3.4.2 Encoder adaptation has minor influence on motor performance

The simulated neuronal network induced a movement pattern that converged to a limit cycle well before the weights of the sensory synergy had converged. In the linear mechanical system, the trajectories of the two masses started as a superposition of the system's two eigenmodes as illustrated in Figure 3.3a. They converged to a synchronous resonance motion along the eigenmode $(1, 1)^T$ over time with a time constant of 6.2 s according to the exponential regression shown in Figure 3.3b. Also the nonlinear leg obtained its peak jumping height within few seconds (Figure 3.3c) and thus about two to three orders of magnitude earlier than the plastic weights of the sensory synergy.

This discrepancy can be explained by the functional role of the robotic encoder. Its transformation weights determine how strongly sensory input from individual joints entrain the phase of all all motor signals. But during fast periodic motion, the proprioceptive

signals from different joints are in phase because the joints move very synchronously [122, 123]. The simulation results thus indicate that the sensory synergy, and the encoder in the robotic autoencoder, have only a minor influence on the motor performance. They need to adjust only to long-lasting and severe conditions occurring, for example, when the proprioceptive nerve in a human or the cable in the robot is severed.

3.4.3 Serotonergic neuromodulation can adapt the decoder

The serotonergic neuromodulation reliably aligned the gains $\boldsymbol{w}_{\mathrm{NM}}$ of motorpools with the dominant eigenmode $\boldsymbol{a}$ of the mechanical system. In contrast to STDP, the neuromodulatory effects acted on just the right time-scale to react to mechanical changes occurring when, for example, the muscles warm up or the stiffness of the running track changes.

Analytic reasoning evaluated a simplified model of serotonergic neuromodulation, summarized by equation (3.7). On this basis, the gains of motorneurons were proven to have the same stable attractor as Oja's rule, which adjusts the transformation weights of the robotic decoder. They thus converge to the same relative values.

The simulations confirmed this behavior for a more complex neuromodulation model described by equation (3.27). The results of the feedforward simulation, which are illustrated in Figure 3.2a, showed that the converged weights $\boldsymbol{w}_{\mathrm{NM}}$ vary with the eigenmode $\boldsymbol{a}$ of the mechanical system according to

$$\frac{w_{\mathrm{NM},1}}{w_{\mathrm{NM},2}} = m \cdot \frac{a_1}{a_2} + b \ , \tag{3.34}$$

$$m = 0.957 \pm 0.031 \tag{3.35}$$

$$b = 0.005 \pm 0.023 \ . \tag{3.36}$$

When the sensory signals were contaminated with increasing levels of white noise, the slope and y-intercept increasingly deviated from their expected value of 1 and 0, respectively. But this deviation amounted to less than 10 % (Figure 3.2b) even with a noise level of $\sigma = 0.13 \cdot \|\boldsymbol{a}\|$ that was added to the intrinsic noise of the Poisson neurons. The algorithmic function of serotonergic neuromodulation is thus very resistant against different kinds and levels of noise. In feedback with the linear mechanical system, neuromodulation also extracted the eigenmode of the linear mechanical system (Figure 3.2d) with an accuracy of

$$\frac{w_{\mathrm{NM},1}}{w_{\mathrm{NM},2}} - \frac{a_1}{a_2} = 0.004 \pm 0.032 \ . \tag{3.37}$$

Also in closed loop with the nonlinear mechanical leg, STDP approximated the linearized eigenmode (Figure 3.2f) with an accuracy of

$$\frac{w_{\mathrm{NM},1}}{w_{\mathrm{NM},2}} - \frac{a_1}{a_2} = -0.064 \pm 0.068 \ . \tag{3.38}$$

The uncertainty resulted from fluctuations of the gain throughout the movement cycle, due to different initial conditions, and, for the nonlinear system, due to the numeric quantification of the eigenmode. The difference of the converged motorpool gains and the dominant eigenmode of the system was smaller than these intrinsic uncertainty. The serotonergic feedback loop can therefore, in theory, reliably extract the dominant eigenmode of the animal's locomotor system.

The effect of serotonin converged within few seconds in all simulations. In the linear

mechanical system, the gains converged with a time constant of 2.9 s, as quantified in an exponential regression shown in Figure 3.2d. This time scale matches the convergence time scale of the movement and of the robotic learning rule (2.6). Unlike ionotropic neuronal mechanisms, neuromodulation thus acts slowly enough to maintain stable weights throughout a movement cycle under constant mechanical conditions. At the same time, serotonin can quickly adapt the motor output when the locomotor system or its environment change.

While serotoninergic neuromodulation and Oja's rule lead to the same actuator forces, they converge along a different path in the parameter space. The CNS accordingly sends out training motor signals to the motorpools. Serotonin subsequently adjusts the neuromodulatory gains. Like a gradient descent algorithm, it mathematically compares the network output with a target output, namely, the motor signals that actuate the joints with the sensory signals that describe the resulting joint movements. The difference between the two signals represents the cost function and the neuromodulatory gains descent along its gradient.

In summary, the present simulations suggest that serotonin neuromodulation performs a non-local gradient descent adaption that obtains the same motoneuronal gains as the learning rule of the robotic decoder. While the weights of the sensory synergy may vary under the influence of STDP without relevant loss in motor performance, the neuromodulatory effect strongly shapes the energy efficiency of an ongoing motion. If, for example, the mechanical environment blocks one joint, the gain of the corresponding motorpools will decay and the muscles will waste no metabolic energy by pressing against the barrier. These conclusions are based on one currently unproven model assumption, namely, that the serotonergic neurons that receive proprioceptive information from an individual joint also project with topographic precision to the motorpools actuating the respective joint. Under this assumption, serotonin will adapt the relative forces of different actuators just like the robotic decoder to minimize the metabolic requirements of fast periodic movements.

CHAPTER 4

Review on the unique algorithmic properties of serotonin

The previous chapter revealed that metabotropic neuromodulation is a promising candidate for the non-local adaptation of ionotropic motor subcircuits. Whereas the ionotropic subcircuits collectively encode predictive models of the locomotor system and its environment based on life-long learning, the disparate metabotropic scaling of their activity can quickly adjust these models to changing mechanical conditions. The robotic decoder shows that this *precision scaling* is an effective and resource-efficient solution to adapt the activation of individual muscle groups to sensory input. While also noradrenaline contributes substantially to the neuromodulation in the ventral spinal cord, only serotonergic neurons receive the proprioceptive information required for motor adaptation [79]. But previous research has not considered serotonin as substrate of non-local learning for two reasons: The first caveat is the common concept that ionotropic effects alone are sufficient to adjust the motor output to arbitrary conditions [124]. This idea has been promoted by the prove that artificial neural networks can approximate every continuous function, a property that relies on their model of neurons as nonlinear integrators of incoming signals [125, 126]. The second caveat is the scientific consensus that monoamines like serotonin are slow and diffuse modulators of the spatially and temporally precise ionotropic connectome [127]. In the spinal cord, serotonin is presumed to equally modulate motorpools innervating several joints even across limbs [78, 79].

The review [27] summarized in this chapter showed that the previous experimental findings on serotonin in spinal circuitry are fully consistent with multiplicative precision scaling. In contrast to the current consensus, it is plausible that serotoninergic neuromodulation, like the robotic decoder, disparately affects individual joints of the same limb and acts on the same time scale as many motor behaviors (section 4.1). It therefore provides the CNS with a unique functionality because recent electrophysiological findings prompt that the spinal ionotropic circuitry is limited to purely linear signal processing, unlike their counterparts in artificial neural networks. Section 4.2 explains this limitation by demonstrating why the special properties of spinal neurons and signals counteract and typically even exclude ionotropic mechanisms proposed for the nonlinear signal integration in other CNS regions.

4.1 Precision of non-local serotonergic motor adaptation

The adaptation rule of the robotic decoder states a clear prediction on the precision of the serotonergic raphe nuclei obscurus (NRO) and pallidus (NRP). They must disparately scale the gains of motorpools that innervate different joints, and their effect must decay on a time scale of hundreds of milliseconds to few seconds. With these characteristics, the NRO and NRP would induce the relative muscle forces that minimize the metabolic demands of fast periodic motion and thus offer a substantial functionality that they cannot provide by diffuse neuromodulation. As detailed below, this precision agrees well with experimental findings on their anatomy and function.

Previous studies show that along the serotonergic feedback pathway each processing step allows for a topographically focused signal transduction. Sensory signals are relayed to the NRP and NRO within 20ms [95]. This short delay indicates a monosynaptic or a strong oligosynaptic input from the peripheral sensors to the NRO and NRP. A likely candidate is disynaptically mediated input via spinal interneurons that typically targets the cerebellum [59] but that may also mediate peripheral inputs to brainstem nuclei [128]. In turn, the approximately 19,000 serotonergic neurons comprised within the human NRP and NRO [129] project almost exclusively to the ventral spinal cord [91–94]. These serotonergic projections show a degree of collateralization that quantitatively resembles that of corticospinal axons. In a previous study, more than 40% of 156 corticospinal neurons responded antidromically to electric stimulation of several segments of the spinal cord in monkeys [130]. Tracers inserted into the spinal cord showed that also the location of the labeled serotonergic cells varied markedly with the region of injection, contrasting the more homogeneous labeling of non-serotonergic cells within the raphe nuclei [131]. Dual retrograde tracers injected into different regions of the ventral horn of rats double-labelled about 50% of cells within the NRP [132]. These serotoninergic projections predominantly terminate in synaptic contacts in the ventral spinal cord and their released 5-HT shows effects of high spatial precision [98, 105, 133]. It is thus plausible that the serotonergic spinal projections, like corticospinal ionotronic projections, comprise not only an anatomically diffuse component [78] but also a separate topographically specific component. In support of this hypothesis, the depletion of 5-HT and the blockage of 5-HT_2 receptors in rats slackens locomotion due to adjustments in the motor signals which disparately affect muscles actuating different joints of the same limb or even the same joint [134–136]. The diffuse projections equally scale the activity of multiple muscles like the amplitude of the proposed robotic autoencoder, denoted $\hat{\theta}_z$ in equation (2.3). In addition, they may increase the overall leg stiffness by co-contraction of antagonistic muscles. Animals use these two strategies to increase their movement speed [137, 138]. The topographically specific serotonergic projections can, in contrast, scale the relative forces of different muscles, represented by the vector $\boldsymbol{\theta}$ in equation (2.4), and thereby increase the energy efficiency of the movement. The joint-specific precision required for this precision scaling is consistent with the experimental insights on the spinal serotonergic system summarized here.

The time scale of metabotropic effects is slow in comparison to ionotropic signal transmission. Following sensory stimulation, the onset of the serotonergic gain scaling is delayed by tens of milliseconds after stimulus cessation in cats [103]. It returns back to baseline within a few seconds in turtles [101], cats [103], and humans [78]. This long time scale might impede fast neuronal calculations within the brain and may also have detrimental effects for motor control under rapidly changing conditions. For example, it may underlie the Kohnstam effect, where the arm involuntarily lifts following the abrupt end of a strong

voluntary contraction of the deltoid. The Kohnstamm effect originates in a persistent activation of the deltoid muscle, which is accompanied by upscaled motor evoked potentials [139, 140]. This excessive activity may be caused by serotonin that is released during the strong contraction of the deltoid and increases the gain of deltoid motoneurons for several seconds after the abrupt end of the contraction. Ongoing movements encountered in everyday life show less-abrupt and extreme switching between conditions. For such natural movements, the time scale of serotonergic effects matches the time scale of the robotic adaptation rule, which is relevant to various motor behaviors.

4.2 Limitations of ionotropic circuitry

The nonlinear scaling renders the metabotropic system functionally unique in the spinal cord. In theory, a similar effect could also be performed by a neuronal network using solely ionotropic synaptic currents. Several ionotropic mechanisms have previously been proposed for such a nonlinear, particularly multiplicative, signal interaction in other CNS regions [141, 142]. But the rapid kinetics of ionotropic receptors [143–145] are ill-suited for a spinal equivalent of the robotic adaptation rule, which accumulates information over the whole movement cycle and induces changes of the motor signals that last for several seconds. In addition, recent studies show that the ionotropic circuitry in the spinal cord is limited to a purely linear integration of their motor commands and sensory signals.

This purely linear behavior has been observed both in spinal interneurons [146–149] and motoneurons [150–154] under physiological conditions *in vivo*. The neurons are active well before overt movement starts and do not saturate [146], implying that they are in their linear regime during a movement. A linear neuron receives ionotropic inputs x_i from the n neurons that converge onto it via synaptic gains w_i. As a result, its output firing rate y linearly increases with the summated input, subtracted by a firing threshold θ,

$$y(x_1, x_2, \ldots) = \sum_{i=1}^{n} w_\mathrm{i} \cdot x_\mathrm{i} - \theta \ . \tag{4.1}$$

An additional ionotropic signal $x_{\mathrm{n}+1}$ will increase the output by an additive constant,

$$y(x_1, x_2, \ldots) = w_{\mathrm{n}+1} \cdot x_{\mathrm{n}+1} + \sum_{i=1}^{n} w_\mathrm{i} \cdot x_\mathrm{i} - \theta \ . \tag{4.2}$$

The serotonin concentration [5-HT] induced by a metabotropic signal will, in contrast, multiplicatively alter the response of the postsynaptic cell to its ionotropic input,

$$y(x_1, x_2, \ldots) = \mathrm{const} \cdot [\text{5-HT}] \cdot \sum_{i=1}^{n} w_\mathrm{i} \cdot x_\mathrm{i} - \theta \ . \tag{4.3}$$

Artificial neural networks have, with the enormous scientific and economical success of artificial intelligence, strongly facilitated the view that also CNS circuits of multiple biological neurons can adjust their output to arbitrarily changing conditions [124]. In mathematical terms, these networks are said to perform universal function approximation, a property that relies on the model of neurons as nonlinear integrators of incoming signals [125, 126]. But when linear neurons synapse together, the resulting spinal circuit is still limited to perform the linear function described by equation (4.1). Neither additional

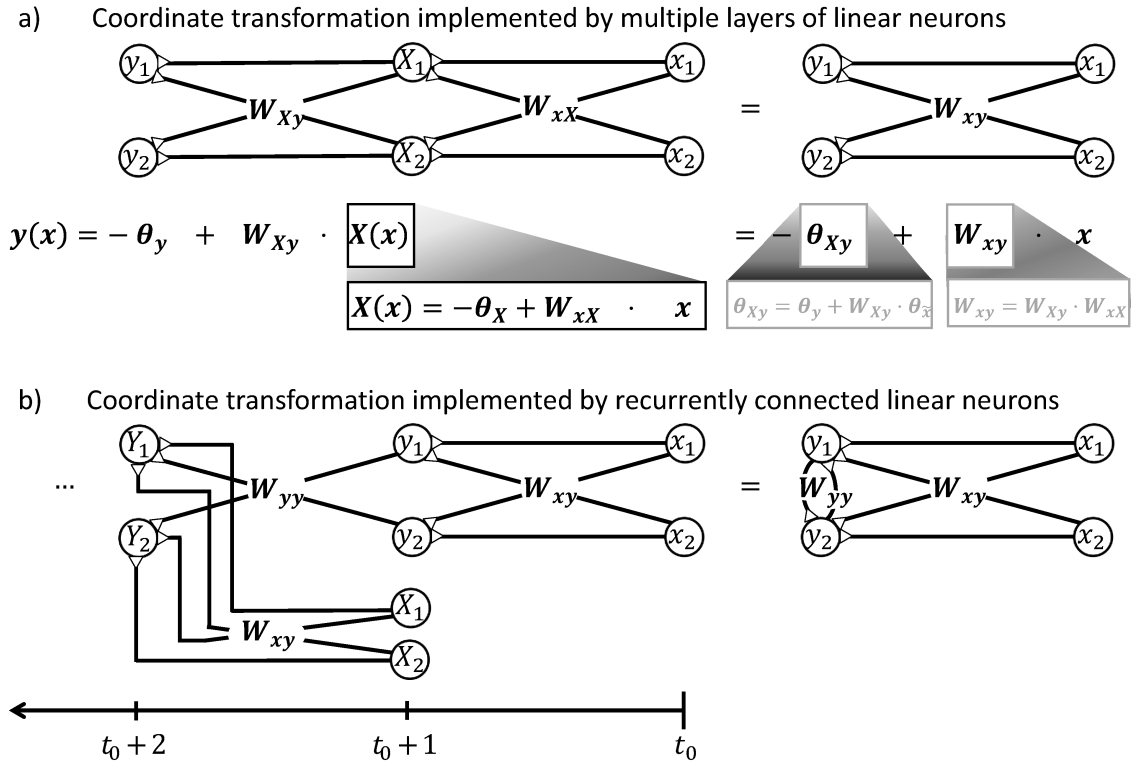

Figure 4.1: A network consisting of linear neurons is restricted to implement a linear function of the form $\boldsymbol{y}(\boldsymbol{x}) = \boldsymbol{w}_{\mathrm{xy}}\boldsymbol{x} - \boldsymbol{\theta}_{\mathrm{y}}$. (a) This relationship is independent of the number of hidden neuronal feedforward layers. Additional layers only alter the linear gains $\boldsymbol{W}$ and y-intercepts $\boldsymbol{\theta}$. (b) To confirm this limitation in a recurrent neuronal networks as illustrated on the right hand side, it is advantageous to unfold the performed calculations. This procedure deduces the hypothetical feedforward network on the left hand side, which computes the same output. When either network receives an input signal $\boldsymbol{x}$ released at t_0, it will produce an output signal $\boldsymbol{y}$ like a simple feedforward network at $t_0 + 1$, i.e. after a short unitary transduction delay. At the next computational step $t_0 + 2$, the output signal $\boldsymbol{Y}$ is determined by the input signal $\boldsymbol{X}$ from time step $t_0 + 1$ and the previous output signal $\boldsymbol{y}$. The previous output signal is thereby fed back by recurrent synapses with weights $\boldsymbol{W}_{\mathrm{yy}}$. Further calculation steps $t_0 + 3, t_0 + 4, \ldots, t$ of the recurrent network can be modeled by iteratively adding layers to the feedforward network that receive the external input at these time steps from an additional pool of input neurons. Thus, the output $\boldsymbol{y}$ of the recurrent network after t time steps is mathematically equivalent to the output produced by a hypothetical feedforward network with $t-1$ hidden and one output layers. During each individual time step, the recurrent network can thus only output a linear function of its input like a feedforward network. Figure modified, with permission, from Stratmann et al. [27].

feedforward layers, nor recurrent synaptic connections remove this functional limitation. If, on the one hand, the neuronal network is extended by intercalating additional layers of linear neurons between the input and output layer, only the effective linear gains $\boldsymbol{w}$ and the threshold θ will change. But the output firing rate will remain a linear function of the network input as illustrated in Figure 4.1a. If, on the other hand, the network is extended by recurrent synaptic connections, it can memorize input and process time-series of data. Thereby, its output may vary nonlinearly with time and, for example, oscillate or converge to a steady state [155]. But Figure 4.1b demonstrates that at each time step the outputs $\boldsymbol{y}$ of the recurrent neuronal network remain a linear function of its previous inputs $\boldsymbol{x}$.

At first glance, the observed linear behavior seems at odds with the scientific consensus

that the ionotropic connectome implements most of the nonlinear functions required for the complex behavioral repertoire of the CNS [127, 156]. But a closer look reveals that the specific characteristics of spinal neurons and signals suppress the mechanisms that multiply ionotropic signals in other CNS regions. These mechanisms can be split into two groups [141]: Some of them work at low firing rates in neurons which show time-sparse encoding, i.e. which encode data in the correlations of spikes. These mechanisms are mainly based on synaptic noise [157–160] and shunting inhibition [161, 162]. They are unlikely to cause gain scaling in the early sensory processing and motor signals of the spinal cord, which is dominated by rate-coded signals [147, 163–167].

Other mechanisms apply to neurons which harness a large range of firing rates to encode information. For neurons which work within this rate-coded regime, like spinal neurons, nonlinear signal interaction can occur due to the short-term synaptic depression (STD) of synaptic efficacy. If a neuron transmits the sum of two excitatory signals, the second signal may push the firing rate into a regime where STD occurs and may therefore divisively scale the circuit response to the first signal [142, 168–170]. This mechanism is metabolically unfavorable compared to other possible nonlinear mechanisms because the neuronal network would transmit a particularly high number of metabolically expensive action and synaptic potentials [171]. In addition, recent recordings on neurons which carry sensory and motor signals show that STD only takes place at the onset of a stimulation train. During sustained firing, STD was found to saturate and remain constant for a wide range of firing rates [172]. Thus, STD is unlikely to occur in spinal calculations during ongoing behavior. A second hypothesis originates from the mathematical fact that the multiplication of two signals turns into a pure addition when the logarithms of the signals are considered,

$$\log(x_1 \cdot x_2) = \log(x_1) + \log(x_2) \ . \tag{4.4}$$

Multiplication thus becomes trivial for signals which are encoded logarithmically [173], such as specific quantities in the visual system [173, 174]. However, many mechanical stimuli are known to be linearly encoded by sensory firing rates [112–116]. Furthermore, a neuronal network which implements this strategy would be restricted to implement exclusively either multiplicative or additive operations on its inputs. To implement both, it would need to implement an additional exponential function to extract the actual coordinates. The third possible nonlinear mechanism uses dendritic properties. Voltage-dependent Na^+ and Ca^{2+} channels, NMDA receptors, and the passive properties of dendrites can individually induce supralinear and sublinear interaction of ionotropic signals [175–182]. The combined effect is strongly determined by the clustering properties of the synaptic inputs that converge onto a dendritic tree. *In vivo* mappings of dendrites from different early sensory systems demonstrated that these inputs are not clustered according to functional similarity [183, 184]. This observation supports a linear signal summation because the concerted nonlinear effects of unclustered inputs typically balance each other out [185]. Indeed, *in vivo* recordings showed that the individual nonlinear effects of active dendrites collectively induce a linear relationship between input current and output firing [186, 187]. The same balance was found for spinal motorneurons in simulations [153] and experiments [154] when any metabotropic input was removed. *In vivo* experiments on the summation of input from both eyes found that sensory systems even use active dendritic properties as a linearizing agent instead of a nonlinear operation. The nonlinear summation of individual signals was found to ensure that the output to binocular stimulation equals the linear summation of input during monocular stimulation [188].

4.3 Summary of the results

The linear behavior that the present review discovers in spinal ionotropic signals offers an attractive explanation of how metabotropic signal processing complements the ionotropic connectome: By nonlinearly adjusting ionotropic motor signals to sensory information, serotonin can provide a functionality that is powerful, resource-efficient, and unique in the spinal circuitry. Metabotropic neuromodulation is the ideal candidate to bridge the fast ionotropic signals and slowly changing behavioral context because its time scale coincides with the time scale of many motor behaviors, including the fast periodic motions considered in this dissertation. Previous studies on the serotonergic neuromodulation are consistent with the proposed hypothesis that their metabotropic effects are, averaged over all serotonergic projections to the ventral spinal cord, at least joint-specific. This finding contradicts the current consensus on serotonergic effects [78, 79] and motivates novel experiments *in vivo* to elucidate how the human CNS applies the unique functionality of the serotonergic spinal circuitry for motor control. The adaptation rule of the robotic decoder offered a clear hypothesis for these experiments, which were performed as described in the next chapter.

CHAPTER 5

Experimental proof in the human central nervous system

The theoretical work in the previous chapters laid the foundation to experimentally test the fundamental question of this dissertation: Does the serotonergic system adapt movement according to the same algorithm as the robotic decoder? So far, it is generally accepted that the spinal serotonergic system acts purely by diffuse modulation of motoneurons innervating several joints, even on other extremities [78, 79]. In contrast, the results presented so far predict that the serotonergic system disparately scales the gain of motorpools acting on different joints of the same limb. In particular, the excitability of motorpools should be higher following highly-dynamic rotations of their innervated joints than after rotations of adjacent joints [27, 36]. The precise details on the experimental validation outlined in the following can be found in the original paper [189].

5.1 Human subject study

To test the stated hypothesis, sixteen healthy, right-handed human subjects (aged 17–30 years, mean 26(4) (s.d.); 12 male) performed motion experiments guided by a manipulandum, i.e., a machine as described in the next section that guides the motion of the subjects' hand by translational forces. In the experiments (section 5.1.2), subjects first repeatedly rotated either their right elbow or shoulder joint with high speed and force. After the movement, the protocol non-invasively quantified the resulting excitability of the motorpools actuating these joints by their monosynaptic reflex response to a rapid joint stretch.

In order to guide the rotation and the stretch with high precision, the human arm was characterized in preliminary experiments (section 5.1.3). A new control architecture was developed for the manipulandum (section 5.1.4) that acted with the high precision required to characterize and constrain the hand movement to involve exclusively rotation of a single joint. At the same time, the controller allowed high forces and speeds during the rotations and subsequently excited the stretch reflex by a rapid joint perturbation. It guaranteed the safe interaction of the subjects with the manipulandum during a total interaction time of more than 70 h despite a potential peak force of more than 1.5 kN [80].

In the analysis, electromyograpy (EMG) quantified the stretch reflex response of the brachioradialis, which actuates the elbow, and of the posterior deltoid, which actuates the

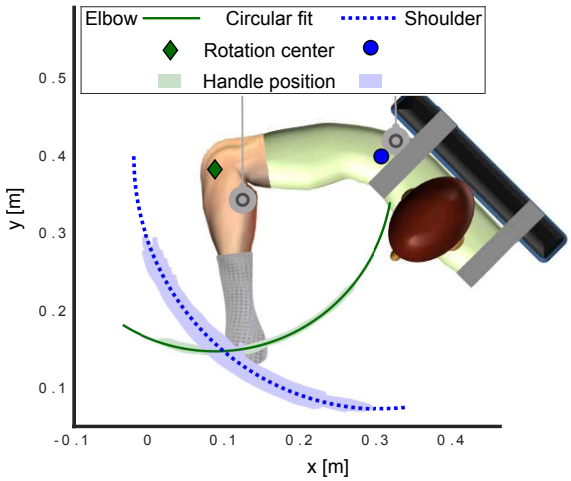

Figure 5.1: Experimental setup. During the experiments, the subjects rotated either their elbow or shoulder joint in a horizontal plane, as guided by a manipulandum. The wrist was immobilized throughout the trials by a stiff splint. After stopping the rotation at the intersection point of the elbow and shoulder rotations, the arm was rapidly perturbed to excite a monosynaptic stretch reflex in either the brachioradialis or the posterior deltoid. The reflex response was measured by EMG electrodes (gray circles). To determine software-based constraints that the manipulandum applies for the guidance of motion, the trajectories of the pure elbow and shoulder rotation were determined prior to the main experiments. For this purpose, the shoulder and elbow were consecutively immobilized by a second splint and the subject rotated the free joint back and forth for 300 s. The resulting hand position was continuously recorded and fitted by a circle to determine the center and radius of rotation of the target trajectory. The schematic shows the exemplary recorded hand positions of one subject.

shoulder (section 5.1.5). The hypothesis of this study predicts an enhanced monosynaptic reflex response of the brachioradialis following elbow rotation, whereas the deltoid should show a higher reflex response following shoulder rotation in the statistical analysis (section 5.1.6). As analyzed mathematically in section 5.1.7, these findings would be incompatible with the diffuse effects that the research community generally attributes to serotonin.

The study was approved by the Ethics Committee of the Technical University of Munich.

5.1.1 Experimental apparatus and setting

Throughout the experiments, the subjects were tightly restrained by seat belts to an adjustable chair and faced the manipulandum. Their right arms were mechanically constrained to form a system with two DOF, resembling the mechanical system in the previous chapters. Subjects could accordingly horizontally flex and extend their elbow and shoulder joint. The manipulandum mechanically blocked any undesired vertical movement of the hand, while a stiff splint prevented wrist movement. This splint also firmly attached the subjects' hands to the endpoint of the manipulandum with their palms facing downwards. To prevent exhaustion, the lower and upper arm were supported against gravity.

For the analysis, electrodes recorded the surface EMG of the brachioradialis and the posterior deltoid. Goniometers and accelerometers additionally measured the angular trajectory and acceleration, respectively, of the elbow and shoulder joint. The manipulandum controller based its control on feedback on the motor positions and forces, the above-mentioned EMG, and the endpoint forces exerted by the subjects.

5.1.2 Main experiments

Each subject performed 120 experimental trials. In an individual trial, the manipulandum first guided the subject to repeatedly perform strong and fast rotations of either their right elbow or shoulder joint (Figure 5.1). After 30 s, the manipulandum stopped the movement in a default arm posture following which the motoneuron excitability was measured in either the brachioradialis or the posterior deltoid muscle. Specifically, the protocol waited until the EMG of the respective muscle had decayed to its resting value and then quantified the motoneuron excitability of either muscle by its EMG response to the monosynaptic stretch reflex. To elicit the reflex, the manipulandum either extended the elbow or flexed the shoulder joint by 10° within 60 ms.

5.1.3 Preliminary experiments

Prior to the experiment, each subject underwent a set of preliminary experiments lasting 2 h in total. The main goal of these experiments was to characterize the subject's arm to ensure that the manipulandum guided the rotations and the perturbations of an individual joint with high precision. In addition, the subjects were habituated to perturbations and the EMG was recorded at maximum voluntary contraction (MVC) to normalize subsequent recordings.

To characterize the elbow and shoulder joint, the subject repeatedly flexed and extended the respective joint for 300 s while the handle position was recorded as shown in Figure 5.1. The other joint was fixed by a splint that had been custom-designed to provide a tight joint fixation but detach if the manipulandum force exceeded a threshold to prevent injuries. This design task was challenging because the skin and muscles of the upper arm allowed for substantial movement of a splint. Circles were fitted [190] to the recordings and showed a high characterization accuracy across all subjects with a standard error in the positions of the rotary axes and in the circular radii of below 5 mm and 6 mm, respectively. As detailed in the original paper [189], the resulting rotary movements were clearly divisible into pure rotations of either the elbow or of the shoulder joint.

5.1.4 Manipulandum control guiding the subjects' motion

The controller of the manipulandum guided pure rotations of either of the two joints by imposing a virtual environment with a clear resonance trajectory. In addition, the controller also artificially compensated three interfering effects originating from the mechanical manipulandum design: the high friction that typifies strong linear motors, the high mass $m = 12.9\,\mathrm{kg}$ of the manipulandum arms and motors which must be moved by the participants, and the coupled dynamics of the manipulandum arms. After compensation, the handle attached to the subject reacted like a frictionless point mass to the forces exerted by the virtual environment and the subject, denoted by $\boldsymbol{F}_e$ and $\boldsymbol{F}_s$, respectively:

$$c_m \cdot m \cdot \boldsymbol{I}\ddot{\boldsymbol{x}} = \boldsymbol{F}_\mathrm{e} + \boldsymbol{F}_\mathrm{s} \ . \tag{5.1}$$

Here, $\boldsymbol{I}$ denotes the 2×2 identity matrix and $\boldsymbol{x} \in \mathbb{R}^2$ is the handle position in the subject's coordinate system. The mass was artificially downscaled by a factor of $c_m = 0.4$.

To enforce the circular movement either along the elbow or shoulder trajectory, the controller exerted the sum of two forces on the subject's arm:

$$\boldsymbol{F}_\mathrm{e} = \boldsymbol{F}_\mathrm{rad} + \boldsymbol{F}_\mathrm{ang} \ . \tag{5.2}$$

The first force $\boldsymbol{F}_{\text{rad}}$ simulated an almost rigid spring which pushed the handle back to its circular resonance trajectory when its distance from the center of the considered joint deviated from the desired radius. The second force $\boldsymbol{F}_{\text{ang}}$ simulated a slack spring which pushed the handle back to its equilibrium position along the circular trajectory. Both forces included an artificial damping term to prevent friction overcompensation, ensuring that the subjects needed to repeatedly push the system to sustain the movement.

Without compensation for the interfering effects, the manipulandum dynamics follows

$$\boldsymbol{M}(\boldsymbol{q})\ddot{\boldsymbol{q}} + \boldsymbol{C}(\boldsymbol{q}, \dot{\boldsymbol{q}})\dot{\boldsymbol{q}} = \boldsymbol{\tau}_{\text{m}} + \boldsymbol{J}^T(\boldsymbol{q})\boldsymbol{F}_{\text{s}} + \boldsymbol{\tau}_{\text{f}} \ . \tag{5.3}$$

The off-diagonal entries in the symmetric, positive-definite inertia matrix $\boldsymbol{M}(\boldsymbol{q})$, along with the generalized Coriolis and the centrifugal matrix $\boldsymbol{C}(\boldsymbol{q}, \dot{\boldsymbol{q}})$, imply a mechanical system with coupled dynamics. The manipulandum is driven by the motor force $\boldsymbol{\tau}_{\text{mot}}$ and the force $\boldsymbol{F}_s$ exerted by the subject on the handle while it shows a friction force $\boldsymbol{\tau}_{\text{f}}$. The equation of motion is stated in the coordinate system spanned by the motor positions $\boldsymbol{q}$,

$$\boldsymbol{q} = \begin{pmatrix} \sqrt{l^2 - x_1^2} - x_2 \\ \sqrt{l^2 - x_2^2} - x_1 \end{pmatrix} \ , \tag{5.4}$$

where l denotes the length of the manipulandum arms. The Jacobian $\boldsymbol{J}(\boldsymbol{q})$ transforms the positions and forces from the subject coordinate system onto the motor coordinate system, in which the forces are denoted by $\boldsymbol{\tau}$.

To decouple the dynamics and scale the mass, the commanded force $\boldsymbol{\tau}_{\text{m}}$ was adjusted to

$$\tilde{\boldsymbol{\tau}}_{\text{mot}} \quad = \frac{1}{c_m \cdot m} \cdot \boldsymbol{J}^T \boldsymbol{\Lambda}(\boldsymbol{x}) \left[\boldsymbol{F}_{\text{e}} + \boldsymbol{F}_s\right] - \boldsymbol{J}^T(\boldsymbol{q})\boldsymbol{F}_s + \boldsymbol{\mu}(\boldsymbol{x}, \dot{\boldsymbol{x}})\dot{\boldsymbol{x}} \ , \tag{5.5}$$

where

$$\begin{aligned} \boldsymbol{\Lambda}(\boldsymbol{x}) \quad &= \boldsymbol{J}^{-T}\boldsymbol{M}(\boldsymbol{q})\boldsymbol{J}^{-1}(\boldsymbol{q}) \ , \\ \boldsymbol{\mu}(\boldsymbol{x}, \dot{\boldsymbol{x}}) &= \boldsymbol{C}(\boldsymbol{q}, \dot{\boldsymbol{q}})\boldsymbol{J}^{-1}(\boldsymbol{q}) - \boldsymbol{M}(\boldsymbol{q})\boldsymbol{J}^{-1}(\boldsymbol{q})\dot{\boldsymbol{J}}(\boldsymbol{q}, \dot{\boldsymbol{q}})\boldsymbol{J}^{-1}(\boldsymbol{q}) \ . \end{aligned} \tag{5.6}$$

For motors exerting the adjusted force $\tilde{\boldsymbol{\tau}}_{\text{mot}}$, the manipulandum dynamics in equation (5.3) can be reformulated as

$$c_m \cdot m \cdot \boldsymbol{I}\ddot{\boldsymbol{x}} = \boldsymbol{F}_{\text{e}} + \boldsymbol{F}_{\text{s}} + c_m \cdot m \cdot \boldsymbol{J}^T \boldsymbol{\Lambda}(\boldsymbol{x})\boldsymbol{\tau}_f \ . \tag{5.7}$$

Under the adjusted motor force, the manipulandum therefore behaves like a point mass that is downscaled by a factor of s. As a beneficial side effect, also the effective friction experienced by the subject was downscaled by the same factor.

The remaining uncompensated friction of the device was compensated by a friction observer based on the theoretical work by Luca et al. [191]. The manipulandum observes the commanded motor force $\tilde{\boldsymbol{\tau}}_{\text{mot}}$ and measures the force $\boldsymbol{F}_{\text{s}}$ exerted by the subject at the handle. The expected resulting movement of a frictionless manipulandum was compared to the actual movement observed by the position sensors in the motors. As shown in the

original paper [189], their deviation allows to estimate the friction by the time integral

$$\boldsymbol{r}(t) = \boldsymbol{K}_I \left[\boldsymbol{p}(t) - \boldsymbol{p}(0) - \int_0^t \left(\boldsymbol{C}^{\boldsymbol{T}} \dot{\boldsymbol{q}} + \tilde{\boldsymbol{\tau}}_\mathrm{m} + \boldsymbol{J}^T(\boldsymbol{q}) \boldsymbol{F}_\mathrm{s} \right) ds \right], \tag{5.8}$$

where the initial condition is $\boldsymbol{r}(0) = 0$, the gain is denoted by $\boldsymbol{K}_I$, and the generalized momentum is given by

$$\boldsymbol{p}(t) = \boldsymbol{M}(\boldsymbol{q}) \dot{\boldsymbol{q}} \ . \tag{5.9}$$

To compensate for the observed friction, the commanded motor force must be reduced by $\boldsymbol{r}(t)$. Therefore, the motor force commanded throughout the experiments was

$$\boldsymbol{\tau}_\mathrm{m} = \tilde{\boldsymbol{\tau}}_\mathrm{mot} - \boldsymbol{r}(t) \ . \tag{5.10}$$

The resulting manipulandum dynamics is then described by plugging $\boldsymbol{\tau}_\mathrm{mot}$, computed by equation (5.10), into the general equation of motion (5.3):

$$c_m \cdot m \cdot \boldsymbol{I} \ddot{\boldsymbol{x}} = \boldsymbol{F}_\mathrm{e} + \boldsymbol{F}_\mathrm{s} + c_m \cdot m \cdot \boldsymbol{J}^T \boldsymbol{\Lambda}(\boldsymbol{x}) \left[\boldsymbol{\tau}_f - \boldsymbol{r} \right] \ . \tag{5.11}$$

From the subject's viewpoint, this compensated mechanical system resembled a point mass $s \cdot m = 5.2\,\mathrm{kg}$ acted upon by forces from the virtual environment and the subject. Extensive experiments confirmed the derived control approach and its implementation on the manipulandum, as summarized in the paper that underlies the present chapter [189].

5.1.5 Electromyography processing

The EMG data were processed first to ensure that the EMG of the observed muscle was at rest prior to its reflex perturbation, and second to quantify the monosynaptic reflex response to mechanical perturbations. Prior to that, all EMG signals were bandpass-filtered between 20 Hz–450 Hz, demeaned, rectified, and normalized to the MVC measurement.

Muscles were ensured to be at rest by measures taken during the experiment and in the data anlysis: During the experiments, the controller delayed the perturbation until the EMG signal had decayed to its resting state and repeated the trial if this did not happen within 3 s after movement cessation. In the post-experimental data analysis, trials were neglected if muscle activity was detected between initiation of a perturbation and onset of the reflex EMG response. This step considered both the recording delay of the EMG electrodes and the neuronal reflex transduction delay. To exclude that any undetected motor activity distorted the results, the pre-reflex activity was matched between different conditions before their comparison.

The analysis quantified the monosynaptic reflex responses of the brachioradialis and deltoid muscles based on their EMG response to the perturbation of their corresponding joint (panel g and h of Figure 5.2). The reflex response occurred after a time delay composed of both the mechanical delay until the accelerometers detected joint movement after onset of the manipulandum perturbation and of the neuronal transduction delay as quantified in previous studies [192, 193]. The EMG reflex was averaged over a time window of 25 ms and normalized by subtracting its resting EMG. As EMG signals were restricted to positive values, the reflex response was defined as the natural logarithm of the EMG response in the statistical analysis to ensure a Gaussian distribution of the data.

5.1.6 Statistical analysis

This study investigated the prediction that the gain increase of motoneurons innervating the brachioradialis is higher after the elbow than shoulder movement and vice versa for the posterior deltoid. To test this hypothesis, a linear mixed-effects model was fitted to the observed reflex responses r_i of these two muscles. The model is given by

$$r_i = \beta_0 + \beta_1 \cdot \mathrm{rot_i} + b_{0,\mathrm{n}} + b_{1,\mathrm{n}} \cdot \mathrm{rot_i} + \epsilon_\mathrm{in} \ . \tag{5.12}$$

Here, β_0 and β_1 denote the fixed-effect regression coefficients, $b_{0,\mathrm{n}}$ and $b_{1,\mathrm{n}}$ are the random-effect regression coefficients, and ϵ_in denotes the residuals. The subjects were denoted by n and differences between them were considered as random effects. The fixed effect $\mathrm{rot_i}$ is a binary variable that amounted to 1 when in trial number i the rotating movement recruited mainly the subsequently perturbed and -1 when it recruited the non-perturbed joint. The assumption states that the reflex response in either of the two muscles is higher after its innervated joint has moved. This implies that $\beta_1 > 0$. The corresponding null hypothesis $\beta_1 = 0$ was tested by a two-tailed t-test. Since the hypothesis predicts that the effect must be significant in both muscles simultaneously, the linear fixed-effects model described in equation (5.12) was individually fitted to the brachioradialis and deltoid measurements, and no correction for multiple comparisons was required.

5.1.7 Analysis of interpretations based on diffuse neuromodulation

It is non-intuitive to see if the predicted changes of motoneuron excitability necessarily rule out diffuse neuromodulation as origin. This is due to the study design, which applied both non-invasive recording techniques and different delays between rotation movement and subsequent excitability measurements to allow motoneurons to come to rest. As summarized here and detailed in the original paper, a mathematical analysis thus tested if the predicted results are theoretically compatible with diffuse neuromodulation of motoneuron excitability.

The present observations may, in principle, also arise from the time delay between each rotation and the subsequent excitability measurement in the face of diffuse neuromodulation. Over the delay interval, the effect underlying increased motoneuron excitability potentially decayed. The delay, which accounted for the time that motoneuron activity required to return to rest, varied from trial to trial. Lower observed motoneuron excitability may thus be caused by a higher delay before the excitability measurement. For this reason, the analysis tested if under conditions of higher motoneuron excitability the delay was lengthened or shortened. This test applied the linear mixed-effect model (5.12) and used the observed time delays as response variable r_i.

The proprioceptive input that triggered the raphe nuclei and the resulting motoneuron gains were quantified in the experiments only by indirect recording methods. These measurements provide only relative statements on these two parameters and prevent determination of their precise units or amplitudes. Given these limitations, the study analyzed if diffuse neuromodulatory mechanisms may explain the observed joint-specific increase of reflex responses following the different rotation conditions or if this finding necessitates topographically precise neuromodulation [189]. This analytic reasoning was based on two assumptions that are supported by previous studies. First, during the present experiments, the sensory input of the elbow muscles to the raphe nuclei was higher during an elbow rotation than during shoulder rotation and vice versa for the shoulder muscles [114–116].

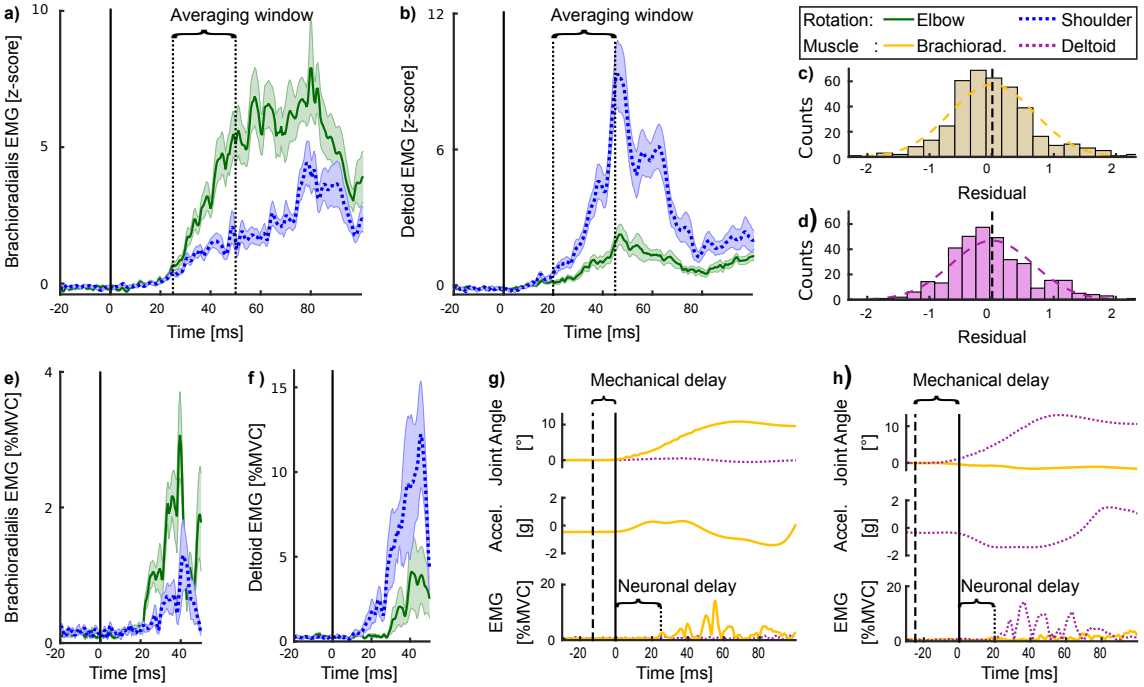

Figure 5.2: Monosynaptic reflex responses after movement of the shoulder or elbow joint. **a)** Averaged over all subjects, the right brachioradialis showed a higher monosynaptic EMG response to stretching after rotating the right elbow than after rotating the right shoulder. **b)** The opposite effect was observed for the right posterior deltoid. Vertical solid lines indicate the onset of the joint perturbation. The shaded areas indicate the standard errors in the EMG signals at each time step. Statistical significance was determined by fitting a linear mixed-effects model to the reflex response, averaged over the indicated window, of the respective muscle. As required for linear mixed-effects models, the residuals for both **c)** the brachioradialis and **d)** the posterior deltoid were well fitted by a normal distribution (dashed curves). Reflex responses of **e)** the right brachioradialis and **f)** the posterior deltoid of an individual subject resembled the subject-averaged responses. Individual reflex responses in **g)** the brachioradialis or **h)** the deltoid were elicited by mechanically perturbing the subject's hand along the elbow or shoulder joint, respectively. The angle of the other joint remained comparatively constant. After a mechanical delay, the perturbation accelerated the lower arm for the brachioradialis or the upper arm for the deltoid, as measured by accelerometers that recorded the horizontal movement of the respective arm segment. Following a neuronal transduction delay, the EMG electrodes recorded the monosynaptic reflex response in the perturbed muscle, while the other muscle remained silent.

Second, the serotonin released by the raphe nuclei onto motoneurons monotonically increases with increasing proprioceptive input [95, 194] and multiplicatively scales the gain of motoneurons [79].

5.2 Summary of the results

In resemblance to the robotic autoencoder, the brachioradialis and the deltoid showed a significantly enhanced monosynaptic reflex response after rotation of their respective actuated joint. Averaging over all subjects, the reflex response of the brachioradialis was significantly higher after elbow than after shoulder rotation at $p = 1.0 \times 10^{-4}$ (Figure 5.2a; linear mixed-effects models and two-tailed t-test: $df = 379$, $t = 3.8$). Conversely, the reflex response of the deltoid was significantly higher after shoulder than after elbow

rotation at $p = 1.7 \times 10^{-4}$ (Figure 5.2b; $df = 338$, $t = 3.9$). The validity of the underlying statistics was emphasized by the fact that the residuals of the linear mixed-effect models fitted to the reflex recordings were normally distributed (panels c and d of Figure 5.2). The predicted reflex behavior was also observed in individual subjects, as illustrated for an exemplary subject in panel e and f of Figure 5.2. For the brachioradialis, the present findings were based on a large set of $n_e = 172$ individual reflex recordings with prior elbow rotation (Figure 5.2g) and $n_s = 209$ reflex responses with prior shoulder rotation which had passed the exclusion criteria stated above. For the deltoid, the respective number of considered reflex responses amounted to $n_e = 203$ and $n_s = 137$ (Figure 5.2h).

While these findings may in theory be caused by non-serotonergic mechanisms, the review in the previous chapter 4 shows that neither known ionotropic nor non-serotonergic metabotropic circuitry provides an alternative explanation for the observed spinal excitability and its time scale. The protocol of the present study suppressed non-serotonergic effects that are known to change motoneuron gain, namely, different joint positions [195], pre-activation of motoneurons [196], and synaptic plasticity [197]. For this purpose, the perturbation parameters, such as the initial position as well as the stretch duration and distance, were kept constant. Additionally, the muscles were at rest prior to perturbation, and the trials under the different conditions were equally distributed over time. Wei et al. [78] reported that the reflex amplification observed several hundred milliseconds after strong proprioceptive input is elevated by serotonin agonists and blocked by its antagonists. Thus, all the evidence suggests that the changes in motoneuron excitability observed here are governed by serotonergic neuromodulation.

The present study proved the topographic precision of gain scaling non-invasively. The study was designed to overcome the specific limitations of the applied indirect recording techniques. In particular, the design overcame the limitation that the joint movement and the muscle EMG is only an indirect measure of the proprioceptive information during the rotatory movements, and that the EMG response to a stretch reflex is an indirect measure of the motorpool gain. These measures yielded only relative values for individual joints or muscles. The recordings demonstrated that the movement and the EMG of the muscles were significantly and substantially more pronounced during rotation than during quiescence of the associated muscle. As both parameters are known to monotonically increase the proprioceptive signals [114–116], it can be deduced that the raphe nuclei received more input from elbow proprioceptors during elbow rotation than during shoulder movement, and vice versa for the shoulder. The resulting excitability of the brachioradialis was higher after elbow movement than after shoulder movement, and vice versa for the deltoid. Mathematically, these findings were sufficient to prove the topographic precision of both the proprioceptive input to the raphe neurons and their projections to motorpools.

CHAPTER 6

Discussion and implications

Science Robotics recently ranked the development of robots that mimic the energy-efficient compliant dynamics of animals as primary challenge to generate *"major breakthroughs, significant research, and/or socioeconomic impact in the next 5 to 10 years"* [198]. But the control of efficient elastic movements in changing environments is largely unknown in both robotics and neuroscience. Bionic approaches to this open question suffer from the difficult identification of functionally distinct circuits within the network of our 86 billion entangled neurons. The present dissertation fully reverses the bionic approach to explain how the human brain controls the compliant body (Figure 6.1). For this endeavor, the highly interdisciplinary research first answered how the dynamics of biomimetic robots can be optimally exploited during fast motions such as jumping.

The simulations and experiments described in chapter 2 demonstrated that a fast, model-free controller induces energy-optimal movement in multiple compliant joints. The algorithm forwards a common signal to drive multiple joints and observes the resulting movement. When the robot or its environment change, the algorithm adapts the common signal for individual motors (Figure 1.1). In the experiments, the algorithm increased the movement amplitude of a jumping robot by up to 67 % without additional energy input.

Motivated by the high performance of the robotic algorithm, chapter 3 used it as a blueprint to develop a comprehensive mathematical model of an analogous brain mechanism (Figure 6.1). The algorithm thereby unites scattered experimental findings on the raphe nuclei in the brain stem. The resulting model describes a motor feedback loop that receives proprioceptive input and releases the monoamine serotonin to metabotropically modulate the gains of motorpools. The loop acts on motor synergies, neuronal circuits which send a common signal to multiple motorpools. Mathematical reasoning and simulations demonstrate that the neuromodulation adjust this common signal to produce the same forces as the adaptive robotic controller. The current consensus in neuroscience assumes that this neuromodulation is diffuse and equally affects muscles even across limbs [78, 79]. In contrast, the new model predicts that the raphe nuclei show topographic precision and predominantly boost the muscles of joints that can be moved with small metabolic expenditure (Figure 1.2). This effect is here denoted as *precision scaling*.

Chapter 4 summarizes a review on the spinal serotonergic system that revealed the plausibility and the unique function of highly precise neuromodulation. The proposed

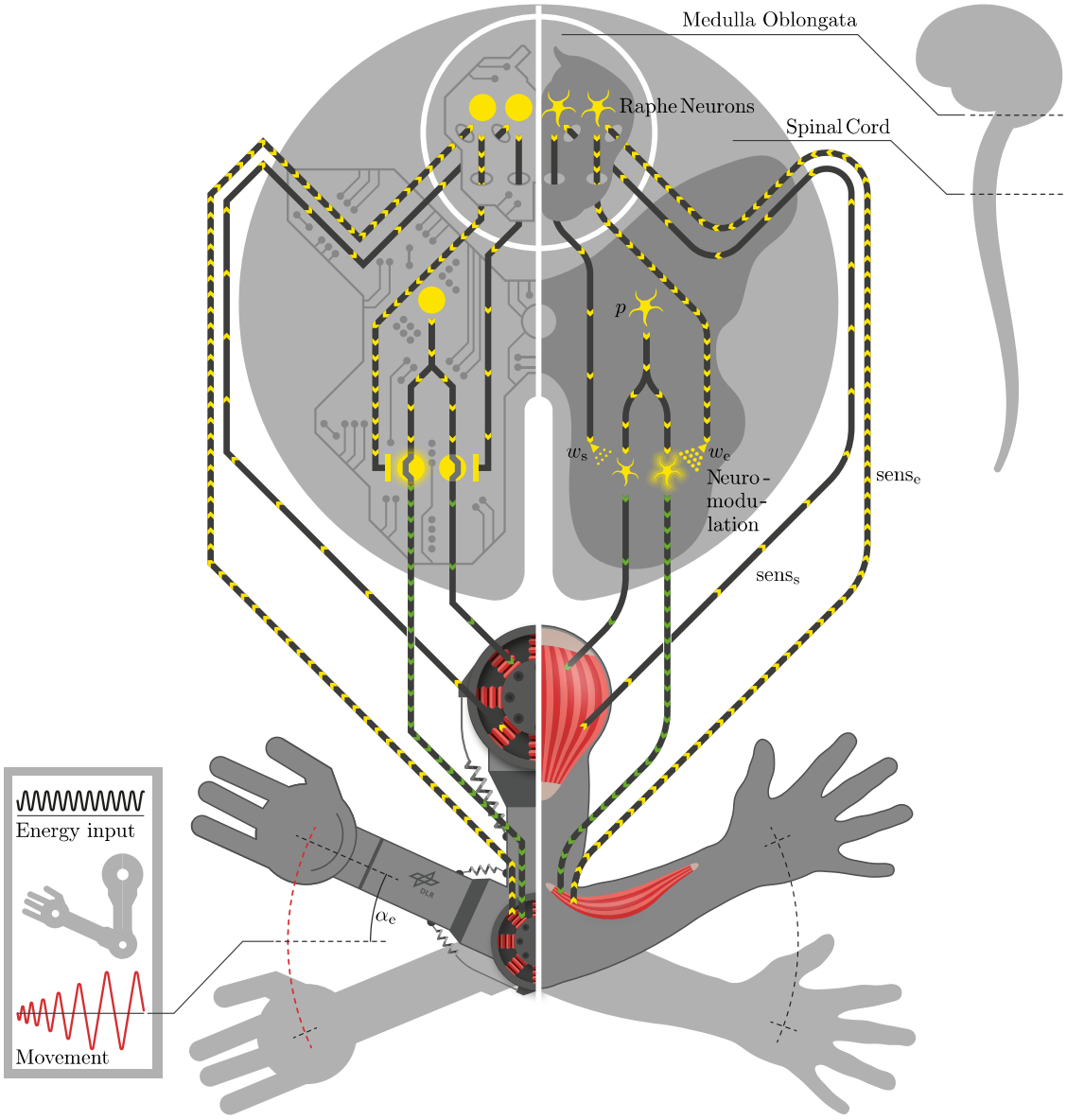

Figure 6.1: Schematic analogy between the robotic controller (left, chapter 2) and the projections from the raphe nuclei in the medulla oblongata to spinal motoneurons (right, chapter 3). The robotic control diagram illustrates that the controller receives sensory information on the position of the elbow, denoted α_e, and the shoulder. In the exemplary setup illustrated here, the shoulder is mechanically blocked. The controller identifies the joints with particularly strong sensory signals (nerve with high density of yellow arrows) and specifically amplifies their motor signals (green arrows). The amplification decays with a time constant of a few 100 ms. The resulting movement is dominated by joints that optimally harness their elastic elements and show optimal energy efficiency even in quickly changing environments. The raphe nuclei similarly receive sensory input from the elbow, $sens_e$, and shoulder, $sens_s$. Accordingly, they modulate the motor signals by releasing serotonin that scales the gains w_e and w_s of motorpools driving the elbow and shoulder, respectively. In contrast to the current neuroscientific consensus, human-subject experiments show that serotonin specifically increases the gain of a motorpool during movement of its innervated joint (chapter 5). This effect drastically simplifies the motor control, because all actuators can be driven by an ionotropic signal from the same synergy circuit p. Illustration by Tilo Wüsthoff.

precise effect of serotonin is fully in line with the experimental state of the art and may extend the purely diffuse effects described by previous reviews [78, 79]. A comparison with other known spinal circuits demonstrated that the serotonergic feedback loop is, according to current data, the only candidate to perform precision scaling in the spinal cord.

Human-subject experiments proved precision scaling, as described in chapter 5. The subjects repeated fast and strong arm motions in environments with clear resonance conditions. After movement of either the elbow or the shoulder joint, the excitability of motoneurons was quantified using a monosynaptic stretch reflex. The electromyographic response to the reflex was increased for motorpools that innervate the moving joint, while motorpools of the resting joint showed a smaller excitability. The increase outlasted the movement that triggered it. Biochemically, this persistent excitability was predicted by the slow decay of serotoninergic neuromodulation. Functionally, the robotic algorithm explains that this slow effect accumulates information over the full movement cycle. The serotonergic system therefore provides a precise adaptation network within the network of the spinal ionotropic motor circuitry and optimizes the controlled highly dynamic motion.

As will be elaborated in this discussion, the summarized findings have important implications for robotics (chapter 6.1), neuroscience (chapter 6.2), and the knowledge exchange between the two fields (chapter 6.3). Roboticists are provided with a modular, computationally cheap controller that maximizes the energy efficiency of multi-joint compliant robots under changing conditions. The algorithm is particularly promising for exoskeletons that support the human locomotor system because the human CNS uses the same control approach. For neuroscientists, serotonergic precision scaling complements the previously observed synaptic plasticity rules which depend solely on local information encoded either within the pre- or postsynaptic neuron [20, 199]. These known, local rules alone make it *"difficult (if not impossible) to learn global functions like [...] motor control"* [200]. Precision scaling adds a spinal mechanism that changes the synaptic strength according to non-local information. Beyond the spinal cord, precision scaling potentially applies also to the other monoaminergic systems, whose malfunction is involved in most neuropsychiatric and neurological disorders [201]. Precision scaling provides an early-level interpretation of the mechanisms of the psychopharmacological drugs administered against the diseases. These far-reaching implications combined reveal that robotic control theory is a promising technique for *"the development of efficient predictive tools [...][to] characterize the pathways between specific types of neuron"*. It therefore boosts an endeavor that Markram [202] denoted as one of the *"fundamental challenges [...] of twenty-first century neuroscience"*.

6.1 Energy-optimal control of compliant biomimetic robots

This project simplifies the powerful controller that Lakatos et al. [17, 18] developed for periodic motions in compliant multi-joint robots. The simplified algorithm is a modular extension for future controllers that learns energy-efficient motions in changing conditions.

The original robotic controller forms an autoencoder as illustrated in Figure 1.1. Its encoder linearly transforms sensory input from the multi-dimensional joint space onto a latent space where it sets the phase of a single timing signal. Its decoder reversely transforms the common timing signal to drive all joints. While the autoencoder was designed based on theoretical considerations, chapters 2 and 3 demonstrate empirically that the encoder can be be neglected without relevant loss in motor performance. In contrast, the results show that the proposed decoder automatically extracts the actuator forces which achieve optimal energy efficiency under changing conditions.

We may gain an intuition for these empirical findings when we reflect how the encoder and decoder contribute to exciting the energy efficient normal modes of a mechanical system. Normal modes are movement cycles where all positions have a constant ratio in linear systems. While complex robots are nonlinear mechanical systems, also they show normal modes either globally [203] or at least locally around their equilibrium position [204, 205]. Once the autoencoder has started a movement, its adaptation algorithm receives information on the motion and adapts the encoder and decoder weights. The adaptation rule stops when the vector of weights is aligned with the joint positions throughout the cycle, implying normal mode movement. Since all joints move in phase, the encoder stage can be left out as it only determines how much impact each of the joints has on the phase and frequency of the timing signal. The decoder adaptation, in contrast, determines how much torque each joint exerts. In a simple example, it will suppress the recruitment of a joint if the joint is dampened by the environment. For this purpose, the decoder adaptation forms a positive feedback loop that increasingly excites the normal mode which yields the largest movement amplitude for a given energy input. The decoder initially exerts an untuned combination of joint forces, exciting multiple normal modes at once. The resulting movement is dominated by the most attractive normal mode that shows particularly low damping and, in nonlinear systems, receives net energy transfers from other modes. The adaptation aligns the output torques with the observed movement and the controller will excite the attractive mode more specifically. In experiments on a complex robotic leg, the model-free decoder adaptation thereby achieved a movement that was identical to the optimal trajectory with an error smaller than the intrinsic fluctuations of the system.

When roboticists extend their controllers by the decoder, they are relieved of the task to generate an individual timing signal for each joint. Instead, the controller needs only a one-dimensional timing signal that is forwarded to all joints. In the one-dimensional latent space, it is particularly simple to combine commands designed to fulfill disparate functions, such as motion stability and path planning, or rely on different sources of information, including sensory input and internal models. The interplay of different commands also becomes accessible to a large range of analysis methods that are well-tested to determine the limit cycle stability, convergence time, and energy efficiency of one-dimensional systems. These include Poincaré maps [206], Lyapunov analysis [207, 208], and analysis of hybrid dynamic systems [209, 210]. During motions that need more than one timing signal because different limbs show out out-of-phase trajectories, the joints of each individual limb will still move with high phase coupling during normal mode oscillations. The decoder will then require a single timing signal per limb. It will thus simplify the generation of energy efficient movement for each limb individually.

Frameworks that reduce the complexity of controllers will be evermore important for robots and exoskeletons that increasingly mimic and support the versatility of biological locomotor systems. Due to the finding that the CNS adapts movements like the decoder (chapter 5), it is likely that the proposed decoder will continuously simplify the control of future robots along their path towards animal-like motor performance.

6.2 Robotics reveals how the brain controls compliant motions

Motivated by the benefits of the decoder adaptation for biomimetic robots, human-subject experiments revealed that the CNS performs a similar function. The results demonstrated that the raphe nuclei in the brain stem react to a movement by releasing serotonin that modulates individual motorpools. According to the known dynamics of serotonin [104],

the detected feedback loop yields the same motor signals as the robotic adaptation rule and thus selects an energy efficient movement pattern from the infinite options of the redundant locomotor system [49]. Since the effect works on spinal motorpools, it simplifies the control performed by all motor circuitry that ultimately projects to the motoneurons. The following reasoning will substantiate that this precision scaling applies to all spinal motor networks. Precision scaling thereby closes a long accepted gap between known plasticity mechanisms and machine learning: like machine learning rules, it can train an ionotropic network according to error signals that are not locally processed by the network. The concept potentially applies also to monoaminergic systems beyond the raphe nuclei and may explain the effects of many psychopharmacological drugs.

6.2.1 Precise serotonergic neuromodulation across spinal motor circuits

While the *in vivo* experiments in this dissertation focus on arm movement, the serotonergic modulation of motoneurons is also essential for locomotion. When a spinal cord injury cuts off descending pathways, therapies must supply serotonin agonists to restore locomotion. For this purpose, the agonists facilitate artificial ionotropic input onto motoneurons, such as input provided by epidural electric stimulation [211–215]. In the healthy spinal cord, the present findings for arm circuitry make it likely that serotonin is distributed with high precision also to the leg circuitry. This owes to the fact that the raphe feedback loop acts very similarly across limbs and motor conditions [78, 216–219]. In addition, serotonin is already known to disparately increase the firing of different muscles in individual legs of lobsters [220]. In the phylogeny from invertebrates [221, 222] up to cats [103] and humans [78], the raphe feedback loop has strikingly maintained its features. It can therefore be expected that precision scaling has been conserved also for locomotion. The ability of precision scaling to utilize compliant elements bears particular benefits for locomotion because the compliant elements are strongly stretched by the high tread forces. The elements thus reuse a large fraction of the high impact energy to boost the next step [9, 11–13]. However, current experimental therapies developed for locomotion rehabilitation replace serotonin in a diffuse way by administering agonists that affect all muscles simultaneously [212–214]. The present research provides a functional and anatomical description of the precise serotonergic motor effects. Future therapies may mimic these discovered effects to substantially enhance the gait amplitude and speed of paraplegic patients.

6.2.2 Adjusting forces by non-local gradient descent

The serotonergic feedback loop extends the neuronal adaptation of synaptic weights, which is largely governed by spike-timing-dependent plasticity [20, 199], by two fundamental functional properties: Its adaptation relies on a continuous firing rate rather than discrete spikes, and it performs non-local learning. The first property results from the fact that the slow neuromodulation smooths the discrete spikes of the raphe neurons to a continuous signal. Chapter 3 demonstrates that the property allows serotonin to minimize the output error of the spinal motor circuitry by descending along the error gradient. In contrast to discrete functions that lack a well-defined gradient, a continuous error function enables the fast and reliable gradient descent approach to adapt a circuit [223]. The second property, non-local learning, solves the long-standing problem that neuronal circuits often need different information for learning than for normal functioning [22]. Local learning alone would rule out some essential adaptation skills. As an example, consider the above-mentioned synergy pool of neurons that forwards a common signal to several motorpools.

The single pool forms a bottleneck that cannot encode muscle-specific sensory information. But this information is required to individually adapt the downstream motorpools when changing mechanical conditions require a different pattern of muscular forces (Figure 1.2). The present findings imply that the raphe nuclei skip this bottleneck and provide non-local sensory information to adapt individual motorpools by gradient descent.

By non-local gradient descent, serotonin closes a fundamental gap between previous models of biological adaptation and machine learning algorithms such as backpropagation [22, 199, 223, 224]. Chapter 3 points out the similarity by a comparison with the delta rule [109], a backpropagation rule for single-layered artificial neural networks [110, 225]. Both serotonin and the delta rule act on networks with a single layered decoder topology (Figure 6.1). The network processes training signals to start the learning process. Subsequently, the raphe nuclei and the delta rule receive target signals, compare them with the actual network output, and then descent the network weights along the gradient of a similar error function. An important distinction is that the CNS does not define the target output in advance. Instead, the musculoskeletal system continuously provides an up-to-date target signal by its response to the network output. General backpropagation algorithms show a further distinction as they propagate the output error backwards through multiple layers of an artificial neural network and read out all synaptic weights to determine the impact of an individual synapse. To read out its synaptic weights, the CNS would need to run designated signals through the neuronal network and thereby block its normal functioning during a special training phase [226]. The serotonergic feedback loop instead forms skip connections that train only one layer without interrupting the normal signal processing. This property prevents severe injuries when serotonin trains motor networks that must continuously perform safety-critical tasks such as balancing.

With its ability to perform non-local gradient descent, serotonin is not the first monoamine that has been linked to principles from machine learning. Wide evidence suggests that midbrain dopaminergic neurons guide a biological form of reinforcement learning as they signal the error between the reward that an animal expects and the reward it receives [227]. The research presented here characterizes the biochemical and mathematical effects of such a monoaminergic error signal on a neuronal level. The extraordinary level of detail was facilitated by the fact that the raphe neurons are connected to spinal circuitry and not higher-level circuitry like the midbrain dopaminergic neurons. Accordingly, it was possible to quantify the sensory input and motor output of the raphe neurons in human-subject experiments without opening the skull or the vertebral column. In addition, it was comparatively straight-forward to interpret how the recorded signals encoded information because they were directly related to physical quantities like muscle forces [228]. In general, monoamines are ideally suited to perform mechanisms that resemble machine learning algorithms: They can adapt the ionotropic connectome while the connectome continuously performs its normal, often safety-critical, signal processing.

6.2.3 An explanation for monoaminergic actions throughout the CNS

Going beyond the spinal cord, monoaminergic systems are in general assumed to show *"extensive branching terminals and diffuse release"* [229] which is *"thought to globally affect all brain areas they project to"* [230]. The present findings question this assumption specifically for serotonin in the spinal cord. Moreover, precision scaling offers a promising big picture for the monoaminergic neuromodulation in all parts of the CNS.

An example for another monoamine whose effects can be modelled by precision scaling comes from the dopaminergic innervation of the retina [156]. The output of the retina

is dominated by cone photoreceptors under bright conditions and by rod photoreceptors under dark conditions. Cone bipolar cells (CBs) form their point of convergence as they receive direct input from cones and indirect input from rods relayed by AII amacrine cells. At increasing light levels, the output of the CBs increasingly drives dopaminergic neurons [231]. In turn, the released dopamine modulates the amacrine cells [232] and disrupts the indirect input of rods onto the CBs [233]. Therefore, dopamine scales the relative impact of cones and rods in order to adjust the overall retinal output under changing light conditions [156, 233, 234]. Dopamine thereby acts analogously to serotonin, which scales the relative muscle signals to optimize the overall force output under changing mechanical conditions. While serotonin achieves its topographic precision by the distribution of terminals on chemical synapses, dopamin performs this effect by actions on gap junctions. This reflects that gap junctions play a minor role in the spinal cord [235] but a major role in the retina [236]. It thus seems that precision scaling has independently evolved in different CNS regions based on the biochemical mechanisms that dominate the local signal processing.

The dopaminergic system illustrates the fact that most monoaminergic systems share the essential features of the serotonergic motor loop. In particular, the systems project predominantly to ionotropic circuitry and typically act by metabotropic effects which change the gain of their target neurons [237–241]. For many projections, preliminary evidence supports topographically specific effects [156, 220, 242, 243]. In turn, the monoaminergic neurons receive feedback on their actions by sensory input or recurrent connections from their targeted circuits [242, 244–246]. In resemblance to the multiple motorpools in the spinal cord, we may assume that also the neocortex comprises multiple ionotropic subcircuits which emit coordinated signals to deal with mental or social situations. Monoaminergic neuromodulation may scale the individual subcircuits to react to unexpected changes, just as serotonin scales different muscle groups depending on the terrain. Since the monoaminergic systems receive feedback on their action, their modulation of individual subcircuits will converge to different set points that suit changing situations.

The model presented in this dissertation offers an early-level explanation for the effects of psychopharmacological drugs that act on the monoaminergic systems. Malfunction of these systems have been *"identified in most, if not all, neuropsychiatric and neurological diseases"* [201]. But the administered drugs often show unpredictable outcomes and, for some of the patients, even no curative effect at all [247–252]. According to the new model, the diseases can arise when the relative scaling of different subcircuits encoding mental models is out of order. As a consequence, the responses to a changing environment would become inadequate, which may start a self-amplifying feedback loop that pushes the relative scaling factors further away from their physiological set points. When a drug diffusely influences the monoaminergic systems, it will push the set points of all subcircuits to new ranges. Even though the new range may turn out to be functionally operative, the doses need to be accurately tuned for each individual and the treatment will not work for some patients irrespective of dose, in line with the clinical observations. Motivated by the research presented here, an *in vivo* study is currently being prepared in the Department of Experimental Medical Science at Lund University (Sweden). The study will evaluate the new model for drugs that replace dopamine in Parkinson's disease.

6.3 Reverse-bionics as generic tool to disentangle CNS circuitry

In addition to the numerous scientific findings, the present project reveals a new methodology for neuroscientific research. In previous research, robotics has provided neuroscience

with analysis tools to investigate biological motions and with biomimetic robots to implement and test the obtained control principles [2–4]. Here, the potential benefit of robotics for neuroscience is fundamentally extended. This dissertation reverses the popular bionic knowledge transfer that applies biological insights as blueprints to create engineering solutions. Instead, the applied *enginic* knowledge transfer applies engineering solutions as blueprints to create biological knowledge.

The enginic transfer of robotic knowledge into neuroscientific insights is a new avenue that is promising, in particular because of recent fundamental changes in the field of robotics. Although many of the early robots already looked like animals, robotics engineers have just recently started to replicate the mechanical foundations for the remarkable biological motor performance. During the last years, an especially promising example of this endeavor has been the incorporation of passive compliant elements in multi-segment robots [23, 24]. The compliant elements have led to robots with intrinsic, stable, energy efficient oscillation modes that can be exploited for versatile gaits [23, 24, 67, 253, 254]. The bionic trend has fundamentally aligned robotic control theory with neuroscience. While conventional robotic algorithms enforce the desired dynamics on a given mechanical system [255–257], roboticists are now also increasingly designing controllers that identify and harness the beneficial intrinsic dynamics of the novel biomimetic robots [18, 258–261]. The resulting algorithms can induce motions that have little energy consumption, are stable and adaptive, and show large movement amplitudes and velocities. The success of the present project shows that these controllers are promising blueprints for analogous, unknown CNS functions as long as the algorithms bear a basic similarity to neuronal arithmetics. This conclusion is in line with the common view that the CNS has primarily been shaped by the evolutionary need for versatile, stable, and efficient movements [5, 6].

The numerous far-reaching results of the present dissertation strongly incentivize future enginic projects. The present findings provide roboticists with a modular framework to minimize the energy consumption of the *"new generation of robots that are multifunctional, power-efficient [and] compliant"* [198]. At the same time, they offer neuroscientists a neuron-level understanding of the strategies that humans apply to exploit their compliant muscles and tendons for energy-efficient and yet powerful movements, with implications for exoskeletons, motor rehabilitation, and even cognitive diseases. As biomimetic robots catch up on the superior motor performance of animals, roboticists design an increasing number of high-performing and well-characterized controllers. Currently, the resulting algorithms are not being explored for their biological plausibility. Future enginic projects can harness this plethora of models to discover the unknown characteristics of neuronal motor circuitry. The algorithms thus diminish the common problem that *"neuroscience is data rich and theory poor"* [262].

Publications

Legged elastic multibody systems: adjusting limit cycles to close-to-optimal energy efficiency

Authors Philipp Stratmann, Dominic Lakatos, Mehmet Özparpucu, Alin Albu-Schäffer

Journal Robotics and Automation Letters

Number of pages 8

Review Peer reviewed

Abstract Compliant elements in robotic systems can strongly increase the energy efficiency of highly dynamic periodic motions with large energy consumption such as jumping. Their control is a challenging task for multi-joint systems. Typical control algorithms are model-based and thus fail to adjust to unexpected mechanical environments or make limited use of mechanical resonance properties. Here, we apply numerical optimal control theory to demonstrate that close-to-optimal energy-efficient movements can be induced from a one-dimensional (1-D) sub-manifold in jumping systems that show nonlinear hybrid dynamics. Linear weights transform sensory information onto this 1-D controller space and reversely transform 1-D motor signals back onto the multi-dimensional joint space. In Monte-Carlo-based simulations and experiments, we show that an algorithm that we derived previously can extract these weights online from sensory information about joint positions of a moving system. The algorithm is computationally cheap, modular, and adjusts to varying mechanical conditions. Our results demonstrate that it reduces the problem of energy-efficient control of multiple compliant joints that move with high synchronicity to a low-dimensional task.

Author contributions Researched literature; co-designed the study; implemented and ran the numerical optimization; ran the experiments; statistically analyzed the results; composed the manuscript; handled review; presented as keynote presentation and interactive session at a major robotics conference.

Legged Elastic Multibody Systems: Adjusting Limit Cycles to Close-to-Optimal Energy Efficiency

Philipp Stratmann[1,2], Dominic Lakatos[2], Mehmet C. Özparpucu[2], Alin Albu-Schäffer[1,2]

***Abstract*—Compliant elements in robotic systems can strongly increase the energy efficiency of highly dynamic periodic motions with large energy consumption such as jumping. Their control is a challenging task for multi-joint systems. Typical control algorithms are model-based and thus fail to adjust to unexpected mechanical environments or make limited use of mechanical resonance properties. Here, we apply numerical optimal control theory to demonstrate that close-to-optimal energy-efficient movements can be induced from a one-dimensional sub-manifold in jumping systems that show nonlinear hybrid dynamics. Linear weights transform sensory information into this one-dimensional controller space and reverse transform one-dimensional motor signals back into the multi-dimensional joint space. In Monte-Carlo-based simulations and experiments, we show that an algorithm that we derived previously can extract these weights online from sensory information about joint positions of a moving system. The algorithm is computationally cheap, modular, and adjusts to varying mechanical conditions. Our results demonstrate that it reduces the problem of energy-efficient control of multiple compliant joints that move with high synchronicity to a low-dimensional task.**

***Index Terms*—Compliance and impedance control, redundant robots, Optimization and Optimal Control.**

I. INTRODUCTION

ROBOTIC platforms are increasingly equipped with compliance in their actuators, which allow to store energy and release it at a later time to increase the energy efficiency of a given movement. These elastic properties significantly influence the dynamics of an actuator at high velocity and force during highly dynamic cyclic movements such as jumping. Different strategies have been proposed to control robots that comprise compliant actuators and multiple degrees of freedom. Most approaches rely on a model and a fixed set of considered initial conditions [1], such as algorithms based on *Poincaré-maps* [2], transverse linearization [3] or optimal control [4]. They lack the ability to adjust to unexpected conditions and environments. Algorithms based on *van der Pol* oscillators often use a nonlinear damping term to enforce a pre-defined limit cycle [5], [6]. This term artificially introduces energy losses and changes the dynamics of the system, which reduces the movement efficiency. An approach to overcome these problems are central pattern generators (CPGs) that mimic animal locomotion control by outputting a default motor signal which adapts according to sensory input. Typically, all joints are driven by individual CPGs that are coupled among each other [7], [8], [9]. These studies focus on the phase relation of the CPGs, but neglect tuning of the relative motor strength, which has a strong influence on the energy efficiency [10].

We have recently demonstrated that under specific intrinsic damping properties of the actuators, the stable control of robotic platforms with several joints may be reduced to a one-dimensional control problem during highly dynamic movements [11], [12]. The algorithm linearly transforms sensory input from the multi-dimensional joint space into a one-dimensional controller space. We analytically derived a learning rule to extract transformation weights which are the optimal, local, linear approximation of the mode of the system in a least-squared sense [11]. The obtained formula is mathematically equivalent to the well-analyzed *Oja's rule* [13], [14]. The input entrains a bang-bang unit, and its motor output is reversely transformed into the joint space. The binary nature of the bang-bang control guarantees convergence to a stable limit cycle within few oscillation periods, as extensively validated both analytically [15] and experimentally [11], [16]. Our approach extends the previous literature by an algorithm that requires neither a priori knowledge of model parameters nor artificial damping. The performed calculations are computationally simple and require to store only the modal transformation weights during execution. The sensory requirements are limited to information about joint forces and positions. Additionally, the chosen modal coordinate transformation is analytically known to allow for resonant relative motor strengths in certain ideal mechanical systems, where it thus achieves a highly energy efficient actuation [11]. We will hereby denote a control law as *energy-efficient* if it maximizes the amplitude of a movement for an energy input of pre-defined magnitude. In particular, the modal weights allow resonant movement in undamped linear mechanical systems which are formed of n elastically coupled bodies, that can be described by a constant diagonal inertia matrix, and which are subject to modal damping and white noise. Such a system has n eigenfrequencies and associated normal modes. If we repeatedly excite the system by deviating all springs simultaneously along any of the eigenmodes, all masses will oscillate in phase with the corresponding eigenfrequency, i.e. mechanical resonance occurs. Oja's rule derives the dominant principal

Manuscript received: September, 09, 2016; Accepted November, 12, 2016.
This paper was recommended for publication by Editor Paolo Rocco upon evaluation of the Associate Editor and Reviewers' comments.

[1]Department of Informatics, Technical University of Munich, 85748 Garching, Germany.
[2]Institute of Robotics and Mechatronics, German Aerospace Center (DLR), Muenchener Strasse 20, 82234 Wessling, Germany.
Contact: philipp.stratmann@dlr.de

Digital Object Identifier (DOI): see top of this page.

component, corresponding to the physical eigenmode that shows the maximum amplitude for the described mechanical system [17], [18]. For a random initial excitation, this is most likely the least damped eigenmode. The performance of Oja's rule is improved by the fact that the bang-bang control inserts energy along the iteratively extracted modal weights, thereby forming a positive feedback loop that enhances the amplitude of the particular mode. In the controller space formed by transformation weights that are extracted by Oja's rule, a one-dimensional timing signal can thus excite all bodies along the least-damped resonant mode. We expect that the modal transformation also allows the control of energy-efficient movement in systems with more general nonlinear dynamics. This is due to the fact that the dominant principle component is the least-square-optimal linear approximation to a data set describing the dynamics [19], which implies that the modal excitation enables close-to-optimal control during the short phase of energy insertion by the bang-bang law.

The present study focuses on the energy optimality of the proposed modal transformation for hybrid compliant mechanical systems subject to nonlinear dynamics. The considerations are based on a periodically jumping leg with two joints, since locomotion bears particular potential for optimization by compliant structures due to its high energy consumption and high occurring impact forces. The hypothesis that our controller induces energy-optimal movement can be divided into three aspects that will be tested individually: Firstly, optimized jumping height is obtained in a stable limit cycle for a modal control approach. A control law that optimizes particularly the last jump in a sequence leads to a periodic trajectory in the preceding jumps and implicitly optimizes each preceding jump individually. Secondly, the optimal transformation weights are constant in time under fixed mechanical conditions. Thirdly, Oja's rule can extract the optimal weights during modally driven jumping movement. We validate the first two assumptions by numerically deriving an optimal control using a Legendre-Gauss-Radau quadrature orthogonal collocation method as implemented in *GPOPS-II* [20]. In a second step, we use a Monte Carlo method to verify that Oja's rule extracts the energy-optimal transformation weights online from sensory signals. We concentrate on a bang-bang control in the controller space as this is the key to the previously observed high movement stability.

In combination with our previous work, we conclude that Oja's rule allows to reduce the generation of stable, adaptable, and energy-efficient movement in multiple compliant joints to a low-dimensional problem. The algorithm may be used in the control of robotic platforms with multiple actuated links as a simple module that adjusts the intra-limb coordination to mechanical changes. Hereby, it optimizes the energy efficiency both of the mechanical actuators and the hardware required to calculate the control law.

II. THE CONTROL ALGORITHM

The modally adaptive bang-bang controller that we recently described [11], [12] controls a multi-body system with n joints driven by series elastic actuators (SEAs). A movement is initiated by deflecting the system from its equilibrium position. The controller observes the movement and adjusts it iteratively until it converges to a stable limit cycle. For this purpose, the controller receives information about the joint torques $\boldsymbol{\tau} \in \mathbb{R}^n$, which are a function of the difference between link and motor coordinates $\boldsymbol{q}, \boldsymbol{\theta} \in \mathbb{R}^n$, respectively,

$$\boldsymbol{\tau} = \boldsymbol{\tau}(\boldsymbol{\theta} - \boldsymbol{q}) \ . \tag{1}$$

The torque is transformed from the joint space into a one-dimensional sub-manifold along the modal weights $\boldsymbol{w} \in \mathbb{R}^n$,

$$\tau_{\mathrm{z}} = \frac{\boldsymbol{w}^T}{\|\boldsymbol{w}\|}\boldsymbol{\tau} \ . \tag{2}$$

Here, it triggers the controller of constant amplitude and threshold $\hat{\theta}_{\mathrm{z}}, \epsilon_\tau \in \mathbb{R}$, respectively,

$$\theta_{\mathrm{z}} = \begin{cases} +\hat{\theta}_{\mathrm{z}} & \text{if } \tau_{\mathrm{z}} > \epsilon_\tau \\ 0 & \text{if } -\epsilon_\tau \leq \tau_{\mathrm{z}} \leq \epsilon_\tau \\ -\hat{\theta}_{\mathrm{z}} & \text{if } \tau_{\mathrm{z}} < -\epsilon_\tau \end{cases} \ . \tag{3}$$

The output is transformed back into the joint space and the motor positions are accordingly updated to

$$\boldsymbol{\theta} = \frac{\boldsymbol{w}}{\|\boldsymbol{w}\|}\theta_{\mathrm{z}} \ . \tag{4}$$

The linear transformation weights are recursively extracted from the joint trajectories according to the learning rule,

$$\dot{\boldsymbol{w}}(t) = \gamma(\boldsymbol{w}(t)^T\boldsymbol{q}(t))\left[\boldsymbol{q}(t) - (\boldsymbol{w}(t)^T\boldsymbol{q}(t))\boldsymbol{w}(t)\right] \ , \tag{5}$$

which is mathematically equivalent to Oja's rule [13]. The adjustment rate γ is chosen smaller than the period frequency of the movement to capture the dynamics of the system during the whole movement cycle.

This study extends the previous description and analysis of the presented control law by energetic considerations. We restrict our simulations to mechanical systems where each actuator comprises a torsional spring with same constant stiffness $k \in \mathbb{R}$. Crossing the threshold $\pm\epsilon_\tau$ switches the torque,

$$\boldsymbol{\tau}_0 = k(-\boldsymbol{q}) \ \rightarrow \ \boldsymbol{\tau}_1 = k\left(\frac{\boldsymbol{w}}{\|\boldsymbol{w}\|}\left[\pm\theta_{\mathrm{z}}\right] - \boldsymbol{q}\right) \ .$$

The performed work equals the change of potential energy,

$$c_{\epsilon\hat{\theta}} = \frac{1}{2}\frac{\boldsymbol{\tau}_1^2}{k} - \frac{1}{2}\frac{\boldsymbol{\tau}_0^2}{k} \tag{6}$$

$$= \mp k\hat{\theta}_{\mathrm{z}}\frac{\boldsymbol{w}^T}{\|\boldsymbol{w}\|}\boldsymbol{q} + \frac{1}{2}k\hat{\theta}_{\mathrm{z}}^2 = \epsilon_\tau\hat{\theta}_{\mathrm{z}} + \frac{1}{2}k\hat{\theta}_{\mathrm{z}}^2 \ . \tag{7}$$

Equation (7) illustrates that the controller amplitude $\hat{\theta}_{\mathrm{z}}$ and threshold ϵ_τ define the energy inserted into the mechanical system. They determine whether the actuated system converges to a limit cycle or falls silent. The latter happens when the modal torque fails to reach the switching threshold.

III. OPTIMALITY OF THE LIMIT CYCLE

In the following sections, we test three aspects of energy efficiency: Here, we check whether optimization of individual jumps is achieved during a limit cycle. Subsequently, whether the energy-optimal modal transformation weights are time-invariant. Finally, whether a bang-bang controller in combination with Oja's rule extracts the optimal transformation weights from sensory information.

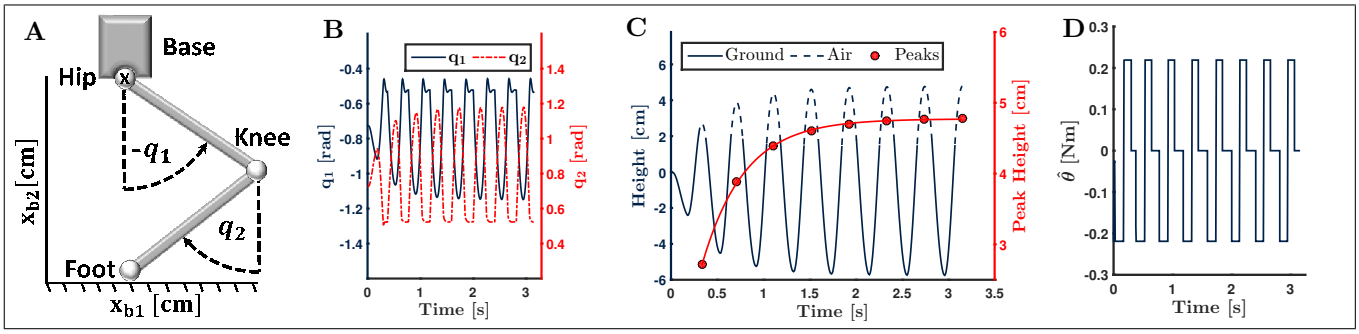

Fig. 1. **(A)** The mechanical test bed consists of a base that is serially connected to two links by a hip and a knee joint. The base coordinates $(x_{\mathrm{b1}}, x_{\mathrm{b2}})$ are measured at the middle of the hip joint, as indicated by an $\boldsymbol{x}$ in the illustration. Joint coordinates (q_1, q_2) are measured clockwise relative to vertically extended links. **(B)** Illustration of movement induced by the optimal controller obtained under the constraint of time-independent transformation weights represented by the weight angle α. Plotted here are the joint coordinates. **(C)** A plot of the resulting trunk trajectory indicates that after eight jumps the trajectory of the leg has approximately converged to a limit cycle. We extracted the peak heights of the jumping movement and plotted them together with a line showing an exponential fit against the second, right y-axis with higher resolution. **(D)** The derived controller is plotted for the whole simulated time. While it is artificially fixed to zero during flying phases, we find clear bang-bang behavior during the standing phase.

A. Methods

Mechanical System: As example system for our considerations, we simulate a floating base with one leg (cf. Fig. 1A) that models the robotic system used for the experimental validation in Sect. V. The floating base can freely translate in a vertical plane and we describe its position by $\boldsymbol{x}_{\mathrm{b}} = (x_{\mathrm{b1}}, x_{\mathrm{b2}})^T \in \mathbb{R}^2$. A trunk of mass $0.49\mathrm{kg}$ is attached by a hip joint to a leg. The leg comprises an upper and lower thigh that have respective masses of $0.059\mathrm{kg}$ and $0.038\mathrm{kg}$, equal length of $8\mathrm{cm}$, and are connected serially by one knee joint. Parameters describing the inertia are obtained from the CAD model of the robot. The respective joint coordinates q_1 and q_2 of the hip and knee joint are measured relative to a vertical orientation of the upper and lower link. We summarize joint and floating base coordinates as $\boldsymbol{x} = (\boldsymbol{x}_{\mathrm{b}}^T, \boldsymbol{q}^T)^T \in \mathbb{R}^4$. The joints are driven by series elastic actuators (SEAs) comprising torsional springs of constant stiffness $k = 1.46\mathrm{N\,m\,rad^{-1}}$ and damping coefficient $c = 0.0219\mathrm{N\,m\,s\,rad^{-1}}$. The actuators deviate the springs by an angle $\boldsymbol{\theta}$ from their equilibrium position. One SEA directly actuates the hip joint, while the second is connected to the knee via a belt drive. The resulting kinematic coupling allows for an independent influence of the SEAs on either joint coordinate [21]. Thus, we can describe the system by

$$\boldsymbol{M}(\boldsymbol{x})\ddot{\boldsymbol{x}} + \boldsymbol{C}(\boldsymbol{x}, \dot{\boldsymbol{x}})\dot{\boldsymbol{x}} + \boldsymbol{g}(\boldsymbol{x}) = \begin{pmatrix} \boldsymbol{0} \\ k(\boldsymbol{\theta} - \boldsymbol{q}) - c\dot{\boldsymbol{q}} \end{pmatrix} + \boldsymbol{\tau}_{\mathrm{contact}} \tag{8}$$

The symmetric, positive definite inertia matrix is denoted by $\boldsymbol{M}(\boldsymbol{x})$, $\boldsymbol{C}(\boldsymbol{x}, \dot{\boldsymbol{x}})$ represents the generalized Coriolis and centrifugal matrix, $\boldsymbol{g}(\boldsymbol{x})$ gravitational forces, and $\boldsymbol{\tau}_{\mathrm{contact}}$ the generalized external force. We describe the controller

$$\boldsymbol{\theta} = \hat{\theta}\frac{\boldsymbol{w}}{\|\boldsymbol{w}\|} = \hat{\theta}\begin{pmatrix} \sin(\alpha) \\ \cos(\alpha) \end{pmatrix} \tag{9}$$

by its Euclidean norm, $\hat{\theta} \in \mathbb{R}_{\geq 0}$, and the angle of the transformation weights, $\alpha \in [\pi, 2\pi]$. The constraint on α prevents ambiguity, since a change of α by π corresponds to a change of sign in $\hat{\theta}$. During jumping movement, the leg forms a hybrid model and alternatively switches between a standing and flying phase. During the contact phase, the foot and the ground form a fixed, unilateral contact point. We apply a rigid ground model because the differential equation solver restricts the use of stiff differential equations. Base rotation is locked, since in the long run we are interested in multi-legged systems. These systems have a high trunk inertia and can adjust their rotation independently from the jumping due to redundant degrees of freedom. Our choice results in fully actuated system dynamics during the stance phase, i.e. the number of actuators equals the number of degrees of freedom of the system. The initial position is defined by a vertical alignment of base and foot. While the foot is initially attached to the ground, we choose the height of the base that prevents any initial vertical acceleration on the trunk. Lift-off occurs when the vertical projection of the force constraining the foot to the ground switches its sign, whereas landing takes place upon ground contact.

Numerical Extraction of Optimal Controller: To find the optimal control law in the modal sub-manifold, we search for the optimal parameter α^* and piece-wise continuous control $\hat{\theta}^*(t)$. By *optimal* we hereby imply that for time-constant α the objective function is minimized, which is given in Mayer form by the negative jumping height

$$\mathcal{J}(\alpha, \hat{\theta}(t)) = -x_{\mathrm{b2}}(t_{\mathrm{end}}) \ . \tag{10}$$

For this purpose, we use a numerical approach for the optimal control of time-continuous multiple-phase dynamical systems as implemented in *GPOPS-II* [20]. The state of the mechanical system is described by $(\boldsymbol{x}^T, \dot{\boldsymbol{x}}^T)$ and the state equation $\boldsymbol{f} = \left(\dot{\boldsymbol{x}}^T, \ddot{\boldsymbol{x}}^T\right)^T$ is obtained from (8). According to the *hp-adaptive Gaussian quadrature collocation* method, GPOPS-II divides the time interval of interest into specific mesh points and discretizes the state at these points. The optimal control problem is then transformed into a nonlinear programming problem and is solved using IPOPT [22]. States are estimated using Lagrange polynomials, and both the number of mesh points and the degree of the polynomial are dynamically adjusted. We allow for a maximal simulated time of 6s and 8 consecutive jumps, which we empirically found to be the maximum number supported by GPOPS-II. The control is only

active during the standing phase and the control set is given by $\alpha \in [\pi, 2\pi]$ as described before and $\hat{\theta} \in [-0.15\text{rad}, 0.15\text{rad}]$. The latter constraint restricts the spring deflections that the controller can induce equivalently to the bang-bang amplitude in (3). The energy inserted during a controller switching decreases linearly with $\boldsymbol{w}^T\boldsymbol{q}$. It is therefore maximized when the joint positions $\boldsymbol{q}$ and the weights $\boldsymbol{w}$ have opposite directions and $\boldsymbol{q}$ has maximum amplitude. A given spring deflection of amplitude $\hat{\theta}_z$ thus inserts the maximum energy at peak positions of $\boldsymbol{q}$, which means that for a given maximum value for $\hat{\theta}_z$ we induce the maximum energy when deflecting the springs instantaneously at the according point in time. The constraint accordingly renders it likely that the derived optimal controller amplitude $\hat{\theta}^*(t)$ will show bang-bang behavior.

B. Results

The derived optimal trajectory requires less than 6s to reach its peak jumping height, which indicates that time does not limit the performance of the derived controller.

As illustrated in Fig. 1B and 1C, the jumping trajectory approximately converges to a limit cycle with duration $T \approx 0.41\text{s}$. The difference between two successive peak heights of the trajectory decreases monotonically. An exponential fit, plotted in the same figure, indicates that the jumping height converges to a final value of 4.77cm. Convergence takes place with a time constant of approximately 2.19s. The optimal transformation weights are represented by $\alpha^* = 1.75\pi$, which corresponds to $(1, -1)^T$ as represented in the spanning set formed by the joint coordinates. This can be considered as a linear eigenvector of the nonlinear system. The orthogonal second eigenvector of the two-dimensional system would be described by $\alpha_{\text{EV2}} = 0.25\pi$. The controller $\hat{\theta}$ shows clear bang-bang-behavior and switches instantly from the minimum to maximum value of the controller set, as demonstrated in Fig. 1D. The switching occurs when the trunk crosses its lowest position with a time difference of $\Delta t < 9.4\text{ms} \approx 0\,02T$ (restricted by the numerical resolution). According to (7), the optimal controller thus inserts the same maximum possible energy into the system during each jump and not just during the final one. All of these findings indicate that the optimal controller, which maximizes the movement amplitude of the final jump, follows the same law during each of the preceding jumps. The goal of optimizing the height of an individual jump therefore requires to optimize each of the preceding jumps, which is achieved in a periodic movement. If only the final standing phase had an influence on the final jumping height, we would expect the controller to insert arbitrary amounts of energy during the earlier phases. All of these findings in summary indicate that a series of equivalently actuated preceding jumps induces maximum movement amplitude and an optimal controller leads to periodic movement.

The results furthermore emphasize the intrinsic stability of our control approach. For a given maximal amplitude $\hat{\theta}_z$, the obtained controller represents a version of our suggested algorithm where α and ϵ_τ are chosen to insert the maximum energy in the most energy-efficient way. Under this extreme condition, the trajectory still converges.

IV. OPTIMALITY OF THE MODAL TRANSFORMATION

We turn the focus to the linear weights of the mapping between the sensory/actuation and controller space. We will first investigate the influence that deviations from the optimal weights have on the controller performance and then test the second assumption of our approach, i.e. that the weights can be assumed constant during the movement cycle.

A. Methods

Deviations from Optimal Value: Using the same mechanical system as described in Sect. III-A, we fix α to 18 equally spaced values within $[1.1\text{rad}, 1.95\text{rad}]$ and leave the remaining parameters of the optimal control problem unchanged. For each trial, the final jumping height is recorded.

Influence of Time Independency: To check whether the optimal transformation weights are time-independent, we allow for $\alpha = \alpha(t)$ and use GPOPS-II to search for $\hat{\theta}^*(t)$ and $\alpha^*(t)$ that maximize the jumping height. All other conditions remain unchanged. Resonance in a linear two-dimensional system would require to drive the system along a constant eigenmode. In an additional trial, we test if a potentially observed deviation from the linearized expectation $\alpha^*(t) = \alpha_{\text{EV1}}$ results from coupling between the linearized eigenmodes either in the inertia matrix $\boldsymbol{M}(\boldsymbol{x})$ or the Coriolis and centrifugal matrix $\boldsymbol{C}(\boldsymbol{x}, \dot{\boldsymbol{x}})$. For this purpose, we reduce the masses of the links to zero. Since the numerically obtained eigenmode $(1, -1)^T$ induces a straight vertical jumping movement of the base in this system, a deviation would be due to coupling in the Coriolis and centrifugal force.

B. Results

Deviations from Optimal Value: When the transformation angle is fixed to different values, the optimal amplitude $\hat{\theta}^*(t)$ remains bang-bang (not illustrated). Figure 2A demonstrates that the maximum jumping height varies between 1.82cm and 4.78cm for different angles. For the current mechanical configuration, weight variations thus allow performance increases in terms of jumping height of up to 263%.

Influence of Time Independency: The optimal controller $\hat{\theta}^*(t)$ continues to show bang-bang-like behavior also under time-varying transformation weights, as illustrated in Fig. 2B. While $\alpha^*(t)$ remains equal to α_{EV1} directly after landing and before take-off for a major proportion of the trajectory, $\alpha^*(t)$ deviates from the linear eigenvector when the joints are increasingly deviated from their equilibrium position. At the point of maximum deviation, i.e. the minimum trunk height, both $\alpha^*(t)$ and $\hat{\theta}^*(t)$ are discontinuous. Expressed in Cartesian coordinates as represented by $\boldsymbol{\theta}(t)$ in (9), the controller describes a continuous semicircle during the standing phase before it is switched off at onset of the flying phase. The time-variation in transformation weights leads to an increase of the final jumping height of 1.9% in comparison to constant weights. The trajectory of the base, shown in Fig. 2C, is a loop. When the link masses are reduced to zero, this behavior remains (cf. same figure). For both systems, it is thus advantageous to insert some energy via the empirically derived eigenmode $(1, 1)^T$ at larger joint deflections, although

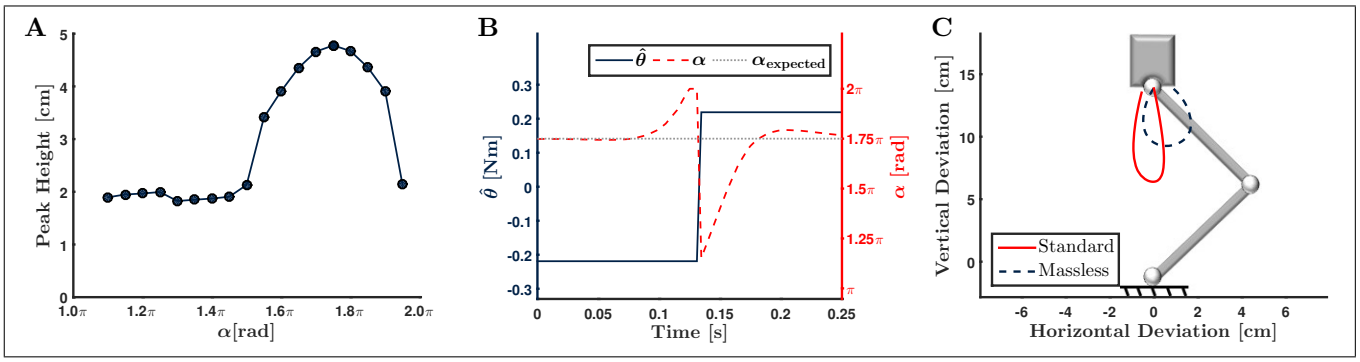

Fig. 2. **(A)** When the optimal control is subject to a pre-defined fixed α, the maximum jumping height varies strongly with the weight angle. The minimum jumping heights are consistently found for $\alpha < 1.5\pi$. This range qualitatively differs from $\alpha > 1.5\pi$, since in the former range both joints share the same sign and one of them will thus always counteract the jumping movement. **(B)** We test the influence of time independency of the transformation weights by allowing for time-dependent weights and search for the controller that maximize the jumping height. The derived control is plotted for one jumping period. Since the control is fixed during the flying phase, only the standing phase is illustrated. The x-axis shows the time that has passed since the onset of the standing phase, not the total simulated time. In agreement with Fig. 1, the controller magnitude $\hat{\theta}$ follows a bang-bang law. The angle $\alpha(t)$ varies continuously with one discontinuous jump from 2π to π, which occurs simultaneously with the sign switch of $\hat{\theta}$. The included reference line shows that the optimal angle agrees with the numerically derived value of $\alpha = 1.75\pi$ at the beginning and the end of the standing phase. **(C)** The trajectory of the base under time-varying weights follows a loop. The dashed line illustrates that it qualitatively remains a loop for massless links, despite quantitative changes.

only $(1,-1)^T$ relates to vertical movement. This agrees with analytic findings by Lakatos et al. [23] who derived the system dynamics with these globally constant eigenvectors of the leg with two mass-less limbs. Based on their derivations, one can transform the damping matrix into the eigenspace and finds that the damping associated to the eigemode $(1,1)^T$ falls below that associated to $(1,-1)^T$ for high deflections. The energy injected into the mode $(1,1)^T$ is transferred into the eigenmode $(1,-1)^T$ via coupling. A significant part of this coupling results from the Coriolis/centrifugal and gravitational force, since the effect qualitatively remains when the masses of the limbs are removed, i.e. the inertia matrix is decoupled in modal coordinates.

V. OPTIMALITY OF OJA'S RULE

Under realistic conditions, the linearized eigenmode of a system is analytically unknown and changes with intrinsic and environmental conditions. In order to maximize the jumping height with minimum energy requirements, our algorithm uses Oja's rule in combination with the modal bang-bang controller to extract an adaptable approximation of the eigenmode from sensory information. In the following, we will evaluate its performance in a simulation and an experiment using parameter screening in combination with a Monte Carlo approach.

A. Methods

Simulation: Our mechanical test bed remains the leg described in Sect. III-A. While the differential equation solver used by GPOPS-II restricted us to a rigid ground model, we here use a more realistic ground model with a stiffness of $10^6\mathrm{N\,m^{-1}}$, a damping coefficient of $2\times10^3\mathrm{N\,s\,m^{-1}}$, and a friction coefficient of 1. We set the bang-bang threshold in (3) to $\epsilon_\tau = 0.5\mathrm{N\,m}$, which we found to prevent decay of the movement for a large parameter range. The time constant of Oja's rule is chosen as $\gamma = 0.1\mathrm{s^{-1}}$. To start the movement, we drop the leg with a vertical distance of $0.02\mathrm{m}$ between foot and ground while the joints are at their equilibrium positions. For the Monte Carlo approach, we assign 40 random 2-tuples to the two remaining free parameters of the model, namely the energy $c_{\epsilon\hat{\theta}}$ injected by the controller and the initial angle α_0 of the transformation weights. The energy $c_{\epsilon\hat{\theta}}$ is drawn from the interval $[0.057\mathrm{N\,m}, 0.563\mathrm{N\,m}]$, which we found to induce stable jumping. For each randomly chosen value $c_{\epsilon\hat{\theta}}$ we empirically derive an interval of values for α that prevent movement decay. An initial angle α_0 is randomly drawn from this interval. During the movement, the weights adjust according to (5). After convergence of the trajectory and weights, the final weight is recorded. We hereby define that the trajectory is converged when the states $(x_{\mathrm{b}2}, q_1, q_2, \dot{q}_1, \dot{q}_2)^T$ at two consecutive peak positions differ by less than $10^{-3}\times(10\mathrm{cm}, \pi\ \mathrm{rad}, \pi\ \mathrm{rad}, \pi\ \mathrm{rad\,s^{-1}}, \pi\ \mathrm{rad\,s^{-1}})^T$. To verify that our algorithm obtains the dominant principal component of the motion, we perform a reference principal component analysis (PCA) of the joint trajectories using the according *Matlab* function for example trials.

The performance of Oja's rule is validated by parameter screening using 40 additional trials with constant weights described by regularly spaced $\alpha \in [1.5\pi, 2\pi]$ for each value of $c_{\epsilon\hat{\theta}}$. After convergence of the trajectory, we record the respective jumping height. In order to find the peak angle, associated with the peak jumping height, with high accuracy for each value of $c_{\epsilon\hat{\theta}}$, we run 20 additional trials for the subinterval between the three values of α associated with the maximum height. This procedure is repeated for a regularly spaced set of $c_{\epsilon\hat{\theta}} \in [0.057\mathrm{N\,m}, 0.563\mathrm{N\,m}]$.

Experiment: The robotic leg used as experimental setup corresponds to the simulation model, is illustrated in Fig. 4A, and has been previously described by [21]. Two servo units are serially coupled via torsional springs with constant stiffness $k \approx 2\mathrm{N\,m\,rad^{-1}}$ to a hip and a knee joint, respectively. Stiffness was determined using force-deflection measurements. The connection of the second SEA to the knee joint is established via belt drives, resulting in kinematic coupling of the joints. The trunk is mounted to a boom which prevents rotation of

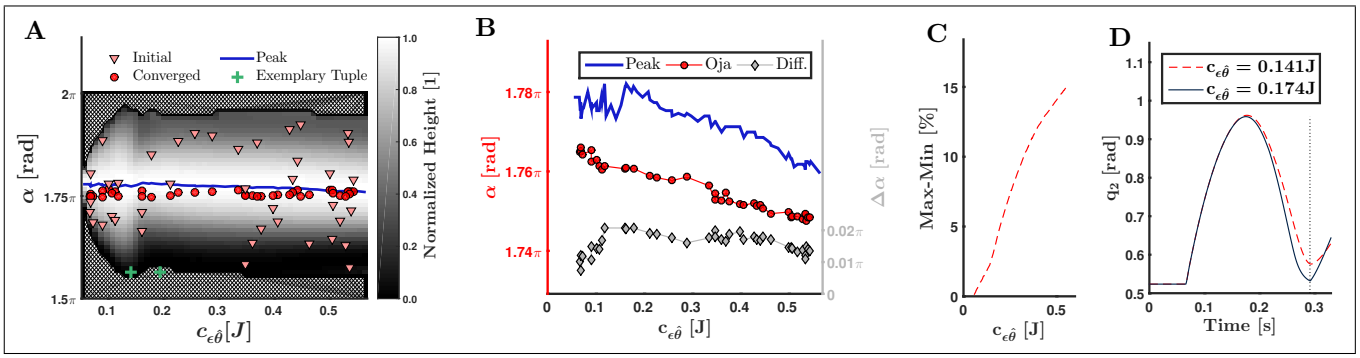

Fig. 3. Simulation results demonstrating the performance of Oja's rule in approximating the local linear eigenmode. **(A)** A parameter screening shows the jumping height as a function of the two free parameters of the bang-bang controller, i.e. the energy $c_{\epsilon\hat{\theta}}$ injected into the system in each jump and the angle α representing the transformation weight vector. The jumping height is normalized for each value $c_{\epsilon\hat{\theta}}$ and the background represents parameter ranges where jumping falls silent. We randomly choose initial tuples $(c_{\epsilon\hat{\theta}}, \alpha_0)$ and initiate jumping of the leg, while the transformation weights adjust according to Oja's rule. The weights converge to values close to the peak line. For values $c_{\epsilon\hat{\theta}} \gtrsim 0.12$J, the range of α that causes stable jumping decreases abruptly, coincident with the transition from oscillations fixed to the ground to a jumping movement. The reason for the abrupt decrease is explained in the text by the two marked exemplary tuples. **(B)** A zoom into the parameter space shows where the converged weights, as obtained by Oja's rule, deviate most from the peak line. We find a minimum deviation for small and large energy input, corresponding to small oscillations without lift-off and large jumping heights. **(C)** For each energy $c_{\epsilon\hat{\theta}}$ within our chosen interval, we show the maximum improvement in jumping height that can be gained by adjusting the transformation weights. Values are given relative to the minimum jumping height when conditions are excluded that cause decay of the movement. **(D)** The trajectory of the knee joint at the beginning of the movement shows qualitative differences for the exemplary tuples marked in sub-figure (A). For larger energy input $c_{\epsilon\hat{\theta}}$, the joint coordinate is not differentiable with respect to time at the marked moment when the leg touches down, indicating removal of kinetic energy. For smaller energy input, the leg remains attached to the ground and thus the joint coordinate remains differentiable.

the trunk while allowing circular horizontal movement around a fixed center and vertical jumping motion. A sensor at the ground fixation point of the boom measures jumping height and horizontal position.

With the motors switched off, we measure the height profile of the ground to correct the jumping height for variations at different horizontal positions. In the beginning, we run the leg using a bang-bang controller with constant weights and wait for the jumping height to converge exponentially while the servo units reach their operating temperature. To prevent overheating, runs lasting 45s are followed by a cooling phase of 120s. At the beginning of each recording sequence, we measure the trunk height while the servos are at rest, $\boldsymbol{\theta} = \mathbf{0}$, and define jumping height relative to this value. An additional height measurement at the end of a recording sequence checks for occurring static hysteresis. We initiate each movement by applying a standardized delta-stimulus and maintain jumping using a bang-bang controller with $\hat{\theta}_z = 0.2$rad.

In a first recording sequence, we record the trajectory for 10 values of $\alpha \in [1.53\pi, 1.98\pi]$. Each run is followed by a reference run with $\alpha = 1\,75\pi$ to check for repeatability. After convergence of the trajectory, which reliably takes place during the first 10 jumps (cf. example trajectory in Fig. 4B), we average the jumping height for each α.

In a second recording sequence, we initiate α_0 with the minimum and maximum value, $\alpha_{0,\min}$ and $\alpha_{0,\max}$, that allow persistent movement and adapt α according to Oja's rule over several subsequent runs of 45s each. To detect convergence, we average α over each run individually. Convergence is declared when this averaged value is smaller than in the preceding run for trials started with $\alpha_0 = \alpha_{0,\min}$ or larger for trials started with $\alpha_0 = \alpha_{0,\max}$. We measure the respective jumping height that is associated with the initial and final transformation weights twice in an alternating fashion.

B. Results

Simulation: An illustrating overview of the results obtained by the parameter screening and the Monte Carlo approach can be found in Fig. 3A. In Fig. 3B, we zoom into the parameter space to evaluate where the converged weight deviates from the conditions associated with maximum jumping height. We find that the peak angle averaged over the full range of $c_{\epsilon\hat{\theta}}$ amounts to $(1.772 \pm 0.006)\pi$ (mean $\pm$ std), which significantly deviates from the expectation of $1.750\,\pi$. The peak angle varies slightly as a function of $c_{\epsilon\hat{\theta}}$.

Oja's rule reliably extracts the dominant principal component, as verified in comparison to the PCA performed by Matlab. It closely aligns the randomly chosen initial weights with the peak angle (cf. Fig. 3A). In 36 out of 40 trials, our algorithm improves the transformation weights and leads to an angle that is associated with an increased jumping height. If improvement was purely based on chance, we would expect to find 20 successful trials, distributed according to a binomial distribution. This assumption can be rejected by $p < 10^{-6}$. Thus, Oja's rule significantly improves the energy efficiency of the movement. The closest match between the peak angle and the converged weights are found for small and large input energy levels (cf. Fig. 3B). These energy domains are least affected by the nonlinear switching phase of the hybrid model and can hence be best described by linear dynamics, i.e. the assumption that underlies our controller design. For small energy levels, the system shows only minor deviations from its equilibrium position and stays attached to the ground, indicating that the dynamics can be well approximated by a continuous, linear differential equation. At high energy levels, the dynamics are mostly determined by the flight phase, where the effect of the nonlinear coupling is reduced.

To quantify the improvement that adjustments of the transformation weight yield, we derive the relative difference between

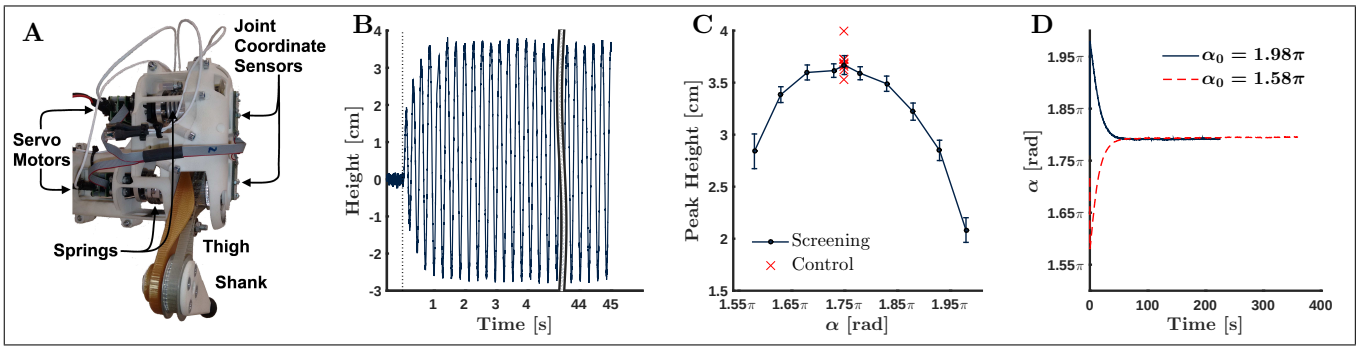

Fig. 4. Results of the experiment. **(A)** The experiments were conducted on a compliant leg that is pictured here. **(B)** An example trunk trajectory. The dotted line indicates the onset of the controller. Fluctuations before this time point illustrate the accuracy of the height sensor. We consistently found that the trajectory converges for less than 10 jumps. **(C)** The average jumping height is plotted as a function of the transformation weights with its peak occurring between $\alpha \in [1.68\pi, 1.78\pi]$. Values of α below the illustrated region lead to a decay of the movement. The parameter space represented in this graph is equivalent to a vertical cross section through Fig. 3A. Each trial is followed by a control recording with $\alpha = 1.75\pi$. The multiple close data points for this value demonstrate that the results are well repeatable throughout the sequence. We averaged them to obtain an additional data point in the screening-curve. Error bars denote the standard deviation over several jumps. **(D)** The transformation weight aligns with the same value under the influence of Oja's rule, independently of the starting conditions. The converged weight lies at the peak of the curve in figure C.

the peak jumping height and the minimum jumping height at each energy value $c_{\epsilon\hat{\theta}}$. Conditions where the leg falls silent are excluded. Figure 3C demonstrates that this difference increases monotonically with $c_{\epsilon\hat{\theta}}$. Within our parameter range, tuning of the transformation weights can lead to relative improvements of more than 15% or 2.6cm.

As a final point that may be noticed in Fig. 3A, the range of transformation weights that lead to periodic movement decreases abruptly for values of $c_{\epsilon\hat{\theta}}$ exceeding approximately 0.12J. This matches the energy required for lift-off, whereas for smaller energies the leg oscillates with the foot attached to the ground. As shown in in Fig. 3D, the touchdown removes kinetic energy from the system, thereby restricting the range of parameters that prevent decay of the movement.

Experiment: In the physical leg, we find that a small range of weights is related to maximum energy efficiency which cannot sensibly be further divided due to natural fluctuations. Our algorithm extracts weights that lie at this plateau and are independent of the initial conditions, as long as these conditions do not directly lead to movement decay. These results are also illustrated in a supplementary video.

In particular, persistent jumping occurs for $\alpha \in [1.58\pi, 1.98\pi]$. In agreement with the simulation results in Fig. 2A, Fig. 4C demonstrates that the jumping height as averaged over several jumps shows a peak for $\alpha \in [1.68\pi, 1.78\pi]$. In the experimental setup, jumping heights associated with this interval differ by less than one standard deviation from the peak height. Thus, a more accurate peak identification is here prevented due to non-periodicity in the limit cycle, sensor noise, and mistakes in the determination of the height profile of the ground. No static hysteresis is found throughout the recordings and the jumping height of the reference measurements at $\alpha = 1.75\pi$ show no obvious tendency over time and as illustrated in Fig. 4C are consistent throughout the recording sequence. Starting from the weights $\alpha_{0,\text{min}} = 1.58\pi$ and $\alpha_{0,\text{max}} = 1.98\pi$, Oja's rule adjusts the weights to $\alpha_{\text{final,min}} = (1.7950 \pm 0.0002)\pi$ and $\alpha_{\text{final,max}} = (1.7920 \pm 0.0002)\pi$, respectively (cf. Fig. 4D). These values lie exactly at the border of the peak area of Fig. 4C, and the associated jumping heights still differ by less than one standard deviation from the peak height. Whereas the simulation results identify a small but significant deviation between converged and optimal weights, the higher noise therefore renders the differences irrelevant in the experiment. Our trials with initial and converged weights quantify the relative improvement of the jumping height to 31% and 67%, respectively. The latter corresponds to an absolute improvement of 1.4cm.

VI. DISCUSSION

We recently suggested a computationally simple control approach that induces stable periodic movement in elastic multibody systems. The present paper concentrates on the proposed system-specific time-independent linear transformation between the joint space and a one-dimensional controller space. While a modal transformation is analytically known to be optimal in terms of energy efficiency for mechanical systems with continuous linear dynamics, we here investigate its performance in the control of resonance in hybrid dynamical systems with nonlinear coupling between the joints. We show that a previously proposed algorithm can use sensory information about joint deflections to extract transformation weights that induce limit cycles of energy efficiency which is indistinguishable from an optimal trajectory for noisy physical systems. This finding is independent of the initial weights.

The simulation results show two shortcomings of our algorithm: Firstly, optimal transformation weights vary during the movement cycle, which improves the performance in the single-digit percentage area. This small increase can be expected to be irrelevant for applications in experimental systems, where model-based optimal control laws suffer from deficits in the underlying model. Furthermore, the difference has minor influence on the jumping height in comparison to adaptations by our (model-free) adaptation law, since the latter can increase the height by several magnitudes. Secondly, our Monte Carlo approach demonstrates that Oja's rule does not precisely extract the optimal linear weights. However, our extracted weights lie on a peak plateau of weights whose mutual

difference in jumping height is obscured by fluctuations due to intrinsic noise of the system.

In accordance with earlier research, the present study focuses on bang-bang controllers. This choice is due to their previously demonstrated robustness properties and the ability to generate asymptotically stable limit cycles. Our algorithm leads to higher relative improvements for a smaller bang-bang threshold, as this decreases the minimum energy required for persistent movement, which lowers the minimum, i.e. reference, jumping height. Thus, we find a smaller relative, but similar absolute, increase in the jumping height in the simulations in comparison to the experiments with smaller threshold. Our experiments show high performance increases of up to 68% and potentially more for higher energy input.

We concentrate on a jumping leg since highly dynamical locomotion is a promising beneficiary of compliant structures due to the high power demands and occurring peak forces. Two findings render our algorithm especially advantageous for this motion type: On the one hand, the optimization of constant weights yields higher improvements here, presumably because higher forces allow elastic elements to store more energy. On the other hand, Oja's rule extracts optimal weights with increasing accuracy at higher motion amplitude.

Oja's rule is widely known as description for calculations performed by the animal nervous system [10], [13]. Furthermore, the presented control approach leads to highly stable motion. Based on these aspects, we previously suggested that the approach may describe aspects of the sophisticated movement control of animals [10], [16]. The obtained strong and reliable increase in jumping performance the we find here emphasizes our hypothesis that it describes neural calculations as shaped by evolutionary constraints.

Our present focus lies on the energy used for mechanical actuation. Our algorithm is additionally energy-efficient in terms of computational power requirements and sensing hardware. While other previously suggested adaptable controllers spend a significant amount of energy for these purposes [24], the calculations of our algorithm are computationally simple and require to store only the modal transformation weights during execution, while information about joint forces and deflections suffice as sensory input.

Future work on the control of elastic multibody systems may use the modular nature of our coordinate transformation, which adjusts a low-dimensional control signal to yield an energy-efficient movement of several joints without constraints on the signal. In the controller sub-manifold, a modular controller may combine commands for non-energetic purposes that have different origins, such as sensory and internally generated signals. Such a controller may also produce two-dimensional commands that target different limbs in anti-phasic gaits like running without considerations about individual joints.

ACKNOWLEDGMENT

Thanks to D. Seidel for infrastructural work on the robot.

REFERENCES

[1] T. Buschmann, A. Ewald, A. von Twickel, and A. Buschges, "Controlling legs for locomotion - insights from robotics and neurobiology," *Bioinspir Biomim*, vol. 10, no. 4, p. 041001, Aug 2015.

[2] K. Sreenath, H.-W. Park, I. Poulakakis, and J. Grizzle, "A compliant hybrid zero dynamics controller for stable, efficient and fast bipedal walking on MABEL," *Int J Robot Res*, 2010.

[3] A. Shiriaev, L. Freidovich, and I. Manchester, "Can we make a robot ballerina perform a pirouette? Orbital stabilization of periodic motions of underactuated mechanical systems," *Annu Rev Control*, vol. 32, pp. 200–211, Jul 2008.

[4] D. J. Braun, M. Howard, and S. Vijayakumar, "Exploiting variable stiffness in explosive movement tasks," in *Robotics: Science and Systems VII*, Los Angeles, CA, USA, June 2011.

[5] G. Garofalo, C. Ott, and A. Albu-Schäffer, "Orbital stabilization of mechanical systems through semidefinite Lyapunov functions," in *2013 American Control Conference*, June 2013, pp. 5715–5721.

[6] S. Stramigioli and M. van Dijk, "Energy conservation limit cycle oscillations," in *International Federation Of Automatic Control, Proceedings Of The 17th World Congress*, 2008, pp. 15 666–15 671.

[7] T. Nachstedt, F. Wörgötter, and P. Manoonpong, "Adaptive neural oscillator with synaptic plasticity enabling fast resonance tuning," in *Artificial Neural Networks and Machine Learning at ICANN 2012*, A. Villa, W. Duch, P. Érdi, F. Masulli, and G. Palm, Eds. Springer Berlin Heidelberg, 2012, vol. 7552, pp. 451–458.

[8] X. Xiong, F. Wörgötter, and P. Manoonpong, "Adaptive and energy efficient walking in a hexapod robot under neuromechanical control and sensorimotor learning," *Cybernetics, IEEE Transactions on*, vol. PP, no. 99, 2015.

[9] J. Buchli and A. J. Ijspeert, "Self-organized adaptive legged locomotion in a compliant quadruped robot," *Autonomous Robots*, vol. 25, no. 4, pp. 331–347, 2008.

[10] P. Stratmann, D. Lakatos, and A. Albu-Schäffer, "Neuromodulation and synaptic plasticity for the control of fast periodic movement: Energy efficiency in coupled compliant joints via PCA," *Front Neurorobot*, vol. 10, no. 2, 2016.

[11] D. Lakatos, M. Gorner, F. Petit, A. Dietrich, and A. Albu-Schäffer, "A modally adaptive control for multi-contact cyclic motions in compliantly actuated robotic systems," in *Intelligent Robots and Systems, 2013 IEEE/RSJ Intl Conf on*, 2013, pp. 5388–5395.

[12] D. Lakatos, F. Petit, and A. Albu-Schäffer, "Nonlinear oscillations for cyclic movements in human and robotic arms," *Robotics, IEEE Transactions on*, vol. 30, no. 4, pp. 865–879, Aug 2014.

[13] E. Oja, "Simplified neuron model as a principal component analyzer," *Journal of Mathematical Biology*, vol. 15, no. 3, pp. 267–273, 1982.

[14] K. D. Miller and D. J. C. MacKay, "The role of constraints in Hebbian learning," *Neural Computation*, vol. 6, pp. 100–126, 1994.

[15] D. Lakatos and A. Albu-Schäffer, "Switching based limit cycle control for compliantly actuated second-order systems," in *Proceedings of the IFAC World Congress*, vol. 19, no. 1, 2014, pp. 6392–6399.

[16] D. Lakatos and A. Albu-Schäffer, "Neuron model interpretation of a cyclic motion control concept," in *5th IEEE Intl Conf on Biomedical Robotics and Biomechatronics*, Aug 2014, pp. 905–910.

[17] B. Feeny and R. Kappagantu, "On the physical interpretation of proper orthogonal modes in vibrations," *J. Sound Vibration*, vol. 211, no. 4, pp. 607 – 616, 1998.

[18] G. Kerschen and J. C. Golinval, "Physical interpretation of the proper orthogonal modes using the singular value decomposition," *Journal of Sound and Vibration*, vol. 249, no. 5, pp. 849 – 865, 2002.

[19] G. Kerschen, J.-c. Golinval, A. F. Vakakis, and L. A. Bergman, "The method of proper orthogonal decomposition for dynamical characterization and order reduction of mechanical systems: An overview," *Nonlinear Dynamics*, vol. 41, no. 1, pp. 147–169, 2005.

[20] M. A. Patterson and A. V. Rao, "GPOPS-II: A MATLAB software for solving multiple-phase optimal control problems using hp-adaptive Gaussian quadrature collocation methods and sparse nonlinear programming," *ACM Trans. Math. Softw.*, vol. 41, no. 1, pp. 1:1–1:37, oct 2014.

[21] D. Lakatos, D. Seidel, W. Friedl, and A. Albu-Schäffer, "Targeted jumping of compliantly actuated hoppers based on discrete planning and switching control," in *Intelligent Robots and Systems (IROS), 2015 IEEE/RSJ Intl Conf on*, Sept 2015, pp. 5802–5808.

[22] T. L. Wächter, Andreasand Biegler, "On the implementation of an interior-point filter line-search algorithm for large-scale nonlinear programming," *Math Program*, vol. 106, no. 1, pp. 25–57, 2005.

[23] D. Lakatos, W. Friedl, and A. Albu-Schäffer, "Modal dynamics matching: embodying fundamental locomotion modes into legged robots with elastic elements," Submitted to RA-L/ICRA, 2017.

[24] Y. Mei, Y.-H. Lu, Y. C. Hu, and C. S. G. Lee, "A case study of mobile robot's energy consumption and conservation techniques," in *ICAR, 12th Intl Conf on Advanced Robotics*, July 2005, pp. 492–497.

Neuromodulation and synaptic plasticity for the control of fast periodic movement: energy efficiency in coupled compliant joints via PCA

Authors Philipp Stratmann, Dominic Lakatos, Alin Albu-Schäffer

Journal Frontiers in Neurorobotics

Number of pages 20 (main article) + 2 (supplementary)

Review Peer reviewed

Abstract There are multiple indications that the nervous system of animals tunes muscle output to exploit natural dynamics of the elastic locomotor system and the environment. This is an advantageous strategy especially in fast periodic movements, since the elastic elements store energy and increase energy efficiency and movement speed. Experimental evidence suggests that coordination among joints involves proprioceptive input and neuromodulatory influence originating in the brain stem. However, the neural strategies underlying the coordination of fast periodic movements remain poorly understood. Based on robotics control theory, we suggest that the nervous system implements a mechanism to accomplish coordination between joints by a linear coordinate transformation from the multi-dimensional space representing proprioceptive input at the joint level into a one-dimensional controller space. In this one-dimensional subspace, the movements of a whole limb can be driven by a single oscillating unit as simple as a reflex interneuron. The output of the oscillating unit is transformed back to the joint space by the reverse transformation. The transformation weights correspond to the dominant principal component of the movement. In this study, we propose a biologically plausible neural network to exemplify that the central nervous system (CNS) may encode our controller design. Using theoretical considerations and computer simulations, we demonstrate that spike-timing-dependent plasticity (STDP) for the input mapping and serotonergic neuromodulation for the output mapping can extract the dominant principal component of sensory signals. Our simulations show that our network can reliably control mechanical systems of different complexity and increase the energy efficiency of ongoing cyclic movements. The proposed network is simple and consistent with previous biologic experiments. Thus, our controller could serve as a candidate to describe the neural control of fast, energy-efficient, periodic movements involving multiple coupled joints

Author contributions Researched literature; derived the hypothesis on the effect of serotonergic modulation in the spinal cord; mathematically modeled and analyzed the effect of serotonin; co-designed the simulations; implemented and ran the simulations; analyzed the results; composed the manuscript; handled review.

frontiers in Neurorobotics

ORIGINAL RESEARCH
published: 08 March 2016
doi: 10.3389/fnbot.2016.00002

Neuromodulation and Synaptic Plasticity for the Control of Fast Periodic Movement: Energy Efficiency in Coupled Compliant Joints via PCA

Philipp Stratmann[1,2]*, *Dominic Lakatos*[2] and *Alin Albu-Schäffer*[1,2]

[1] Department of Informatics, Sensor Based Robotic Systems and Intelligent Assistance Systems, Technische Universität München, Garching, Germany, [2] Institute of Robotics and Mechatronics, German Aerospace Center, Weßling, Germany

There are multiple indications that the nervous system of animals tunes muscle output to exploit natural dynamics of the elastic locomotor system and the environment. This is an advantageous strategy especially in fast periodic movements, since the elastic elements store energy and increase energy efficiency and movement speed. Experimental evidence suggests that coordination among joints involves proprioceptive input and neuromodulatory influence originating in the brain stem. However, the neural strategies underlying the coordination of fast periodic movements remain poorly understood. Based on robotics control theory, we suggest that the nervous system implements a mechanism to accomplish coordination between joints by a linear coordinate transformation from the multi-dimensional space representing proprioceptive input at the joint level into a one-dimensional controller space. In this one-dimensional subspace, the movements of a whole limb can be driven by a single oscillating unit as simple as a reflex interneuron. The output of the oscillating unit is transformed back to joint space via the same transformation. The transformation weights correspond to the dominant principal component of the movement. In this study, we propose a biologically plausible neural network to exemplify that the central nervous system (CNS) may encode our controller design. Using theoretical considerations and computer simulations, we demonstrate that spike-timing-dependent plasticity (STDP) for the input mapping and serotonergic neuromodulation for the output mapping can extract the dominant principal component of sensory signals. Our simulations show that our network can reliably control mechanical systems of different complexity and increase the energy efficiency of ongoing cyclic movements. The proposed network is simple and consistent with previous biologic experiments. Thus, our controller could serve as a candidate to describe the neural control of fast, energy-efficient, periodic movements involving multiple coupled joints.

Keywords: movement generation, compliant actuators, control theory, spike-timing-dependent plasticity, neuromodulation, principal component analysis

OPEN ACCESS

Edited by:
Miriam Zacksenhouse, Technion - IIT, Israel

Reviewed by:
Cristiano Alessandro, Northwestern University, USA
Poramate Manoonpong, The University of Southern Denmark, Denmark

***Correspondence:**
Philipp Stratmann
philipp.stratmann@dlr.de

Received: *13 October 2015*
Accepted: *22 February 2016*
Published: *08 March 2016*

Citation:
Stratmann P, Lakatos D and Albu-Schäffer A (2016) Neuromodulation and Synaptic Plasticity for the Control of Fast Periodic Movement: Energy Efficiency in Coupled Compliant Joints via PCA. Front. Neurorobot. 10:2. doi: 10.3389/fnbot.2016.00002

1. INTRODUCTION

During fast periodic motions, such as jumping or drumming, animals exploit the natural dynamics of their elastic locomotor systems to achieve high velocity in an energy-efficient manner (Bar-Cohen, 2011, p. 514). Their central nervous systems (CNSs) are able to quickly adjust the control of periodic movements that involve several joints to face changes of their environment or intrinsic body properties (Hatsopoulos and Warren, 1996; Zondervan et al., 2014). The underlying control problem is highly complex, as the locomotor systems have multiple joints that have non-linear compliances and are dynamically coupled. For a controller algorithm to replicate the CNS's locomotion control, it must be able to induce stable movement and quickly tune it to high energy efficiency under varying mechanical conditions, while being consistent with biological experiments.

Fast, or explosive, movements such as jumping are typically compound movements that involve synchronous trajectories of several joints in a single or several limbs (Freund and Büdingen, 1978; Morasso, 1981). The synchronicity enables high maximum force and thereby allows to take advantage of elastic dynamics. This can increase the resulting energy efficiency and thereby movement speed. Energy efficiency implies that for constant energy input a controller increases the energy within a mechanical system, as e.g., represented by an increased jump height (cf. Section 4.7.3). In systems with one degree of freedom, maximum energy efficiency implies correct timing of the controller output. In natural explosive movements involving several joints, it also requires the adjustment of the relative amplitude of motor signals at different joints. For the remainder of this article, the latter mechanism shall be denoted as *intra-limb coordination*.

In neuroscience, both theoretical and experimental studies have described neural mechanisms that can induce stable movements in an elastic locomotor system via central pattern generators (CPGs) or reflex arcs (cf. Buschmann et al., 2015 for a review). Theoretical research has extensively analyzed the question on how compliant systems can be tuned to yield energy-efficient movements on artificial models with a single joint (Brambilla et al., 2006; Righetti et al., 2006; Pelc et al., 2008; Barikhan et al., 2014; Huang et al., 2014). Studies considering multiple joints showed that frequency adjustment can be achieved by multiple coupled CPGs, one for each joint involved, that are entrained to proprioceptive input. Multiple CPGs are especially beneficial in non-synchronous movements of the joints, where phase-tuning between different joints is required and where different joints in a limb could execute functionally different tasks, such as forward/backward movement vs. elevation/depression in insect gaits (Nachstedt et al., 2012; Xiong et al., 2015). Buchli and Ijspeert (2008) demonstrate that multiple coupled CPGs, one for each actuated joint, can also be used to find the resonance frequency of fast compound periodic movements. However, the use of multiple CPGs neglects the described synchronicity in joint trajectories. Furthermore, tuning for higher energy efficiency also requires intra-limb tuning, i.e., to adjust the relative amplitude of motor signals at different joints.

Previous experimental research has considered both frequency and intra-limb tuning. Measurements on decerebrate cats demonstrated that signals from individual group I nerves converge in spinal pathways to entrain the frequency of all muscles involved (Whelan et al., 1995a; Hiebert et al., 1996). The efficacy of individual nerves to cause entrainment is dependent on their activity. The influence of a silenced nerve decreases with time, whereas an increased influence is found for nerves originating from muscles that assist in the same movement as the silenced one (Whelan et al., 1995b). Intra-limb coordination of explosive movements was found to be controlled by circuits in the brain stem and cerebellum (MacKay-Lyons, 2002; Shemmell et al., 2009). Furthermore, Animal studies found a disruption of intra-limb coordination after administration of a serotonin-antagonist (Pearlstein et al., 2005; Harris-Warrick, 2011). Serotonin (5-HT) metabotropically increases the excitability of motoneurons (Heckmann et al., 2005; Heckman et al., 2008; Perrier et al., 2013). It is released into the spinal cord by the raphe nucleus obscurus, pallidus and medianus (Jacobs et al., 2002), which reside in the brain stem. Since they receive proprioceptive input (Springfield and Moolenaar, 1983), the raphe neurons may be part of a motor feedback loop. The resulting absolute strength of motor signals during ballistic periodic movements can largely exceed the signal during maximum voluntary contractions (Dietz et al., 1979). Despite these experimental findings, neural pathways underlying the control of stable and energy-efficient explosive movements are poorly understood (Taube et al., 2012). In summary, current knowledge about the algorithm that the CNS encodes to tune ballistic periodic movements does not explain how the CNS maintains stable movement while tuning the frequency and inter-joint coordination to high energy efficiency. A physically motivated theoretical control approach would allow to link the experimental knowledge into a comprehensive framework.

Roboticists increasingly mimic the non-linear compliances of muscles and tendons in joints of mechanical robotic systems such as *BigDog* by *Boston Dynamics* (Raibert et al., 2008) or the *Hand Arm System* from the *German Aerospace Center* (*DLR*; Grebenstein et al., 2011). The control approaches developed by robot designers for controlling these bio-inspired robots can be a valuable source of hypotheses for neuroscientists. Several control algorithms have been suggested to induce stable and energy-efficient limit-cycle movements in compliant hybrid systems. However, their characteristics disqualify most designs as hypothesis for neural movement control. Van-der-Pol oscillators (Stramigioli and van Dijk, 2008) artificially damp systems and thereby reduce the energy efficiency of the movement. Poincaré-map based algorithms (Sreenath et al., 2010) cannot adequately adjust to different environments due to their dependence on a prior model and a fixed set of considered initial conditions. The same point argues against optimal-control algorithms, which additionally require numerical approaches and thus high computational power for multiple joints (Braun et al., 2011).

In this study, we propose an algorithm that was purely derived by engineering considerations on the control of biomechanically inspired robotic systems, to describe how the CNS may

tune ballistic periodic movements to energy efficiency. We have previously shown that under specific intrinsic damping properties of muscles, tendons, and joints, the control of fast periodic movements can be reduced to exciting the local linear approximation of the non-linear mode of the system (Lakatos and Albu-Schäffer, 2014a; Lakatos et al., 2014). The corresponding algorithm linearly transforms sensory input from the multi-dimensional joint space into a one-dimensional controller space. The input entrains a driving unit, and the driving motor output is reversely transformed into the joint space. Multiplicative transformation weights are recurrently adapted and a driving unit as simple as a single reflex interneuron can adjust movements to unknown oscillatory patterns within few step cycles (Lakatos et al., 2013a,b).

Our algorithm does not share the adverse characteristics with the previous robotic control approaches mentioned above. It requires no prior model but needs only sensory information about joint deflections or forces. Additionally, the algorithm performs only linear calculations. This agrees with the recent findings from calculations performed by spinal interneurons (Spanne et al., 2014). In our previous work, we analytically proved stability of controlled mechanical systems with a single degree of freedom (Lakatos and Albu-Schäffer, 2014b). We numerically demonstrated stability in simulations for a controlled quadruped with 12 hinge joints (Lakatos and Albu-Schäffer, 2014a) and in a real robotic platform with four joints (Lakatos et al., 2013b).

For the remainder of this paper, we propose an exemplary neural network implementation of this algorithm in Section 2. By theoretical considerations and simulations of this network in Sections 2.2 and 2.3, respectively, we justify that the algorithm proposed by Lakatos et al. (2013b) may be implemented by the CNS to control fast periodic movements that involve several synchronously moving joints. At the input stage, we suggest that proprioceptive input converges from all muscles involved in a movement onto a single interneuron. Synaptic weights can align with the appropriate linear transformation weights under the influence of spike-timing-dependent plasticity (STDP). At the output stage, we show that serotonergic amplification of motoneuron output can produce the reverse transformation via the described motor feedback of medullary raphe nuclei. Our simulations substantiate that the proposed network can induce highly energy-efficient, stable, periodic movements in mechanical systems of different complexity. While we demonstrate in Section 3.2.2 that our neural sub-networks are consistent with previous experiments, we emphasize that our general controller design may be implemented by alternative circuits. Therefore, we discuss general mathematical requirements set by the controller and provide experimentalists with a checklist of necessary characteristics of a neural implementation in Section 3.3.

Our proposed transformation provides a functional unit that drives several joints with a sensory entrainment signal. The reverse transformation applied to the driving signal leads to correct intra-limb coordination. We argue in the discussion that the driving unit itself can be a pool of reflex interneurons, a CPG or a combination of both.

2. RESULTS

Following an overview on the controller introduced by Lakatos et al. (2013b) and illustrated in **Figure 1A** (cf. Section 2.1.1), we present models of two neural sub-networks that we propose based on previous animal experiments (cf. Sections 2.2.1 and 2.2.2, **Figure 1B**). We theoretically demonstrate that the network performs the proposed coordinate transformations.

In Section 2.3, we simulate our sub-networks in closed-loop simulations to verify that they can reliably excite stable, energy-efficient periodic movement. Detailed methodological descriptions of the simulations can be found in Section 4.

2.1. Controller Theory

2.1.1. Basic Controller Concept

We consider fast periodic movements with high synchronicity in the joint trajectories. The mathematical controller receives sensory information describing the observed movement, represented by the deflections $\varphi_i(t)$ of joints i from their respective zero position. Using the joint-specific weight vector with entries w_i, sensory signals are linearly combined to obtain a single controller coordinate

$$\varphi_z(t) = \boldsymbol{w}^T(t)\boldsymbol{\varphi}(t). \tag{1}$$

All motor units receive the same timing signal $f_z(t)$ that initiates force production when φ_z crosses a threshold,

$$f_z(t) = \begin{cases} \hat{c}_f & \text{if } \varphi_z(t) > c_\epsilon \\ 0 & \text{otherwise,} \end{cases} \tag{2}$$

where $\hat{c}_f$ and c_ϵ are positive constants. Equation (2) functionally describes both the timing and driving unit as illustrated in **Figure 1B**. It is transformed back into a change of force, $f_i(t)$, in the individual joints i by multiplication with the same weight vector $\boldsymbol{w}$,

$$\boldsymbol{f}(t) = \boldsymbol{w}(t)f_z(t). \tag{3}$$

Exerting these forces on the joints induces stable energy-efficient movements due to correct timing and relative force amplitude (Lakatos et al., 2013b,a).

2.1.2. Transformation Weights

In this study, we focus on the adaptation of the weight vector $\boldsymbol{w}$. It is recursively updated and supposed to converge toward the dominant principal component of the data covariance matrix of the movement, which we denote the principal oscillation mode of the system. This can be achieved using

$$\frac{\mathrm{d}}{\mathrm{d}t}\boldsymbol{w}(t) = \gamma[\boldsymbol{w}^T(t)\boldsymbol{\varphi}(t)]\left(\boldsymbol{\varphi}(t) - [\boldsymbol{w}^T(t)\boldsymbol{\varphi}(t)]\boldsymbol{w}(t)\right), \tag{4}$$

where $\gamma \ll 1$ (Oja, 1992). The formula keeps weights bounded and generally increases the relative magnitude of weights for joints that are heavily involved in a movement.

It is assume that neuroscientific quantities representing weights w_i and sensory input φ_i are positive. We prove in

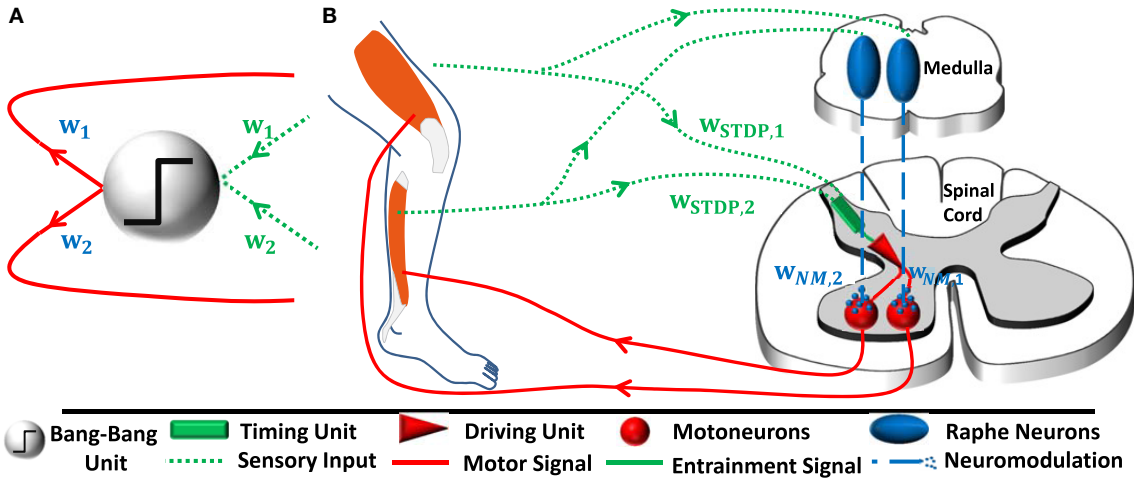

FIGURE 1 | (A) In the mathematical controller design as proposed by Lakatos et al. (2013b), sensory input from each joint *i* is transformed into a one-dimensional coordinate space. For this purpose, the sensory inputs are multiplied by weights w_i. The input entrains a thresholding bang-bang unit, which produces a motor signal. The driving signal is transformed back into the original joint space via the same respective weights. The output transformation accomplishes correct relative force weighting of the individual joints (Figure based on Lakatos and Albu-Schäffer, 2014a). **(B)** In our hypothetical neural controller implementation, sensory input from the joints also converges. The synaptic weights $w_{STDP,i}$ change according to spike-timing-dependent plasticity. We emphasize that the bang-bang controller can be separated into two functionally distinct unit: A timing unit entrains a driving unit, which sends motor signals to muscles innervating all joints involved in a given periodic movement. While functionally distinct, these units do not have to be spatially separated in general. In our model, a single pool of reflex interneurons represents both units and outputs correctly timed motor signals. A parallel, joint-specific, sensory feedback pathway via raphe nuclei releases serotonin into motorpools. This amplifies the common motor output by $w_{NM,i}$ and increases the relative strength of muscles that are more involved in the movement.

the **Presentation 1** that under this assumption the simplified formula

$$\frac{\mathrm{d}}{\mathrm{d}t}\boldsymbol{w}(t) = c_w\boldsymbol{\varphi}(t) - \frac{1}{\tau_{\mathrm{eff}}}\boldsymbol{w}(t), \tag{5}$$

where c_w and τ_{eff} denote arbitrary positive constants, aligns weights $\boldsymbol{w}$ with the result of Equation (4). Using either learning rule, the system will be excited along the principal oscillation mode of the observed movement.

2.2. Neural Implementation of Coordinate Transformations

2.2.1. Input Transformation: Plasticity

For the input transformation, we suggest a simple neural timing network, where proprioceptive input $\nu_{\varphi,i}$ from all synchronously acting muscles converges on a single postsynaptic timing neuron via synapses with weight $w_{\mathrm{STDP},i}$ (cf. *timing unit* in **Figure 1B**). This single neuron could in nature correspond to a pool of postsynaptic neurons. Our network is based on the findings from previous experiments, which have shown that proprioceptors innervating single muscles involved in a periodic movement can adjust the timing of the motor signal that drives all muscles (Whelan et al., 1995a). Under the approximation of linear input summation, the firing rate ν_{post} of the postsynaptic neuron amounts to

$$\nu_{\mathrm{post}}(t) = \boldsymbol{w}^T_{\mathrm{STDP}}(t)\nu_{\boldsymbol{\varphi}}(t). \tag{6}$$

The efficacy of individual muscles to change the timing was found to be subject to plasticity (Whelan et al., 1995b). Assuming that the weights are subject to Hebbian plasticity combined with synaptic scaling, Oja (1982) demonstrated that the weight change of our network can be described by

$$\frac{\mathrm{d}}{\mathrm{d}t}\boldsymbol{w}_{\mathrm{STDP}}(t) = \gamma[\boldsymbol{w}^T_{\mathrm{STDP}}(t)\boldsymbol{\nu}_{\varphi}(t)] \times \left(\boldsymbol{\nu}_{\varphi}(t) - [w^T_{\mathrm{STDP}}(t)\boldsymbol{\nu}_{\varphi}(t)]\boldsymbol{w}_{\mathrm{STDP}}(t)\right). \tag{7}$$

In case that $\nu_{\varphi,i} \propto \varphi_i$, Oja's rule equals Equation (4), and our neural network would transform the input signals from the multi-dimensional joint space into the controller space, i.e., would implement Equation (1).

STDP extends the idea of Hebbian plasticity. It considers both the case of a causally related and unrelated firing of the pre- and postsynaptic neurons. In later simulations, we numerically address the question if also biologically more realistic STDP rules extract the dominant principal component of the motion.

2.2.2. Output Transformation: Neuromodulation

For the output transformation, we model a motor feedback loop via the raphe nucleus medianus, obscurus and pallidus, which release serotonin (5-HT) into the spinal cord. The released 5-HT leads to metabotropic enhancement of motoneuron output (Heckman et al., 2008; Perrier et al., 2013). The feedback loop is based on the fact that the same nuclei receive proprioceptive information and quickly increase their firing rates with sensory input (Springfield and Moolenaar, 1983; Jacobs et al., 2002).

We assume that for each joint *i* involved in the periodic movement there is a group of serotonergic medullary neurons

that receives proprioceptive input $\nu_{\varphi,i}$ via proprioceptors from a joint and project back to the motoneurons innervating this joint exclusively. Their firing rate is thus $\nu_{\text{ser},i} = \nu_{\varphi,i}$ (cf. *raphe neurons* in **Figure 1B**).

The concentration of 5-HT in the extracellular space, denoted [5-HT], increases proportionally to the firing rate of the releasing raphe neurons, ν_{ser} (Hentall et al., 2006; Best et al., 2010). Depletion of 5-HT can occur by reuptake into the cytosol of the cell by the *serotonin transporter* (*SERT*; denoted by V_{SERT}), due to catabolism mainly by monoamine oxidase and aldehyde dehydrogenase (denoted by V_{cat}), or by removal due to glia or diffusion (denoted by V_{rem}) (Best et al., 2010). The rate of change thus amounts to

$$\frac{\text{d[5-HT]}}{\text{d}t} = c_{\text{ser}}\nu_{\text{ser}} - V_{\text{SERT}} - V_{\text{cat}} - V_{\text{rem}}, \tag{8}$$

where c_{ser} is a constant.

Diffusion of 5-HT can be neglected in the spinal cord (Brumley et al., 2007). The remaining mechanisms of disappearance of 5-HT follow Michaelis-Menten kinetics,

$$V_x = \frac{v^x_{\max}}{\frac{k^x_m}{\text{[5-HT]}} + 1} \tag{9}$$

$$\approx \frac{v^x_{\max}}{k^x_m}\text{[5-HT]} \qquad \text{if} \qquad \text{[5-HT]} \ll k^x_m \tag{10}$$

where $v^x_{\max}$ denotes the maximal rate of disappearance and k^x_m the respective Michaelis-constant of mechanism x (Best et al., 2010). The Michaelis constant for depletion due to reuptake by SERTs ranges between 170 and 410nM (Verleysdonk et al., 2004; Best et al., 2010), is larger than 94,000nM for catabolism (Molodtsova, 1983; Best et al., 2010), and around 400nM for glia cells (Katz and Kimelberg, 1985).

After high-frequency stimulation of raphe nuclei *in vivo*, [5-HT] $\ll k^x_m$ in the spinal cord (Hentall et al., 2006). Therefore, the approximation in Equation (10) is valid and Equation (8) reduces to

$$\frac{\text{d[5-HT]}}{\text{d}t} \approx c_{\text{ser}}\nu_{\text{ser}} - \left(\frac{v^{\text{SERT}}_{\max}}{k^{\text{SERT}}_m} + \frac{v^{\text{cat}}_{\max}}{k^{\text{cat}}_m} + \frac{v^{\text{rem}}_{\max}}{k^{\text{rem}}_m}\right)\text{[5-HT]} \tag{11}$$

$$= c_{\text{ser}}\nu_{\text{ser}} - \frac{1}{\tau_{\text{eff}}}\text{[5-HT]}. \tag{12}$$

Extracellular serotonin concentration in a motorpool monotonically and linearly increases the slope of the input-output function of the motoneurons (Heckman et al., 2003). Therefore, we can define multiplicative neuromodulatory weights that describe the amplification of ionotropic input as

$$w_{\text{NM},i} = c_{\text{NM}}\text{[5-HT]}_i. \tag{13}$$

Equation (12) can thus be reformulated to

$$\frac{\text{d}w_{\text{NM},i}}{\text{d}t} = \hat{c}_{\text{ser}}\nu_{\varphi,i} - \frac{1}{\hat{\tau}_{\text{eff}}}w_{\text{NM},i}. \tag{14}$$

Since this is equivalent to Equation (5), our network will lead to an output transformation equivalent to Equation (3).

We suggest that both neural sub-systems finally converge on motorpools. The ionotropic input represented by ν_{post} is proportionally transformed into a motor signal by multiplication with a constant m_f,

$$f_z(t) = m_f\nu_{post}(t) \tag{15}$$

and the motoneurons exert a force (sliding joint) or torque (rotatory joint) on the joints i they innervate of

$$f_i(t) = w_{\text{NM},i}(t)f_z(t). \tag{16}$$

2.3. Simulations

We test the neural implementation of our algorithm using three different simulations. The first one is a simple feed-forward implementation to show that the sub-networks are able to extract the dominant mode from a large variety of sensory input. In the second closed-loop implementation, the neural network receives sensory input from and control the motor output to a linear mechanical system with known resonance behavior. This mechanical system is finally replaced by a more realistic system approximating a hopping leg. The feedback systems show that the neural network is able to induce energy-efficient movements in biomechanical systems with multiple joints and realistic ground contact situations.

2.3.1. Open-Loop Implementation

The open-loop feed-forward implementation is comprised of two sensory neurons which are connected to a postysnaptic timing neuron and to the parallel serotonergic feedback system (cf. **Figure 2**). Each sensory neuron represents the pool of proprioceptive neurons responsible for one joint i. The individual neurons fire according to Poisson statistics with mean firing rates $\nu_{\varphi,i}$ which oscillate in phase with different amplitudes a_i (cf. **Figure 3A**). To test if the system is robust against disturbances, we add Gaussian white noise $\boldsymbol{n}(\sigma)$ with standard deviation $\sigma = 0.1$ to the sensory input. An additional sinusoidal contribution $\boldsymbol{b}$ of Euclidean vector norm smaller than $\boldsymbol{a}$ simulates a secondary eigenmode of the biomechanical system. The firing rates thus amount to

$$\begin{pmatrix}\nu_{\varphi,1}(t)\\ \nu_{\varphi,2}(t)\end{pmatrix} = 40Hz[\begin{pmatrix}a_1\\ a_2\end{pmatrix}\sin(2\pi t) + \boldsymbol{b}\sin(8\pi t) + \boldsymbol{n}(\sigma)]. \tag{17}$$

In the timing sub-network, the sensory neurons are directly connected to a third Poisson-neuron that represents the timing unit. This postsynaptic neuron fires with a rate of

$$\nu_{\text{post}}(t) = \boldsymbol{w}^T_{\text{STDP}}(t)\boldsymbol{\nu_\varphi}(t). \tag{18}$$

The synaptic weights are subject to an STDP rule that is based on previous experiments (Pfister and Gerstner, 2006) which considered the effect of spike triplets (e.g., two pre- and one postsynaptic spike). We stabilize the weights using synaptic scaling as homeostatic mechanism (cf. Section 4.2).

Each sensory neuron is connected to a corresponding raphe neuron. Spikes of each raphe neuron increase the serotonin concentration in a respective pool. The concentrations [5-HT]$_i$

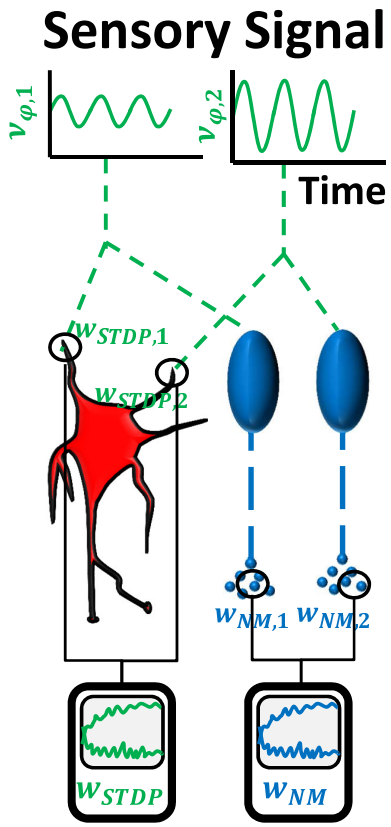

FIGURE 2 | In the first experiment, we verify the possibility to use STDP and serotonin dynamics to obtain the dominant principle component of input signals, by simulating two sensory Poisson neurons. Shown here are their firing rates that evolve according to sinus functions $\nu_{\varphi,1}$ and $\nu_{\varphi,2}$ with different amplitude and underlying white noise (noise not illustrated in the picture). The neurons drive a third Poisson neuron (center left). Synaptic weights $w_{\text{STDP},i}$ are subject to STDP and their ratio is expected to converge toward the amplitude ratio of the input sinus functions. Additionally, the input neurons drive two raphe neurons (center right), which release serotonin into separate pools. The serotonin concentration decreases according to Michaelis-Menten dynamics. The ratio of serotonin concentrations is proportional to the ratio of the neuromodulatory weights, $w_{\text{NM},1}/w_{\text{NM},2}$, and is also expected to converge toward the amplitude ratio of the input signals.

in the two pools i decrease according to Michaelis-Menten kinetics. Our derivation, which shows that serotonergic dynamics can extract the dominant principle component, assumes that [5-HT] $\ll k_m^x$ (cf. Equation 10). Therefore, simulations implementing a small value for the Michaelis constant represent the strongest validation of our derivation. We choose the smallest Michaelis constant suggested by the literature mentioned in Section 2.2.2: $k_m = 170nM$.

The vector of input weights $\boldsymbol{w}_{\text{STDP}}$ and output weights $\boldsymbol{w}_{\text{NM}}$ should converge toward $(a_1, a_2)^T$. We simulate the neural network with 19 different ratios $\frac{a_1}{a_2}$ ranging between 0.05 and 0.95 and set $\|\boldsymbol{a}\| = 1$. Both $\boldsymbol{w}_{NM} = c_{\text{NM}}([5\text{-HT}]_1, [5\text{-HT}]_2)^T$ and $\boldsymbol{w}_{\text{STDP}}$ are supposed to align with the eigenmode. This implies $\frac{w_{\text{NM},1}}{w_{\text{NM},2}} = \frac{w_{\text{STDP},1}}{w_{\text{STDP},2}} = \frac{a_1}{a_2}$. We hence fit the converged ratio $\frac{w_{\text{NM},1}}{w_{\text{NM},2}}$ and $\frac{w_{\text{STDP},1}}{w_{\text{STDP},2}}$ vs. $\frac{a_1}{a_2}$.

Figures 3B–E illustrate the convergence of weights. The ratio of input weights are best fit by a line described by

$$\frac{w_{\text{STDP},1}}{w_{\text{STDP},2}} = m\frac{a_1}{a_2} + b, \tag{19}$$

$$m = 0.952 \pm 0.005 \tag{20}$$

$$b = 0.040 \pm 0.003 \tag{21}$$

$$R^2_{\text{adj}} = 0.999. \tag{22}$$

R^2_{adj} denotes the adjusted R^2-value. We obtain similar findings for the neuromodulatory weights,

$$\frac{w_{\text{NM},1}}{w_{\text{NM},2}} = m\frac{a_1}{a_2} + b, \tag{23}$$

$$m = 0.945 \pm 0.033 \tag{24}$$

$$b = 0.015 \pm 0.019 \tag{25}$$

$$R^2_{\text{adj}} = 0.979. \tag{26}$$

To test the influence of the initial conditions, we run nine additional trials with random initial synaptic weights and serotonin concentrations. Averaging the parameters over all ten trials yields

$$m = 0.979 \pm 0.010 \tag{27}$$

$$b = 0.016 \pm 0.002 \tag{28}$$

for synaptic weights while we obtain for neuromodulatory weights

$$m = 0.957 \pm 0.031 \tag{29}$$

$$b = 0.005 \pm 0.023. \tag{30}$$

Our theoretical considerations predict a slope of $m = 1$ and an intercept of $b = 0$. The slope representing both synaptic and neuromodulatory weights and the intercept of synaptic weights deviate from the expectation values by several standard deviations. The deviations are thus small, but significant. Under the influence of white noise, Oja's rule, Equation (4), converges toward the dominant principal component of input data (Oja, 1982), which is equivalent to the dominant eigenmode in a linear system (Feeny and Kappagantu, 1998). Hence, the deviations of the slope and intercept from their expectation values derive on the one hand from the minor eigenmode and the Poisson noise underlying the neural firing statistics, and on the other hand from the deviations between calculations performed by the implementation of STDP and Michaelis-Menten kinetics from Oja's rule.

To show robustness against sensory noise, we vary the standard deviation of the Gaussian white noise in the sensory input. We sweep through a range of σ between 0.01 and 1.0. **Figures 3F–H** illustrate the slope, y-intercept and adjusted R^2 value for each noise level. We see that the linear approximation remains valid for high noise levels, as represented by a R^2_{adj} close to unity at $\sigma = 1$. The slope and y-intercept increasingly deviate from the expectation for higher noise levels. However, the

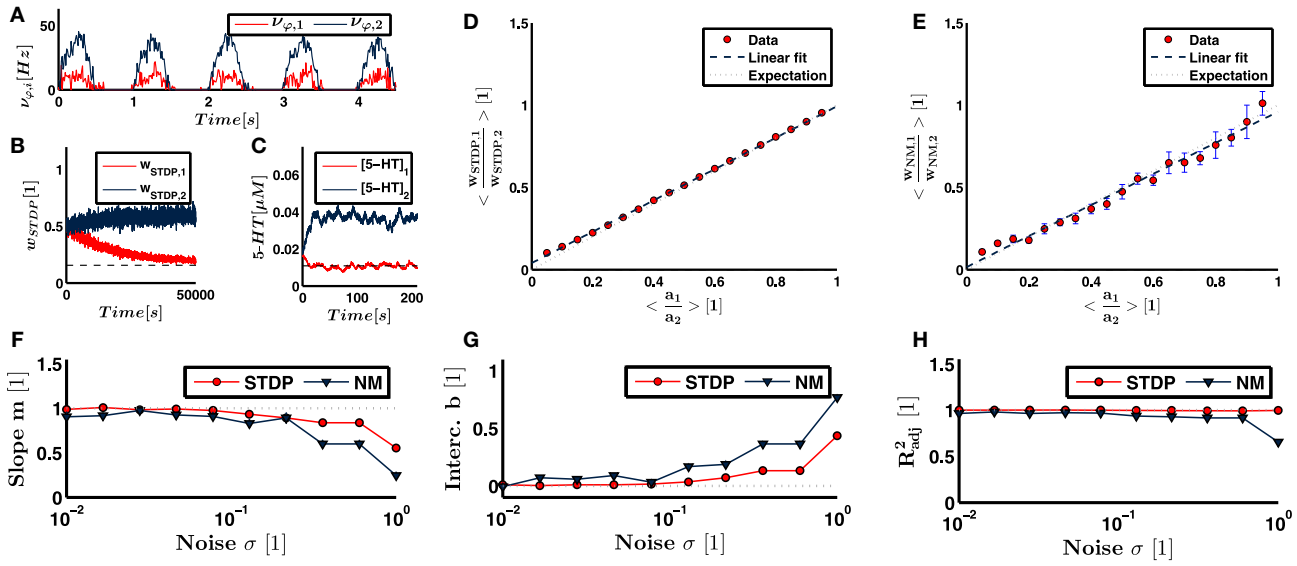

FIGURE 3 | Illustrated here are the results of the feed-forward neural network. (A) The firing rate of the sensory input neurons from joint 1 and 2 for one example run with an underlying eigenmode described by the ratio $a_1/a_2 = 0.3$. Both input and output weights are supposed to align with the dominant principal component, i.e., eigenmode. **(B)** The evolution of the synaptic input weights under the influence of STDP for the two neuron pools. The expected ratio $w_{\text{STDP},1}/w_{\text{STDP},2} = 0.3$ and the converged synaptic strength corresponding to joint 2, $w_{\text{STDP},2}$, determine the expectation value for $w_{\text{STDP},1}$. The expectation value is indicated as dashed line. **(C)** Same illustration for the serotonin concentration, which corresponds to output weighting. **(D)** The ratio of plastic input weights linearly increases with the expected ratio, i.e., a_1/a_2. **(E)** demonstrates the same behavior for the neuromodulatory output weights. Theoretically predicted is a line of unit slope and zero y-intercept. **(F,G)** When the noise in the sensory input increases, the slope and intercept of the linear fit increasingly deviate from the expectation. **(H)** Even for large noise levels, we find an adjusted R^2 value close to 1. This indicates that our linear fits, and hence the obtained values for the slope and y-intercept, remain reasonable.

slope and intercept representing synaptic and neuromodulatory weights deviate by less than 10% from the expected value for noise levels $\sigma < 0.2$ and $\sigma < 0.13$, respectively. Since the dominant eigenmode $\boldsymbol{a}$ is normalized, a value of $\sigma = 0.1$ implies that the firing frequency of any sensory or the postsynaptic neuron is influenced by noise by more than 10% on average. Thus, within a given time step, the probability that either an occurring neural spike is due to noise or that a neural spike is inhibited because of noise is higher than 10%. These results suggest a strong robustness of neural calculations performed by our network against noise.

2.3.2. Closed-Loop Implementation

In order to test the ability of our neural controller to drive a mechanical system with multiple degrees of freedom, we simulate the complete neural network in a closed-loop feedback system (cf. **Figure 4**) .

We implement the two neural sub-systems in parallel, each receiving proprioceptive input. The deflection of each joint is signaled by a pool of Poisson neurons firing with an average rate proportional to the deflection. The sensory neurons are connected to a pool of leaky integrate-and-fire (LIF) neurons. Synaptic weights are subject to the same STDP rule as described above. Since the instantaneous pool-averaged firing rate of the LIF neurons, $\bar{\nu}_{\text{post}}$, serves as ionotropic input to the motoneurons, the neuron pool functionally represents the timing and the driving unit (cf. **Figure 1B**).

The sensory neurons of each individual joint are additionally connected to a respective pool of serotonergic raphe nuclei. The raphe nuclei are also composed of Poisson neurons. Every spike of a raphe neuron releases 5-HT into the corresponding motorpool. Within an individual motorpool, the release is spatially uniform. Depletion takes place according to Michaelis-Menten kinetics. Once again, we choose the smallest suggested Michaelis constant. The resulting [5-HT] is here given in units of mol/l= M. The motoneuron firing rate is amplified proportionally to [5-HT] (Heckman et al., 2003).

We consider two mechanical systems; one is simple and analytically solvable (cf. **Figure 5A**), the other more complex and biologically realistic (cf. **Figure 6A**).

The first system consists of two masses, each representing one joint, that are serially coupled by a spring. Each mass is connected to muscles by further springs of equal stiffness. The system is driven by forces f_i of the muscles, which stretch and squeeze the springs. As illustrated in **Figure 5B**, the system is analytically known to follow the eigenmodes $(1, 1)^T$ (phasic oscillation) and $(1, -1)^T$ (anti-phasic oscillation).

Figures 5D,E shows that the weights of both joints converge toward the same values. This corresponds to phasic resonance movements of the two joints. Fitting exponential functions to the ratio of $\frac{w_{\text{STDP},1}}{w_{\text{STDP},2}}(t)$ and $\frac{w_{\text{NM},1}}{w_{\text{NM},2}}(t)$ shows that the input and output weights converge toward unity with exponential time constants of $\tau_{\text{STDP}} = 2.65 \times 10^3\,\text{s}$ and $\tau_{\text{NM}} = 2.93\,\text{s}$ (cf. **Figures 5G,H**). These time constants differ by three orders of

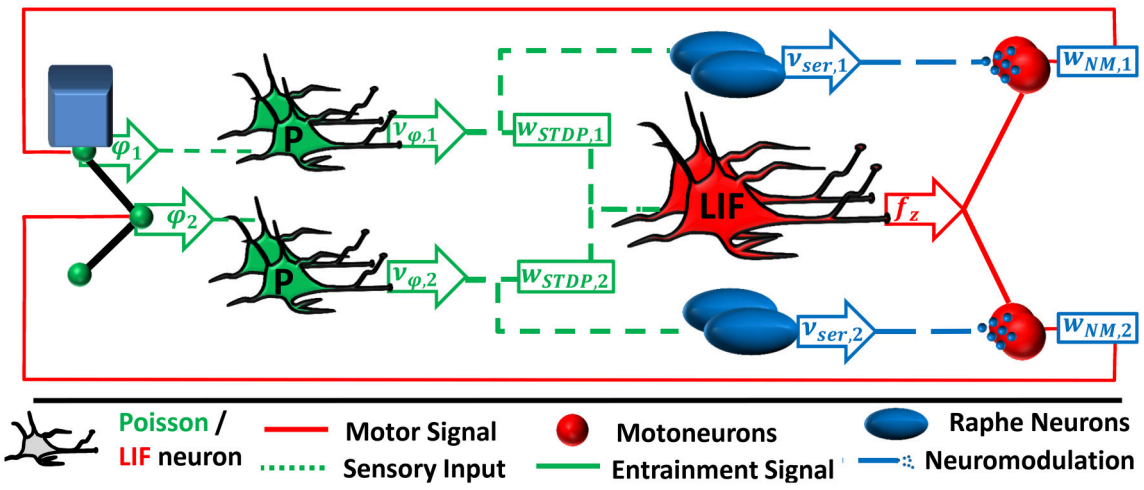

FIGURE 4 | The neural feedback network is an extended version of the feed-forward network as described in Figure 2. In contrast, the spinal interneurons are implemented as leaky integrate-and-fire (LIF) neurons. Their pool averaged firing rate is proportionally transformed into a motor signal f_z. The motor signal is amplified by a factor $w_{NM,i}$ due to serotonergic neuromodulation and is projected back to the muscles.

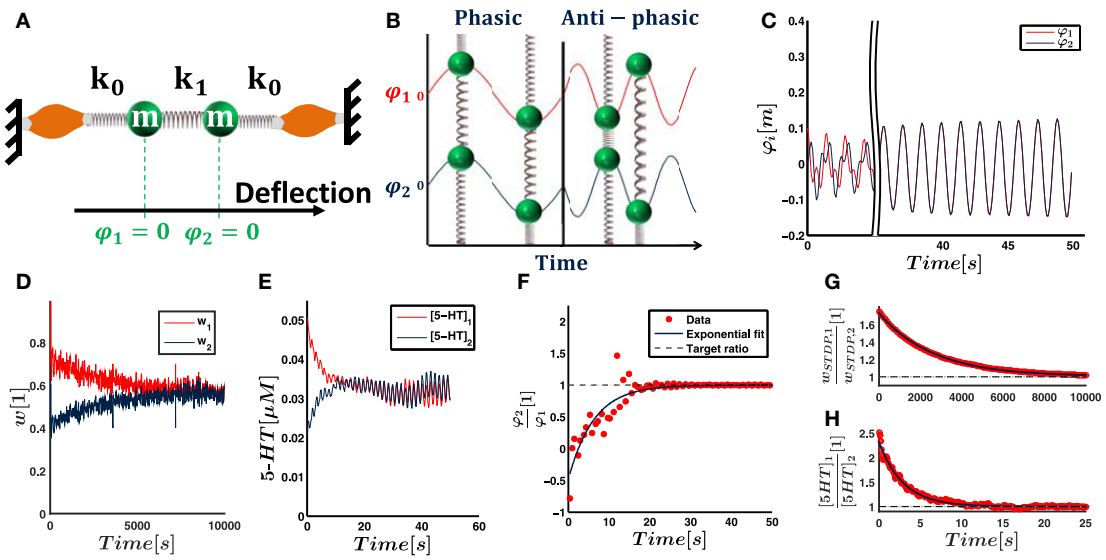

FIGURE 5 | The neural network as described in Figure 4 is initially supposed to control a simple mechanical system. (A) Two masses m are connected by springs of stiffness k_0 and k_1 and driven by muscles that can stretch the springs. Zero positions are given by the equilibrium positions when no force is applied. The deviations of the masses from their zero positions are used as joint deflections φ_i. The neural network as described in **Figure 4** controls the muscles' forces. **(B)** The system has analytically known resonance modes of $(1, 1)^T$ and $(-1, 1)^T$, i.e., the masses either oscillate in phase or anti-phasic. The task of our controller is to excite the system along any of the two eigenmodes with corresponding respective eigenfrequency. The other eigenmode decays due to friction. The final movement is thus resonant. **(C)** The deflection trajectories of both joints align and show phasic resonant movement after few seconds. **(D)** shows that the input weights, which are subject to STDP, converge toward the same value within hours. They therefore also align with the phasic resonance mode $(1, 1)^T$ of the mechanical system. **(E)** shows that the 5-HT concentration within both motoneuron pools, and hence the output weights, converge toward the same value within seconds. **(F)** The alignment of the trajectories is illustrated by the deflection ratio φ_2/φ_1 at peak positions of mass m_1. Shown here is the time evolution of this ratio and an exponential fit. **(G,H)** The ratio of the synaptic and neuromodulatory weights converge to unity with different time scales, as illustrated by respective exponential fits. (All results illustrate the simulation with non-random initial weights).

magnitude and we refer to Section 3.1.1 for a discussion of the different time scales. As shown in **Figure 5C**, the resulting motion trajectory of the mechanical system starts as a superposition of its eigenmodes, showing no obvious relationship in phase or amplitude between the two masses. The trajectories of the two masses converge to synchronous resonant movements over time.

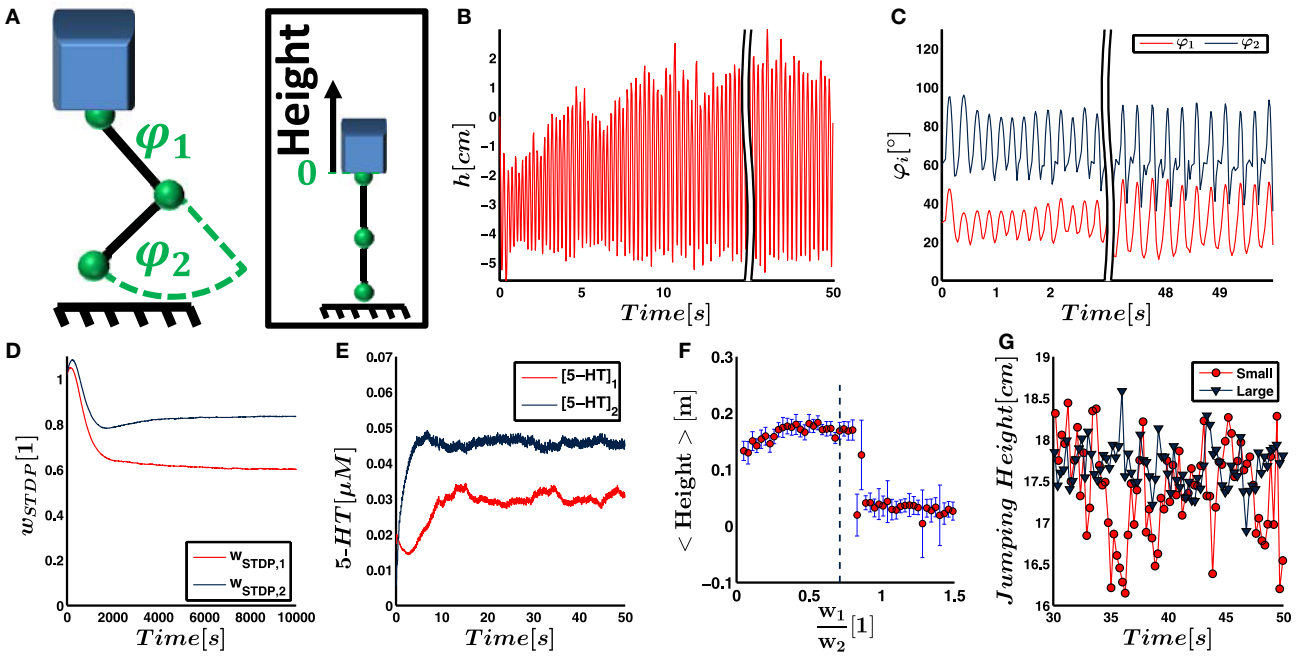

FIGURE 6 | (A) In the final simulation, the neural network as described in **Figure 4** is designed to control a more biologically realistic trunk model that has a jumping leg with two joints influenced by gravity. The neural network gets sensory input about joint deflections and controls the torque within these joints. The jump height is taken as indicator for energy efficiency. It is measured as height of the trunk relative to its position when both joints are fully extended. **(B)** The jump height of the leg increases as a result of the weight adjustment by the neural network. **(C)** The joint deflections are linearly converted to firing rates of the sensory neurons and therefore also represent the sensory input to the neural network. **(D)** The synaptic weights from proprioceptors innervating muscles of joint 1 and 2 to the pool of postsynaptic LIF neuron converge on a time scale of hours. **(E)** Neuromodulatory weights are proportional to the serotonin concentration. They converge faster than the synaptic weights, and the serotonergic concentration within the two motoneuron pools starts to fluctuate around its final value after seconds. **(F)** To find conditions for energy efficiency of the controller numerically, we fix the Euclidean norm of the weight vectors describing the synaptic input and neuromodulatory output weights. We vary the ratio w_1/w_2 both for input and output weights, run a separate simulation for each ratio and record the respective jump height. As illustrated, the jump height has a maximum plateau for ratios between 0.4 and 0.75. This ratio is in agreement with the weight ratios obtained by STDP and serotonin dynamics. **(G)** Even after convergence, the jump height, illustrated as maximum height above the ground here, shows fluctuations with time. We suggest that this is due to noise and the small number of leaky integrate-and-fire neurons that is intrinsic to the controller network. Accordingly, increasing the network size from small to large significantly decreases the fluctuations. (All results illustrate the simulation with non-random initial weights).

Fitting an exponential function to the ratio of joint deflections $\frac{\varphi_2}{\varphi_1}(t)$ at peaks of the first joint deflection, we find that this synchronization takes place with a time constant $\tau_{\text{traj}} = 6.24\,\text{s}$ (cf. **Figure 5F**).

To test the dependence of our results on the initial conditions, we randomly vary the initial synaptic weights and serotonin concentrations in nine additional trials. As an average over all ten trials, we find

$$\frac{w_{\text{STDP},1}}{w_{\text{STDP},2}} = 1.005 \pm 0.011 \tag{31}$$

$$\frac{w_{\text{NM},1}}{w_{\text{NM},2}} = 1.004 \pm 0.032. \tag{32}$$

These values agree with our expectation of unit weight ratios.

The second mechanical system represents a vertically jumping leg consisting of a trunk, a thigh, and a shank, which are connected by rotatory hip and knee joints. When the leg touches down, the joints are deflected, which leads to a stretching of the elastic elements. This stretching triggers the firing of the sensory neurons and activates the reflex arc. The respective torque f_i is exerted on the joint i according to Equation (16) and the leg pushes off the ground.

Figures 6D,E demonstrate for one run that the input and output weights converge on a time scale of seconds and hours, respectively. A video illustrating this simulation can be found in **Video 1**. Again, we perform nine additional runs to test for stability against changes of the initial conditions. As an average over all 10 simulations, we obtain

$$\frac{w_{\text{STDP},1}}{w_{\text{STDP},2}} = 0.724 \pm 0.021 \tag{33}$$

$$\frac{w_{\text{NM},1}}{w_{\text{NM},2}} = 0.703 \pm 0.062. \tag{34}$$

The jump height increases with time and reaches its maximum within seconds (cf. **Figures 6B,C**). The increasing jump height indicates that the movement is tuned to yield higher energy efficiency. To validate that the network increases the energy efficiency of the movement, we run the simulation with different fixed input and output weights. In each trial, we set the norm of the weight vectors equal to the converged norm as obtained in

the trial illustrated in **Figures 6B–E**. We only vary the ratio of the weights, i.e., the orientation of the weight vector. **Figure 6F** illustrates that the final jump height has a maximum plateau for weight ratios $\frac{w_1}{w_2}$ between 0.4 and 0.75.

We analyze the alignment of our weights with the dominant principal component of the movement. For this analysis, we extract the dominant principal component $\boldsymbol{a}$ of the joint trajectory $\boldsymbol{\varphi}(t)$ for each of the ten runs. The average ratio amounts to $\frac{a_1}{a_2} = 0.767 \pm 0.027$. In comparison to the initial synaptic weights, the converged synaptic weights are closer to the ratio of the principal dominant component in 9 out of 10 trials. Assuming that this alignment happens by chance, we would expect to see alignment on average in 50% of the runs. This hypothesis can be rejected by a probability $p < 0.05$. For the serotonin concentration in the two motorpools, we find alignment in 10 out of 10 runs, indicating $p < 0.001$.

As shown in **Figure 6B**, the peak jump height does not converge but shows fluctuations. Considering the average in the window of 30–50 s of simulated time, the jump height shows a standard deviation of 5.8mm. A possible reason for the fluctuations is the intrinsic (Poisson) noise in the system and a relatively small number of only six LIF controller neurons which is chosen due to computational restrictions. To test the influence of noise and the network size, we increase the number of sensory input neurons by a factor of 3 and the number of LIF neurons by a factor of 2. For reasons of comparison, we keep the strength of the input to the LIF neurons as well as the motor signal approximately equal. As a result, we decrease the initial synaptic weights and the neuromodulatory amplification factor c_{NM} by the same respective factors. The standard deviation of the jump height decreases to 2.7mm (cf. **Figure 6G**). The 76 measurement points of jump height recorded for either network do not show any outliers, are not significantly correlated with time, and do not significantly deviate from a normal distribution. They therefore fulfill the requirements to test for different standard deviations using an F-test. The test shows that the standard deviation in the jump height controlled by the large and small network deviate by $p < 0.001$. Therefore, a larger network size and reduced sensory noise decreases fluctuations in the joint trajectories.

3. DISCUSSION

In this study, we consider how the CNS may coordinate fast periodic movements involving several joints. We propose a simple algorithm for this task and confirm that a neural implementation, which is consistent with previous experiments, may explain the correct inter-joint coordination between joints that act with high phase synchronicity as observed for explosive movements. The controller excites the mechanical system along the dominant local eigenmode by a coordinate transformation of proprioceptive inputs from the joint space into a one-dimensional controller space and an inverse transformation of driving controller output. The eigenmode is recursively extracted from the proprioceptive input describing the movement.

We demonstrate that this weighting can be performed by a small network of sensory afferents that converge onto a common pool of spinal interneurons via plastic synapses. Similarly, we reason that a motor feedback loop from proprioceptors via medullary serotonergic neurons may approximate the appropriate output weighting.

3.1. Advantages of the Controller Design

3.1.1. Stability and Energy Efficiency

Our controller design generates stable and energy-efficient periodic movement. In previous research, we have demonstrated that the basic controller design can induce stable movements in robotic platforms (Lakatos et al., 2013b; Lakatos and Albu-Schäffer, 2014a,b). In our simulations, the neural implementation can also induce stable movements in two mechanical systems of different complexity. The induced movement is stable over hours for both the linear and the non-linear mechanical system, as tested for a large range of initial conditions. Our results emphasize that the two neural sub-networks reliably extract the dominant principle component of sensory input signals even in the presence of different disturbances. In particular, we tested stability against noise and perturbations resulting from excitation of a second eigenmode. The converged weights did not fully align with the dominant principle components since their calculations deviate from the mathematical controller design due to different biological features. These firstly include signal transduction durations as included by delays of sensory signals in the network driving the mechanical leg (cf. Section 4.4.2). Second, the mathematical descriptions of STDP and neuromdoulation are based on experimental measurements and deviate strongly from Oja's rule, which underlies the robotic controller design. This deviation is increased by the fact that the spiking of sensory and the postsynaptic neurons in the feed-forward simulation bear Poisson noise. Third, the input-output function of spiking LIF neurons deviate from the basic bang-bang controller (defined by Equation 2) as described in the discussion in Section 4.4.2. Another reason for the deviation in the feed-forward simulation comes from the fact that we added a secondary minor eigenmode to the sensory firing rates to test for stability against disturbances. Despite these constraints, the feed-forward simulations show that a strong alignment of weights with the dominant principal component does take place. Extending the sample size of simulations with different initial conditions, levels of noise and disturbances would quantify more precisely the level of alignment. But a value quantifying the alignment of weights in a feed-forward simulation under a limited variety of disturbances results only indirectly in a statement about the ability of the neural network to control biomechanical systems, which may show an arbitrary variation of disturbances, in a feedback loop. Thus, a more precise quantification of the alignment, i.e., more trials, would only yield little advantage. In the feedback system where the neural network controls the simple mechanical system, the weights seem to align even more reliably with the theoretical expectation. Here, an increased number of neurons decreases the relative influence of Poisson noise in the sensory input. Additionally, the final movement can be fully described by a single eigenmode of the system. Therefore, the sensory signals are not disturbed by a secondary eigenmode in the end of the simulation. With the biological constraints

still in place, these factors lead to a better agreement between expectation and theory in the simple feedback simulation.

Tuning of the movements to increase energy efficiency by our controller design is strongly linked to linearization of the mechanical system. The dominant principle component of a movement is equivalent to the eigenmode of a linear mechanical system associated with the largest eigenvalue of the covariance matrix (Feeny and Kappagantu, 1998), i.e., the eigenmode that best describes the observed movement trajectories. An eigenmode that is e.g., only lightly damped and close to the initial weights is likely to dominate the overall movement and the controller will favor to excite this eigenmode over others. Our controller hence aligns the transformation weights with one of the eigenmodes, $(1, 1)^T$ in our simulations, and thereby obtains resonance tuning for systems such as our simple mechanical model.

For non-linear systems such as our leg, this is not necessarily the case. However, our controller design assumes that energy is only inserted into the system by the bang-bang controller during a relatively short period of the movement cycle. It is therefore reasonable in practice to compute the control action based on the linearization of the non-linear system at the current state. Our simulation of the mechanical leg emphasizes this point. The synaptic input and neuromodulatory output weights start from random initial values in the range of 0.67–1.5 for relative weights $\frac{w_{\mathrm{STDP},1}}{w_{\mathrm{STDP},2}}$ and 0.1–10 for $\frac{w_{\mathrm{NM},1}}{w_{\mathrm{NM},2}}$, respectively. The weight ratio reliably converges toward a value of about 0.7. **Figure 6F** illustrates the jump height as a function of the ratio $\frac{w_{\mathrm{STDP},1}}{w_{\mathrm{STDP},2}} = \frac{w_{\mathrm{NM},1}}{w_{\mathrm{NM},2}}$. It shows that the value of 0.7 is clearly in the range of ratios that maximize the jump height. In Section 4.7.3, we explain that this finding implies tuning to energy efficiency. These results suggest our controller design and our neural models in particular as a candidate to explain how the CNS may excite stable and energy-efficient fast periodic movements. We are currently conducting further testing to analyze in detail the conditions that allow our controller to increase energy efficiency.

Our neural sub-networks show that the control algorithm may be implemented by two spatially separated units. One unit consists of the ionotropic sensory neurons and spinal interneurons and acts at the sensory input level of the spinal cord. A second unit performs individual amplification of the motor signal for each joint. We consider the role of each unit individually.

The output amplification, i.e., the second unit, is necessary for energy-efficient control. If the two masses of our linear mechanical system were excited with forces of different amplitude, the mass trajectories would never converge to resonant movement. This agrees with the fact that the output weights and joint trajectories in our feedback simulations converge on a similar time scale.

The weights in the input network in contrast converge on a slower time scale of hours. They can therefore not react to quick changes of the environment, but to slow biomechanical changes. We intentionally set this slow time scale in agreement with experiments on STDP *in vivo* (e.g., Nishimura et al., 2013; cf. Section 4.2). The discrepancy between this time scale and the fast convergence of joint trajectories as found in our simulations can be explained by the mentioned high synchronicity of joint motions in the considered fast periodic movements. The input weighting determines how strongly sensory input from each joint participates in the entrainment of motor output. If all joints would move in phase, the motor output could be entrained to an arbitrary linear combination of the sensory input. Therefore, the input weighting is not strictly necessary for energy-optimal tuning. In contrast to an approach where motor output is entrained to the signal of only a single nerve, our input network would have three features better suited for animals. First, the motion of joints in biomechanical systems will not be exactly in phase. In this case, our controller gives higher priority to the timing of muscles that are more important. Second, our network gives higher efficacy to nerve fibers that fire more strongly. Under the influence of additive noise, higher activity is connected to a better signal to noise ratio. Thus, entrainment is mainly affected by nerves that show the highest signal to noise ratio. Third, considering all sensory inputs reduces the risk to failure, e.g., when individual nerve fibers are damaged.

To summarize, output weighting by the CNS is required for energy-optimized movement. The fast time scale of neuromodulation may thus allow animals to quickly adjust their movements to changes in the environment. In contrast, the CNS must not necessarily implement the input stage of our controller. However, since the input transformation is advantageous, it is plausible that the neural timing network that we propose may adjust weighting on a longer time scale to compensate for slow mechanical changes.

3.1.2. Dimensionality Reduction

The design of our proposed neural network implies characteristic features of the functional driving unit of considered movements (cf. **Figure 1B**). In our simulations, the pool of timing neurons functionally represents also the driving unit and form a reflex arc.

The driving unit is effectively one dimensional. It receives input from all joints and sends the same motor signal to all motorpools. This single signal is weighted by the neuromodulatory weights to project the one dimensional controller signal back into joint space. At the stage of the timing unit, the input and output weights have thus transformed the control of the mechanical systems to a one-dimensional problem.

This is obvious for the control of the simple mechanical system, which only comprises a single reflex interneuron to create the motor signal to all joints. However, the neural controller of the mechanical leg has six timing neurons. Nonetheless, they act as a single functional unit. The reason is that each timing neuron receives input from a large pool of sensory neurons from each joint. Each sensory neuron has the same probability to connect to any of the six timing neurons, and the pools of sensory neurons projecting to the individual timing neurons largely overlap. The motor signal is furthermore averaged over all six timing neurons, and the same signal is transferred to both motorpools, where it is amplified by neuromodulation. Therefore, the control is still transformed to a functionally one-dimensional problem despite the existence of the six timing neurons. There are three reasons

why we decided for a neuron pool instead of a single timing neuron: First, it makes the model more realistic. Second, it reduces the influence that Poisson noise in the sensory neurons has on synaptic weights. Third, it smooths the output signal of the pool of LIF neurons.

3.1.3. Interplay of Reflexes and CPGs

Although not considered in our simulations, the timing and driving unit may be spatially separated. The driving unit must produce rhythmic output that is phase-coupled to the output of the timing unit. For example, Xiong et al. (2015) and Buchli and Ijspeert (2008) proposed CPG models that fulfill a task similar to our driving unit. It is alternatively possible that the one-dimensional task is achieved by a parallel combination of a CPG and reflex arcs that are both entrained by the timing signal and converge onto or prior to the motoneurons. The CNS may tune the relative contribution of our proposed reflex arc and a parallel CPG according to a secondary task. For example, in the beginning of a periodic movement, the reflex arc may be more active in order to react to unforeseen perturbations. When the periodic movement remains unperturbed for a longer period of time, the contribution of the CPG may increase. The serotonergic feedback network acts on the motorneurons and could thus adjust the relative strength of the motor signal without affecting the driving unit itself.

3.2. Biological Considerations

3.2.1. From Joint to Muscular Level

Our neural controller design acts on a joint level due to its origin in robotics control theory. In animals, proprioceptive input originates from individual muscles, and the motor signal also exerts force on a muscular level. We assume that in the CNS the neural implementation of our controller would adjust weights of individual muscles and not joints. If two muscles of the control loop need to equally assist in a given movement to tune it to yield high energy efficiency, e.g., because the joints that they actuate are equally important for a given movement, they would be assigned similar weights. Antagonistic muscles would be assigned weights of opposite sign. In our simulations, weights are adjusted according to sensory signals representing joint deflections. Corresponding signals on a muscular level, which would represent muscle length, may originate in type II nerve fibers.

3.2.2. Model Validity

Although the CNS may use different mechanisms for the implementation of our proposed control algorithm, our neural models are based on substantiated experimental observations.

Our sub-network for input weighting is based on the finding that proprioceptive nerve fibers from leg muscles converge in the spinal cord (Jankowska, 1992), and that the stimulation of individual fibers in decerebrate cats can change the timing of all muscles involved in a movement (Whelan et al., 1995a; Hiebert et al., 1996; Rossignol et al., 2006). Circuits underlying this behavior seem to reside fully in the spinal cord (Conway et al., 1987; Hiebert et al., 1996). The efficacy of fibers from individual muscles to cause entrainment undergoes use-dependent plastic changes. The efficacy of the fibers positively corresponds to the level of their participation in the entrainment (Whelan et al., 1995b). This agrees with Oja's rule, which underlies our controller design. We suggest to link these findings with STDP, which has been reported in the spinal cord of animals at various ages (Kim et al., 2003; Schouenborg, 2004; Nishimura et al., 2013).

Our hypothesis about the serotonergic sub-network performing output weighting is comprised of a motor feedback loop via the raphe obscurus, pallidus and potentially medianus. We propose this feedback loop in Section 1 based on a large range of experimental evidence (Veasey et al., 1995; Bennett et al., 1998; Hultborn, 1999; Jacobs et al., 2002; Heckman et al., 2008; p. 46f). Using theoretical considerations, we demonstrate that serotonin dynamics can be approximated by Equation (5) and show that this equation is equivalent to Oja's rule under physiologically reasonable conditions. Therefore, it is plausible that 5-HT dynamics extract the dominant principle component of sensory input onto serotonergic neurons. Our simulations emphasize that 5-HT produces enhancement of the motoneuron output along the dominant principal component of the movement. In agreement with our simulation results, the time scale of motoneuron excitability following raphe stimulation is of the order of several seconds (Perrier and Delgado-Lezama, 2005).

The precision of sensory input to the raphe nuclei and serotonergic output onto motoneurons is a matter of current debates (Hyngstrom et al., 2007; Heckman et al., 2008; Johnson and Heckman, 2014). Our proposed serotonergic network would require the topography of the feedback arc to be at least joint-specific. This is reasonable for somatosensory input to the raphe nuclei obscurus, pallidus and medianus, since it has a delay of about 20 ms (Springfield and Moolenaar, 1983). Such a short delay favors a neural pathway with few synapses, maybe bypassing the cerebellum as has previously been described for somatosensory input to other brain stem nuclei (Landgren and Silfvenius, 1971; Johansson and Silfvenius, 1977). There are different indications for topography in spinal projections of the raphe nucleus (Skagerberg and Bjorklund, 1985; Bacon et al., 1990; Cope, 2001; Brumley et al., 2007; Perrier et al., 2013; p. 53). Sufficient topographic precision is plausible; whereas other raphe nuclei project to areas throughout the whole brain and release serotonin in a paracrine manner, projections from the considered raphe nuclei project primarily to the spinal cord (Jacobs et al., 2002; Nieuwenhuys et al., 2007, p. 896) and form well-defined synaptic connections on motoneurons (Perrier et al., 2013).

Furthermore, experiments on the level of neural networks agree with our hypothesis for the functional consequence of serotonergic modulation of motoneuron excitability. Cats show walking patterns which lack refinement after their spinal cord is transected, but not if only influence from the cerebral cortex is cut off (MacKay-Lyons, 2002). The lack of cortical influence in humans was shown for reflex modulation during explosive movements, i.e., those that benefit from the elastic dynamics, in contrast to precision tasks (Shemmell et al., 2009). Our proposed algorithm observes arbitrary movements and tunes

inter-muscular coordination accordingly. In Section 3.2.1, we suggest that the PCA algorithm of our basic controller principle would assign weights of opposite sign to antagonistic muscles. The antagonistic muscles would be excited with a phase shift of 180°. In biological terms, this means that the motor signal of these two muscles (measured by EMG) would become anti-correlated over time. Our hypothesis suggests that blockade of 5-HT_2 receptors, which are assumed to be responsible for enhanced motoneuron excitability upon 5-HT application (Sławińska et al., 2014), will disrupt this tuning. Pearlstein et al. (2005) observed exactly this behavior in rats when measuring the ventral root activity of antagonistic muscles acting on the same limb. Upon addition of a 5-HT_2 antagonist, the cyclic movement continued while the correlation coefficient of motor signals in the ventral roots of antagonistic muscles changed highly significantly from a negative to a positive value (Pearlstein et al., 2005, **Figure 5**).

3.2.3. Movement Initiation

Since our controller design represents a reflex arc, it can only shape an ongoing but not initiate a new periodic movement. In our simulations, the mechanical systems move because they start from an imbalanced initial position. In nature, the CNS must initiate the movement with an intrinsically produced motor signal that is sent to all motor neurons. In our simulations, the relative strength of the first motor signals produced by the reflex arc are randomly chosen. Therefore, a motor signal that initiates the periodic movement does not need to be specifically tuned, either. It is sufficient to send an appropriately strong motor signal to all joints involved in the movement. This motor signal may originate in cortical areas. A CPG that may functionally replace or support the reflex interneurons at intermediate spinal levels, as proposed in Section 3.1.3, is an alternative explanation for movement initiation.

3.3. Implications for Research

Our proposed neural sub-networks link different experimental findings into a coherent framework. Their validation would require to show that the repeated passive movement of a single joint increases the motoneuron excitability of corresponding muscles exclusively. The change in excitability must be due to 5-HT.

Our simulation results show that the presented concept of an adaptive coordinate transformation between joint and controller space is a promising hypothesis for neural calculations. While our sub-networks are plausible, we must emphasize that alternative neural implementations of our algorithm may exist and we encourage other ideas for neural interpretations. The controller design provides experimenters with guidelines for a neural circuit to search for. In the following, we provide a check list of characteristics that circuits must provide in order to tune periodic movements according to our algorithm. The circuits must

- adjust motor output for the whole limb during fast periodic movements based on proprioceptive signals.
- scale the output of motor signals to individual motoneuron pools. The relative strength of muscles must be amplified when the joint they act on shows larger deflections during the movement.
- average sensory input representing joint deflections on a time scale of seconds. This time scale must be sufficiently fast to react to environmental changes, but significantly longer than the cycle duration of the movement to prevent substantial variations during the cycle.
- include a function that keeps the strength amplification bounded. In addition, the mechanism itself must not alter relative amplifications between the muscles.
- not alter the frequency of the motor signal.

As discussed in Section 3.1.1, adjustment of the input transformation is not strictly necessary, but advantageous from viewpoint of convergence to energy-efficient fast periodic movements. A circuit that implements the input transformation must

- receive sensory information from several joints that converge onto a single functional unit. This unit must influence muscles in the whole limb.
- entrain the output frequency of this driving unit to proprioceptive signals. Hereby, the relative entrainment efficacy of a signal must be amplified when the corresponding joint shows larger deflections during the movement.
- change the relative efficacy of a signal based on the sensory information about the joint deflections as averaged on a time scale of at least seconds. This lower boundary on the time scale is in contrast e.g., to the typically short time scale of influences by a single ionotropic input. It prevents substantial variations of the weights during the movement cycle. As discussed in Section 3.1.1, there is no strict upper boundary for this time scale.
- include a mechanism that keeps the efficacy bounded, i.e., prevent runaway behavior. The mechanism must not alter the relative efficacy between the muscles.

In contrast to these requirements on the sensory input and motor output stage of the spinal cord, our algorithm and the proposed neural implementations place minimal restriction on circuits generating the ionotropic motor signal of a whole limb. Our controller design provides a driving circuit with an entrainment signal that is continuously optimized for local eigenmodes of the controlled mechanical system under changing environmental and biomechanical conditions. Similarly, it achieves correct inter-joint coordination of the motor output. Since the eigenmode is determined by the mechanical system, our controller effectively adjusts movements to biomechanical and environmental properties. As discussed in Section 3.1.3, our proposed controller and network may thus effectively simplify the dynamical interplay of CPGs and reflexes in explosive periodic movements to a one-dimensional problem.

Our results emphasize the benefits of control strategies for bio-mimicking robotic systems derived by engineering considerations, which can be well verified experimentally. We suggest that neuroscientific research can use these strategies as source for promising hypothesis about neural calculations.

4. MATERIAL AND METHODS

We test our proposed neural implementation of the discussed controller using three different systems of increasing complexity. In the beginning, we model the neural network in a simple feed-forward simulation to test its ability to extract the dominant principal component of the movement. Using the feedback of a simple, analytically solvable, mechanical system, we test the network's ability to induce stable energy-efficient movement. Finally, we demonstrate that the neural network is able to control a more realistic mechanical model of a leg with two joints that provides sensory feedback.

4.1. Neuron Models

We model spiking neural networks, in which cells are represented either by Poisson or leaky integrate-and-fire (LIF) neurons. In every time step dt, the probability for a Poisson neuron to fire is given by a Poisson distribution with mean $\nu(t)\mathrm{d}t$, where $\nu(t)$ represents the instantaneous firing rate. The spike train of neuron n is described by $S_n(t) = \sum_k \delta(t - t_n^k)$, where t_n^k are the spiking times and δ denotes the delta distribution.

Where not otherwise stated, differential equations describing LIF neurons are taken from Zenke et al. (2013). Constants that have been changed in comparison to their paper are given in **Table 1**. Each LIF neuron has an associated membrane voltage U_n which changes as

$$\tau^m \frac{\mathrm{d}U_n}{\mathrm{d}t} = (U^{\mathrm{rest}} - U_n) + g_n^{\mathrm{exc}}(t)(U^{\mathrm{exc}} - U_n) + g_n^{\mathrm{inh}}(t)(U^{\mathrm{inh}} - U_n), \tag{35}$$

with membrane time scale τ^m and membrane conductances g^x. As soon as the voltage crosses the threshold $\vartheta^{\mathrm{rest}}$, a spike is triggered and U_n is reset to U^{rest}. Our model deviates in the form of the subsequent refractory period. Zenke et al. (2013) implemented the refractory period by a time-dependent spiking threshold following a neural spike. This implementation does not consider the effect of channel inactivation on the time course of the membrane voltage, and hence its primary function is to delay the next spike. We implement a refractory period by fixing the membrane voltage of the neuron to its resting level for a time period τ_{thr}. Our approach more closely models the absolute refractory time. It introduces a delay of same time scale between two spikes and therefore has the same functional consequence. However, it saves computational power, since the membrane and synaptic dynamics do not need to be updated during the refractory period.

TABLE 1 | Parameters of the neuron models and the structure of the neural network.

	Feed-Forward	Feedback	
		Simple	Complex
τ_{thr}	5 ms	5 ms	5 ms
n_{sens}	1	290	130
n_{inh}	0	0	100
n_{tim}	0	1	6
m_{sens}	/	10 Hz m^{-1}	9 Hz rad^{-1}
p_{con}	1	1	0.7
w_{ext}	/	0.1	0.1
ν_{ext}	/	3 Hz	3 Hz
$\tau_{\mathrm{del,STDP}}$	0 ms	0 ms	30 ms
$\tau_{\mathrm{del,NM}}$	0 ms	0 ms	200 ms

The feedback model is subdivided according to the simple and complex mechanical system that it controls. We state only those parameters that deviate from the original implementation as described by Zenke et al. (2013).

The synaptic conductances of neuron n are updated following a spike of the upstream neurons m according to

$$g_n(t) = \frac{1}{2}\left(g_n^{\mathrm{ampa}}(t) + g_n^{\mathrm{nmda}}(t)\right), \tag{36}$$

where

$$\frac{\mathrm{d}g_n^{\mathrm{ampa}}}{\mathrm{d}t} = -\frac{g^{\mathrm{ampa}}}{\tau^{\mathrm{ampa}}} + \sum_m w_{\mathrm{STDP},mn} S_m \tag{37}$$

$$\frac{\mathrm{d}g_n^{\mathrm{nmda}}}{\mathrm{d}t} = -\frac{g_n^{\mathrm{nmda}}}{\tau^{\mathrm{nmda}}} + \frac{g_n^{\mathrm{ampa}}}{\tau^{\mathrm{nmda}}}. \tag{38}$$

The weight of the synapse connecting neuron m to n is given by $w_{\mathrm{STDP},mn}$. The time evolution of conductances differentiates between a component due to AMPA and NMDA to account for different time constants of the corresponding channels. We modified Equation (37) to align units.

4.2. Plasticity

We also adapt our plasticity model from Zenke et al. (2013), who described a triplet-based STDP model based on experimental observations performed by Pfister and Gerstner (2006) and Sjöström et al. (2001). Zenke et al. defined synaptic traces z_n^{slow}, z_n^-, and z_n^+ of neuron n by

$$\frac{\mathrm{d}z_n^x}{\mathrm{d}t} = -\frac{z_n^x}{\tau^x} + S_n(t). \tag{39}$$

with time constants τ^{slow}, τ^-, and τ^-, respectively. Synaptic weights change according to

$$\frac{\mathrm{d}w_{\mathrm{STDP},nm}}{\mathrm{d}t} = \eta\left(A^+ z_n^+(t) z_m^{\mathrm{slow}}(t-\epsilon) S_m(t) - A^- z^-(t) S_n(t)\right) + \Delta w_{\mathrm{scal},nm}(t), \tag{40}$$

where ϵ is a small time constant and $\Delta w_{\mathrm{scal},nm}$ a homeostatic weight change as described below. Zenke et al. introduced the learning rate η as conversion factor between their plasticity model and the true biological scale, which we set to unity to match model and biological scale. They additionally scaled the rate of weight change by the initial synaptic weights. Since we consider this to be an arbitrary choice, we omit the factor. Additionally, we decrease the amplitude of long term potentiation (LTP), A^+,

and long term depression (LTD), A^-, by two orders of magnitude (cf. **Table 2**). Due to the high firing rates of our neural network, we found a fast convergence of weights to their final values within tens of seconds up to minutes. Such a fast convergence would be advantageous for our consideration (cf. Section 3.1.1). However, measurements by Nishimura et al. (2013) in behaving monkeys suggest that STDP *in vivo* is more likely to act on a time scale of hours, which we account for by the decrease in amplitude. Weights in our model are altered following both pre- and postsynaptic spikes and weights of sensory neurons from joint i are initialized to $w_{\text{STDP},in,0}$.

To introduce stability, we use synaptic scaling as homeostatic mechanism as described by Zenke et al. (2013), who adapted it from van Rossum et al. (2000). Scaling adjusts Equation (40) by

$$\Delta w_{\text{scal},nm}(t) = \frac{1}{\tau_s \nu_{\text{tar}}} \left(\nu_{\text{tar}} - \left(\frac{\bar{\nu}_n}{\nu_{\text{tar}}^2} \right) \right), \tag{41}$$

where τ_s is a time constant, ν_{tar} the target firing rate, and $\bar{\nu}_n$ the average firing rate of the postsynaptic neuron n as represented by the low-pass-filtered spike train to arrive at

$$\tau_{\text{rs}} \frac{\mathrm{d}\bar{\nu}_n}{\mathrm{d}t} = -\bar{\nu}_n + S_n(t). \tag{42}$$

4.3. Neuromodulation

The motoneuron pool innvervating joint i starts with a serotonergic concentration of $[5\text{-HT}]_{i,0}$. Upon spiking of a raphe neuron, a fixed amount of 5-HT is released into the corresponding motoneuron pool, which subsequently diminishes according to Michaelis-Menten kinetics. The resulting concentration in motoneuron pool i due to the corresponding neurons n is described by

$$\frac{\mathrm{d}[5\text{-HT}]_i}{\mathrm{d}t} = c_{\text{ser}} \sum_n S_n(t) - \frac{\nu_{\max}}{\frac{k_m}{[5\text{-HT}]_i} + 1}, \tag{43}$$

as derived in Section 2.2.2. Since we use spike-based neural networks, the firing rate in Equation (8) is replaced with the spike train. The serotonin concentration increases proportionally to the firing rate. Hence, it can be approximated that each spike releases the same quantity of serotonin. We choose $\nu_{\max}$ according to Hentall et al. (2006) and k_m as the smallest value suggested by the literature (Molodtsova, 1983; Katz and Kimelberg, 1985; Verleysdonk et al., 2004; Best et al., 2010). We set c_{ser} appropriately to yield [5-HT] between 0.01 and 0.1μM (Hentall et al., 2006) (cf. **Table 3**).

4.4. Neural Network

As mentioned, we test our neural network in three simulations. The computational implementation of the neural network differs for each. We use a simple computational neural model for the feed-forward simulation. A more detailed second model is used as controller for the two mechanical systems in the second and third (feedback) simulations.

4.4.1. Simulation 1: Feed-Forward

The feed-forward network receives sensory input from two sensory Poisson neurons. They fire with mean firing rates that show a sinusoidal oscillation along a dominant eigenmode ***a*** plus a small sinusoidal component from a minor eigenmode,

$$\begin{pmatrix} \nu_{\varphi,1}(t) \\ \nu_{\varphi,2}(t) \end{pmatrix} = 40\,Hz[\begin{pmatrix} a_1 \\ a_2 \end{pmatrix} \sin(2\pi t) + \begin{pmatrix} 0.05 \\ 0.05 \end{pmatrix} \sin(8\pi t) + \begin{pmatrix} n(\sigma = 0.1) \\ n(\sigma = 0.1) \end{pmatrix}]. \tag{44}$$

The last term represents Gaussian noise with zero mean and standard deviation σ. Negative firing rates are considered as zero. These presynaptic neurons are connected via plastic synapses to a third postsynaptic Poisson neuron that fires with a rate of

$$\nu_{\text{post}} = \sum_i w_{\text{STDP},i} \nu_{\varphi,i}. \tag{45}$$

The neuromodulator system consists of two serotonergic Poisson neurons that fire according to Equation (44) and release 5-HT into two separate motoneuron pools i.

4.4.2. Simulation 2 and 3: Feedback

The feedback neural network controlling the two mechanical systems is illustrated in **Figure 4**. It receives input from n_{sens}

TABLE 2 | Parameters of the synaptic plasticity model.

	Feed-Forward	Feedback	
		Simple	Complex
$w_{\text{STDP},1,0}$	0.5	0.7	1
$w_{\text{STDP},2,0}$	0.5	0.4	1
A^+	6.5d-5	6.5d-5	6.5d-5
A^-	1.1d-5	1.1d-5	1.1d-5
τ_S	50 s	50 s	15,000 s
τ_{rs}	5 s	5 s	300 s
ν_{tar}	8 Hz	30 Hz	15 Hz

The feedback model is subdivided according to the simple and complex mechanical system that it controls. We state only those parameters that deviate from the original implementation as described by Zenke et al. (2013).

TABLE 3 | Parameters of the serotonergic dynamics model.

	Feed-Forward	Feedback	
		Simple	Complex
$[5\text{-HT}]_{1,0}$	17 nM	50 nM	18 nM
$[5\text{-HT}]_{2,0}$	17 nM	20 nM	6 nM
c_{ser}	300 pM	40 pM	5 pM
$\nu_{\max}$	$0.1\frac{1}{s}$	$0.1\frac{1}{s}$	$0.1\frac{1}{s}$
k_m	170 nM	170 nM	170 nM

The feedback model is subdivided according to the simple and complex mechanical system that it controls.

Poisson neurons per joint that fire with rates proportionally related to the respective joint deflection φ_i,

$$\nu_{\varphi,i}(t) = \begin{cases} m_{\text{sens}}\varphi_i(t) & \text{if } \varphi_i(t) > 0 \\ 0 & \text{otherwise} \end{cases} \tag{46}$$

Sensory neurons from joint i are randomly connected with a probability p_{con} to each of n_{tim} LIF neurons via plastic synapses. In the network controlling the complex mechanical system, the information about spikes from the sensory neurons reaches the LIF neurons with a delay of $\tau_{\text{del,STDP}}$. We choose the delay in agreement with experiments on reflex arcs in the human leg (Friemert et al., 2005). Additionally, the LIF neurons receive input from n_{inh} external inhibitory Poisson neurons firing with a constant rate of ν_{ext}. The external neurons allowed us to quickly scale the resting excitability of LIF neurons. This scaling was required due to the small number of neurons in the network. The LIF neurons accumulate synaptic input and fire as described in Section 4.1, which results in adaptation of the plastic synapses as described in Section 4.2. The spike trains of the LIF neurons are low-pass-filtered according to Equation (42) with time constant τ_f and averaged over the LIF neuron pool. This instantaneous average firing rate $\bar{\nu}_{\text{post}}$ is proportionally converted to a generalized muscle force,

$$f_z(t) = m_f \bar{\nu}_{\text{post}}. \tag{47}$$

In the mathematical controller algorithm, converged synaptic input is transformed into an output motor signal by a step function, Equation (2). The input-output function of the LIF neurons is a smoothed approximation of this signal. The neurons are silent for small synaptic input due to the firing threshold and their firing rates saturate at high input due to the refractory period. The saturation, together with velocity dependent damping of the mechanical system as described below, ensures mechanical stability since it prevents possible positive feedback loops. For intermediate input strengths, the firing rates increase with synaptic input. The low-pass-filter, Equation (42), furthermore smooths the firing rate over time.

A number of n_{ser} serotonergic Poisson neurons fire with a rate that is linearly related to the joint coordinates,

$$\nu_{\text{ser},i}(t) = \begin{cases} b_{\text{ser}} + m_{\text{ser}}\varphi_i(t) & \text{if } \varphi_i(t) > -\frac{b_{\text{ser},1}}{m_{\text{ser},1}} \\ 0 & \text{otherwise} \end{cases} \tag{48}$$

Resulting spikes are delayed by $\tau_{\text{del,NM}}$ in the complex model. Our proposed serotonergic motor feedback loop has not been described previously and the signal delay is hence not experimentally determined. It can be assumed that the function of the network improves with shorter delays. As a safe estimation, we choose a relatively long delay which is larger than the measured delay between proprioceptive input and activity of serotonergic neurons (Springfield and Moolenaar, 1983) by one order of magnitude. Each spike increases $[5\text{-HT}]_i$ according to Equation (43). The serotonin concentration in the motoneuron pool of the individual joints amplify the force/torque exerted on this joint proportionally, i.e., increase it by weights

$$\begin{pmatrix} w_{\text{NM},1}(t) \\ w_{\text{NM},2}(t) \end{pmatrix} = c_{\text{NM}} \begin{pmatrix} [5\text{-HT}]_1(t) \\ [5\text{-HT}]_2(t) \end{pmatrix}. \tag{49}$$

The chosen value for c_{NM} guarantees an amplification ranging between 1 and 3 (Heckman et al., 2008).

4.5. Mechanical Models

We test our neural feedback controller on two mechanical systems. The first consists of two masses m that represent the joints and are connected by a spring of stiffness k_1 (cf. **Figure 5A**). Both masses are connected to muscles via a spring k_0. The muscles exert forces on the masses according to

$$f(t) = \boldsymbol{w}_{\mathbf{NM}}(t) f_z(t). \tag{50}$$

The deflections $\boldsymbol{\varphi} \in \mathbb{R}^2$ of the masses represent the joint coordinates and are measured relative to their resting positions in the absence of any force. They follow

$$\frac{\mathrm{d}^2}{\mathrm{d}t^2}\boldsymbol{\varphi}(t) = -\frac{d_0}{m}\frac{\mathrm{d}}{\mathrm{d}t}\boldsymbol{\varphi}(t) - \begin{pmatrix} \frac{k_0+k_1}{m} & -\frac{k_1}{m} \\ -\frac{k_1}{m} & \frac{k_0+k_1}{m} \end{pmatrix}\boldsymbol{\varphi}(t) + \frac{1}{m}\boldsymbol{f}(t), \tag{51}$$

where d_0 is a damping constant. The solution for constant muscle force is the sum of two sinusoidal oscillations with eigenvectors $(1, 1)$ and $(-1, 1)$. Additionally, a small damping term causes decay of minor eigenmodes. The mechanical parameters have not been specifically tuned and can be found in **Table 4**. Zero positions $\boldsymbol{\varphi} = \mathbf{0}$ are defined as equilibrium positions. We excite oscillations by initially deviating the system to $\boldsymbol{\varphi}(t = 0s) = (0m, 0.1m)^T$. This is a linear combination of the eigenmodes. Hence, we initially excite both eigenmodes simultaneously.

The second mechanical system consists of a trunk of mass m_0 connected to one rod-like thigh of mass m_1 and length l via a rotatory hip joint (cf. **Figure 6A**). The shank of same mass and length is connected to the thigh via a rotatory knee joint. The joint angles define the coordinates $\boldsymbol{\varphi} \in \mathbb{R}^2$ and are measured

TABLE 4 | Parameters of the mechanical models.

	Simple		Complex
τ_f	100 ms		5 ms
m_f	10 mN Hz^{-1}		525 μN m Hz^{-1}
c_{NM}	15/μM		65/μM
m_{ser}	9 Hz m^{-1}		1 kHz rad−1
b_{ser}	900 mHz		0 Hz
k_0	8 N m−1		0.75 N m rad^{-1}
k_1	15 N m−1		0.75 N m rad^{-1}
m	500 g	m_0	500 g
d_0	300 mN s m^{-1}	m_1	100 g
		d_0	11,250 μN m s rad^{-1}
		d_1	11,250 μN m s rad^{-1}

Subdivided into the simple and complex model.

relative to a fully extended leg. The trunk is constrained to a one-dimensional vertical jumping movement. We set its zero-position $h = 0$ to its height when both hip and knee are fully extended, i.e., $\boldsymbol{\varphi} = \mathbf{0}$. Gravity pulls the system down. The joints are each driven by one motor, which exerts force via a torsional spring. These springs have a torsion coefficient of k_0 and k_1 and an angular damping coefficient of d_0 and d_1 for the hip and knee joint, respectively. The equilibrium positions of the springs are defined by joint angles of $\boldsymbol{\varphi_0} = (\frac{1}{6}\pi, \frac{2}{6}\pi)^T$. The values of these parameters, as given in **Table 4**, are adjusted according to an existing prototype of a legged robot at our institute. The muscles exert forces on the joints by stretching the springs. The resulting torque amounts to

$$\boldsymbol{f}(t) = \begin{pmatrix} k_0 \\ k_1 \end{pmatrix} \left(w_{\mathrm{NM}}(t) f_z(t) - \boldsymbol{\varphi}(t) + \boldsymbol{\varphi_0} \right) - \begin{pmatrix} d_0 \\ d_1 \end{pmatrix} \frac{\mathrm{d}}{\mathrm{d}t} \varphi(t). \quad (52)$$

After touch down, contact with the ground is modeled by forces acting on the contact point of the foot via a compliant ground model as described by Azad and Featherstone (2010) and implemented in *Spatial_v2* (Featherstone, 2012).

We define the generalized velocity $\boldsymbol{v} = (\frac{\mathrm{d}}{\mathrm{d}t} h, \frac{\mathrm{d}}{\mathrm{d}t} \boldsymbol{\varphi})^T$. Then, the movement can be described by

$$\boldsymbol{M}(\boldsymbol{\varphi}) \frac{\mathrm{d}}{\mathrm{d}t} \boldsymbol{v} + \boldsymbol{p}(\boldsymbol{\varphi}, \boldsymbol{v}) = \boldsymbol{f} + \sum_k \boldsymbol{J_k}(h, \boldsymbol{\varphi})^T \boldsymbol{F_k}. \quad (53)$$

The inertia matrix is denoted by $\boldsymbol{M} \in \mathbb{R}^{3\times3}$ and the Coriolis, centrifugal and gravity forces are summarized by $\boldsymbol{p}$. The ground contact wrench $\boldsymbol{F_k}$ is mapped to the generalized forces by the transposed Jacobian matrix $\boldsymbol{J_k}$. To initiate the movement, we drop the leg from $h = 0$m, while the joints are at $\boldsymbol{\varphi_0}$.

4.6. Parameters of the Numerical Simulations

We simulate our network using *Matlab* and *Simulink*. Differential equations are integrated using simple Euler integration with time steps of $\mathrm{d}t = 10^{-3}$ s in the feed-forward simulation and 10^{-4} s in the simulation comprising the simple mechanical model. To speed up the complex model, we use $\mathrm{d}t = 10^{-4}$ s only for the plasticity model and the LIF neurons, 10^{-3} s for the serotonergic dynamics, and variable time steps for the mechanical model.

4.7. Analysis of Simulations

4.7.1. Simulation 1: Feed-Forward

We run the feed-forward model for ten different ratios $\frac{a_1}{a_2} \in [0.05, 0.95]$. Each run takes 60,000 s of simulated time. Synaptic weights are initiated as described in **Table 2** and recorded each 1s during the whole simulation, serotonin concentrations are initiated as described in **Table 3** and monitored in each time step during the first 500 s. During the last 50 s of the recordings, we average the ratio both of serotonergic amplification weights, $\frac{w_{\mathrm{NM},1}}{w_{\mathrm{NM},2}}$, and of the synaptic weights, $\frac{w_{\mathrm{STDP},1}}{w_{\mathrm{STDP},2}}$, for each ratio $\frac{a_1}{a_2}$ separately. Standard deviations of these values represent the fluctuation of weight ratios during the 50 s. We fit the converged ratios $\frac{w_{\mathrm{NM},1}}{w_{\mathrm{NM},2}}$ and $\frac{w_{\mathrm{STDP},1}}{w_{\mathrm{STDP},2}}$ vs. $\frac{a_1}{a_2}$ using a weighted linear least-square fit.

To verify robustness of our network against noise as stated in Equation (44), we vary the standard deviation, σ, in 10 logarithmically spaced steps between 10^{-2} and 10^{0}. The trial for each noise level is analyzed as described in the last paragraph. We plot the slope and intercept of the linear fit as a function of σ.

In nine additional simulations with random initial weights, we test the robustness against changes in the initial conditions. Therefore, we allocate a random weight in the interval [0.1, 1.0] to $w_{\mathrm{STDP},1}$ and $w_{\mathrm{NM},1}$ and another random weight to $w_{\mathrm{STDP},2}$ and $w_{\mathrm{NM},2}$ in each trial. We run the simulations as described above and calculate a linear fit for each of these runs. The average and standard deviation of the slope and intercept are derived over all of these nine trials plus the initial simulation.

4.7.2. Simulation 2: Feedback, Simple Mechanical Model

The simulation including the simple mechanical model runs for 10,000 s of simulated time. Synaptic and neuromodulatory weights are recorded each 0.1 s only, which is due to computational restrictions. We average the weight ratios over the last 50 s of simulated time. Their respective initial values are stated in **Tables 2**, **3**.

In nine additional trials, we verify the reliability of the results against changing initial conditions. For this test, we choose random initial concentrations $[5\text{-HT}]_{i,0} \in [6\text{nM}, 60\text{nM}]$ and random initial synaptic weights $w_{\mathrm{STDP},i,0} \in [0.8, 1.2]$ for each run. We average the ratios of synaptic and neuromodulatory weights over the last 50s of all ten trials.

4.7.3. Simulation 3: Feedback, Complex Mechanical Model

We run the simulation of the neural feedback network that controls the mechanical leg for 10,000s of simulated time. Synaptic and neuromodulatory weights are recorded each 0.25 s. Their respective initial values are given in **Tables 2**, **3**. Joint coordinates and the height of the leg are recorded for the last 70,000 time steps and for all numerical time steps during the first 50 s. Sampling of more data was not possible due to memory restrictions. We average the weight ratios during the last 50 s.

We would like to verify that the converged weight ratios maximize the energy efficiency of the movement. Therefore, we record the Euclidean vector norm of the converged synaptic and neuromodulatory weight vector of the first trial. We subsequently implement the other simulations with weight vectors that are constant over time and share the vector norm with the converged network. We vary the ratio $\frac{w_{\mathrm{STDP},1}}{w_{\mathrm{STDP},2}} = \frac{w_{\mathrm{NM},1}}{w_{\mathrm{NM},2}}$ between 0.05 and 1.5 in steps of 0.03 and run each simulation for 20 s of simulated time. In each trial, we average the jump height over the last 20 jumps.

The jump height as function of the weight ratio is taken as a measure for the energy efficiency of the neural control. At the peak of the jumping movement, the energy within the system is given by the potential energy. Since most of the mass of the system is confined to the trunk, the potential energy is approximately linearly related to the jump height. In the original bang-bang controller, switching of the bang-bang controller leads

to a force $f_i = w_i \hat{c}_f$ in joint i (Equation 3). The energy inserted into the system in each jump is thus given by

$$E = \frac{1}{2}\hat{c}_f^2 \left(\frac{w_1^2}{k_0} + \frac{w_2^2}{k_1} \right). \quad (54)$$

We choose equal spring constants $k_0 = k_1$ for the joints. Hence, the Euclidean vector norm of the weight vector determines the energy inserted into the system. Since we fix the vector norm for each trial, the energy inserted into the system is constant. We define energy efficiency as energy within the system divided by the energy that we insert. According to our argumentation, jump height can thus be assumed to represent this quantity.

In addition, we once again perform nine trials with randomly initialized weights. The range of initial weights is the same as for the simple mechanical system described in the last section. We average the weight ratio over the last 50 s of these nine trials plus the trial described in the beginning of the present section.

To show if our neural network extracts the dominant principle component of their sensory input, we use the same ten trials with different initial conditions. As described above, we record the joint coordinates for each time step during the first 50 s of the runs. Using the Matlab-function *pca*, we extract the dominant principle component of the joint coordinates for each trial.

In a final simulation, we elucidate how the network size influences fluctuations in the jump height of the leg. We therefore increase the number of sensory input neurons to the LIF neurons by a factor of 3 and the number of LIF neurons by 2. We decrease the initial synaptic weights and the amplification factor of neuromodulation, c_{NM}, by the same respective factors and run the simulation for 50 s. During the last 20 s, we calculate the standard deviation of the jump height over all jumps as a measure for the fluctuation level. Using a one-sided F-test, we compare this value to the standard deviation obtained for the initial simulation. The p-value indicates whether increasing the network size decreases fluctuations in the jumping trajectories. We use three approaches to test the assumptions underlying an F-test: First, we visually inspect a plot of jump height vs. time for obvious outliers for the small and large network individually. Second, we test for a significant correlation between jump height and time. Finally, we test either sample for normality using a Lillie test.

AUTHOR CONTRIBUTIONS

AA, DL developed the hypothesis that the mathematical controller may be implemented in the nervous system. PS researched the literature. PS derived the hypothesis about the proposed serotonergic modulation. DL supported PS to find a control theoretically thorough biological implementation of DL control approach. AA, PS, DL designed the simulations. AA supervised the project. DL, PS implemented the simulations. PS ran the simulations and analyzed the results. AA, PS composed the paper. DL critically revised the paper.

ACKNOWLEDGMENTS

The authors cordially thank H. Jörntell for critical and helpful discussions about the biological hypotheses and the description of their consequences for biological research as presented in this paper. They express their thanks to N. Lii for his help in revising the paper. The authors also very much appreciate F. Röhrbein's help.

SUPPLEMENTARY MATERIAL

The Supplementary Material for this article can be found online at: http://journal.frontiersin.org/article/10.3389/fnbot.2016.00002

Video 1 | An illustration of the controller behavior. We show here the controlled movement of our complex mechanical system, i.e., a trunk with an attached leg. An included graph shows how the serotonin concentration within the motoneuron pools of muscles innervating joint 1 (hip) and 2 (knee) converge with time. We created the animation using *Showmotion*, which is a part of *Spatial_v2* Featherstone (2012).

Presentation 1 | Proof of the convergence of our simplified version of Oja's rule, Equation (5).

REFERENCES

Azad, M., and Featherstone, R. (2010). "Modelling the contact between a rolling sphere and a compliant ground plane," in *Australasian Conference Robotics and Automation* (Brisbane, QLD).

Bacon, S., Zagon, A., and Smith, A. (1990). Electron microscopic evidence of a monosynaptic pathway between cells in the caudal raphe nuclei and sympathetic preganglionic neurons in the rat spinal cord. *Exp. Brain Res.* 79, 589–602. doi: 10.1007/BF00229327

Bar-Cohen, Y. (2011). *Biomimetics: Nature-Based Innovation*. Biomimetics series. Boca Raton, FL; London; New York, NY: Taylor & Francis.

Barikhan, S. S., Wörgötter, F., and Manoonpong, P. (2014). "Multiple decoupled cpgs with local sensory feedback for adaptive locomotion behaviors of bio-inspired walking robots," in *From Animals to Animats 13*, Vol. 8575 of *Lecture Notes in Computer Science*, eds A. del Pobil, E. Chinellato, E. Martinez-Martin, J. Hallam, E. Cervera, and A. Morales (Cham; Heidelberg; New York, NY; Dordrecht; London: Springer International Publishing), 65–75.

Bennett, D. J., Hultborn, H., Fedirchuk, B., and Gorassini, M. (1998). Short-term plasticity in hindlimb motoneurons of decerebrate cats. *J. Neurophysiol.* 80, 2038–2045.

Best, J., Nijhout, H. F., and Reed, M. (2010). Serotonin synthesis, release and reuptake in terminals: a mathematical model. *Theor. Biol. Med. Model.* 7:34. doi: 10.1186/1742-4682-7-34

Brambilla, G., Buchli, J., and Ijspeert, A. (2006). "Adaptive four legged locomotion control based on nonlinear dynamical systems," in *From Animals to Animats 9*, *Vol. 4095 of Lecture Notes in Computer Science*, eds S. Nolfi, G. Baldassarre, R. Calabretta, J. Hallam, D. Marocco, J.-A. Meyer, O. Miglino, and D. Parisi (Berlin; Heidelberg: Springer), 138–149.

Braun, D. J., Howard, M., and Vijayakumar, S. (2011). "Exploiting variable stiffness in explosive movement tasks," in *Robotics: Science and Systems VII* (Los Angeles, CA: University of Southern California).

Brumley, M. R., Hentall, I. D., Pinzon, A., Kadam, B. H., Blythe, A., Sanchez, F. J., et al. (2007). Serotonin concentrations in the lumbosacral spinal cord of the adult rat following microinjection or dorsal surface application. *J. Neurophysiol.* 98, 1440–1450. doi: 10.1152/jn.00309.2007

Buchli, J., and Ijspeert, A. (2008). Self-organized adaptive legged locomotion in a compliant quadruped robot. *Auton. Robot.* 25, 331–347. doi: 10.1007/s10514-008-9099-2

Buschmann, T., Ewald, A., von Twickel, A., and Buschges, A. (2015). Controlling legs for locomotion-insights from robotics and neurobiology. *Bioinspir. Biomim.* 10:041001. doi: 10.1088/1748-3190/10/4/041001

Conway, B. A., Hultborn, H., and Kiehn, O. (1987). Proprioceptive input resets central locomotor rhythm in the spinal cat. *Exp. Brain Res.* 68, 643–656.

Cope, T. (2001). *Motor Neurobiology of the Spinal Cord*. Frontiers in Neuroscience. Boca Raton, FL; London; New York, NY; Washington, DC: CRC Press.

Dietz, V., Schmidtbleicher, D., and Noth, J. (1979). Neuronal mechanisms of human locomotion. *J. Neurophysiol.* 42, 1212–1222.

Featherstone, R. (2012). *Spatial_v2: Spatial Vector and Rigid-Body Dynamics Software*. Technical report, Australian National University.

Feeny, B., and Kappagantu, R. (1998). On the physical interpretation of proper orthogonal modes in vibrations. *J. Sound Vibration* 211, 607–616.

Freund, H.-J., and Büdingen, H. (1978). The relationship between speed and amplitude of the fastest voluntary contractions of human arm muscles. *Exp. Brain Res.* 31, 1–12.

Friemert, B., Faist, M., Spengler, C., Gerngross, H., Claes, L., and Melnyk, M. (2005). Intraoperative direct mechanical stimulation of the anterior cruciate ligament elicits short- and medium-latency hamstring reflexes. *J. Neurophysiol.* 94, 3996–4001. doi: 10.1152/jn.00410.2005

Grebenstein, M., Albu-Schäffer, A., Bahls, T., Chalon, M., Eiberger, O., Friedl, W., et al. (2011). "The dlr hand arm system," in *Robotics and Automation (ICRA), 2011 IEEE International Conference* (Shanghai: IEEE), 3175–3182.

Harris-Warrick, R. M. (2011). Neuromodulation and flexibility in Central Pattern Generator networks. *Curr. Opin. Neurobiol.* 21, 685–692. doi: 10.1016/j.conb.2011.05.011

Hatsopoulos, N. G. and Warren, W. H. Jr. (1996). Resonance tuning in rhythmic arm movements. *J. Mot. Behav.*, 28, 3–14.

Heckman, C., Lee, R. H., and Brownstone, R. M. (2003). Hyperexcitable dendrites in motoneurons and their neuromodulatory control during motor behavior. *Trends Neurosci.* 26, 688–695. doi: 10.1016/j.tins.2003.10.002

Heckman, C. J., Hyngstrom, A. S., and Johnson, M. D. (2008). Active properties of motoneurone dendrites: diffuse descending neuromodulation, focused local inhibition. *J. Physiol.* 586, 1225–1231. doi: 10.1113/jphysiol.2007.145078

Heckmann, C. J., Gorassini, M. A., and Bennett, D. J. (2005). Persistent inward currents in motoneuron dendrites: implications for motor output. *Muscle Nerve* 31, 135–156. doi: 10.1002/mus.20261

Hentall, I. D., Pinzon, A., and Noga, B. R. (2006). Spatial and temporal patterns of serotonin release in the rat's lumbar spinal cord following electrical stimulation of the nucleus raphe magnus. *Neuroscience* 142, 893–903. doi: 10.1016/j.neuroscience.2006.06.038

Hiebert, G. W., Whelan, P. J., Prochazka, A., and Pearson, K. G. (1996). Contribution of hind limb flexor muscle afferents to the timing of phase transitions in the cat step cycle. *J. Neurophysiol.* 75, 1126–1137.

Huang, Y., Vanderborght, B., Van Ham, R., and Wang, Q. (2014). Torque-stiffness-controlled dynamic walking with central pattern generators. *Biol. Cybern.* 108, 803–823. doi: 10.1007/s00422-014-0625-3

Hultborn, H. (1999). "Plateau potentials and their role in regulating motoneuronal firing," in *Peripheral and Spinal Mechanisms in the Neural Control of Movement*, Progress in Brain Research, ed M. Binder (Elsevier Science), 39–48.

Hyngstrom, A. S., Johnson, M. D., Miller, J. F., and Heckman, C. J. (2007). Intrinsic electrical properties of spinal motoneurons vary with joint angle. *Nat. Neurosci.* 10, 363–369. doi: 10.1038/nn1852

Jacobs, B. L., Martin-Cora, F. J., and Fornal, C. A. (2002). Activity of medullary serotonergic neurons in freely moving animals. *Brain Res. Rev.* 40, 45–52. doi: 10.1016/S0165-0173(02)00187-X

Jankowska, E. (1992). Interneuronal relay in spinal pathways from proprioceptors. *Prog. Neurobiol.* 38, 335–378.

Johansson, H., and Silfvenius, H. (1977). Connexions from large, ipsilateral hind limb muscle and skin afferents to the rostral main cuneate nucleus and to the nucleus x region in the cat. *J. Physiol.* 265, 395–428.

Johnson, M. D., and Heckman, C. J. (2014). Gain control mechanisms in spinal motoneurons. *Front. Neural Circuits* 8:81. doi: 10.3389/fncir.2014.00081

Katz, D. M., and Kimelberg, H. K. (1985). Kinetics and autoradiography of high affinity uptake of serotonin by primary astrocyte cultures. *J. Neurosci.* 5, 1901–1908.

Kim, D. K., Jung, S. J., Kim, S. J., Kwak, J., and Kim, J. (2003). Dependence of long-term potentiation on the interval between A- and C-responses of the spinal dorsal horn neurons in rats. *Neurosci. Lett.* 348, 33–36. doi: 10.1016/S0304-3940(03)00651-7

Lakatos, D., and Albu-Schäffer, A. (2014a). "Neuron model interpretation of a cyclic motion control concept," in *Biomedical Robotics and Biomechatronics, 2014 5th IEEE RAS EMBS International Conference* (São Paulo: IEEE), 905–910.

Lakatos, D., and Albu-Schäffer, A. (2014b). "Switching based limit cycle control for compliantly actuated second-order systems," in *Proceedings of the IFAC World Congress*, Vol. 19 (Cape Town), 6392–6399.

Lakatos, D., Garofalo, G., Petit, F., Ott, C., and Albu-Schaffer, A. (2013a). "Modal limit cycle control for variable stiffness actuated robots," in *Robotics and Automation (ICRA), 2013 IEEE International Conference* (Karlsruhe: IEEE), 4934–4941.

Lakatos, D., Gorner, M., Petit, F., Dietrich, A., and Albu-Schäffer, A. (2013b). "A modally adaptive control for multi-contact cyclic motions in compliantly actuated robotic systems," in *Intelligent Robots and Systems (IROS), 2013 IEEE/RSJ International Conference* (Tokyo: IEEE), 5388–5395.

Lakatos, D., Petit, F., and Albu-Schaffer, A. (2014). Nonlinear oscillations for cyclic movements in human and robotic arms. *Robot. IEEE Trans.* 30, 865–879. doi: 10.1109/TRO.2014.2308371

Landgren, S., and Silfvenius, H. (1971). Nucleus z, the medullary relay in the projection path to the cerebral cortex of group i muscle afferents from the cat's hind limb. *J. Physiol.* 218, 551–571.

MacKay-Lyons, M. (2002). Central pattern generation of locomotion: a review of the evidence. *Phys. Ther.* 82, 69–83. Available online at: http://ptjournal.apta.org/content/82/1/69.long

Molodtsova, G. F. (1983). [Effect of prolonged cold exposure on monoamine oxidase activity and kinetics and on serotonin metabolism in the rat brain]. *Biull. Eksp. Biol. Med.* 96, 16–18.

Morasso, P. (1981). Spatial control of arm movements. *Exp. Brain Res.* 42, 223–227.

Nachstedt, T., Wörgötter, F., and Manoonpong, P. (2012). "Adaptive neural oscillator with synaptic plasticity enabling fast resonance tuning," in *Artificial Neural Networks and Machine Learning at ICANN 2012, Vol. 7552 of Lecture Notes in Computer Science*, eds A. Villa, W. Duch, P. ÃĽrdi, F. Masulli, and G. Palm (Berlin; Heidelberg: Springer), 451–458.

Nieuwenhuys, R., Voogd, J., and van Huijzen, C. (2007). *The Human Central Nervous System: A Synopsis and Atlas*. Berlin; Heidelberg: Steinkopff.

Nishimura, Y., Perlmutter, S. I., Eaton, R. W., and Fetz, E. E. (2013). Spike-timing-dependent plasticity in primate corticospinal connections induced during free behavior. *Neuron* 80, 1301–1309. doi: 10.1016/j.neuron.2013.08.028

Oja, E. (1982). Simplified neuron model as a principal component analyzer. *J. Math. Biol.* 15, 267–273.

Oja, E. (1992). Principal components, minor components, and linear neural networks. *Neural Netw.* 5, 927–935.

Pearlstein, E., Ben Mabrouk, F., Pflieger, J. F., and Vinay, L. (2005). Serotonin refines the locomotor-related alternations in the *in vitro* neonatal rat spinal cord. *Eur. J. Neurosci.* 21, 1338–1346. doi: 10.1111/j.1460-9568.2005.03971.x

Pelc, E. H., Daley, M. A., and Ferris, D. P. (2008). Resonant hopping of a robot controlled by an artificial neural oscillator. *Bioinspir. Biomim.* 3:026001. doi: 10.1088/1748-3182/3/2/026001

Perrier, J. F., and Delgado-Lezama, R. (2005). Synaptic release of serotonin induced by stimulation of the raphe nucleus promotes plateau potentials in spinal motoneurons of the adult turtle. *J. Neurosci.* 25, 7993–7999. doi: 10.1523/JNEUROSCI.1957-05.2005

Perrier, J. F., Rasmussen, H. B., Christensen, R. K., and Petersen, A. V. (2013). Modulation of the intrinsic properties of motoneurons by serotonin. *Curr. Pharm. Des.* 19, 4371–4384. doi: 10.2174/1381612811319990341

Pfister, J.-P., and Gerstner, W. (2006). Triplets of spikes in a model of spike timing-dependent plasticity. *J. Neurosci.* 26, 9673–9682. doi: 10.1523/JNEUROSCI.1425-06.2006

Raibert, M., Blankespoor, K., Nelson, G., Playter, R., and the BigDog Team (2008). "Bigdog, the rough-terrain quadruped robot," in *Proceedings of the 17th World Congress*, Vol. 17 (Seoul), 10822–10825.

Righetti, L., Buchli, J., and Ijspeert, A. J. (2006). Dynamic hebbian learning in adaptive frequency oscillators. *Phys. D Nonlinear Phenomena* 216, 269–281. doi: 10.1016/j.physd.2006.02.009

Rossignol, S., Dubuc, R., and Gossard, J. P. (2006). Dynamic sensorimotor interactions in locomotion. *Physiol. Rev.* 86, 89–154. doi: 10.1152/physrev.00028.2005

Schouenborg, J. (2004). Learning in sensorimotor circuits. *Curr. Opin. Neurobiol.* 14, 693–697. doi: 10.1016/j.conb.2004.10.009

Shemmell, J., An, J. H., and Perreault, E. J. (2009). The differential role of motor cortex in stretch reflex modulation induced by changes in environmental mechanics and verbal instruction. *J. Neurosci.* 29, 13255–13263. doi: 10.1523/jneurosci.0892-09.2009

Sjöström, P. J., Turrigiano, G. G., and Nelson, S. B. (2001). Rate, timing, and cooperativity jointly determine cortical synaptic plasticity. *Neuron* 32, 1149–1164. doi: 10.1016/S0896-6273(01)00542-6

Skagerberg, G., and Bjorklund, A. (1985). Topographic principles in the spinal projections of serotonergic and non-serotonergic brainstem neurons in the rat. *Neuroscience* 15, 445–480.

Sławińska, U., Miazga, K., and Jordan, L. M. (2014). $[5\text{-HT}]_2$ and $[5\text{-HT}]_7$ receptor agonists facilitate plantar stepping in chronic spinal rats through actions on different populations of spinal neurons. *Front. Neural Circuits* 8:95. doi: 10.3389/fncir.2014.00095

Spanne, A., Geborek, P., Bengtsson, F., and Jörntell, H. (2014). Spike generation estimated from stationary spike trains in a variety of neurons *in vivo*. *Front. Cell. Neurosci.* 8:199. doi: 10.3389/fncel.2014.00199

Springfield, S. A., and Moolenaar, G.-M. (1983). Differences in the responses of raphe nuclei to repetitive somatosensory stimulation. *Exp. Neurol.* 79, 360–370.

Sreenath, K., Park, H.-W., Poulakakis, I., and Grizzle, J. W. (2010). A compliant hybrid zero dynamics controller for stable, efficient and fast bipedal walking on MABEL. *Int. J. Robot. Res.* 30, 1170–1193. doi: 10.1177/0278364910379882

Stramigioli, S., and van Dijk, M. (2008). "Energy conservation limit cycle oscillations," in *International Federation Of Automatic Control, Proceedings Of The 17th World Congress* (Seoul), 15666–15671.

Taube, W., Leukel, C., and Gollhofer, A. (2012). How neurons make us jump: the neural control of stretch-shortening cycle movements. *Exerc. Sport Sci. Rev.* 40, 106–115. doi: 10.1097/JES.0b013e31824138da

van Rossum, M. C., Bi, G. Q., and Turrigiano, G. G. (2000). Stable Hebbian learning from spike timing-dependent plasticity. *J. Neurosci.* 20, 8812–8821. Available online at: http://www.jneurosci.org/content/20/23/8812.long

Veasey, S. C., Fornal, C. A., Metzler, C. W., and Jacobs, B. L. (1995). Response of serotonergic caudal raphe neurons in relation to specific motor activities in freely moving cats. *J. Neurosci.* 15(7 Pt 2), 5346–5359.

Verleysdonk, S., Hamprecht, B., Rapp, M., and Wellard, J. (2004). Uptake and metabolism of serotonin by ependymal primary cultures. *Neurochem. Res.* 29, 1739–1747. doi: 10.1023/B:NERE.0000035810.08543.97

Whelan, P. J., Hiebert, G. W., and Pearson, K. G. (1995a). Stimulation of the group I extensor afferents prolongs the stance phase in walking cats. *Exp. Brain Res.* 103, 20–30.

Whelan, P. J., Hiebert, G. W., and Pearson, K. G. (1995b). Plasticity of the extensor group I pathway controlling the stance to swing transition in the cat. *J. Neurophysiol.* 74, 2782–2787.

Xiong, X., Wörgötter, F., and Manoonpong, P. (2015). Adaptive and energy efficient walking in a hexapod robot under neuromechanical control and sensorimotor learning. *Cybern. IEEE Trans.* doi: 10.1109/TCYB.2015.2479237. [Epub ahead of print].

Zenke, F., Hennequin, G., and Gerstner, W. (2013). Synaptic plasticity in neural networks needs homeostasis with a fast rate detector. *PLoS Comput. Biol.* 9:e1003330. doi: 10.1371/journal.pcbi.1003330

Zondervan, D. K., Duarte, J. E., Rowe, J. B., and Reinkensmeyer, D. J. (2014). Time flies when you are in a groove: using entrainment to mechanical resonance to teach a desired movement distorts the perception of the movement's timing. *Exp. Brain Res.* 232, 1057–1070. doi: 10.1007/s00221-013-3819-3

Conflict of Interest Statement: The authors declare that the research was conducted in the absence of any commercial or financial relationships that could be construed as a potential conflict of interest.

Supplemental Data: Neuromodulation and Synaptic Plasticity for the Control of Fast Periodic Movement: Energy Efficiency in Coupled Compliant Joints via PCA

Philipp Stratmann, Dominic Lakatos, Alin Albu-Schäffer
*Correspondence:
Philipp Stratmann
Philipp.Stratmann@dlr.de

P1 PROOF OF THE CONVERGENCE OF OUR SIMPLIFIED VERSION OF OJA'S RULE

In the following, we want to show that the update rule, eq. (5) in the article,

$$\frac{\mathrm{d}}{\mathrm{dt}}\boldsymbol{w}(t) = c_w\boldsymbol{\varphi} - \frac{1}{\tau_{eff}}\boldsymbol{w},$$

leads to a weight vector that is aligned with the result of Oja's rule, eq. (4) in the article, despite having a different magnitude. We claim that this is true as long as the weights and sensory signals are positive. We consider the case of two joints, a higher-dimensional consideration of Oja's rule (but not its simplified form) has been performed by Miller and MacKay (1994). The controller assumes that the dynamics of the oscillating mechanical system can be linearized and described by a linear second order system (Lakatos et al., 2013),

$$\ddot{\boldsymbol{\varphi}} + \boldsymbol{B}\boldsymbol{\varphi} = 0. \tag{1}$$

Using orthogonal eigenmodes $\boldsymbol{a}_k$, its trajectories are given by

$$\boldsymbol{\varphi}(t) = \sum_k \boldsymbol{a}_k \sin(\omega_k t + \phi_k) \tag{2}$$

and the dominant principal component corresponds to the dominant eigenmode $\boldsymbol{a}_1$ (Feeny and Kappagantu, 1998).

P1.1 Finding Fixed Points

We are only interested in the relative magnitude of weights corresponding to joints i, j and hence define

$$w_{i/j} := \frac{w_i}{w_j} \tag{3}$$

$$\varphi_{i/j} := \frac{\varphi_i}{\varphi_j} \tag{4}$$

to rearrange Oja's rule, eq. (4) in the article, to

$$\frac{\mathrm{d}}{\mathrm{dt}} w_{i/j} = \gamma(w_{i/j}\varphi_i + \varphi_j)\varphi_j \left[\varphi_{i/j} - w_{i/j}\right] \tag{5}$$

and the simplified update rule, eq. (5) in the article, to

$$\frac{\mathrm{d}}{\mathrm{dt}} w_{i/j} = c_w \frac{\varphi_j}{w_j} \left[\varphi_{i/j} - w_{i/j}\right] \tag{6}$$

The relative magnitude of weights is a fixed point when $\frac{d}{dt}(w_{i/j}) = 0$. For $c_w,\ w_i,\ w_j,\ \varphi_i,\ \varphi_j > 0$, both derivations imply the same fixed point

$$\frac{w_i}{w_j} = \frac{\varphi_i}{\varphi_j} = const. \tag{7}$$

This term is constant when all summands except for one have decayed in eq. (2).

P1.2 Stability

In order to prove stability, we linearize eq. (5) and eq. (6) around the fixed points. For Oja's rule we find

$$\frac{\mathrm{d}}{\mathrm{d}w_{i/j}}(\frac{\mathrm{d}}{\mathrm{dt}} w_{i/j}) = \gamma\varphi_i\varphi_j \left[\varphi_{i/j} - w_{i/j}\right] - \gamma(w_{i/j}\varphi_i + \varphi_j)\varphi_j \tag{8}$$

$$= -\gamma(\varphi_i^2 + \varphi_j^2) < 0. \tag{9}$$

For the simplified rule we find

$$\frac{\mathrm{d}}{\mathrm{d}w_{i/j}}(\frac{\mathrm{d}}{\mathrm{dt}} w_{i/j}) = c_w\varphi_j \left[\varphi_{i/j} - w_{i/j}\right] \frac{d(\frac{1}{w_j})}{dw_{i/j}} - c_w\frac{\varphi_j}{w_j} \tag{10}$$

$$= c_w\varphi_j \left[\varphi_{i/j} - w_{i/j}\right] \frac{1}{w_{i/j}} - c_w\frac{\varphi_j}{w_j} \tag{11}$$

$$= -c_w\frac{\varphi_j}{w_j}, \tag{12}$$

which is < 0 as long as weights and sensory signals are strictly positive. Therefore, both update rules converge towards the same relative weights, i.e. the weight vectors subject to either plasticity rule align.

REFERENCES

Feeny, B. and Kappagantu, R. (1998). On the physical interpretation of proper orthogonal modes in vibrations. *Journal of Sound and Vibration* 211, 607 – 616

Lakatos, D., Gorner, M., Petit, F., Dietrich, A., and Albu-Schäffer, A. (2013). A modally adaptive control for multi-contact cyclic motions in compliantly actuated robotic systems. In *Intelligent Robots and Systems (IROS), 2013 IEEE/RSJ International Conference on*. 5388–5395

Miller, K. D. and MacKay, D. J. C. (1994). The role of constraints in hebbian learning. *Neural Computation* 6, 100–126

Manuscript Guidelines

Open access and copyright

https://www.frontiersin.org/about/author-guidelines, accessed on 02.11.2018

Scaling our world view: how monoamines can put context into brain circuitry

Authors Philipp Stratmann, Alin Albu-Schäffer, Henrik Jörntell

Journal Frontiers in Cellular Neuroscience

Number of pages 22

Review Peer reviewed

Abstract Monoamines are presumed to be diffuse metabotropic neuromodulators of the topographically and temporally precise ionotropic circuitry which dominates CNS functions. Their malfunction is strongly implicated in motor and cognitive disorders, but their function in behavioral and cognitive processing is scarcely understood. In this paper, the principles of such a monoaminergic function are conceptualized for locomotor control. We find that the serotonergic system in the ventral spinal cord scales ionotropic signals and shows topographic order that agrees with differential gain modulation of ionotropic subcircuits. Whereas the subcircuits can collectively signal predictive models of the world based on life-long learning, their differential scaling continuously adjusts these models to changing mechanical contexts based on sensory input on a fast time scale of a few 100 ms. The control theory of biomimetic robots demonstrates that this precision scaling is an effective and resource-efficient solution to adapt the activation of individual muscle groups during locomotion to changing conditions such as ground compliance and carried load. Although it is not unconceivable that spinal ionotropic circuitry could achieve scaling by itself, neurophysiological findings emphasize that this is a unique functionality of metabotropic effects since recent recordings in sensorimotor circuitry conflict with mechanisms proposed for ionotropic scaling in other CNS areas. We substantiate that precision scaling of ionotropic subcircuits is a main functional principle for many monoaminergic projections throughout the CNS, implying that the monoaminergic circuitry forms a network within the network composed of the ionotropic circuitry. Thereby, we provide an early-level interpretation of the mechanisms of psychopharmacological drugs that interfere with the monoaminergic systems.

Author contributions Initiated and managed the collaboration; co-developed the structure of the paper; researched literature and authored sections 1–7 and 9; handled reviews.

frontiers in Cellular Neuroscience

HYPOTHESIS AND THEORY
published: 20 December 2018
doi: 10.3389/fncel.2018.00506

Scaling Our World View: How Monoamines Can Put Context Into Brain Circuitry

Philipp Stratmann[1,2*], *Alin Albu-Schäffer*[1,2] *and Henrik Jörntell*[3]

[1] *Sensor Based Robotic Systems and Intelligent Assistance Systems, Department of Informatics, Technical University of Munich, Garching, Germany,* [2] *German Aerospace Center (DLR), Institute of Robotics and Mechatronics, Weßling, Germany,* [3] *Neural Basis of Sensorimotor Control, Department of Experimental Medical Science, Lund University, Lund, Sweden*

Monoamines are presumed to be diffuse metabotropic neuromodulators of the topographically and temporally precise ionotropic circuitry which dominates CNS functions. Their malfunction is strongly implicated in motor and cognitive disorders, but their function in behavioral and cognitive processing is scarcely understood. In this paper, the principles of such a monoaminergic function are conceptualized for locomotor control. We find that the serotonergic system in the ventral spinal cord scales ionotropic signals and shows topographic order that agrees with differential gain modulation of ionotropic subcircuits. Whereas the subcircuits can collectively signal predictive models of the world based on life-long learning, their differential scaling continuously adjusts these models to changing mechanical contexts based on sensory input on a fast time scale of a few 100 ms. The control theory of biomimetic robots demonstrates that this precision scaling is an effective and resource-efficient solution to adapt the activation of individual muscle groups during locomotion to changing conditions such as ground compliance and carried load. Although it is not unconceivable that spinal ionotropic circuitry could achieve scaling by itself, neurophysiological findings emphasize that this is a unique functionality of metabotropic effects since recent recordings in sensorimotor circuitry conflict with mechanisms proposed for ionotropic scaling in other CNS areas. We substantiate that precision scaling of ionotropic subcircuits is a main functional principle for many monoaminergic projections throughout the CNS, implying that the monoaminergic circuitry forms a network within the network composed of the ionotropic circuitry. Thereby, we provide an early-level interpretation of the mechanisms of psychopharmacological drugs that interfere with the monoaminergic systems.

Keywords: monoamine neurotransmitter disorders, motor control, motor learning, neuromodulation, principal component analysis, raphe nuclei, serotonin, spinal cord

OPEN ACCESS

Edited by:
Jing-Ning Zhu,
Nanjing University, China

Reviewed by:
Jian Jing,
Nanjing University, China
Tjeerd V. Olde Scheper,
Oxford Brookes University,
United Kingdom

***Correspondence:**
Philipp Stratmann
philipp.stratmann@tum.de

Received: *13 September 2018*
Accepted: *06 December 2018*
Published: *20 December 2018*

Citation:
Stratmann P, Albu-Schäffer A and Jörntell H (2018) Scaling Our World View: How Monoamines Can Put Context Into Brain Circuitry. Front. Cell. Neurosci. 12:506. doi: 10.3389/fncel.2018.00506

1. INTRODUCTION

Metabotropic neuromodulators are ubiquitous in the CNS. Together with acetylcholine (Picciotto et al., 2012), the four monoamines serotonin (5-HT), dopamine, noradrenaline, and histamine dominate neuromodulatory effects in the CNS (Cools et al., 2011; O'Donnell et al., 2012; Yu et al., 2015). These molecules are strongly implicated in mood and affective state, while their malfunction is tightly linked to cognitive disorders (Kurian et al., 2011; Howell and Cunningham, 2015; Ng et al., 2015; Mather and Harley, 2016). A common view is that brain function emanates

from signal processing of the ionotropic functional and anatomical connectome of the brain, which occurs with high topographic and temporal precision. In contrast to ionotropic neurotransmission, neuromodulation produces no direct excitatory or inhibitory effects mediated by the activation of the fast-acting ionotropic glutamate or GABA receptors. Instead, neuromodulation acts on G protein-coupled receptors and thereby changes the surface expression or efficacy of potassium, calcium, or sodium channels. This scales the general excitability, or gain, of the neuron (Haas et al., 2008; Rosenbaum et al., 2009; Beaulieu and Gainetdinov, 2011; Bargmann, 2012; Picciotto et al., 2012; Perrier et al., 2013; Husch et al., 2015; Perrier and Cotel, 2015). So far, monoamines are presumed to provide a diffuse general modulation of large connectome circuits (Fuxe et al., 2010). But knowledge of the specific functional contributions of monoaminergic neuromodulators to neuronal processing and the resulting integrative behavior is scarce.

In this paper, a novel functional principle is deduced for monoamines as temporal- and subcircuit-precise gain modulators. Whereas the ionotropic subcircuits can collectively signal predictive models of the world based on life-long learning, monoamines are shown to scale the influence of functionally distinct neuronal subcircuits individually. Hereby, their effects show just the right time constant to adjust the models to quickly changing contexts. By this precision scaling, monoamines provide an operation which may overcome functional limitations of ionotropic networks that apply under physiological conditions. The principle emerges from an analysis of monoaminergic effects in the specific context of locomotion, which integrates control theory of biomimetic robots, motor control neuroscience, and neurobiological findings on monoamine systems. Accordingly, serotonin must be assumed to scale motorpools of an individual joint when it shows particularly large movement, because this implies that the respective joint can be moved with smaller metabolic requirements. This precision scaling dramatically simplifies motor control adaptation in the face of gradually changing mechanical conditions which, for example, take place as one steps from a solid to a soft ground or lifts a load. But the principle of precision scaling is also tentatively applicable to general computational interactions between neuronal populations throughout the CNS and may thus support various high- and low-level functions.

Here we focus on the spinal motor circuitry to deduce if the CNS applies precision scaling. This focus has two reasons: First, it is comparatively easy to interpret how information is encoded and reconstruct how information is processed, because the spinal circuitry is the final motor output stage and the entry stage of low-level sensory feedback signals (Franklin et al., 2016). In contrast, higher-level systems operate by using more abstracted information that can be hard to interpret. Second, the control of body movement is widely assumed to be a major, if not the most important, factor for the evolution of the CNS (Wise and Shadmehr, 2002; Babič et al., 2016). This implies that cognitive levels evolved while being constrained by the spinal motor output and sensory input circuitry. Motor control can therefore be regarded as a basis to understand such higher integrative circuits.

In order to understand the spinal motor control, modern robotics control theory, which has been developed for robots with increasing functional similarity to biological locomotor systems, offers multiple advantages: Robotic control theory can provide comprehensive and well-tested analytical tools. If the major constraints of the CNS are taken into account, it further offers highly specific interpretational frames for understanding observations of sensorimotor control in the CNS. It goes without saying that early-stage testing of concepts for biological motor control is easier in robots than in biological systems.

In the present paper, we suggest that the mode of operation of various monoaminergic systems in the CNS is *precision scaling*, i.e., a topographically and temporally specific gain control of local neuronal operation. In the chain of argumentation that leads up to this prediction, we start out by comparing the functional operations within monoamine-driven metabotropic systems with those observed in ionotropic circuitry. Accordingly, the spinal ionotropic circuitry integrates descending motor commands and sensory signals and linearly processes them into muscle signals. By this function, it dominates the spinal generation of motor patterns, which has further contributions from gap junctions and diffuse metabotropic effects. Mathematically, the ionotropic circuitry transforms between the different representations, or the different "views," of the world as they are encoded by the individual processing stages (section 2). Nonlinear signal processing is required to adjust these transformations to changing contexts. Based on neurophysiological findings, these non-linear adjustments are ideally solved by neuromodulatory scaling of the ionotropic signals due to the properties of the serotonergic system (section 3). The scaling effect renders the metabotropic system functionally unique, given that ionotropic effects proposed for non-linear signal processing in other CNS areas are unlikely to apply to spinal circuitry conditions *in vivo* according to recent experimental studies (section 4). Subsequently, the spatial and temporal precision of the spinal serotonergic system is evaluated to see if it may perform tasks that cannot be obtained by ionotropic circuitry under the influence of exclusively diffuse neuromodulation. Insights from robotic control and motor neuroscience are combined to identify such a task and deduce how focused serotonin must act, both anatomically and temporally, in order to solve it (sections 5, 6). This functionally required precision is demonstrated to coincide with the neuroscientifically observed topographic and temporal precision of serotonergic effects in the spinal cord (section 7). Monoamines must therefore be considered, at least partly, subcircuit- and temporally-specific gain modulators of ionotropic circuitry, motivating the term *precision scaling*. As will be shown toward the end of this paper, precision scaling can potentially apply to multiple levels of CNS function and may explain the effects of psychopharmacological drugs that act on monoamine systems in the brain (section 8).

2. THE SPINAL CORD AS TRANSFORMER OF WORLD VIEWS

The function of the CNS emanates from the neurophysiological processes in the individual neurons and the precise network

of connections between them. In order to understand how monoaminergic neuromodulatory influences neuronal circuitry, it is important to first understand how functions arise in networks of ionotropic circuitry.

2.1. Linear Signal Processing Transforms How Spinal Neurons Encode the World

An individual neuron primarily works by integrating information in the form of the electrical signals it receives from other neurons by synaptic transmission. In response to the summated effect of those inputs, it issues electrical signals that reach other neurons. Hence, it can be said to process information. In the spinal cord, recent electrophysiological findings suggest that the neurons are hereby limited to linear processing of information encoded by ionotropic signals: Spinal interneurons which are subject to increasing single or multiple synaptic inputs respond linearly under physiological conditions *in vivo* (Prut and Perlmutter, 2003; Shalit et al., 2012; Spanne et al., 2014; Zelenin et al., 2015). In particular, they are active well before overt movement starts and do not saturate (Prut and Perlmutter, 2003), implying that they are in their linear regime during a movement. Investigations assign the same linear response to spinal motorneurons in anesthetized animals and *in vitro* (Powers and Binder, 1995, 2000; Hultborn et al., 2003; Cushing et al., 2005; Hyngstrom et al., 2008).

As the CNS forwards information from one group of neurons to another, it filters out irrelevant aspects, combines data of different origin, and adjusts the way the information is encoded. All CNS functions can be traced back to such basal neuronal circuitry mechanisms. These basal mechanisms can be cascaded and integrated to create interesting local functions. The local functions can to a large extent be shaped by learning and can be regarded as partial, often predictive, models of the world, e.g., describing how photoreceptors are distributed across the retina or what motor signals must be elicited to perform a particular task (Brown and Brüne, 2012; Bhanpuri et al., 2013). What model of the world a neuronal circuit contains is determined by an associated coordinate space. For motor control, illustrative examples of coordinate spaces are found in visual reaching tasks: The target position is initially encoded as a pixelated image mapped in a retinotopic reference frame (Heed et al., 2015). To reach the target, the incoming visual signal requires neuronal processing and merging with additional information represented in non-retinotopic reference frames (cf. **Figure 1**). Processing generates an appropriate movement intention and an according signal in a musculotopic coordinate space at the level of the spinal motorneurons (Graziano, 2006; Yanai et al., 2008). Describing how a neuronal circuit encodes its associated coordinate space requires knowledge of the set of qualitatively relevant categories of encoded information. The categories may in principle be directly linked to physical quantities (Franklin et al., 2016), such as the activation of different muscles. But at integrative stages, they may also be linked to more high-level quantities like the social status and familiarity that an animal takes into account before approaching a potential partner. They may even be linked to highly abstract quantities with no direct counterpart in the physical world. Given appropriate coordinates, it is convenient to describe the information encoded in a group of neurons as a vector,

$$\boldsymbol{x} = \begin{pmatrix} x_1 \\ x_2 \\ \vdots \end{pmatrix}. \tag{1}$$

Each coordinate x_1, x_2, ... would in the mentioned examples describe the motor signal driving a single muscle or a component of a higher-level quantity encoded by the CNS. It can be represented by the signal of individual, or groups of, neurons (Cunningham and Yu, 2014).

Between coordinate spaces, linear neurons as found in the spinal cord perform affine transformations. Affine transformations, which are exemplified in **Figure 1**, are heavily used by engineers since they often approximate general transformations involving arbitrary mathematical functions very well for a limited range of input values around an operating point (Cohen and Tan, 2012). In a network consisting of linear neurons, each neuron j receives sensory inputs from presynaptic neurons i, which is represented by a firing rate x_i for rate-coding neurons. The inputs are weighted by synaptic weights w_{ij} and subject to a neuron-specific firing threshold θ_j. In summary, the output firing rate y_j in neuron j can be described by the linear function

$$y_j(x_1, x_2, \ldots) = \sum_i w_{\mathrm{ij}} \cdot x_i - \theta_j. \tag{2}$$

Equation (2) can be represented in vector notation as

$$\boldsymbol{y}(\boldsymbol{x}) = \boldsymbol{W}_{\mathrm{xy}} \cdot \boldsymbol{x} - \boldsymbol{\theta}_{\mathrm{y}}. \tag{3}$$

It defines the affine transformation between two coordinate spaces in which the signal can be represented by coordinates $\boldsymbol{x}$ and $\boldsymbol{y}$, respectively.

A spinal ionotropic network consisting of linear neurons is limited to implement an affine transformation which can be described by Equation (3). Neither additional feedforward layers, nor recurrent synaptic connections can change this functional property. If the neuronal network is extended by intercalating further layers of linear neurons between the input and output layer, only the effective transformation weights $\boldsymbol{W}_{\mathrm{xy}}$ and threshold $\boldsymbol{\theta}_{\mathrm{y}}$ of the transformation will change. As shown in **Figure 2A**, the output firing rate will remain a linear function of the network input. If the network is extended by recurrent synaptic connections, it can memorize input and process time-series of data. Thereby, its output may vary non-linearly with time and, for example, converge to a steady state or oscillate (Dayan and Abbott, 2001). But at each time step, the network output $\boldsymbol{y}$ remains a linear function of its previous input $\boldsymbol{x}$ at previous time steps, as illustrated in **Figure 2B**.

2.2. Non-linear Signal Processing Is Required When the World Changes

Artificial neural networks have, with the enormous scientific and economical success of deep learning in particular and

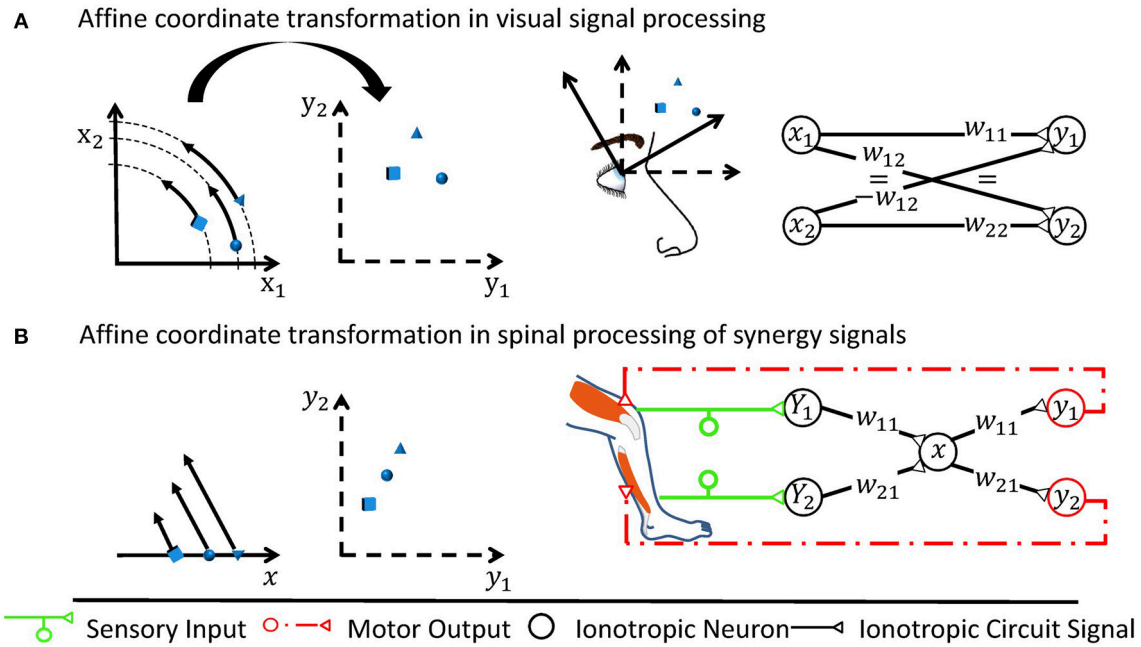

FIGURE 1 | Two examples of affine transformations and their simplest neuronal circuitry connectivity solution. Each transformation is made from a coordinate space represented by neuronal states (x_1, x_2) or x to a space represented by (y_1, y_2), respectively. For rate-coded models, these neuronal states would be equivalent to firing rates of neurons or neuron pools. Sketches of neuronal networks show the simplest possible way by which the CNS might implement each transformation. As illustrated for each panel, the networks in effect re-calculate individual signals encoded by the neuronal states into new individual neuronal states, where the re-calculation is the specific transformation made and is illustrated by arrows in the leftmost graph. **(A)** A rotation is assumed to occur when neurons transform retinotopic neuronal signals occurring at early visual processing stages to a head-centered representation at later stages (Heed et al., 2015). **(B)** Shown here is the transformation underlying a motor synergy, i.e., a spinal circuit which emits common ionotropic signals to actuate muscles that the neuronal synergy models as agonists (Santello et al., 2016). The low-dimensional synergy signal x is thereby transformed into the high-dimensional musculotopic space represented by coordinates (y_1, y_2). Signals (Y_1, Y_2), such as sensory signals, can be transformed into this low-dimensional synergistic subspace by orthogonal projections.

of artificial intelligence in general, strongly facilitated the view that also biological neuronal networks can approximate general transformations which adjust the output of the network to arbitrarily changing conditions (Chen et al., 2015). In mathematical terms, they are said to perform universal classification and function approximation. This view relies on the model of neurons as non-linear integrators of incoming signals (Cybenko, 1989; Hornik, 1991). While this contrasts the observed linear interaction of ionotropic signals for the specific example of the spinal circuitry, it must be assumed that also the spinal cord needs mechanisms which non-linearly combine external signals with the ionotropic inputs that the neuronal network processes. This becomes particularly obvious under quickly changing mechanical conditions of the environment and the locomotor system. Hereby, the changing context often requires that the CNS reacts differently to the same inputs. The multiplicative transformation weights of Equation (2) must therefore be context-dependent and change with a signal s which encodes the external cue,

$$y_j(x_1, x_2, \ldots, s) = \sum_i w_{ij}(s) \cdot x_i - \theta_j \,. \qquad (4)$$

This implies a non-linear integration of the signals s and x_i. In contrast, adding the signal s as an additional linear input, e.g., by a reflex loop that signals s and also converges onto the neurons j, would only additively increase the output of the network. In effect, it would only change its firing threshold θ_j.

By adjusting individual transformation weights independently from each other, the motor circuitry can gain a unique functionality. **Figure 3** illustrates this functionality based on the transformation of context-dependent motor signals from M1 onto the musculotopic motor output within spinal circuits. Hereby, pools of M1 neurons typically elicit a common motor command which is transformed into musculotopic signals as it is transmitted to spinal motorneurons either directly or through spinal interneurons (Yanai et al., 2008). The transformed motor command activates the spinal motorneuron pools of several muscles to produce a meaningful pattern of muscle contraction (Graziano, 2006; Overduin et al., 2012; Gallego et al., 2017). In this circuit, the transformation weights along the path between M1 and the motorneuron pools will need to be scaled in a pool-specific manner if a new mechanical condition necessitates that the involved muscles change their force output relative to each other. Similar examples for neuronal operations that require changing transformation weights can be found in integrative circuits such as the ventral intraparietal area. This area encodes an abstract representation of vestibular self-motion signals that is independent of head and eye position (Chen et al., 2013). To

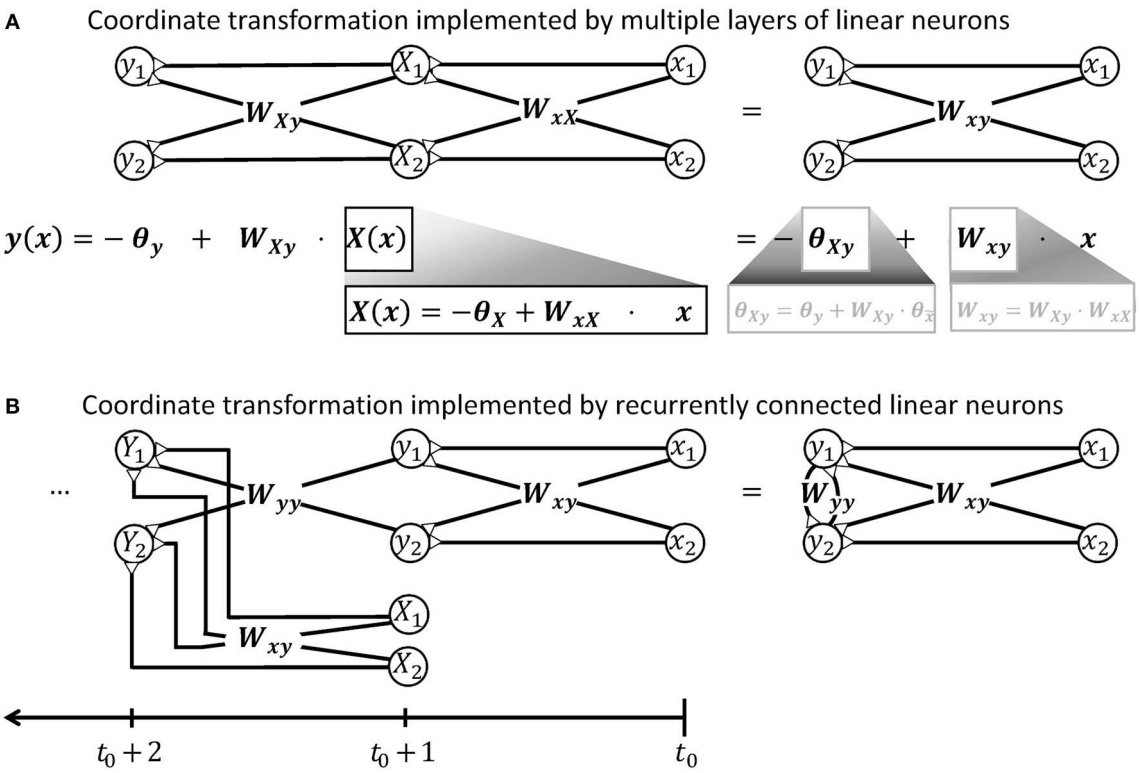

FIGURE 2 | Illustration demonstrating that a network of linear neurons is restricted to implement an affine coordinate transformation of the form $\boldsymbol{y}(\boldsymbol{x}) = \boldsymbol{W}_{\mathrm{xy}}\boldsymbol{x} - \boldsymbol{\theta}_{\boldsymbol{y}}$. **(A)** This relationship is independent of the number of incorporated neuronal feedforward layers. Adding additional layers of neurons changes the input-independent transformation weight $\boldsymbol{W}$ and the shift $\boldsymbol{\theta}$ of the basis, but the mathematical form remains. **(B)** Neuronal networks with recurrent connections are subject to the same limitation. To confirm this, it is advantageous to unfold the calculations performed by the recurrent network shown on the right hand side and deduce a hypothetical feedforward network that computes the same output. When the recurrent network receives an input signal $\boldsymbol{x}$ released at t_0, it will produce an output signal $\boldsymbol{y}$ like a simple feedforward network at $t_0 + 1$, i.e., after a short unitary transduction delay. At the next computational step $t_0 + 2$, the output signal $\boldsymbol{Y}$ is determined by the input signal $\boldsymbol{X}$ from time step $t_0 + 1$ and the previous output signal $\boldsymbol{y}$. The previous output signal is thereby feed back by recurrent synapses with weights $\boldsymbol{W}_{\mathrm{yy}}$. To model this recurrent calculation, one may extend the hypothetical feedforward network by a further layer of linear neurons as shown on the left hand side. These neurons receive the previous output $\boldsymbol{y}$ via synaptic weights $\boldsymbol{W}_{\mathrm{yy}}$. They also receive the further input signal $\boldsymbol{X}$ from time step $t_0 + 1$ from an additional pool of input neurons which synapse via synaptic weights $\boldsymbol{W}_{\mathrm{xy}}$. Further calculation steps $t_0 + 3, t_0 + 4, \ldots, t$ of the recurrent network can be modeled in the feedforward network by iteratively adding layers with the same properties. Thus, the output $\boldsymbol{y}$ of the recurrent network after t time steps is mathematically equivalent to the output produced by a hypothetical feedforward network with $t - 1$ intermediate and one output layers. According to the argument in the beginning of this caption, this multi-layered feedforward network implements an affine coordinate transformation. During each individual time step, also the recurrent network can thus only perform an affine coordinate transformation on its input.

decouple vestibular signals from head and eye movement, the transformation of vestibular signals onto intraparietal neurons must be adjusted according to time-varying signals encoding the motion (Salinas and Sejnowski, 2001). While the ionotropic signal processing is shaped by synaptic plasticity, it is important to notice that its non-linear adjustment during ongoing motor control inherently differs from synaptic plasticity rules in two ways. First, synaptic plasticity acts on a time scale of minutes to hours in motor circuitry (Nishimura et al., 2013), which is too slow for adjustments to changing mechanical contexts. Second, synaptic plasticity is typically local (Gerstner, 2016), whereas the external signal s modulates the transformation weights between multiple pre- and postsynaptic neurons that encode input signals x_i but not the signal s itself. The spinal cord needs to implement such a mechanism which non-linearly integrates signals in order to adjust transformations between neuronal information at different stages of processing, or abstraction, according to changing context.

3. MONOAMINES SCALE SIGNALS IN SPINAL MOTOR CIRCUITS

How would such a non-linear signal integration occur? Functional and anatomical evidence suggests that, in contrast to ionotropic receptors, metabotropic neuromodulation enables non-linear signal integration within spinal motor circuits. A serotonergic signal s is thereby a promising candidate for adjusting the spinal signal processing in line with Equation (4), as it can encode the changing context.

Serotonin (5-HT) released within the ventral spinal cord increases the gain or response of both spinal motorneurons (Hochman et al., 2001; Heckman et al., 2008) and ventral spinal

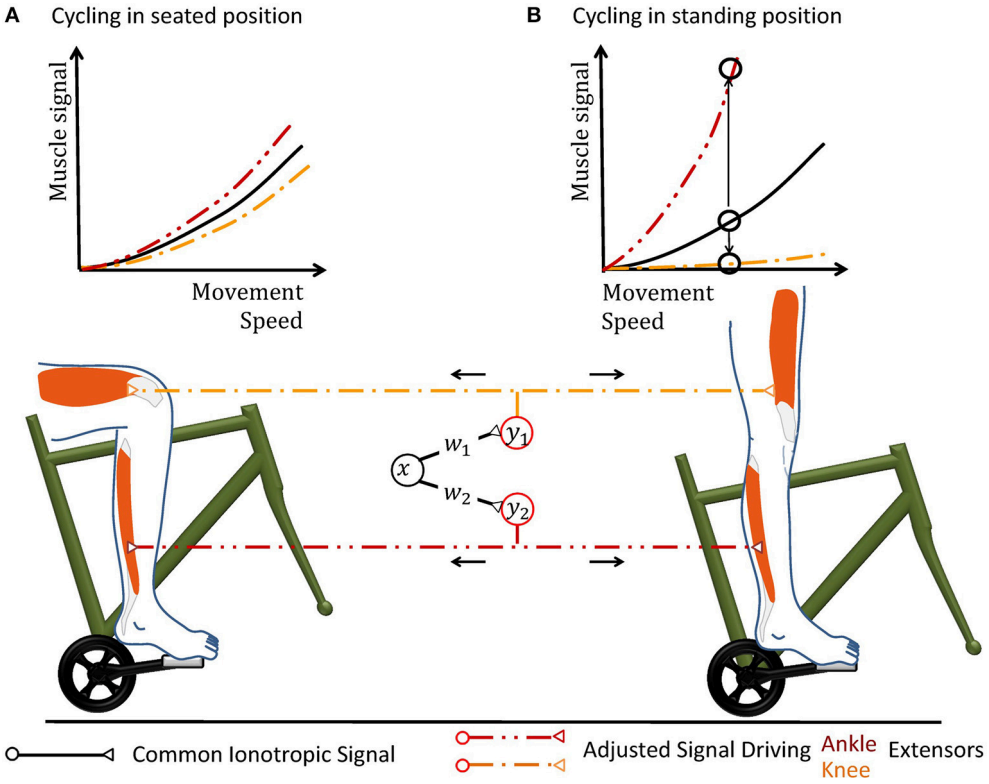

FIGURE 3 | Cycling can illustrate why a hypothetical coordinate transformation requires topographically precise non-linear scaling under varying conditions. The pedal forms a mechanical environment that constrains the movement and the muscular forces required to excite it in a particularly strict way. In the hypothetical neuronal circuit, a group of neurons carries a motor signal *x* that triggers several groups of muscles. As the motor signal is forwarded to spinal interneurons and motorneurons, it is transformed according to the transformation weights w_i. The resulting musculotopic signals y_i simultaneously actuate muscles involved in pushing the pedal, e.g., extensor muscles of the knee and ankle. Increasing the movement speed can be performed by an overall increase of the common motor signal. **(A)** When the person sits on the saddle, both knee and ankle extensors need to be actuated simultaneously. The weights of the synapses transferring the hypothetical motor signal *x* to the respective motorneuron pools are hereby chosen accordingly to achieve the required respective muscular signals. **(B)** When the mechanical properties of the environment changes during an ongoing movement, e.g., because the subject stands up to accelerate, the same muscle groups need to alter their output during the same phase of locomotion. In the standing position, knee actuation cannot exert force along the pedal trajectory. Thus, knee extensors should receive almost no muscle signal, while ankle extensors need to be activated more in order to keep up a given movement speed. Ankle and knee extensors thus need a scaling of different polarity, as illustrated by the upwards and downwards arrow in the graph. Under changing mechanical conditions, all motorneuron pools can thus still be actuated by the same abstract ionotropic motor signal from the hypothetical neuronal synergy, which just needs to be scaled differentially according to sensory information.

interneurons (Abbinanti and Harris-Warrick, 2012; Abbinanti et al., 2012; Husch et al., 2015; Perrier and Cotel, 2015) to ionotropic input, without affecting their baseline excitation. This effect is functionally equivalent to an increase of the transformation weights onto motorneurons. It results from a stimulation of 5-HT_2 receptors, which triggers a range of biochemical mechanisms as extensively reviewed previously (Abbinanti and Harris-Warrick, 2012; Perrier et al., 2013). Stimulating 5-HT_2 receptors by descending 5-HT is crucial in particular for the generation of rhythmic movement in mammals, such as whisking in rats (Hattox et al., 2003) and weight-supported locomotion (Slawińska et al., 2014). By activating 5-HT_{1A} receptors, the CNS can in turn divisively scale down the transformation weights of ionotropic circuitry converging onto motorneurons. The underlying decrease of motorneuronal gain has been suggested to occur during muscle fatigue, when 5-HT spills over its synaptic release site after prolonged release and diffuses to the axon initial segment (Cotel et al., 2013). Before fatigue occurs, the CNS can scale up the firing rate of spinal neurons monotonously and multiplicatively by a factor of up to 10 by increasing the concentrations of 5-HT (Heckman et al., 2008).

In the ventral spinal cord, neuromodulatory effects are dominated not only by 5-HT, but also by noradrenaline (Heckman et al., 2008) and neuropeptides (Thörn Pérez et al., 2015). Neuropeptides are co-released with monoamines and partly trigger similar biomechanic mechanisms (Thörn Pérez et al., 2015), but their predominant trophic effects are very slow (Svensson et al., 2001). In contrast to noradrenaline, 5-HT particularly stands out as candidate for multiplicative operations governed by a mechanical context, as serotonergic neurons receive proprioceptive information on a given movement and implement a distinct motor feedback loop as illustrated in **Figure 4**. About 90% of the 5-HT present within the spinal cord

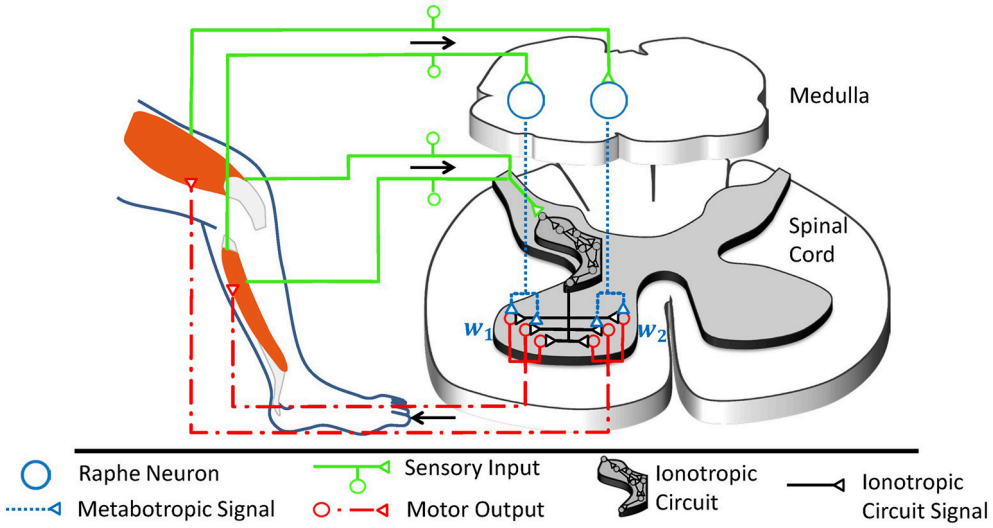

FIGURE 4 | The raphe nuclei obscurus and pallidus form a motor feedback loop. They receive proprioceptive signals and accordingly release serotonin into the ventral spinal cord. The resulting higher serotonin concentration metabotropically increases the excitability of spinal motorneurons as well as associated interneurons at the motor output stage. Collectively, these serotonergic raphe projections change the relative multiplicative weights w_j, which describe how ionotropic signals are transformed into musculotopic motor output. The serotonergic feedback loop acts in parallel to the ionotropic processing of sensory signals. Ionotropic circuitry could operate independently of the metabotropic weight adjustments at the motor output stage and could implement, for example, a low-dimensional control circuit as illustrated here and in **Figure 1B**. Those projections of the raphe nuclei obscurus and pallidus which target interneurons within the low-dimensional circuit will scale the overall spinal ionotropic motor signal without affecting the relative strength w_j of the signals actuating different muscles. In this figure, the ionotropic circuit and each motorneuron pool are represented by several neurons, which appear to be functionally redundant. However, neurons within a subcircuit may have dissimilar connections that assign them to different subcircuits during other tasks. Figure modified, with permission, from Stratmann et al. (2016).

originates from the raphe nuclei (ElBasiouny et al., 2010). In the ventral spinal cord, 5-HT originates primarily from the nucleus raphe obscurus (NRO) and pallidus (NRP), which in turn project almost exclusively to the ventral spinal motor circuitry (Martin et al., 1978; Loewy, 1981; Nieuwenhuys et al., 2008; Watson et al., 2012). These medullary nuclei receive proprioceptive inputs, potentially including inputs from cutaneous mechanoreceptors, and increase the firing rate of their serotonergic neurons accordingly (Springfield and Moolenaar, 1983; Veasey et al., 1995; Fornal et al., 1996). In agreement with the concept of a motor feedback loop, ionotropic motor output is functionally facilitated by 5-HT as an after-effect following strong muscle contraction (Crone et al., 1988; Wei et al., 2014).

There is one pivotal caveat to the presented concept of serotonin as the modulator of individual transformation weights in the ionotropic processing of information: Monoamines are typically considered to be slow and diffuse modulators of a spatially and temporally precise ionotropic circuitry. In fact, the ventral spinal serotonergic system will have a topographically diffuse effect on motor output for the reason that it partly projects to spinal interneurons, which often target several groups of muscles simultaneously (Santello and Lang, 2015; Pérez-Nombela et al., 2017; Takei et al., 2017). The diffuse component will scale the overall Spinal ionotropic motor signal without affecting the relative strength of signals actuating different muscles. But as will be detailed below, recent work suggests that the ventral spinal projections of the NRO and NRP have also a topographically specific component which performs precision scaling (Stratmann et al., 2016). In the following sections, the chain of argumentation will demonstrate that previous findings on the described serotonergic motor feedback loop are consistent with a role as a functionally specific multiplicative operator. By this precision scaling, the raphe nuclei accordingly overcome the limitations of ionotropic circuitry. The arguments run along three lines: First, metabotropic systems are shown to offer a unique functionality in the spinal cord, since ionotropic mechanisms cannot implement non-linear interaction of signals in this CNS region. Second, a fundamental motor control task is considered to define what spatial and temporal precision the serotonergic system needs in order to offer a meaningful functionality that cannot be obtained by diffuse neuromodulation. For this purpose, the particular affine transformation involved in synergy control is chosen as the system of study, as it is both likely implemented by spinal ionotropic circuits and solves motor tasks that would benefit from a subcircuit-specific gain-scaling mechanism. Third, the functionally required spatial and temporal precision will be compared with the experimentally observed precision of the serotonergic feedback loop.

4. LIMITATIONS OF IONOTROPIC SIGNAL INTERACTION *IN VIVO*

The adjustment of coordinate transformations to external signals could theoretically be performed by a neuronal network using

solely ionotropic synaptic currents. Based on neurophysiological findings, several mechanisms have previously been proposed for non-linear, particularly multiplicative, interactions of ionotropic signals. They are typically linked to specific respective CNS regions, have recently been reviewed in detail (Silver, 2010; Carandini and Heeger, 2012) and are summarized in **Table 1**. As mentioned before, the spinal interaction of ionotropic signals is known to be highly linear. This can be attributed to the properties of spinal neurons and signals, which make mechanisms suggested for other CNS regions physically implausible and typically even impossible.

Mechanisms of multiplicative signal interactions can be split into two groups (Silver, 2010): Some mechanisms work in neurons which show time-sparse encoding, i.e., which encode data in the correlations of spikes. Other mechanisms apply to neurons which show a rate-based encoding of information, implying that the neurons process information by exploiting a large range of firing rates.

For neuronal networks working in temporally sparse coding regimes with low firing rates, two main mechanisms for non-linear interaction have been proposed. The first is based on changing levels of synaptic noise emerging from balanced excitatory and inhibitory input (Berg et al., 2007), which can change the gain of the input-output function for neurons operating around their spiking threshold (Chance et al., 2002; Mitchell and Silver, 2003; Higgs et al., 2006). The second is based on shunting inhibition produced by inhibitory input in spatial proximity to the soma (Sherman and Koch, 1986; Isaacson and Scanziani, 2011). These mechanisms are unlikely to cause gain scaling in spinal circuitry, where the early sensory processing and motor output are dominated by rate-coded signals under normal behavior (Ahissar, 1998; Maier et al., 1998; Perlmutter et al., 1998; van Rossum et al., 2002; Stein et al., 2005; Shalit et al., 2012).

For neurons that work within a rate-coded regime, non-linear signal interaction can occur due to the short-term synaptic depression (STD) of synaptic efficacy. If a neuron transmits the sum of two excitatory signals, the second signal may push the firing rate into a regime where STD occurs and may therefore divisively scale the circuit response to the first signal (Carandini et al., 2002; Ozeki et al., 2009; Rothman et al., 2009; Carandini and Heeger, 2012). Using this mechanism is metabolically unfavorable compared to other possible non-linear mechanisms, as the neuronal network would transmit a particularly high number of metabolically expensive action and synaptic potentials (Magistretti and Allaman, 2015). In addition, recent recordings on rate-coding neurons which carry sensor and motor signals show that STD only takes place at the onset of a stimulation train (McElvain et al., 2015). During sustained firing, STD was found to saturate and remain constant for a wide range of firing rates. Thus, STD is unlikely to occur in spinal calculations during ongoing behavior. A second hypothesis originates from the mathematical fact that the multiplication of two signals turns into a pure addition when the logarithms of the signals are considered,

$$\log(x_1 \cdot x_2) = \log(x_1) + \log(x_2)\,. \tag{5}$$

For signals which are encoded logarithmically, such as specific quantities in the visual systems (Gabbiani et al., 2002; Jones and Gabbiani, 2012), multiplication thus becomes trivial (Jones and Gabbiani, 2012). However, many mechanical stimuli are known to be linearly encoded by sensory firing rates (Hensel, 1973; Davis, 1975; Rothwell, 1987; Muniak et al., 2007; Bensmaia, 2008). Furthermore, a neuronal network which implements this strategy would be restricted to implement exclusively either multiplicative or additive operations on its inputs. To implement both, it would need to implement an additional exponential function to extract the actual coordinates. The third possible non-linear mechanism uses active properties of dendrites. Voltage-dependent Na^+ and Ca^{2+} channels as well as NMDA receptors can individually induce supralinear and sublinear interaction of ionotropic signals (Oviedo and Reyes, 2002; Williams and Stuart, 2002; Mehaffey et al., 2005; Losonczy and Magee, 2006; Rhodes, 2006; Remy et al., 2009; Major et al., 2013). In concert, the non-linear effects can counteract the sublinear integration of signals caused either by passive dendritic properties (Segev et al., 1994) or by other voltage-dependent channels (Mehaffey et al., 2005; Rhodes, 2006; Palmer, 2014). The resulting overall effect is strongly determined by the clustering properties of converging synaptic inputs. Individual non-linear effects of unclustered inputs typically balance out to a linear signal summation (Priebe and Ferster, 2010). And indeed, *in vivo* mappings of the full dendritic tree of neurons at early sensory stages demonstrated that synaptic input is not clustered according to functional similarity, a finding which is consistent across different sensory systems (Jia et al., 2010; Varga et al., 2011). In agreement, other *in vivo* recordings showed that the individual non-linear effects of active dendrites are highly balanced and in effect facilitate a linear relationship between input current and output firing (Cash and Yuste, 1998, 1999). The same balance was found for spinal motorneurons in simulations (Cushing et al., 2005) and experiments (Hyngstrom et al., 2008) when neuromodulatory metabotropic input was removed. *In vivo* experiments on non-linear input summation of input from both eyes further emphasized that the CNS uses active dendritic properties not as a non-linear operation, but as a linearizing agent in sensory systems. The non-linear summation of individual signals was found to ensure that the output to binocular stimulation equals the linear summation of input during monocular stimulation (Longordo et al., 2013).

In conclusion, the specific physiological conditions of the spinal cord explain and emphasize that spinal neurons are linear integrators of incoming ionotropic signals. Therefore, the spinal cord needs to take advantage of the metabotropic serotonergic system in order to implement a non-linear interaction of signals.

5. LIGHTENING THE BURDEN OF FREEDOM

5.1. Synergies Simplify the Control of Redundant Locomotor Systems

In order to understand how serotonergic precision scaling can improve motor behavior, it is necessary to consider a typical

TABLE 1 | Overview of various mechanisms proposed for multiplicative interaction of neuronal signals.

Coding regime mechanism	Explanation	References
Time-sparse encoding		
Synaptic noise from balanced excitatory and inhibitory input	Noise triggers membrane voltage to cross threshold by chance and thus smooths input-output function around spiking threshold.	Pyramidal neurons from somatosensory cortex: Chance et al. (2002); Higgs et al. (2006). Motoneurons from spinal cord: Berg et al. (2007).
Shunting inhibition	Inhibitory input in proximity to the soma increases the membrane conductance, which divisively scales the postsynaptic potentials	Theoretical explanation: Isaacson and Scanziani (2011). Neurons from lateral geniculate nucleus: Sherman and Koch (1986). Granule neurons from cerebellum: Mitchell and Silver (2003).
Rate-based encoding		
Short-term synaptic depression	Divisively scales input when a further signal is added.	Neurons from V1: Carandini et al. (2002); Ozeki et al. (2009); Carandini and Heeger (2012). Granule cells from cerebellum: Rothman et al. (2009).
Logarithmic signals	Multiplication of signals x_i turns into a summation upon their logarithmic transformation: $\log(x_1 \cdot x_2) = \log(x_1) + \log(x_2)$.	Locust lobula giant motion detector: Jones and Gabbiani (2012).
Active dendrites	Voltage dependent channels can induce sub- or supralinear signal interaction.	Theoretical explanation: Segev et al. (1994); Rhodes (2006). Pyramidal neurons from sensorimotor cortex: Oviedo and Reyes (2002); Williams and Stuart (2002). Pyramidal neurons from hippocampus: Losonczy and Magee (2006); Remy et al. (2009). Pyramidal neurons from neocortex: Major et al. (2013).
Monoaminergic neuromodulation	Activation of G protein-coupled receptors changes neuronal excitability.	Review on general monoaminergic functions: Bargmann (2012). Review on dopamine receptors: Beaulieu and Gainetdinov (2011). Review on cholinergic receptors: Picciotto et al. (2012). Serotonergic receptors in the spinal cord: Perrier et al. (2013); Husch et al. (2015); Perrier and Cotel (2015); this paper.

coordinate transformations implemented by ionotropic spinal circuitry.

Synergies are an example of spinal transformations which neuroscientists have analyzed in detail. They are formed by interneurons that either receive many input signals or project to motoneurons of several muscles. As illustrated in **Figure 1B**, the CNS thereby transforms high-dimensional sensory information into the low-dimensional synergy space and transforms the motor output from the synergistic circuitry into the high-dimensional musculotopic space (Lacquaniti et al., 2012; Alessandro et al., 2013; Santello et al., 2016). The input sensory synergy filters out information which is unnecessary for a specific motor task. It therefore chooses a particular combination of sensory information from the infinite combinatorial possibilities of sensory signals. The output motor synergy predetermines coordinated activation of a group of muscles elicited by a single circuit. It allows the CNS to choose from an infinite number of possible movement patterns in a locomotor system with more degrees of freedom than is required for a specific task (Bernstein, 1967). The human hand is the most obvious example for such a redundant mechanical system (Santello et al., 2016). But also each lower human limb comprises more than 50 muscles which are to a major extent recruited together for locomotion (Lacquaniti et al., 2012). This redundancy provides a high versatility of possible movements.

Behaviorally, neuronal synergies become detectable as a spatiotemporal pattern of EMG signals emanating from different muscles. They can be extracted mathematically by linear source decomposition methods like principal component analysis (Naik et al., 2016). Human locomotion shows four to five basic patterns (Lacquaniti et al., 2012), which are reproducible when locomotion is perturbed (Chvatal and Ting, 2012). To change locomotion speed, their relative recruitment is shifted gradually (Hagio et al., 2015).

Neurophysiological analysis indicates that the spinal cord is an important basis for synergy control (Santello et al., 2013; Jörntell, 2016; Kiehn, 2016). The majority of spinal interneurons combine signals from different modalities into sensory synergies (Jankowska, 1992). In turn, groups of interneurons elicit a synergistic pattern of muscle activations (Clark et al., 2010; Levine et al., 2014; Danner et al., 2015; Santello and Lang, 2015; Pérez-Nombela et al., 2017; Takei et al., 2017). Synergy output is thereby transformed into the high-dimensional musculotopic space and may be further routed through a separate neuronal layer before it reaches the motoneurons (Zhong et al., 2012). The cerebellum links the individual synergies into more elaborate synergies or into sequential patterns (Bengtsson and Jörntell, 2014; Jörntell, 2017). Descending cortical motor commands may accordingly excite individual synergies to produce meaningful, complex behavior (Graziano, 2006; Overduin et al., 2012; Gallego et al., 2017). These commands may in fact be partly transferred by diffuse neuromodulation, which is known to activate movement patterns or increase the movement frequency (Jing et al., 2009; Harris-Warrick, 2011). In summary, the evidence implies that spinal interneurons often combine information in a low-dimensional synergy space, and the synergistic muscle output is transformed and forwarded to the redundant locomotor system.

Understanding synergies is essential for studies on integrative motor circuits. They can be regarded as a library of re-usable modular building blocks, which the brain combines in order to

construct a large range of complex learned and new movements from basic old ones. In the low-dimensional synergy space, the brain can integrate descending pathways, reflexes, and central pattern generators, i.e., neuronal circuits which produce rhythmic movement without rhythmic input (Ijspeert, 2008; Guertin, 2013; Ijspeert et al., 2013; Dzeladini et al., 2014; Kiehn, 2016; Minassian et al., 2017).

5.2. Robotics Control Theory Explains Synergistic Motor Control

Functional insights on the use of synergies can be obtained from robotics control theory. In recent work, an artificial neural network, which formed a similar network structure as a sensorimotor synergy, was trained to encode meaningful motor primitives within the intermediate synergy layer (Chen et al., 2015). The underlying type of artificial neural networks is called *autoencoder* and is typically used in in the field of deep learning to reduce the dimensionality of data (Hinton and Salakhutdinov, 2006). But while autoencoders in general deploy non-linear quasi-ionotropic mechanisms in the simulated neurons, also the use of more biologically plausible linear synergy spaces have been functionally well-examined for the control of biomimetic robotic hands (Bicchi et al., 2011; Santello et al., 2016) and legged systems (Aoi et al., 2017; Lakatos et al., 2017). The tools that have been developed in this endeavor are mathematically advanced and well-tested. Neuroscientists can thus use them to functionally explain or even predict a specific synergistic behavior.

For low movement speeds, the robotic control strategy of null space projections explains how several tasks, which are individually solved by a respective synergy, can be executed simultaneously (Dietrich et al., 2015). The top-priority command is executed using the full capability of the locomotor system, such as a synergy responsible to keep balance. If the locomotor system is redundant for that specific task, a lower-priority task, e.g., defined by a secondary synergy, can be executed to the greatest possible extent as long as it does not interfere with the top-priority task. For this purpose, an affine transformation projects the secondary task into a space formed by the redundant degrees of freedom, and the resulting motor signal is added to the signal of the top-priority command. The transformation weights depend on the current positions of the actuators, and their adjustments requires a precise model of the locomotor system and its environment (Featherstone and Khatib, 1997). The need for precise models applies to most strategies devised to control low movement speed (Braun et al., 2011). To adjust complex movements at low movement speed to changing conditions, it is therefore likely that human neuronal control circuits also require precise models of their locomotor system. Accordingly, the underlying circuits require high topographic precision. Since the fine-control of complex slow movements strongly relies on the supraspinal circuitry (MacKay-Lyons, 2002; Shemmell et al., 2009), it is reasonable to assume that the required precise models are encoded in the more sophisticated supraspinal neuronal networks. The slow movement speed allows for a heavy recruitment of these networks despite their long feedback delays.

5.3. Synergies for the Control of Highly Dynamic Movement

Here, we want to define a minimal precision that serotonergic effects need to show in order to perform a task that cannot be explained by diffuse neuromodulation. This suggests considering control strategies that require little model precision. It is likely that the CNS recruits such strategies more during fast and strong movements like running. These are strongly shaped by the inertia and elasticity of the system, i.e., quantities which can only be modeled with high inaccuracies and change over time (Nakanishi et al., 2008; Peters et al., 2008; Dietrich et al., 2015). Biomechanical locomotor systems are substantially more complex than robotic systems, as their dynamics critically depend on a particularly large range of parameters such as non-linear muscle elasticities, hysteresis effects, and the changing muscular 3D structure (Siebert and Rode, 2014). This emphasizes that control strategies which require a minimal model precision can control highly dynamic movements in biomechanical locomotor systems much more robustly than model-dependent strategies. A second advantage of considering the control of highly dynamic movement is the associated high consumption of metabolic energy within muscles. The metabolic demands can be drastically lowered by a control strategy utilizing elastic elements within tendons and muscles, as these elastic elements store kinetic energy during a ground impact and release it for recoil (Holmes et al., 2006; Sawicki et al., 2009; Lai et al., 2014). During the evolutionary development of the CNS, strategies for the energy-efficient control of this movement type were thus most likely a critical selection factor. For these reasons, control strategies for highly dynamic movements are likely to be implemented by the CNS. They require a minimum of model knowledge and are thus promising to estimate the minimum precision that serotonergic effects need to show.

For highly dynamic motion, robot control theory showed that a simple synergy controller can generate movement which is stable (Lakatos et al., 2013; Lakatos and Albu-Schäffer, 2014a,b) and makes optimal use of elastic elements in the locomotor system to minimize the consumption of metabolic energy (Stratmann et al., 2017). According to this control strategy, sensory information is linearly transformed into the one-dimensional synergy coordinate space, where it periodically drives a synergy controller (cf. **Figure 5**). Its output is reversely transformed into the musculotopic space using the transformation weights $\boldsymbol{w}$ to drive the joint actuators. Functionally, precise output weights are critical, whereas the input weights may strongly vary without relevant loss in movement performance (Stratmann et al., 2016). Within the synergy space, a circuit as simple as a pool of excitatory reflex interneurons can control the movement (Stratmann et al., 2016). This control law is a promising hypothesis for neuronal motor control for three reasons: First, it requires information about the number of degrees of freedom prior to movement onset and thus minimum model knowledge. Second, it requires only information about muscular deflections and forces during an ongoing movement, as provided by proprioceptive fibers. Third, a linear ionotropic synergy circuit can implement this controller for unchanging environments. To adjust the control law to

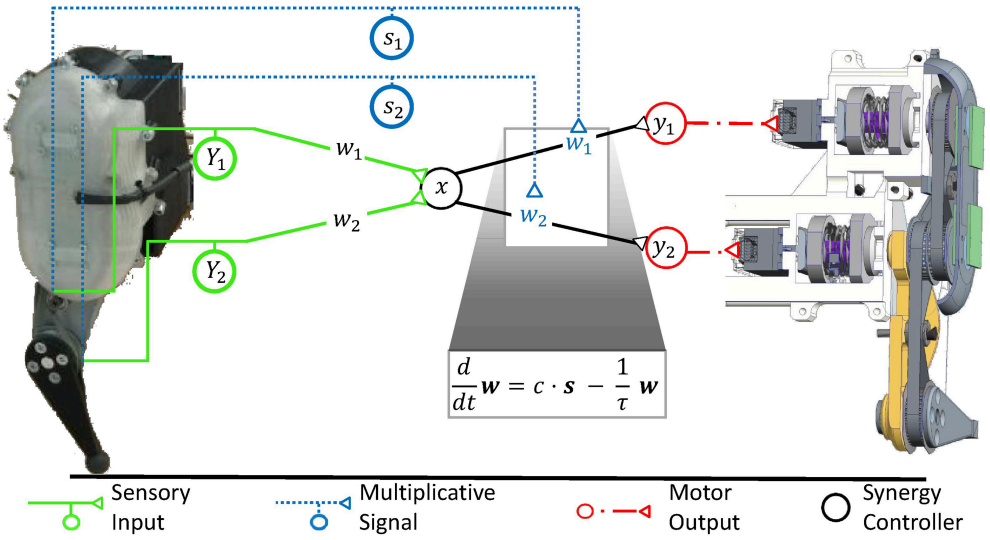

FIGURE 5 | The robotic controller, which was previously developed to maintain a stable, fast, and strong movement, is mathematically equivalent to a synergy controller as illustrated in **Figure 1B**. Sensory input (Y_1, Y_2) signals the movement of individual degrees of freedom of the mechanical system. It is transformed into the low-dimensional synergy space and adjusts the phase and frequency of a synergistic motor signal x. Since the different mechanical degrees of freedom move with high synchrony during fast locomotion, the input weights can be chosen arbitrarily without loss in movement performance (Stratmann et al., 2016). The motor signal x is reversely transformed along the weights (w_1, w_2) to drive the actuators of the same robot. These weights are functionally critical, as the relative forces (y_1, y_2) of different actuators determine, among others, how well the robot can take advantage of its elastic elements to store energy upon ground impact and release it for recoil. In robotic systems, springs typically dominate the elastic properties of the system, as shown on the right hand side of this figure in a cross-sectional illustration of the exemplary robot. As detailed in section 6, the synergy controller can maintain an elastic movement with optimal energy efficiency under changing mechanical conditions. For this purpose, the controller receives sensory inputs s_1 and s_2, which signal the deflections of the degrees of freedom such as joint angles. To adjust to changing mechanical conditions, the controller needs to multiplicatively scale the output transformation weights w_1 and w_2 according to these inputs s_1 and s_2, respectively (Stratmann et al., 2017). A common multiplicative factor c determines the jumping height or distance. To keep the weights bounded, they need to decay exponentially with a time constant τ. The ventral spinal serotonergic system forms a motor feedback loop, as illustrated in **Figure 4**, which functionally resembles the loop of the multiplicative signals presented here.

changing environments, multiplicative scaling of the neuronal gains $\boldsymbol{w}$ at the motor output stage is required, as will be explained in the following section. Since the number of degrees of freedom is the only required model knowledge, this control law is an ideal example to determine what minimal topographic precision serotonergic effects need at least in order to adjust synergies to changing contexts.

6. MULTIPLICATIVE GAIN SCALING MAINTAINS SYNERGIES IN CHANGING CONTEXTS

6.1. Gain Scaling Offers Unique Advantages to Neuronal Signal Processing

Mathematically, multiplicative gain scaling is a core principle for the extension of affine transformations. As will be shown, this principle can strongly enhance the presented robotic synergy controller. Thereby, it is possible to derive the spatial and temporal precision required by the serotonergic system to adjust synergic signal processing to changing contexts. Prior to that, it is important to consider how well multiplication can fulfill this task for realistic locomotor systems under arbitrary conditions. As will be shown, multiplication can in theory extend linear neuronal networks to fulfill this task arbitrarily well, because it allows them the implementation of arbitrary general transformations. Multiplication is furthermore a straightforward, functionally powerful operation for this task. These advantages of gain scaling are so fundamental that they apply to affine transformations in general, even beyond motor control. They motivate and help understand why precision scaling may have evolved during evolution.

Weierstrass and Stone (1948) have mathematically demonstrated that arbitrary continuous transformations $y(x)$ can be approximated to any desired precision for a restricted interval of possible input values $\boldsymbol{x}$ by the sum of exponentiation powers in the input,

$$\boldsymbol{y}(\boldsymbol{x}) = +(-\boldsymbol{\theta}_y) + \boldsymbol{W}_{xy}\boldsymbol{x}^1 + \dots . \tag{6}$$

Each summand comprises a power of the input with increasing exponent. Engineers often use this finding since this sum can be used to approximate arbitrary transformations which cannot be derived mathematically or are changing unpredictably with time. An affine transformation implemented by a linear neuronal network, as described by Equation (3), is a first-order approximation. That means it includes a constant, i.e., a term proportional to the zeroth power $\boldsymbol{x}^0 = \boldsymbol{1}$ in the input, and a summand that is proportional to the first power $\boldsymbol{x}^1$ in the input. Taylors theorem, one of the basic theorems

in mathematical analysis, states that adding summands of higher exponent continuously improves the approximation. But given an approximation with summands up to a particular exponent, the benefit gained by adding further summands of higher exponent becomes increasingly negligible (Cohen and Tan, 2012). As affine transformations include terms up to the first power of the input, a linear neuronal network offers a general circuit scheme that captures a major portion of a general transformation. Linear neurons which are further able to multiply signals can be combined in several layers to calculate arbitrary powers of its inputs. In contrast to a purely linear neuronal network, such a network can implement Equation (6) and therefore perform each possible transformation on its inputs with arbitrary precision.

Deep learning shows that multiplication is only one out of many arithmetic operations which a neuronal network can implement in order to act as universal approximator of general transformations (Stone, 1948; Cybenko, 1989; Hornik, 1991; Chen et al., 2015). Hereby, the artificial networks typically implement a single function which seemingly resembles ionotropic signal processing, but may in fact represent the collective effect of ionotropic, metabotropic, and other mechanisms. While a multiplicative mechanism that parallels the ionotropic circuitry is not the only mechanism that allows implementing a universal approximator, it allows a particularly powerful, straightforward, and resource-efficient adjustment of an affine transformation to changing contexts. Adjusting an affine transformation,

$$y_j = \sum_i w_{\mathrm{ij}} x_i - \theta_j \,,$$

according to the external signal s encoding the context implies that individual transformation weights w_{ij} must change with s. If the CNS multiplies the inputs x_i with the external signal, it effectively performs an affine transformation with transformation weights

$$w_{\mathrm{ij}}(s) = w_{\mathrm{ij,c}} \cdot s \,, \tag{7}$$

which increase with the constant of proportionality $w_{\mathrm{ij,c}}$. The resulting affine transformation

$$y_{\mathrm{j}} = \sum_i w_{\mathrm{ij,c}} x_{\mathrm{i}} s - \theta_{\mathrm{j}} \tag{8}$$

can be seen as a Taylor approximation which models the interaction between inputs x_{i} and context s up to second order. As explained in the previous paragraph, such a second-order approximation captures a large portion of an arbitrary interaction, which eases the functional need for further resource-consuming neuronal operations. In agreement with this functional benefit, experiments typically link changing coordinate transformations to gain modulation, as reviewed by Salinas and Sejnowski (2001). For example, motor output following stimulations of M1 is multiplicatively modulated by proprioceptive information (Graziano et al., 2004), which can at least partly be attributed to serotonergic gain scaling at the level of spinal motorneurons (Wei et al., 2014).

6.2. How Gain Scaling Can Enhance Synergy Control

In the specific context of robotic synergies, it is possible to derive the spatial and temporal precision that the spinal serotonergic system needs for precision scaling. Scaling the gains of the output transformation hereby leverages the above-described robotic control law, as it decouples the synergy circuitry from changes in the mechanical context of the movement (Lakatos et al., 2013). The synergy itself is therefore unaffected, for example, when one runs from a solid to a soft ground or changes body posture during cycling (cf. **Figure 3**). The common synergistic motor signal can be individually scaled by separate output gains w_{j} to calculate the respective motor signal for each functional group j of muscles acting on a single degree of freedom. A degree of freedoms is thereby typically formed by an individual joint (Lakatos et al., 2013, 2017). The index i of the synaptic weights w_{ij} is neglected, as the synergy circuit functionally outputs only a single ionotropic signal x.

Robotic control theory predicts how the gains w_{j} within the biological neuronal network must be adjusted to changing mechanical contexts in order to minimize metabolic demands (Lakatos et al., 2013). To explore a given mechanical context, the ionotropic synergy circuitry provides input to all involved muscles and excites a non-optimal movement. As the controller adapts to the mechanical context, it increasingly optimizes the movement. The control approach derived for this purpose (cf. **Figure 5**) resembles the function performed by the serotonergic feedback loop (cf. **Figure 4**) in all of its three main characteristics: First, the controller receives sensory input about the resulting joint deflections, resembling the proprioceptive information converging onto the raphe nuclei. Second, the controller uses this information to update its model of the body and its environment. For this purpose, it adjusts the transformation weights from the motor synergy to groups of actuators driving the involved joints. The updated transformation weights improve the movement and recursively lead to updated sensory signals. Also this characteristic resembles the function of the raphe nuclei, which scale ionotropic synergy signals as they arrive on motorpools. Third, the multiplicative transformation weights $\boldsymbol{w}$ converge toward the dominant principal component of the sensory signals $\boldsymbol{s}$ encoding the deflections of individual joints. Based on work by Lakatos et al. (2013), Stratmann et al. (2016) demonstrated that the alignment can be achieved by multiplying the output of the synergy circuitry by weights that increase with the sensory signals. In order to keep the weights within a physiological regime, decay of the weights over time is required as counteracting mechanism. These two effects can be summarized as

$$\frac{d}{dt}\boldsymbol{w} = w_{\mathrm{c}} \cdot \boldsymbol{s} - \frac{1}{\tau}\boldsymbol{w} \,. \tag{9}$$

The constant factor w_{c} scales the overall force output. The time constant τ describes the gain decay and must be of the same order of magnitude as the typical cycle duration of biomechanical movement. This time scale guarantees constant gains throughout the movement cycle in a sustained context. Meanwhile, the dominant changes of transformation weights, and thus most of

the functional impact on metabolic costs, occurs already during the first step cycles, i.e., for quickly-changing contexts (Stratmann et al., 2017). Stratmann et al. (2016) demonstrated analytically and in neuromechanical simulations that previous models of the kinematics of released serotonin are fully consistent with Equation (9). But it remained unclear if the serotonergic feedback loops shows the same temporal and topographic precision as the controller.

The resemblance between the serotonergic motor feedback loop and the controller is remarkable, as the controller has been derived based purely on considerations about the dynamics of biomimetic systems. After controller convergence, the synergy controller makes optimal use of the energy saving capacity offered by the elastic elements within the mechanical locomotor system. This result was consistently obtained under the influence of physical noise, mechanical damping, and non-linear dynamics (Stratmann et al., 2017). This means that the actuators require a minimum of metabolic energy to sustain the highly dynamic locomotion. Throughout the adaptation, the mechanical system shows stable movement. This stability results from the weight decay and from the friction within the mechanical system. The friction implements a further negative feedback loop as it increases with higher movement velocity, i.e., a stronger motor signal (Lakatos and Albu-Schäffer, 2014b). Videos illustrating the emerging movement have been published previously for elastic robotic systems mimicking the leg of a small mammal (Stratmann et al., 2017), human legs (Löffl et al., 2016), and a human arm (Lakatos et al., 2013). Under the assumption that the raphe nuclei show sufficient topographic and temporal precision, also the simulated raphe nuclei optimized the energy efficiency of motion induced in a leg which was either mechanically constraint, resembling cycling as illustrated in **Figure 3**, or free to move along a trail (Stratmann et al., 2016).

The robotics control approach explains the functional advantage of a raphe motor feedback loop that shows precision scaling rather than a diffuse neuromodulation of motorpools. Thereby, it predicts that the serotonergic feedback loop must show gain scaling which acts on a time scale of hundreds of milliseconds to few seconds and which is at least joint-specific. In particular, it must amplify motorpools driving joints that show a large deflection throughout the movement and thus send out large proprioceptive signals s_i. With these characteristics, the raphe nuclei would ensure that simple ionotropic synergies can induce highly dynamic rhythmic movements with minimum metabolic demands under changing context.

7. SEROTONIN PROVIDES SUBCIRCUIT-SPECIFIC GAIN SCALING

The functional considerations offer a benchmark for the anatomical and functional precision that the serotonergic feedback loop requires to perform precision scaling.

Neuroscientific studies considering the topographic precision suggest that along the serotonergic feedback pathway, each processing step allows for a spatially focused signal transduction. Sensory signals are relayed to the NRP and NRO within 20 ms (Springfield and Moolenaar, 1983). This short delay indicates a monosynaptic or a strong oligosynaptic input from the peripheral sensors to the NRO and NRP. A likely candidate is disynaptically mediated input via spinal interneurons that typically targets the cerebellum (Jörntell, 2017) but that may also mediate peripheral inputs to brainstem nuclei (Johansson and Silfvenius, 1977) as illustrated in **Figure 6**. The efferent serotonergic projections of the approximately 19,000 serotonergic neurons comprised within the human NRP and NRO (Hornung, 2003) target almost exclusively the ventral spinal cord (Martin et al., 1978; Loewy, 1981; Nieuwenhuys et al., 2008; Watson et al., 2012). These projections have been suggested to comprise both an anatomically diffuse component and a separate topographically specific component (Huisman et al., 2011). The diffuse projections as well as projections to ventral interneurons within a neuronal synergy affect the overall gain like the factor w_c in Equation (9) and may additionally increase the overall leg stiffness by co-contraction of antagonistic muscles. Both effects have been suggested to underlie increases of the movement speed (Heglund and Taylor, 1988; Ferris et al., 1998). They explain functional findings demonstrating that the 5-HT released by the action of one limb amplifies motor signals that target the muscles in other limbs as well (Wei et al., 2014). Previous anatomical studies allow a quantification of the spatially focused projection onto spinal motorneurons and interneurons associated with specific motorneuron pools. Tracers inserted into the spinal cord showed that the location of the labeled serotonergic cells vary markedly with the region of injection, contrasting the more homogeneous labeling of non-serotonergic cells within the raphe nuclei (Skagerberg and Bjorklund, 1985). Dual retrograde tracers injected into different regions of the ventral horn of rats double-labeled about 50% of cells within the NRP (Cavada et al., 1984). This degree of collateralization resembles that of corticospinal axons, for which more than 40% of 156 neurons could be activated antidromically from several segments of the spinal cord in monkeys (Shinoda et al., 1979). In the ventral spinal cord, serotoninergic projections predominantly terminate in synaptic contacts and the release of 5-HT shows effects of high spatial precision (Brumley et al., 2007; Cotel et al., 2013; Perrier et al., 2013). In agreement with a topographically precise spinal serotonergic system, depletion of 5-HT and blockage of 5-HT_2 receptors in rats slackens locomotion due to adjustments in the motor signals which differentially affect muscles acting at different joints of the same limb or even the same joint (Myoga et al., 1995; Pflieger et al., 2002; Pearlstein et al., 2005). Evidence therefore suggests that the serotonergic system is able to induce effects which are at least joint-specific.

The time scale of metabotropic effects is slow in comparison to ionotropic signal transmission. Following sensory stimulation, the onset of the serotonergic multiplication effect was found to be delayed by tens of milliseconds after stimulus cessation in cats (Crone et al., 1988). It was shown to return back to baseline within a few seconds in turtles (Perrier and Delgado-Lezama, 2005), cats (Crone et al., 1988) and humans (Wei et al., 2014). This long time scale might impede fast neuronal calculations within the brain and may also have detrimental effects for motor control under rapidly changing conditions.

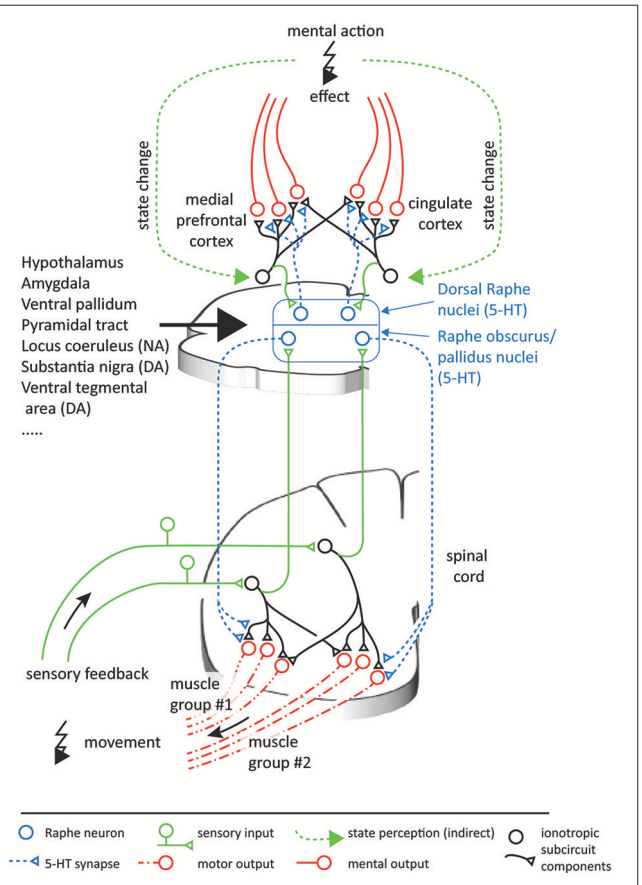

FIGURE 6 | Possible analogous organization of serotonergic function in the spinal cord and the neocortex. In both CNS areas, populations of serotonergic projections originating in the raphe nuclei can be assumed to multiplicatively scale the output of individual ionotropic subcircuits. In turn, the projecting raphe neurons receive feedback on the outcome of their effects, thus forming feedback loops. The ionotropic signals in the spinal cord can be interpreted relatively easily, as they are directly linked to physical muscles and sensors. As in the case of the spinal circuitry, neocortical circuitry operations likely involve integration of information from groups of neurons, which are innervated by different combinations of serotonergic neurons. In contrast, the information encoded in the neocortex can be expected to be more abstract and less directly intelligible, and at present it is therefore less clear what coordinate spaces the neocortex combines. Nevertheless, as a first-level descriptive model of the functional mechanisms monoamines have in neocortical systems, the functional principle presented here can help understand the principles of the effects elicited by psychopharmacological drugs.

For example, it may underlie the Kohnstam effect, where the arm involuntarily lifts following the abrupt end of a strong voluntary contraction. The Kohnstamm effect lasts for several seconds and originates in a persistent activation of the deltoid muscle, which is accompanied by higher motor evoked potentials. The underlying mechanisms are assumed to have a dominant spinal origin (Mathis et al., 1996; Ghosh et al., 2014). These properties are consistent with the idea that the excessive activity observed during the Kohnstamm effect is caused by serotonin that is released during a strong muscle contraction and increases the motoneuron gain of the deltoid specifically. Ongoing movements encountered in everyday life show less-abrupt and extreme switching between conditions. For such non-artificial movements, the time scale of serotonergic effects matches the time scale relevant to various motor behaviors.

To summarize, a joint-specific multiplicative effect which decreases on a time scale of seconds agrees well with the functional requirements determined for the stable and energy-efficient control of highly dynamic movement. The presented control-theoretical framework therefore links the previous experimental findings on monoamines into a new operational principle of temporally- and subcircuit-specific gain modulators. By this precision scaling, the serotoninergic projections to the ventral spinal cord can be assumed to strongly simplify motor control adaptation.

8. MONOAMINES SCALE SIGNALS THROUGHOUT THE CNS

8.1. A Principle Common Across Serotonergic Systems

The previous section considered the parts of the serotonergic system that target the spinal cord. But the functional interpretation developed so far may, in principle, also apply to the serotonergic innervation of other parts of the central nervous system. It may even apply to those CNS areas which may achieve precision scaling using non-linear ionotropic mechanisms, possibly by combining many non-linear neurons into a network that approximates more general transformations mediated by network effects. These CNS areas may take advantage of the parallel, resource-efficient implementation of precision scaling originating from monoaminergic systems. Serotonergic innervation is present in practically all parts of the CNS, including the striatum, amygdala, thalamus, and hippocampus (Vertes and Linley, 2008; Daubert and Condron, 2010). But in this paper, a specific interpretational example will be developed for the frontal and cingulate areas of the neocortex, where many researchers locate at least part of the effects caused by psychopharmacological drugs interfering with the serotonergic system.

The proposed framework suggests a generic function for 5-HT as a subcircuit- and temporally specific non-linear gain modulator which scales individual weights of transformations between different processing stages by postsynaptic effects. An important component of this framework is formed by the feedback connections which evaluate the contextual conditions to update the drive on the serotonergic gain modulation (cf. **Figure 4**). Because of the subcircuit-specificity, there is differential gain scaling. This is useful if changes in conditions require the transformation of different aspects of the overall information to be multiplied with different factors to correctly interact with the external world. For the 5-HT innervation of the prefrontal cortex (PFC), most of these requirements seem to be confirmed. First, there are topographically precise projections with well-defined synapses from the nucleus raphe dorsalis (NRD) to the PFC (Bang et al., 2012; Belmer et al., 2017). Second,

there is a topographically precise feedback inhibition from the PFC to the NRD (Jankowski and Sesack, 2004) and the NRD affects the neuronal gain in the layer V pyramidal cells of the PFC (Zhang and Arsenault, 2005). Considering these apparent functional homologies with the serotonergic innervation of the spinal circuitry, **Figure 6** illustrates a possible scenario for the functional organization of the serotonergic innervation of the PFC / cingulate areas.

In the spinal cord, the functional principle proposed for 5-HT is the multiplicative scaling of individual transformation weights in order to adjust transformations between different coordinate spaces. Whereas for the spinal circuitry one can speak in relatively concrete terms of what is being represented and on what bases the coordinates exist, the coordinates relevant to integrative neocortical systems are likely to have much more abstract bases and are anyway not well-known at the moment. However, there are studies of correlations between certain abstract measures and the activity of the neurons, which can serve as approximations of what kinds of representations are involved. Primate PFC neurons can encode at least in part the monitored actions (Yoshida et al., 2011) and the errors of action of other monkeys (Yoshida et al., 2012). In the anterior cingulate cortex, neurons strongly respond to rewards delivered to other monkeys, while orbitofrontal neurons are more biased toward rewards delivered to the recorded monkey (Chang et al., 2013). An effect of lesions in the orbitofrontal cortex is abnormal social and emotional judgements of facial expressions (Willis et al., 2010; Watson and Platt, 2012) possibly associated with autism or sociopathy (Chang et al., 2013). In rodents, an optogenetic stimulation of PFC neurons that project to the NRD creates abnormal avoidance behavior (Warden et al., 2012; Challis et al., 2014).

Consider the possibility that the neocortex, as we envisaged for the spinal circuitry organization around synergy control, consists of multiple subcircuits, or groups of neurons. Each subcircuit carries representations of specific parameters which are directly or indirectly relevant to dealing with situations arising mentally or in the social world. Because the subcircuits interact, the optimal weighting of each subcircuit will depend on context, similar to the relative muscle forces needed for locomotion across different terrains. In this case, the serotonergic system may scale the relative contributions of different subcircuits so that their contributions to the output become proportional to the required contributions which are imposed by the situation (cf. **Figure 6**).

Attempts toward more holistic models of the functional role of 5-HT have emerged from studies on lower animals, such as the lobster (Kravitz, 2000). In the social life of the lobster, 5-HT levels are assumed to gradually build up during encounters with other lobsters. Encounters typically end up in a gradually escalating demonstration of power in which the lobster with the most imposing body language, or, more rarely, physically proven superiority, will maintain high 5-HT levels and an imposing body posture. Conversely, the individual losing the social tete-a-tete will rapidly develop a subordinate body posture which is assumed to be associated with a dramatic decline in 5-HT levels. The subordinate will subsequently avoid engagement in social fighting for a long time. This acquired unwillingness to engage in fighting can be discharged, however, by an experimental manipulation of the 5-HT levels (Kravitz, 2000). In this model system with a low degree of behavioral diversification, 5-HT will hence affect social interactions and the level of 5-HT will also be a consequence of the behavioral outcome on the social stage. In mammals, possessing a more highly developed neocortex and hence a more diversified and richer understanding of the external world, one would expect a more complex set of feedback regulations of the serotonergic system. Still, the serotonergic system may abide the same principle, i.e., the serotonin level is a consequence of the actions we take and the effects we perceive them to produce. A high or a low level of 5-HT is not necessarily good or bad, but the level should rather be appropriate for how we perceive our position with respect to the external world.

Applying this type of functional model of 5-HT actions also to mental brain functions can offer a novel interpretational framework for the action of psychopharmacological drugs linked to malfunction of the monoaminergic system. Associated disorders include depression, melancholia, social anxiety disorder, obsessive compulsive disorders, panic disorders, posttraumatic stress syndrome, and generalized anxiety disorder. Drugs which are used against these disorders and interact with serotonin and monoamine synaptic transmission are sometimes viewed as pharmaceutical pushbuttons for specific emotional qualities, even though there seems to be no good support for assuming direct causality (Ruhe et al., 2007). However, as portrayed above, the cortical systems that can be expected to be ultimately responsible for the perception of our mood appear to provide feedback projections permitting them to regulate their own 5-HT release (Peyron et al., 1998). As in every negative feedback system, a set point of activity that the system strives toward will tend to arise. Temporary variations around that set point can be triggered by novel estimates of the prevailing conditions based on inputs from the ionotropic circuitry. Hence, according to this view, psychiatric disorders that are susceptible to treatment with drugs interfering with the 5-HT system may arise when the multiplicative coordination of activity for different subcircuits have fallen outside their normally functioning set points. If the scaling of the relative contributions of different subcircuits carrying mental models is out of order, the responses to a changing environment would become inadequate, which may start a vicious circle in which the system digresses further away from its functional set points. In principle, this could occur as a consequence of behavior and would thus be acquired, although internal predisposition factors could exist as well. Interference with 5-HT transmission by the clinical administration of seletive serotonin reuptake inhibitors (SSRIs) could theoretically push the set points of 5-HT in the different subcircuits to new ranges. In some patients, these emerging ranges turn out to be functionally operative. In many cases, however, the doses need to be individually adjusted over a long time. And for some patients SSRI treatment does not work irrespective of dose (Rush et al., 2006; Trivedi et al., 2006). Another feature of SSRI treatment that seems to indicate the existence of internal set points for 5-HT activity is that the therapeutic effect of SSRI is often delayed by some two weeks. One part of this delay has been hypothesized to be due to the autoreceptors on the synaptic terminal that releases

serotonin (Richardson-Jones et al., 2010). The autoreceptors exert a negative feedback on the amount of serotonin released by the terminal and thus forms another natural negative feedback system. However, a negative feedback acting across such a short diffusion range and with effects isolated to the own terminal would seem unlikely to normally take two weeks to find a new set point. But the long-range feedback connections back to the raphe nuclei, involving subcircuits of ionotropic neurons, where each neuron may be expected to have a differentially time-varying activity across different conditions, could well result in feedback systems with very long time constants. Hence, they seem to be a more logical explanatory model for such extremely delayed effects.

8.2. A Principle Common Across Monoaminergic Systems

Other monoaminergic systems than the raphe nuclei also function according to principles that strongly resemble the precision scaling function that is proposed here for serotonin in the spinal cord.

A beautiful and perhaps unexpected example comes from the apparent function of the dopaminergic innervation of the retina (Bargmann, 2012). Retinal processing is dominated by cone photoreceptors in bright light and by rod photoreceptors in low light. Both sensor types converge on cone bipolar cells, which receive direct input from cones as well as indirect input from rods relayed through intermediate rod bipolar cells and AII amacrine cells. When the light level is high, the responsible dopaminergic neurons are activated (Brainard and Morgan, 1987) and the gap junctions between AII amacrine cells and cone bipolar cells are uncoupled. This uncoupling is triggered by the action of dopamine at gates exclusively on the amacrine side, implying that it does not interfere with the processing of inputs from the cone photoreceptors (Xia and Mills, 2004). Uncoupling can be considered to be a multiplicative effect, in which the aim is to find the relative scaling that gives the best overall information for the current light level (Mills and Massey, 1995; Xia and Mills, 2004; Bargmann, 2012). This function is akin to the proposed effect of 5-HT in the ventral spinal cord, which scales the relative motor signals actuating individual groups of muscles according to sensory signals in order to optimize the overall force output.

In general, most monoaminergic systems share the principal features that underlie the model of serotonergic precision scaling presented in this paper. In particular, they are under the tight control of the hypothalamus (Veazey et al., 1982; Villalobos and Ferssiwi, 1987). In some cases, they are even part of the hypothalamic nuclear complex (Ugrumov, 1997), as for example the tuberomammillary nucleus of the hypothalamus in case of histaminergic neurons (Haas et al., 2008). The monoaminergic systems send dense projections to each other, suggesting that their respective activities are under mutual control (Ericson et al., 1989; Nakamura, 2013). They all have widespread terminations in most major structures of the CNS (Samuels and Szabadi, 2008; Vertes and Linley, 2008; Daubert and Condron, 2010; Nestler et al., 2015; Yu et al., 2015). They receive feedback connections from the structures they target and they have autoreceptors for the local feedback of their synaptic release (Douglas et al., 2001; Garcia et al., 2004; Richardson-Jones et al., 2010; Ford, 2014). The bulk of their projections go to the ionotropic circuitry where they act primarily by changing conductances which modulate gains (Foehring et al., 1989; Dong and White, 2003; Surmeier et al., 2007; Yu et al., 2015) in the targeted neurons. Among others, targets include the neocortex, thalamus, striatum, cerebellum, hippocampus, and amygdala. In many cases, there is support for a subcircuit-specific regulation (Blandina et al., 2012).

8.3. A Principle Preserved Across Phylogeny

The presented evidence suggests that precision scaling fundamentally extends the functions of the ionotropic circuitry. Therefore, it comes as no surprise that the monoaminergic systems have emerged very early in phylogeny (Parent, 1984) and that their effects have often been strikingly preserved in the course of natural selection. The serotonergic motor feedback loop, which we describe in detail for mammals, can for example be traced back to invertebrates. Also in these animals, serotonergic neurons strongly innervate motor circuits and receive corresponding feedback (Gillette, 2006). Once serotonin is released, motoneurons show equal reactions across species boundaries and increase their gain in Aplysia (Mackey et al., 1989) as well as in cats (Crone et al., 1988) and humans (Wei et al., 2014). In the lobster, it is known that serotonin can act with topographic precision and specifically increase the firing of flexor muscles. This increased flexor excitation induces the imposing body posture which was described above for dominant lobsters (Kravitz, 2000). Similar to the serotonergic motor feedback loop described here, the amacrine dopaminergic system in the retina has been found also in cartilaginous fishes and amphibians (Yamamoto and Vernier, 2011). A difference from the spinal circuitry is that the topographic precision of the population-integrated dopaminergic projection to the retina is not achieved by the distribution of presynaptic terminals and their amplification of ionotropic currents, but by acting on gap junctions. This reflects that gap junctions play a major role in retinal signal processing (Bloomfield and Volgyi, 2009), whereas the influence of electrical coupling within the spinal cord strongly decreases with developmental age (Li and Rekling, 2017). Thus, it is likely that precision scaling has independently emerged in different CNS regions based on the biochemical mechanisms that dominate the respective signal processing.

9. EXPERIMENTAL PREDICTIONS AND CONCLUSIONS

In order to test if the CNS takes advantage of monoaminergic precision scaling, it is most convenient to investigate the serotonergic motor feedback loop implemented by the raphe nuclei. For this circuit, the control of biomimetic robots clearly predicts the hypothesis that must be evaluated: The excitability of a motorpool actuating a specific joint must increase primarily after subjects have moved the respective

joint rather than other joints of the same limb. As serotonergic effects on motoneurons remain for several 100 ms, the increased excitability must be observable also after cessation of the movement and the motor signals that drive it. Given this predicted topographic precision, the raphe nuclei can adapt motor control to changing conditions and ensure highly-dynamic locomotion under minimum metabolic demands.

While this paper elaborates subcircuit-specific neuromodulation mainly for spinal circuitry, precision scaling presents a big picture which frames the ubiquitous monoaminergic neuromodulation across the CNS. Accordingly, monoaminergic systems represent a computational network within the network formed by the ionotropic circuitry. While subcircuits can collectively encode predictive models of the world, monoamines adapt these models to contextual changes by scaling the ionotropic output signals. This concept offers an attractive explanation of how metabotropic signal processing complements the ionotropic functional and anatomical connectome: By scaling individual ionotropic signals, monoamines can provide functionality that is powerful, resource-efficient and, at least in the spinal circuitry, unique. Furthermore, the slow time scale of metabotropic effect coincides with the time scale of many motor behaviors, rendering monoamines ideal candidates to bridge the fast ionotropic signals and slowly changing behavioral context. In turn, the long time scale of metabotropic mechanisms can impose testable detrimental limits on the speed of behavioral adaptation, as exemplarily observed in the persistent impairment of precision movements resulting from serotonergic effects after high muscular force production (Wei et al., 2014). Given these facts, it is not surprising that malfunction of monoaminergic systems is strongly implicated in motor and cognitive disorders. Conceptualizing monoaminergic systems as subcircuit-specific modulators of ionotropic circuitry thus helps scale our view on why diffuse psychopharmacological drugs often show unpredictable treatment outcomes in such disorders.

AUTHOR CONTRIBUTIONS

AA-S, HJ, and PS developed the structure of the paper. PS authored sections 1–7 and 9. HJ authored section 8. AA-S, HJ, and PS critically revised the paper.

REFERENCES

Abbinanti, M. D., and Harris-Warrick, R. M. (2012). Serotonin modulates multiple calcium current subtypes in commissural interneurons of the neonatal mouse. *J. Neurophysiol.* 107, 2212–2219. doi: 10.1152/jn.00768.2011

Abbinanti, M. D., Zhong, G., and Harris-Warrick, R. M. (2012). Postnatal emergence of serotonin-induced plateau potentials in commissural interneurons of the mouse spinal cord. *J. Neurophysiol.* 108, 2191–2202. doi: 10.1152/jn.00336.2012

Ahissar, E. (1998). Temporal-code to rate-code conversion by neuronal phase-locked loops. *Neural Comput.* 10, 597–650.

Alessandro, C., Delis, I., Nori, F., Panzeri, S., and Berret, B. (2013). Muscle synergies in neuroscience and robotics: from input-space to task-space perspectives. *Front. Comput. Neurosci.* 7:43. doi: 10.3389/fncom.2013.00043

Aoi, S., Manoonpong, P., Ambe, Y., Matsuno, F., and Wörgötter, F. (2017). Adaptive control strategies for interlimb coordination in legged robots: a review. *Front. Neurorobot.* 11:39. doi: 10.3389/fnbot.2017.00039

Babič, J., Oztop, E., and Kawato, M. (2016). Human motor adaptation in whole body motion. *Sci. Rep.* 6:32868. doi: 10.1038/srep32868

Bang, S. J., Jensen, P., Dymecki, S. M., and Commons, K. G. (2012). Projections and interconnections of genetically defined serotonin neurons in mice. *Eur. J. Neurosci.* 35, 85–96. doi: 10.1111/j.1460-9568.2011.07936.x

Bargmann, C. I. (2012). Beyond the connectome: how neuromodulators shape neural circuits. *Bioessays* 34, 458–465. doi: 10.1002/bies.201100185

Beaulieu, J.-M., and Gainetdinov, R. R. (2011). The physiology, signaling, and pharmacology of dopamine receptors. *Pharmacol. Rev.* 63, 182–217. doi: 10.1124/pr.110.002642

Belmer, A., Klenowski, P. M., Patkar, O. L., and Bartlett, S. E. (2017). Mapping the connectivity of serotonin transporter immunoreactive axons to excitatory and inhibitory neurochemical synapses in the mouse limbic brain. *Brain Struct. Funct.* 222, 1297–1314. doi: 10.1007/s00429-016-1278-x

Bengtsson, F., and Jörntell, H. (2014). Specific relationship between excitatory inputs and climbing fiber receptive fields in deep cerebellar nuclear neurons. *PLOS ONE* 9:e84616. doi: 10.1371/journal.pone.0084616

Bensmaia, S. J. (2008). Tactile intensity and population codes. *Behav. Brain Res.* 190, 165–173. doi: 10.1016/j.bbr.2008.02.044

Berg, R. W., Alaburda, A., and Hounsgaard, J. (2007). Balanced inhibition and excitation drive spike activity in spinal half-centers. *Science* 315, 390–393. doi: 10.1126/science.1134960

Bernstein, N. A. (1967). *The Co-ordination and Regulation of Movements, 1st english Edn*. Oxford: Pergamon Press.

Bhanpuri, N. H., Okamura, A. M., and Bastian, A. J. (2013). Predictive modeling by the cerebellum improves proprioception. *J. Neurosci.* 33, 14301–14306. doi: 10.1523/JNEUROSCI.0784-13.2013

Bicchi, A., Gabiccini, M., and Santello, M. (2011). Modelling natural and artificial hands with synergies. *Philos. Trans. R. Soc. Lond. B Biol. Sci.* 366, 3153–3161. doi: 10.1098/rstb.2011.0152

Blandina, P., Provensi, G., Munari, L., and Passani, M. B. (2012). Histamine neurons in the tuberomamillary nucleus: a whole center or distinct subpopulations? *Front. Syst. Neurosci.* 6:33. doi: 10.3389/fnsys.2012.00033

Bloomfield, S. A., and Volgyi, B. (2009). The diverse functional roles and regulation of neuronal gap junctions in the retina. *Nat. Rev. Neurosci.* 10, 495–506. doi: 10.1038/nrn2636

Brainard, G. C., and Morgan, W. W. (1987). Light-induced stimulation of retinal dopamine: a dose-response relationship. *Brain Res.* 424, 199–203. doi: 10.1016/0006-8993(87)91211-X

Braun, D., Howard, M., and Vijayakumar, S. (2011). "Exploiting variable stiffness in explosive movement tasks," in *Proceedings of Robotics: Science and Systems* (Los Angeles, CA).

Brown, E., and Brüne, M. (2012). The role of prediction in social neuroscience. *Front. Hum. Neurosci.* 6:147. doi: 10.3389/fnhum.2012.00147

Brumley, M. R., Hentall, I. D., Pinzon, A., Kadam, B. H., Blythe, A., Sanchez, F. J., et al. (2007). Serotonin concentrations in the lumbosacral spinal cord of the adult rat following microinjection or dorsal surface application. *J. Neurophysiol.* 98, 1440–1450. doi: 10.1152/jn.00309.2007

Carandini, M., and Heeger, D. J. (2012). Normalization as a canonical neural computation. *Nat. Rev. Neurosci.* 13, 51–62. doi: 10.1038/nrn3136

Carandini, M., Heeger, D. J., and Senn, W. (2002). A synaptic explanation of suppression in visual cortex. *J. Neurosci.* 22, 10053–10065. doi: 10.1523/JNEUROSCI.22-22-10053.2002

Cash, S., and Yuste, R. (1998). Input summation by cultured pyramidal neurons is linear and position-independent. *J. Neurosci.* 18, 10–15.

Cash, S., and Yuste, R. (1999). Linear summation of excitatory inputs by ca1 pyramidal neurons. *Neuron* 22, 383–394.

Cavada, C., Huisman, A. M., and Kuypers, H. G. (1984). Retrograde double labeling of neurons: the combined use of horseradish peroxidase and diamidino yellow dihydrochloride (DY·2HCl) compared with true blue and DY·2HCl in rat descending brainstem pathways. *Brain Res.* 308, 123–136.

Challis, C., Beck, S., and Berton, O. (2014). Optogenetic modulation of descending prefrontocortical inputs to the dorsal raphe bidirectionally bias socioaffective choices after social defeat. *Front. Behav. Neurosci.* 8:43. doi: 10.3389/fnbeh.2014.00043

Chance, F. S., Abbott, L. F., and Reyes, A. D. (2002). Gain modulation from background synaptic input. *Neuron* 35, 773–782. doi: 10.1016/S0896-6273(02)00820-6

Chang, S. W., Gariepy, J. F., and Platt, M. L. (2013). Neuronal reference frames for social decisions in primate frontal cortex. *Nat. Neurosci.* 16, 243–250. doi: 10.1038/nn.3287

Chen, N., Bayer, J., Urban, S., and van der Smagt, P. (2015). "Efficient movement representation by embedding dynamic movement primitives in deep autoencoders," in *2015 IEEE-RAS 15th International Conference on Humanoid Robots (Humanoids)* (Seoul), 434–440.

Chen, X., DeAngelis, G. C., and Angelaki, D. (2013). Diverse spatial reference frames of vestibular signals in parietal cortex. *Neuron* 80, 1310–1321. doi: 10.1016/j.neuron.2013.09.006

Chvatal, S. A., and Ting, L. H. (2012). Voluntary and reactive recruitment of locomotor muscle synergies during perturbed walking. *J. Neurosci.* 32, 12237–12250. doi: 10.1523/JNEUROSCI.6344-11.2012

Clark, D. J., Ting, L. H., Zajac, F. E., Neptune, R. R., and Kautz, S. A. (2010). Merging of healthy motor modules predicts reduced locomotor performance and muscle coordination complexity post-stroke. *J. Neurophysiol.* 103, 844–857. doi: 10.1152/jn.00825.2009

Cohen, M. A., and Tan, C. O. (2012). A polynomial approximation for arbitrary functions. *Appl. Math. Lett.* 25, 1947–1952. doi: 10.1016/j.aml.2012.03.007

Cools, R., Nakamura, K., and Daw, N. D. (2011). Serotonin and dopamine: unifying affective, activational, and decision functions. *Neuropsychopharmacology* 36, 98–113. doi: 10.1038/npp.2010.121

Cotel, F., Exley, R., Cragg, S. J., and Perrier, J.-F. (2013). Serotonin spillover onto the axon initial segment of motoneurons induces central fatigue by inhibiting action potential initiation. *Proc. Natl. Acad. Sci. U.S.A.* 110, 4774–4779. doi: 10.1073/pnas.1216150110

Crone, C., Hultborn, H., Kiehn, O., Mazieres, L., and Wigstrom, H. (1988). Maintained changes in motoneuronal excitability by short-lasting synaptic inputs in the decerebrate cat. *J. Physiol.* 405, 321–343.

Cunningham, J. P., and Yu, B. M. (2014). Dimensionality reduction for large-scale neural recordings. *Nat. Neurosci.* 17, 1500–1509. doi: 10.1038/nn.3776

Cushing, S., Bui, T., and Rose, P. K. (2005). Effect of nonlinear summation of synaptic currents on the input–output properties of spinal motoneurons. *J. Neurophysiol.*, 94(5):3465–3478. doi: 10.1152/jn.00439.2005

Cybenko, G. (1989). Approximation by superpositions of a sigmoidal function. *Math. Control Signals Syst.* 2, 303–314.

Danner, S. M., Hofstoetter, U. S., Freundl, B., Binder, H., Mayr, W., Rattay, F., et al. (2015). Human spinal locomotor control is based on flexibly organized burst generators. *Brain* 138, 577–588. doi: 10.1093/brain/awu372

Daubert, E. A., and Condron, B. G. (2010). Serotonin: a regulator of neuronal morphology and circuitry. *Trends Neurosci.* 33, 424–434. doi: 10.1016/j.tins.2010.05.005

Davis, J. N. (1975). The response to stretch of human intercostal muscle spindles studied *in vitro*. *J. Physiol.* 249, 561–579.

Dayan, P., and Abbott, L. (2001). "Chapter Network Models: Recurrent Networks," in *Theoretical Neuroscience: Computational and Mathematical Modeling of Neural Systems*, eds T. J. Sejnowski and T. Poggio (Cambridge, MA; London: Computational Neuroscience Series. Massachusetts Institute of Technology Press), 244–265.

Dietrich, A., Ott, C., and Albu-Schäffer, A. (2015). An overview of null space projections for redundant, torque-controlled robots. *Int. J. Robot. Res.* 34, 1385–1400. doi: 10.1177/0278364914566516

Dong, Y., and White, F. J. (2003). Dopamine d1-class receptors selectively modulate a slowly inactivating potassium current in rat medial prefrontal cortex pyramidal neurons. *J. Neurosci.* 23, 2686–2695. doi: 10.1523/JNEUROSCI.23-07-02686.2003

Douglas, C. L., Baghdoyan, H. A., and Lydic, R. (2001). M2 muscarinic autoreceptors modulate acetylcholine release in prefrontal cortex of c57bl/6j mouse. *J. Pharmacol. Exp. Ther.* 299, 960–966.

Dzeladini, F., Ijspeert, A., and van den Kieboom, J. (2014). The contribution of a central pattern generator in a reflex-based neuromuscular model. *Front. Hum. Neurosci.* 8:371. doi: 10.3389/fnhum.2014.00371

ElBasiouny, S. M., Schuster, J. E., and Heckman, C. J. (2010). Persistent inward currents in spinal motoneurons: Important for normal function but potentially harmful after spinal cord injury and in amyotrophic lateral sclerosis. *Clin. Neurophysiol.* 121, 1669-1679. doi: 10.1016/j.clinph.2009.12.041

Ericson, H., Blomqvist, A., and Köhler, C. (1989). Brainstem afferents to the tuberomammillary nucleus in the rat brain with special reference to monoaminergic innervation. *J. Comp. Neurol.* 281, 169–192. doi: 10.1002/cne.902810203

Featherstone, R., and Khatib, O. (1997). Load independence of the dynamically consistent inverse of the jacobian matrix. *Int. J. Robot. Res.* 16, 168–170.

Ferris, D. P., Louie, M., and Farley, C. T. (1998). Running in the real world: adjusting leg stiffness for different surfaces. *Proc. R. Soc. Lond. B Biol. Sci.* 265, 989–994.

Foehring, R. C., Schwindt, P. C., and Crill, W. E. (1989). Norepinephrine selectively reduces slow ca2+- and na+-mediated k+ currents in cat neocortical neurons. *J. Neurophysiol.* 61, 245–256.

Ford, C. P. (2014). The role of D2-autoreceptors in regulating dopamine neuron activity and transmission. *Neuroscience* 282, 13–22. doi: 10.1016/j.neuroscience.2014.01.025

Fornal, C. A., Metzler, C. W., Marrosu, F., do Valle, L. E. R., , and Jacobs, B. L. (1996). A subgroup of dorsal raphe serotonergic neurons in the cat is strongly activated during oral-buccal movements. *Brain Res.* 716, 123–133.

Franklin, D. W., Batchelor, A. V., and Wolpert, D. M. (2016). The sensorimotor system can sculpt behaviorally relevant representations for motor learning. *eNeuro* 3:ENEURO.0070-16.2016. doi: 10.1523/ENEURO.0070-16.2016

Fuxe, K., Dahlström, A. B., Jonsson, G., Marcellino, D., Guescini, M., Dam, M., Manger, P., et al. (2010). The discovery of central monoamine neurons gave volume transmission to the wired brain. *Prog. Neurobiol.* 90, 82–100. doi: 10.1016/j.pneurobio.2009.10.012

Gabbiani, F., Krapp, H. G., Koch, C., and Laurent, G. (2002). Multiplicative computation in a visual neuron sensitive to looming. *Nature* 420, 320–324. doi: 10.1038/nature01190

Gallego, J. A., Perich, M. G., Miller, L. E., and Solla, S. A. (2017). Neural manifolds for the control of movement. *Neuron* 94, 978–984. doi: 10.1016/j.neuron.2017.05.025

Garcia, A. S., Barrera, G., Burke, T. F., Ma, S., Hensler, J. G., and Morilak, D. A. (2004). Autoreceptor-mediated inhibition of norepinephrine release in rat medial prefrontal cortex is maintained after chronic desipramine treatment. *J. Neurochem.* 91, 683–693. doi: 10.1111/j.1471-4159.2004.02748.x

Gerstner, W. (2016). "Chapter 6: Hebbian learning and plasticity," in *From Neuron to Cognition Via Computational Neuroscience*, eds, M. A. Arbib and J. J. Bonaiuto (Cambridge, MA; London: Computational Neuroscience Series, MIT Press), 199–218.

Ghosh, A., Rothwell, J., and Haggard, P. (2014). Using voluntary motor commands to inhibit involuntary arm movements. *Proc. R. Soc. Lond. B Biol. Sci.* 281:20141139. doi: 10.1098/rspb.2014.1139

Gillette, R. (2006). Evolution and function in serotonergic systems. *Integr. Comp. Biol.* 46, 838–846. doi: 10.1093/icb/icl024

Graziano, M. (2006). The organization of behavioral repertoire in motor cortex. *Annu. Rev. Neurosci.* 29, 105–134. doi: 10.1146/annurev.neuro.29.051605.112924

Graziano, M. S. A., Patel, K. T., and Taylor, C. S. R. (2004). Mapping from motor cortex to biceps and triceps altered by elbow angle. *J. Neurophysiol.* 92, 395–407. doi: 10.1152/jn.01241.2003

Guertin, P. (2013). Central pattern generator for locomotion: anatomical, physiological, and pathophysiological considerations. *Front. Neurol.* 3:183. doi: 10.3389/fneur.2012.00183

Haas, H. L., Sergeeva, O. A., and Selbach, O. (2008). Histamine in the nervous system. *Physiol. Rev.* 88, 1183–1241. doi: 10.1152/physrev.00043.2007

Hagio, S., Fukuda, M., and Kouzaki, M. (2015). Identification of muscle synergies associated with gait transition in humans. *Front. Hum. Neurosci.* 9:48. doi: 10.3389/fnhum.2015.00048

Harris-Warrick, R. M. (2011). Neuromodulation and flexibility in central pattern generator networks. *Curr. Opin. Neurobiol.* 21, 685–692. doi: 10.1016/j.conb.2011.05.011

Hattox, A., Li, Y., and Keller, A. (2003). Serotonin regulates rhythmic whisking. *Neuron* 39, 343–352. doi: 10.1016/S0896-6273(03)00391-X

Heckman, C. J., Hyngstrom, A. S., and Johnson, M. D. (2008). Active properties of motoneurone dendrites: diffuse descending neuromodulation, focused local inhibition. *J. Physiol.* 586, 1225–1231. doi: 10.1113/jphysiol.2007.145078

Heed, T., Buchholz, V. N., Engel, A. K., and Röder, B. (2015). Tactile remapping: from coordinate transformation to integration in sensorimotor processing. *Trends Cogn. Sci.* 19, 251–258. doi: 10.1016/j.tics.2015.03.001

Heglund, N. C., and Taylor, C. R. (1988). Speed, stride frequency and energy cost per stride: how do they change with body size and gait? *J. Exp. Biol.* 138, 301–318.

Hensel, H. (1973). "Cutaneous thermoreceptors," in *Somatosensory System*, ed A. Iggo (Berlin; Heidelberg: Springer), 79–110.

Higgs, M. H., Slee, S. J., and Spain, W. J. (2006). Diversity of gain modulation by noise in neocortical neurons: regulation by the slow afterhyperpolarization conductance. *J. Neurosci.* 26, 8787–8799. doi: 10.1523/JNEUROSCI.1792-06.2006

Hinton, G. E., and Salakhutdinov, R. R. (2006). Reducing the dimensionality of data with neural networks. *Science* 313, 504–507. doi: 10.1126/science.1127647

Hochman, S., Garraway, S. M., Machacek, D. W., and Shay, B. L. (2001). "5-ht receptors and the neuromodulatory control of spinal cord function," in *Motor Neurobiology of the Spinal Cord*, ed T. Cope (Boca Raton, FL; London; New York, NY; Washington, DC), 47–88.

Holmes, P., Full, R. J., Koditschek, D., and Guckenheimer, J. (2006). The dynamics of legged locomotion: models, analyses, and challenges. *SIAM Rev.* 48, 207–304. doi: 10.1137/S0036144504445133

Hornik, K. (1991). Approximation capabilities of multilayer feedforward networks. *Neural Netw.* 4, 251–257.

Hornung, J.-P. (2003). The human raphe nuclei and the serotonergic system. *J. Chem. Neuroanat.* 26, 331–343. doi: 10.1016/j.jchemneu.2003.10.002

Howell, L. L., and Cunningham, K. A. (2015). Serotonin 5-HT2 receptor interactions with dopamine function: implications for therapeutics in cocaine use disorder. *Pharmacol. Rev.* 67, 176–197. doi: 10.1124/pr.114.009514

Huisman, A. M., Kuypers H. G. J. M., and Verburgh, C. A. (2011). "Differences in collateralization of the descending spinal pathways from red nucleus and other brain stem cell groups in cat and monkey," in *Descending Pathways to the Spinal Cord*, eds H. Kuypers and G. Martin (Amsterdam; New York, NY; Oxford: Elsevier Science), 185–218.

Hultborn, H., Denton, M. E., Wienecke, J., and Nielsen, J. B. (2003). Variable amplification of synaptic input to cat spinal motoneurones by dendritic persistent inward current. *J. Physiol.* 552(Pt 3), 945–952. doi: 10.1113/jphysiol.2003.050971

Husch, A., Dietz, S. B., Hong, D. N., and Harris-Warrick, R. M. (2015). Adult spinal v2a interneurons show increased excitability and serotonin-dependent bistability. *J. Neurophysiol.* 113, 1124–1134. doi: 10.1152/jn.00741.2014

Hyngstrom, A. S., Johnson, M. D., and Heckman, C. J. (2008). Summation of excitatory and inhibitory synaptic inputs by motoneurons with highly active dendrites. *J. Neurophysiol.* 99, 1643–1652. doi: 10.1152/jn.01253.2007

Ijspeert, A. J. (2008). Central pattern generators for locomotion control in animals and robots: a review. *Neural Netw.* 21, 642–653. doi: 10.1016/j.neunet.2008.03.014

Ijspeert, A. J., Nakanishi, J., Hoffmann, H., Pastor, P., and Schaal, S. (2013). Dynamical movement primitives: learning attractor models for motor behaviors. *Neural Comput.* 25, 328–373. doi: 10.1162/NECO_a_00393

Isaacson, J., and Scanziani, M. (2011). How inhibition shapes cortical activity. *Neuron* 72, 231–243. doi: 10.1016/j.neuron.2011.09.027

Jankowska, E. (1992). Interneuronal relay in spinal pathways from proprioceptors. *Prog. Neurobiol.* 38, 335–378.

Jankowski, M. P., and Sesack, S. R. (2004). Prefrontal cortical projections to the rat dorsal raphe nucleus: Ultrastructural features and associations with serotonin and gamma-aminobutyric acid neurons. *J. Comp. Neurol.* 468, 518–529. doi: 10.1002/cne.10976

Jia, H., Rochefort, N. L., Chen, X., and Konnerth, A. (2010). Dendritic organization of sensory input to cortical neurons *in vivo*. *Nature* 464, 1307–1312. doi: 10.1038/nature08947

Jing, J., Gillette, R., and Weiss, K. R. (2009). Evolving concepts of arousal: insights from simple model systems. *Rev. Neurosci.* 20, 405–427. doi: 10.1515/REVNEURO.2009.20.5-6.405

Johansson, H., and Silfvenius, H. (1977). Connexions from large, ipsilateral hind limb muscle and skin afferents to the rostral main cuneate nucleus and to the nucleus X region in the cat. *J. Physiol.* 265, 395–428.

Jones, P. W., and Gabbiani, F. (2012). Logarithmic compression of sensory signals within the dendritic tree of a collision-sensitive neuron. *J. Neurosci.* 32, 4923–4934. doi: 10.1523/JNEUROSCI.5777-11.2012

Jörntell, H. (2016). "Synergy control in subcortical circuitry: Insights from neurophysiology," in *Human and Robot Hands: Sensorimotor Synergies to Bridge the Gap Between Neuroscience and Robotics*, eds M. Bianchi and A. Moscatelli (Cham: Springer International Publishing), 61–68.

Jörntell, H. (2017). Cerebellar physiology: links between microcircuitry properties and sensorimotor functions. *J. Physiol.* 595, 11–27. doi: 10.1113/JP272769

Kiehn, O. (2016). Decoding the organization of spinal circuits that control locomotion. *Nat. Rev. Neurosci.* 17, 224–238. doi: 10.1038/nrn.2016.9

Kravitz, E. A. (2000). Serotonin and aggression: insights gained from a lobster model system and speculations on the role of amine neurons in a complex behavior. *J. Comp. Physiol. A* 186, 221–238. doi: 10.1007/s003590050423

Kurian, M. A., Gissen, P., Smith, M., Heales, S. J., and Clayton, P. T. (2011). The monoamine neurotransmitter disorders: an expanding range of neurological syndromes. *Lancet Neurol.* 10, 721–733. doi: 10.1016/S1474-4422(11)70141-7

Lacquaniti, F., Ivanenko, Y. P., and Zago, M. (2012). Patterned control of human locomotion. *J. Physiol.* 590, 2189–2199. doi: 10.1113/jphysiol.2011.215137

Lai, A., Schache, A. G., Lin, Y.-C., and Pandy, M. G. (2014). Tendon elastic strain energy in the human ankle plantar-flexors and its role with increased running speed. *J. Exp. Biol.* 217, 3159–3168. doi: 10.1242/jeb.100826

Lakatos, D., and Albu-Schäffer, A. (2014a). "Neuron model interpretation of a cyclic motion control concept," in *Biomedical Robotics and Biomechatronics, 2014 5th IEEE RAS EMBS International Conference* (Sao Paulo), 905–910.

Lakatos, D., and Albu-Schäffer, A. (2014b). "Switching based limit cycle control for compliantly actuated second-order systems," in *Proceedings of the IFAC World Congress, Vol. 19* (Cape Town), 6392–6399.

Lakatos, D., Friedl, W., and Albu-Schäffer, A. (2017). Eigenmodes of nonlinear dynamics: Definition, existence, and embodiment into legged robots with elastic elements. *IEEE Robot. Automat. Lett.* 2, 1062–1069. doi: 10.1109/LRA.2017.2658018

Lakatos, D., Görner, M., Petit, F., Dietrich, A., and Albu-Schäffer, A. (2013). "A modally adaptive control for multi-contact cyclic motions in compliantly actuated robotic systems," in *Intelligent Robots and Systems (IROS), 2013 IEEE International Conference on* (IEEE) (Tokyo), 5388–5395.

Levine, A. J., Hinckley, C. A., Hilde, K. L., Driscoll, S. P., Poon, T. H., Montgomery, J. M., et al. (2014). Identification of a cellular node for motor control pathways. *Nat. Neurosci.* 17, 586–593. doi: 10.1038/nn.3675

Li, W.-C., and Rekling, J. C. (2017). "Electrical coupling in the generation of vertebrate motor rhythms," in *Network Functions and Plasticity: Perspectives from Studying Neuronal Electrical Coupling in Microcircuits*, ed J. Jing (London; San Diego, CA; Cambridge, MA; Oxford: Elsevier Science), 243–264.

Loewy, A. (1981). Raphe pallidus and raphe obscurus projections to the intermediolateral cell column in the rat. *Brain Res.* 222, 129–133.

Löffl, F., Werner, A., Lakatos, D., Reinecke, J., Wolf, S., Burger, R., et al. (2016). "The dlr c-runner: Concept, design and experiments," in *2016 IEEE-RAS 16th International Conference on Humanoid Robots (Humanoids)* (Cancun), 758–765.

Longordo, F., To, M. S., Ikeda, K., and Stuart, G. J. (2013). Sublinear integration underlies binocular processing in primary visual cortex. *Nat. Neurosci.* 16, 714–723. doi: 10.1038/nn.3394

Losonczy, A., and Magee, J. C. (2006). Integrative properties of radial oblique dendrites in hippocampal ca1 pyramidal neurons. *Neuron* 50, 291–307. doi: 10.1016/j.neuron.2006.03.016

MacKay-Lyons, M. (2002). Central pattern generation of locomotion: a review of the evidence. *Phys. Ther.* 82, 69–83. doi: 10.1093/ptj/82.1.69

Mackey, S., Kandel, E., and Hawkins, R. (1989). Identified serotonergic neurons lcb1 and rcb1 in the cerebral ganglia of aplysia produce presynaptic facilitation of siphon sensory neurons. *J. Neurosci.* 9, 4227–4235.

Magistretti, P. J., and Allaman, I. (2015). A cellular perspective on brain energy metabolism and functional imaging. *Neuron* 86, 883–901. doi: 10.1016/j.neuron.2015.03.035

Maier, M. A., Perlmutter, S. I., and Fetz, E. E. (1998). Response patterns and force relations of monkey spinal interneurons during active wrist movement. *J. Neurophysiol.* 80, 2495–2513.

Major, G., Larkum, M. E., and Schiller, J. (2013). Active properties of neocortical pyramidal neuron dendrites. *Annu. Rev. Neurosci.* 36, 1–24. doi: 10.1146/annurev-neuro-062111-150343

Martin, R. F., Jordan, L. M., and Willis, W. D. (1978). Differential projections of cat medullary raphe neurons demonstrated by retrograde labelling following spinal cord lesions. *J. Comp. Neurol.* 182, 77–88. doi: 10.1002/cne.901820106

Mather, M., and Harley, C. W. (2016). The locus coeruleus: Essential for maintaining cognitive function and the aging brain. *Trends Cogn. Sci.* 20, 214–226. doi: 10.1016/j.tics.2016.01.001

Mathis, J., Gurfinkel, V., and Struppler, A. (1996). Facilitation of motor evoked potentials by postcontraction response (kohnstamm phenomenon). *Electroencephalogr. Clin. Neurophysiol.* 101, 289–297.

McElvain, L., Faulstich, M., Jeanne, J., Moore, J., and du Lac, S. (2015). Implementation of linear sensory signaling via multiple coordinated mechanisms at central vestibular nerve synapses. *Neuron.* 85, 1132–1144. doi: 10.1016/j.neuron.2015.01.017

Mehaffey, W. H., Doiron, B., Maler, L., and Turner, R. W. (2005). Deterministic multiplicative gain control with active dendrites. *J. Neurosci.* 25, 9968–9977. doi: 10.1523/JNEUROSCI.2682-05.2005

Mills, S. L., and Massey, S. C. (1995). Differential properties of two gap junctional pathways made by AII amacrine cells. *Nature* 377, 734–737.

Minassian, K., Hofstoetter, U. S., Dzeladini, F., Guertin, P. A., and Ijspeert, A. (2017). The human central pattern generator for locomotion: does it exist and contribute to walking? *Neuroscientist* 23, 649–663. doi: 10.1177/1073858417699790

Mitchell, S. J., and Silver, R. A. (2003). Shunting inhibition modulates neuronal gain during synaptic excitation. *Neuron* 38, 433–445. doi: 10.1016/S0896-6273(03)00200-9

Muniak, M. A., Ray, S., Hsiao, S. S., Dammann, J. F., and Bensmaia, S. J. (2007). The neural coding of stimulus intensity: linking the population response of mechanoreceptive afferents with psychophysical behavior. *J. Neurosci.* 27(43):11687–11699. doi: 10.1523/JNEUROSCI.1486-07.2007

Myoga, H., Nonaka, S., Matsuyama, K., and Mori, S. (1995). Postnatal development of locomotor movements in normal and para-chlorophenylalanine-treated newborn rats. *Neurosci. Res.* 21, 211 – 221.

Naik, G. R., Selvan, S. E., Gobbo, M., Acharyya, A., and Nguyen, H. T. (2016). Principal component analysis applied to surface electromyography: a comprehensive review. *IEEE Access* 4, 4025–4037. doi: 10.1109/ACCESS.2016.2593013

Nakamura, K. (2013). The role of the dorsal raphe nucleus in reward-seeking behavior. *Front. Integr. Neurosci.* 7:60. doi: 10.3389/fnint.2013.00060

Nakanishi, J., Cory, R., Mistry, M., Peters, J., and Schaal, S. (2008). Operational space control: a theoretical and empirical comparison. *Int. J. Robot. Res.* 27, 737–757. doi: 10.1177/0278364908091463

Nestler, E. J., Hyman, S. E., Holtzman, D. M., and Malenka, R. C. (eds.). (2015). "Chapter 6: Widely projecting systems: Monoamines, acetylcholine, and orexin," in *Molecular Neuropharmacology: A Foundation for Clinical Neuroscience, 3e* (New York, NY: McGraw-Hill Education), 149–183.

Ng, J., Papandreou, A., Heales, S., and Kurian, M. (2015). Monoamine neurotransmitter disorders - clinical advances and future perspectives. *Nat. Rev. Neurol.* 11, 567-84. doi: 10.1038/nrneurol.2015.172

Nieuwenhuys, R., Voogd, J., and van Huijzen, C. (eds.). (2008). "The reticular formation and the monoaminergic and cholinergic cell groups," in *The Human Central Nervous System* (Berlin; Heidelberg: Springer), 889–916.

Nishimura, Y., Perlmutter, S. I., Eaton, R. W., and Fetz, E. E. (2013). Spike-timing-dependent plasticity in primate corticospinal connections induced during free behavior. *Neuron* 80, 1301–1309. doi: 10.1016/j.neuron.2013.08.028

O'Donnell, J., Zeppenfeld, D., McConnell, E., Pena, S., and Nedergaard, M. (2012). Norepinephrine: A neuromodulator that boosts the function of multiple cell types to optimize cns performance. *Neurochem. Res.* 37, 2496–2512. doi: 10.1007/s11064-012-0818-x

Overduin, S. A., d'Avella, A., Carmena, J. M., and Bizzi, E. (2012). Microstimulation activates a handful of muscle synergies. *Neuron* 76, 1071–1077. doi: 10.1016/j.neuron.2012.10.018

Oviedo, H., and Reyes, A. (2002). Boosting of neuronal firing evoked with asynchronous and synchronous inputs to the dendrite. *Nat. Neurosci.* 5, 261–266. doi: 10.1038/nn807

Ozeki, H., Finn, I. M., Schaffer, E. S., Miller, K. D., and Ferster, D. (2009). Inhibitory stabilization of the cortical network underlies visual surround suppression. *Neuron* 62, 578–592. doi: 10.1016/j.neuron.2009.03.028

Palmer, L. M. (2014). Dendritic integration in pyramidal neurons during network activity and disease. *Brain Res. Bull.* 103(Suppl. C), 2–10. doi: 10.1016/j.brainresbull.2013.09.010

Parent, A. (1984). Functional anatomy and evolution of monoaminergic systems1. *Am. Zool.* 24, 783–790.

Pearlstein, E., Ben Mabrouk, F., Pflieger, J. F., and Vinay, L. (2005). Serotonin refines the locomotor-related alternations in the *in vitro* neonatal rat spinal cord. *Eur. J. Neurosci.* 21, 1338–1346. doi: 10.1111/j.1460-9568.2005.03971.x

Pérez-Nombela, S., Barroso, F., Torricelli, D., de Los Reyes-Guzman, A., Del-Ama, A. J., Gomez-Soriano, J., et al. (2017). Modular control of gait after incomplete spinal cord injury: differences between sides. *Spinal Cord* 55, 79–86. doi: 10.1038/sc.2016.99

Perlmutter, S. I., Maier, A. M., and Fetz, E. E. (1998). Activity of spinal interneurons and their effects on forearm muscles during voluntary wrist movements in the monkey. *J. Neurophysiol.* 80, 2475–2494.

Perrier, J.-F., and Cotel, F. (2015). Serotonergic modulation of spinal motor control. *Curr. Opin. Neurobiol.* 33, 1–7. doi: 10.1016/j.conb.2014.12.008

Perrier, J.-F., and Delgado-Lezama, R. (2005). Synaptic release of serotonin induced by stimulation of the raphe nucleus promotes plateau potentials in spinal motoneurons of the adult turtle. *J. Neurosci.* 25, 7993–7999. doi: 10.1523/JNEUROSCI.1957-05.2005

Perrier, J.-F., Rasmussen, H. B., Christensen, R. K., and Petersen, A. V. (2013). Modulation of the intrinsic properties of motoneurons by serotonin. *Curr. Pharmaceut. Design* 19, 4371–4384. doi: 10.2174/1381612811319990341

Peters, J., Mistry, M., Udwadia, F., Nakanishi, J., and Schaal, S. (2008). A unifying framework for robot control with redundant dofs. *Auton. Robots* 24, 1–12. doi: 10.1007/s10514-007-9051-x

Peyron, C., Petit, J. M., Rampon, C., Jouvet, M., and Luppi, P. H. (1998). Forebrain afferents to the rat dorsal raphe nucleus demonstrated by retrograde and anterograde tracing methods. *Neuroscience* 82, 443–468.

Pflieger, J.-F., Clarac, F., and Vinay, L. (2002). Postural modifications and neuronal excitability changes induced by a short-term serotonin depletion during neonatal development in the rat. *J. Neurosci.* 22, 5108–5117. doi: 10.1523/JNEUROSCI.22-12-05108.2002

Picciotto, M., Higley, M., and Mineur, Y. (2012). Acetylcholine as a neuromodulator: cholinergic signaling shapes nervous system function and behavior. *Neuron* 76, 116–129. doi: 10.1016/j.neuron.2012.08.036

Powers, R. K., and Binder, M. D. (1995). Effective synaptic current and motoneuron firing rate modulation. *J. Neurophysiol.* 74, 793–801.

Powers, R. K., and Binder, M. D. (2000). Summation of effective synaptic currents and firing rate modulation in cat spinal motoneurons. *J. Neurophysiol.* 83, 483–500. doi: 10.1152/jn.2000.83.1.483

Priebe, N. J., and Ferster, D. (2010). Neuroscience: each synapse to its own. *Nature* 464, 1290–1291. doi: 10.1038/4641290b

Prut, Y., and Perlmutter, S. I. (2003). Firing properties of spinal interneurons during voluntary movement. I. State-dependent regularity of firing. *J. Neurosci.* 23, 9600–9610. doi: 10.1523/JNEUROSCI.23-29-09600.2003

Remy, S., Csicsvari, J., and Beck, H. (2009). Activity-dependent control of neuronal output by local and global dendritic spike attenuation. *Neuron* 61, 906–916. doi: 10.1016/j.neuron.2009.01.032

Rhodes, P. (2006). The properties and implications of nmda spikes in neocortical pyramidal cells. *J. Neurosci.* 26, 6704–6715. doi: 10.1523/JNEUROSCI.3791-05.2006

Richardson-Jones, J. W., Craige, C. P., Guiard, B. P., Stephen, A., Metzger, K. L., Kung, H. F., et al. (2010). 5-HT1A autoreceptor levels determine vulnerability to stress and response to antidepressants. *Neuron* 65, 40–52.

Rosenbaum, D. M., Rasmussen, S. G., and Kobilka, B. K. (2009). The structure and function of G-protein-coupled receptors. *Nature* 459, 356–363. doi: 10.1016/j.neuron.2009.12.003

Rothman, J. S., Cathala, L., Steuber, V., and Silver, R. A. (2009). Synaptic depression enables neuronal gain control. *Nature* 457, 1015–1018. doi: 10.1038/nature07604

Rothwell, J. C. (ed.). (1987). "Proprioceptors in muscle, joint and skin," in *Control of Human Voluntary Movement* (Boston, MA: Springer), 74–104.

Ruhe, H. G., Mason, N. S., and Schene, A. H. (2007). Mood is indirectly related to serotonin, norepinephrine and dopamine levels in humans: a meta-analysis of monoamine depletion studies. *Mol. Psychiatry* 12, 331–359. doi: 10.1038/sj.mp.4001949

Rush, A. J., Trivedi, M. H., Wisniewski, S. R., Nierenberg, A. A., Stewart, J. W., Warden, D., et al. (2006). Acute and longer-term outcomes in depressed outpatients requiring one or several treatment steps: a star*d report. *Am. J. Psychiatry* 163, 1905–1917. doi: 10.1176/ajp.2006.163.11.1905

Salinas, E., and Sejnowski, T. J. (2001). Gain modulation in the central nervous system: where behavior, neurophysiology, and computation meet. *Neuroscientist* 7, 430–440. doi: 10.1177/107385840100700512

Samuels, E. R., and Szabadi, E. (2008). Functional neuroanatomy of the noradrenergic locus coeruleus: its roles in the regulation of arousal and autonomic function part I: principles of functional organisation. *Curr. Neuropharmacol.* 6, 235–253. doi: 10.2174/157015908785777229

Santello, M., Baud-Bovy, G., and Jörntell, H. (2013). Neural bases of hand synergies. *Front. Comput. Neurosci.* 7:23. doi: 10.3389/fncom.2013.00023

Santello, M., Bianchi, M., Gabiccini, M., Ricciardi, E., Salvietti, G., Prattichizzo, D.,et al. (2016). Hand synergies: Integration of robotics and neuroscience for understanding the control of biological and artificial hands. *Phys. Life Rev.* 17, 1–23. doi: 10.1016/j.plrev.2016.02.001

Santello, M., and Lang, C. E. (2015). Are movement disorders and sensorimotor injuries pathologic synergies? when normal multi-joint movement synergies become pathologic. *Front. Hum. Neurosci.* 8:1050. doi: 10.3389/fnhum.2014.01050

Sawicki, G. S., Lewis, C. L., and Ferris, D. P. (2009). It pays to have a spring in your step. *Exerc. Sport Sci. Rev.* 37, 130–138. doi: 10.1097/JES.0b013e31819c2df6

Segev, I., Rinzel, J., and Shepherd, G. (1994). *The Theoretical Foundation of Dendritic Function: Selected Papers of Wilfrid Rall with Commentaries*. Cambridge, MA; London: MIT Press.

Shalit, U., Zinger, N., Joshua, M., and Prut, Y. (2012). Descending systems translate transient cortical commands into a sustained muscle activation signal. *Cereb. Cortex* 22, 1904–1914. doi: 10.1093/cercor/bhr267

Shemmell, J., An, J. H., and Perreault, E. J. (2009). The differential role of motor cortex in stretch reflex modulation induced by changes in environmental mechanics and verbal instruction. *J. Neurosci.* 29, 13255–13263. doi: 10.1523/JNEUROSCI.0892-09.2009

Sherman, S. M., and Koch, C. (1986). The control of retinogeniculate transmission in the mammalian lateral geniculate nucleus. *Exp. Brain Res.* 63, 1–20.

Shinoda, Y., Zarzecki, P., and Asanuma, H. (1979). Spinal branching of pyramidal tract neurons in the monkey. *Exp. Brain Res.* 34, 59–72.

Siebert, T., and Rode, C. (2014). "Computational modeling of muscle biomechanics," in *Computational Modelling of Biomechanics and Biotribology in the Musculo-skeletal System, 1 Edn*, ed Z. Jin (Amsterdam; Boston, MA; Heidelberg; London; New York, NY; Oxford; Paris; San Diego CA; San Francisco CA; Singapore; Sydney, NSW; Tokyo: Woodhead Publishing; Elsevier), 173–204.

Silver, R. A. (2010). Neuronal arithmetic. *Nat. Rev. Neurosci.* 11, 474–489. doi: 10.1038/nrn2864

Skagerberg, G., and Bjorklund, A. (1985). Topographic principles in the spinal projections of serotonergic and non-serotonergic brainstem neurons in the rat. *Neuroscience* 15, 445–480.

Slawińska, U., Miazga, K., and Jordan, L. M. (2014). $[5\text{-HT}]_2$ and $[5\text{-HT}]_7$ receptor agonists facilitate plantar stepping in chronic spinal rats through actions on different populations of spinal neurons. *Front. Neural Circuits* 8:95. doi: 10.3389/fncir.2014.00095

Spanne, A., Geborek, P., Bengtsson, F., and Jörntell, H. (2014). Spike generation estimated from stationary spike trains in a variety of neurons *in vivo*. *Front. Cell. Neurosci.* 8:199. doi: 10.3389/fncel.2014.00199

Springfield, S. A., and Moolenaar, G.-M. (1983). Differences in the responses of raphe nuclei to repetitive somatosensory stimulation. *Exp. Neurol.* 79, 360–370.

Stein, R. B., Gossen, E. R., and Jones, K. E. (2005). Neuronal variability: noise or part of the signal? *Nat. Rev. Neurosci.* 6, 389–397. doi: 10.1038/nrn1668

Stone, M. H. (1948). The generalized weierstrass approximation theorem. *Math. Mag.* 21, 167–184. doi: 10.2307/3029750

Stratmann, P., Lakatos, D., and Albu-Schäffer, A. (2016). Neuromodulation and synaptic plasticity for the control of fast periodic movement: energy efficiency in coupled compliant joints via PCA. *Front. Neurorobot.* 10:2. doi: 10.3389/fnbot.2016.00002

Stratmann, P., Lakatos, D., Özparpucu, M. C., and Albu-Schäffer, A. (2017). "Legged elastic multibody systems: adjusting limit cycles to close-to-optimal energy efficiency," in *IEEE Robotics and Automation Letters*, 1–1.

Surmeier, D. J., Ding, J., Day, M., Wang, Z., and Shen, W. (2007). D1 and D2 dopamine-receptor modulation of striatal glutamatergic signaling in striatal medium spiny neurons. *Trends Neurosci.* 30, 228–235. doi: 10.1016/j.tins.2007.03.008

Svensson, E., Grillner, S., and Parker, D. (2001). Gating and braking of short- and long-term modulatory effects by interactions between colocalized neuromodulators. *J. Neurosci.* 21, 5984–5992. doi: 10.1523/JNEUROSCI.21-16-05984.2001

Takei, T., Confais, J., Tomatsu, S., Oya, T., and Seki, K. (2017). Neural basis for hand muscle synergies in the primate spinal cord. *Proc. Natl. Acad. Sci. U.S.A.* 114, 8643–8648. doi: 10.1073/pnas.1704328114

Thörn Pérez, C., Hill, R. H., and Grillner, S. (2015). Substance p depolarizes lamprey spinal cord neurons by inhibiting background potassium channels. *PLOS ONE* 10:e0133136. doi: 10.1371/journal.pone.0133136

Trivedi, M. H., Rush, A. J., Wisniewski, S. R., Nierenberg, A. A., Warden, D., Ritz, L., et al. (2006). Evaluation of outcomes with citalopram for depression using measurement-based care in star*d: Implications for clinical practice. *Am. J. Psychiatry* 163, 28–40. doi: 10.1176/appi.ajp.163.1.28

Ugrumov, M. V. (1997). Hypothalamic monoaminergic systems in ontogenesis: development and functional significance. *Int. J. Dev. Biol.* 41, 809–816.

van Rossum, M. C. W., Turrigiano, G. G., and Nelson, S. B. (2002). Fast propagation of firing rates through layered networks of noisy neurons. *J. Neurosci.* 22, 1956–1966. doi: 10.1523/JNEUROSCI.22-05-01956.2002

Varga, Z., Jia, H., Sakmann, B., and Konnerth, A. (2011). Dendritic coding of multiple sensory inputs in single cortical neurons *in vivo*. *Proc. Natl. Acad. Sci. U.S.A.* 108, 15420–15425. doi: 10.1073/pnas.1112355108

Veasey, S. C., Fornal, C. A., Metzler, C. W., and Jacobs, B. L. (1995). Response of serotonergic caudal raphe neurons in relation to specific motor activities in freely moving cats. *J. Neurosci.* 15(7 Pt 2), 5346–5359. doi: 10.1523/JNEUROSCI.15-07-05346.1995

Veazey, R. B., Amaral, D. G., and Cowan, W. M. (1982). The morphology and connections of the posterior hypothalamus in the cynomolgus monkey (macaca fascicularis). ii. efferent connections. *The J. Comp. Neurol.* 207, 135–156.

Vertes, R. P., and Linley, S. B. (2008). "Efferent and afferent connections of the dorsal and median raphe nuclei in the rat," in *Serotonin and Sleep: Molecular, Functional and Clinical Aspects* (Basel: Birkhäuser Basel), 69–102.

Villalobos, J., and Ferssiwi, A. (1987). The differential descending projections from the anterior, central and posterior regions of the lateral hypothalamic area: an autoradiographic study. *Neurosci. Lett.* 81, 95–99.

Warden, M. R., Selimbeyoglu, A., Mirzabekov, J. J., Lo, M., Thompson, K. R., Kim, S. Y., et al. (2012). A prefrontal cortex-brainstem neuronal projection that controls response to behavioural challenge. *Nature* 492, 428–432. doi: 10.1038/nature11617

Watson, C., Paxinos, G., and Puelles, L. (2012). *The Mouse Nervous System*. Amsterdam; Boston MA; Heidelberg; London; New York, NY; Oxford; Paris; San Diego, CA; San Francisco, CA; Singapore; Sydney, NSW; Tokyo: Academic Press; Elsevier Academic Press.

Watson, K., and Platt, M. (2012). Social signals in primate orbitofrontal cortex. *Curr. Biol.* 22, 2268–2273. doi: 10.1016/j.cub.2012.10.016

Wei, K., Glaser, J. I., Deng, L., Thompson, C. K., Stevenson, I. H., Wang, Q., et al. (2014). Serotonin affects movement gain control in the spinal cord. *J. Neurosci.* 34, 12690–12700. doi: 10.1523/JNEUROSCI.1855-14.2014

Williams, S. R., and Stuart, G. J. (2002). Dependence of epsp efficacy on synapse location in neocortical pyramidal neurons. *Science* 295, 1907–1910. doi: 10.1126/science.1067903

Willis, M. L., Palermo, R., Burke, D., McGrillen, K., and Miller, L. (2010). Orbitofrontal cortex lesions result in abnormal social judgements to emotional faces. *Neuropsychologia* 48, 2182 – 2187. doi: 10.1016/j.neuropsychologia.2010.04.010

Wise, S. P., and Shadmehr, R. (2002). "Motor control," in *Encyclopedia of the Human Brain, Vol. 3*, ed V. S. Ramachandran (Amsterdam; Boston MA; Heidelberg; London; New York, NY; Oxford; Paris; San Diego, CA; San Francisco, CA; Singapore; Sydney, NSW; Tokyo: Academic Press), 137–158.

Xia, X.-B., and Mills, S. L. (2004). Gap junctional regulatory mechanisms in the aii amacrine cell of the rabbit retina. *Vis. Neurosci.* 21, 791–805. doi: 10.1017/S0952523804215127

Yamamoto, K., and Vernier, P. (2011). The evolution of dopamine systems in chordates. *Front. Neuroanat.* 5:21. doi: 10.3389/fnana.2011.00021

Yanai, Y., Adamit, N., Israel, Z., Harel, R., and Prut, Y. (2008). Coordinate transformation is first completed downstream of primary motor cortex. *J. Neurosci.* 28, 1728–1732. doi: 10.1523/JNEUROSCI.4662-07.2008

Yoshida, K., Saito, N., Iriki, A., and Isoda, M. (2011). Representation of others' action by neurons in monkey medial frontal cortex. *Curr. Biol.* 21, 249–253. doi: 10.1016/j.cub.2011.01.004

Yoshida, K., Saito, N., Iriki, A., and Isoda, M. (2012). Social error monitoring in macaque frontal cortex. *Nat. Neurosci.* 15, 1307–1312. doi: 10.1038/nn.3180

Yu, X., Ye, Z., Houston, C., Zecharia, A., Ma, Y., Zhang, Z., et al. (2015). Wakefulness is governed by gaba and histamine cotransmission. *Neuron*, 87:164–178. doi: 10.1016/j.neuron.2015.06.003

Zelenin, P. V., Hsu, L. J., Lyalka, V. F., Orlovsky, G. N., and Deliagina, T. G. (2015). Putative spinal interneurons mediating postural limb reflexes provide a basis for postural control in different planes. *Eur. J. Neurosci.* 41, 168–181. doi: 10.1111/ejn.12780

Zhang, Z. W., and Arsenault, D. (2005). Gain modulation by serotonin in pyramidal neurones of the rat prefrontal cortex. *J. Physiol.* 566(Pt 2), 379–394. doi: 10.1113/jphysiol.2005.086066

Zhong, G., Shevtsova, N. A., Rybak, I. A., and Harris-Warrick, R. M. (2012). Neuronal activity in the isolated mouse spinal cord during spontaneous deletions in fictive locomotion: insights into locomotor central pattern generator organization. *J. Physiol.* 590, 4735–4759. doi: 10.1113/jphysiol.2012.240895

Conflict of Interest Statement: The authors declare that the research was conducted in the absence of any commercial or financial relationships that could be construed as a potential conflict of interest.

Manuscript Guidelines

Open access and copyright

https://www.frontiersin.org/about/author-guidelines, accessed on 02.11.2018

Focused neuromodulation of individual motorpools: confirmation of predictions from the efficient control of biomimetic robots

Authors Philipp Stratmann, Hannes Höppner, David Franklin, Patrick van der Smagt, Alin Albu-Schäffer

Journal Undetermined (in preparation)

Number of pages 16 (main article) + 4 (supplementary)

Review Not peer-reviewed, yet

Abstract Serotonin is assumed to alter motoneuron excitability through diffuse neuromodulation that equally affects several muscles, even across limbs. However, the control theory of biomimetic robots predicts that the serotonergic system should disparately amplify the motorpools that supply different joints of the same limb in order to optimally adapt strong periodic movements to changing environments. Here, we confirm that the human central nervous system tunes the excitability of motorpools innervating different joints with the predicted specificity after a periodic motion. Guided by a mechanical device, participants first repeatedly rotated either their right elbow or shoulder joint for thirty seconds. The device then rapidly perturbed either joint to elicit a monosynaptic reflex which quantifies the motoneuron excitability. Enhanced excitability was observable for several hundred milliseconds after movement cessation. These observations assign serotonergic neuromodulation with the time scale necessary to accumulate information across the movement cycle and yet react quickly to changing environments.

Author contributions Initiated and managed the collaboration; researched the literature; co-designed the study hypotheses; designed the step-to-step study protocol; obtained the ethical approval; developed the robotic controller for the manipulandum; co-restructured the manipulandum's mechanics; created the splints required for safe interaction; managed the restructuring of the manipulandum's electronics; recruited the subjects; performed the experiments; developed the statistical models; statistically analyzed the data; derived mathematical proof of topographic precision; composed the manuscript.

Focused neuromodulation of individual motorpools: confirmation of predictions from the efficient control of biomimetic robots.

Philipp Stratmann[1,2,*], Hannes Höppner[2,3], David Franklin[4], Patrick van der Smagt[5], Alin Albu-Schäffer[1,2]

[1] Department of Informatics, Technical University of Munich, 85748 Garching, Germany.
[2] Institute of Robotics and Mechatronics, German Aerospace Center (DLR), Münchener Straße 20, 82234 Weßling, Germany.
[3] Institute for Applied Training Science, Marschnerstraße 29, 04109 Leipzig, Germany.
[4] Department of Sport and Health Sciences, Georg-Brauchle-Ring 60-62/II, 80992 Munich, Germany.
[5] Machine Learning Research Lab, Volkswagen Group, Ungererstraße 69, 80805 Munich, Germany.

Corresponding author:	Philipp Stratmann philipp.stratmann@tum.de Chair for Sensor Based Robotic Systems and Intelligent Assistance Systems Department of Informatics Technical University of Munich DE-85748 Garching
Number of figures:	4
Number of tables:	0
Number of words Abstract:	150/150
Number of words Main Text:	3740/5000
Number of words Methods:	2224/3000

Abstract

Serotonin is assumed to alter motoneuron excitability through diffuse neuromodulation that equally affects several muscles, even across limbs. However, the control theory of biomimetic robots predicts that the serotonergic system should disparately amplify the motorpools that supply different joints of the same limb in order to optimally adapt strong periodic movements to changing environments. Here, we confirm that the human central nervous system tunes the excitability of motorpools innervating different joints with the predicted specificity after a periodic motion. Guided by a mechanical device, participants first repeatedly rotated either their right elbow or shoulder joint for thirty seconds. The device then rapidly perturbed either joint to elicit a monosynaptic reflex which quantifies the motoneuron excitability. Enhanced excitability was observable for several hundred milliseconds after movement cessation. These observations assign serotonergic neuromodulation with the time scale necessary to accumulate information across the movement cycle and yet react quickly to changing environments.

Introduction

During strong and fast periodic motions, humans rely on the passive compliant elements in their muscles and tendons. These elastic elements store energy on impact with the environment and convert it back to kinetic energy for acceleration, enabling fast and large movements with reduced expenditure of metabolic energy [1, 2, 3]. The neuronal control of compliant movements must provide fast feedback, necessitating limited cortical influence [4]. Functionally, the central nervous system (CNS) adapts to mechanical changes, such as the compliance of the environment or the body posture, by changing the task-dependent excitability of the neuronal circuitry [5, 6]. Anatomically, the underlying mechanisms act at least partially at the motor output stage and amplify motoneuron responses to ionotropic input [7, 8] up to several seconds after the motor signals have ceased [9]. Experiments applying serotonin antagonists show that these effects are caused by serotonergic raphe nuclei in the medulla [9]. These raphe nuclei form a motor feedback loop, because they receive proprioceptive input [10, 11, 12] and consequently release serotonin into the spinal cord [13, 14], where it increases motoneuron excitability [15, 16, 17]. How the serotonergic neuromodulation and other mechanisms in the spinal cord accomplish the highly skilled human control of compliant movement is scarcely unraveled [18], because the fast motion induces pronounced movement of the spine within the vertebral column, obstructing invasive recordings [19]. But based on the low precision of monoaminergic neuromodulation in other CNS regions [20], it is generally accepted that also the spinal serotonergic system acts purely by the diffuse modulation of motoneurons innervating several joints [9, 16].

However, recent research on the control of compliant biomimetic robots has challenged this concept based on the dynamics of these mechanical systems. The resulting robotic controller shows a high functional similarity to the raphe nuclei (Figure 1) but predicts that the serotonergic system should disparately scale the gains of motorpools acting on different joints of the same limb [21]. If serotonin predominantly amplifies the actuators of the joints showing particularly large movements, it will reduce, for example, recruitment of a muscle whose actuated joint is mechanically blocked. Experiments on biomimetic robots have also shown that under less extreme changes in the mechanical conditions, which just favors the movement of a particular joint, the energy consumption after joint-specific gain scaling matches the performance of computing-intensive optimal control [22]. The raphe feedback loop is the unique candidate for this functionality, as it forms the only known circuit that accumulates information on the joint movement and accordingly scale the gains of the involved actuators [23].

The present paper experimentally demonstrates that the central nervous system (CNS) indeed applies spinal neuromodulation with the predicted high topographic precision while it controls compliant motion. When subjects perform large movements of an individual joint, the CNS specifically increases the excitability of the motoneurons driving the respective joint. The same motoneurons are significantly less excitable after movement of other joints on the same limb. The excitability change is observable long after the cessation of the motor signals and the movements that triggered it.

These findings demonstrate that during changing mechanical conditions, serotonergic neuromodulation adapts the relative muscle forces across an individual limb. The ionotropic motor circuits that drive the muscles are relieved of this task and may even consist of a simple neuronal synergy circuit which sends a timing signal to all involved actuators simultaneously. As the effect is observable for a few hundred milliseconds after cessation of the triggering stimulus, neuromodulation can adjust the motoneuron gain to the information accumulated across the movement cycle, while being fast enough to react to changing mechanical contexts. Robotic control theory thus leads to the insight that the simple serotonergic motor feedback loop can maximize the amplitude of an ongoing highly dynamic movement and reduce its metabolic demands.

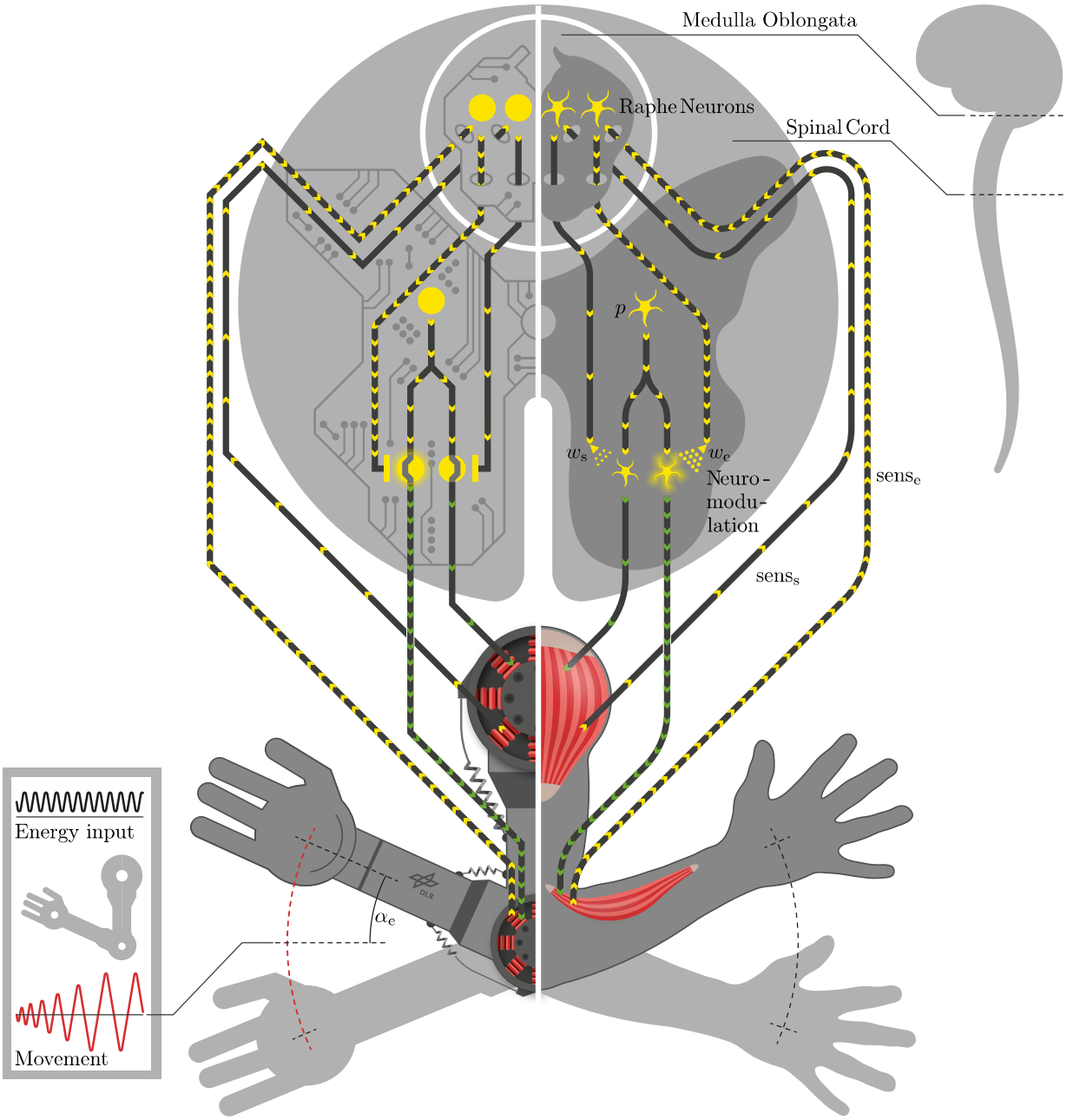

Figure 1: Schematic analogy between the robotic controller (left) that predicts topographically specific neuromodulation and the projections from the raphe nuclei to spinal motoneurons (right). The robotic control diagram illustrates that the controller receives sensory information on the position of the elbow, denoted α_e, and the shoulder, which is mechanically blocked in the exemplary setup illustrated here. The controller identifies the joints with particularly strong sensory signals (paths with high arrow density), and specifically amplifies their motor signals. The amplification decays with a time constant of few 100 ms. The resulting movement is dominated by joints that optimally exploit their elastic elements and was demonstrated to show optimal energy efficiency even in quickly changing environments. The raphe nuclei similarly receive sensory input from the elbow, $sens_e$, and shoulder, $sens_s$. Accordingly, they modulate the motor signals by releasing serotonin that scales the gains w_e and w_s of motorpools driving the elbow and shoulder, respectively. According to the present experiments, serotonin specifically increases the gain of a motorpool during movement of its innervated joint. This effect drastically simplifies the motor control, because all actuators can be driven by an ionotropic signal from the same synergy circuit p. Such a synergy signal may originate from a single pool of reflex neurons, M1 neurons, or a central pattern generator. Figure by Tilo Wüsthoff.

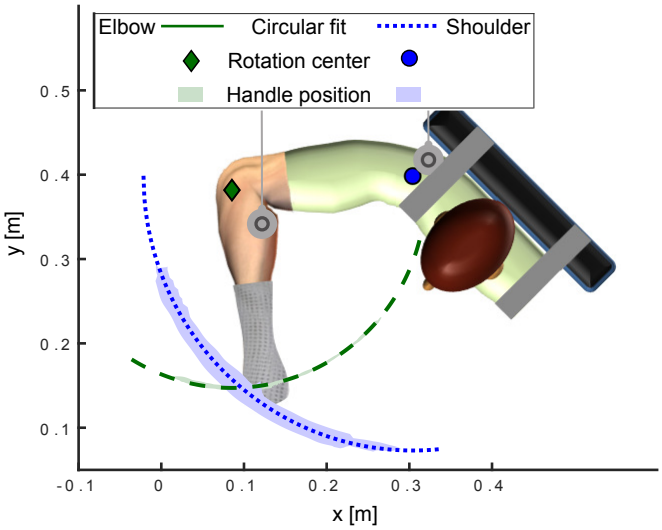

Figure 2: Experimental setup. During the experiments, the subjects rotated either their elbow or shoulder joint in a horizontal plane, as guided by a manipulandum. The wrist was immobilized throughout the trials by a stiff splint. After stopping the rotation at the intersection point of the elbow and shoulder rotations, the arm was rapidly perturbed to excite a monosynaptic stretch reflex in either the brachioradialis or posterior deltoid. The reflex response was measured by EMG electrodes (gray circles). To determine software-based constraints that the manipulandum applies for the guidance of motion, the trajectories of the pure elbow and shoulder rotation were determined prior to the main experiments. For this purpose, the shoulder and elbow were consecutively immobilized by a second splint and the subject rotated the free joint back and forth for 300 s. The resulting hand position was continuously recorded and fitted by a circle to determine the center and radius of rotation of the target trajectory. The schematic shows the exemplary recorded hand positions of one subject.

Results

The predicted topography of the raphe motor feedback loop was experimentally tested on human subjects. The functional hypothesis predicts that the excitability of motorpools is higher following rotation of their innervated joint than after rotations of other joints in the same limb [21, 23]. In each trial, the subject first repeated strong and fast rotations of either the right elbow or right shoulder joint for 30 s. The rotations were guided by a manipulandum, i.e., a machine that applies translational forces to the arm based on its state (Figure 2). After 30 s, the manipulandum stopped the movement in a predefined default arm posture, and the motoneuron excitability was measured in either the brachioradialis or posterior deltoid muscles. Specifically, after the electromyography (EMG) signal of the respective muscle had decayed to its resting value, the motoneuron excitability of either muscle was quantified by its EMG response to a monosynaptic stretch reflex. The reflex was elicited by mechanically perturbing the target joint. According to the study hypothesis, rotating a joint should enhance the monosynaptic reflex response of its associated muscle. Thus, the monosynaptic reflex response of the brachioradialis should be enhanced following elbow rotation, whereas the deltoid should show a higher reflex response following shoulder rotation.

Topographically precise gain scaling

As predicted, the brachioradialis and the deltoid showed a significantly enhanced monosynaptic reflex response after rotation of their respective actuated joint. Averaging over all subjects, the reflex response of the brachioradialis was higher after elbow than after shoulder rotation at $p = 1.0 \times 10^{-4}$ (Figure 3a; linear mixed-effects models and two-tailed t-test: $df = 379$, $t = 3.8$). Conversely, the reflex response of the deltoid was higher after shoulder than after elbow rotation at $p = 1.7 \times 10^{-4}$ (Figure 3b; $df = 338$, $t = 3.9$). When fitting the linear mixed-effect models to the reflex recordings, the residuals were normally distributed (panels c and d of Figure 3). The predicted reflex behavior was also observed in individual subjects, as illustrated for an exemplary subject in panel e and f of Figure 3. The individual reflexes were elicited by the manipulandum, which rapidly moved the subject's wrist. The response EMG occurred after a delay, which consisted of a mechanical delay until accelerometers detected the stretch onset at the perturbed joint, and of the neuronal transduction time (panel g and h of Figure 3). For the statistical analysis,

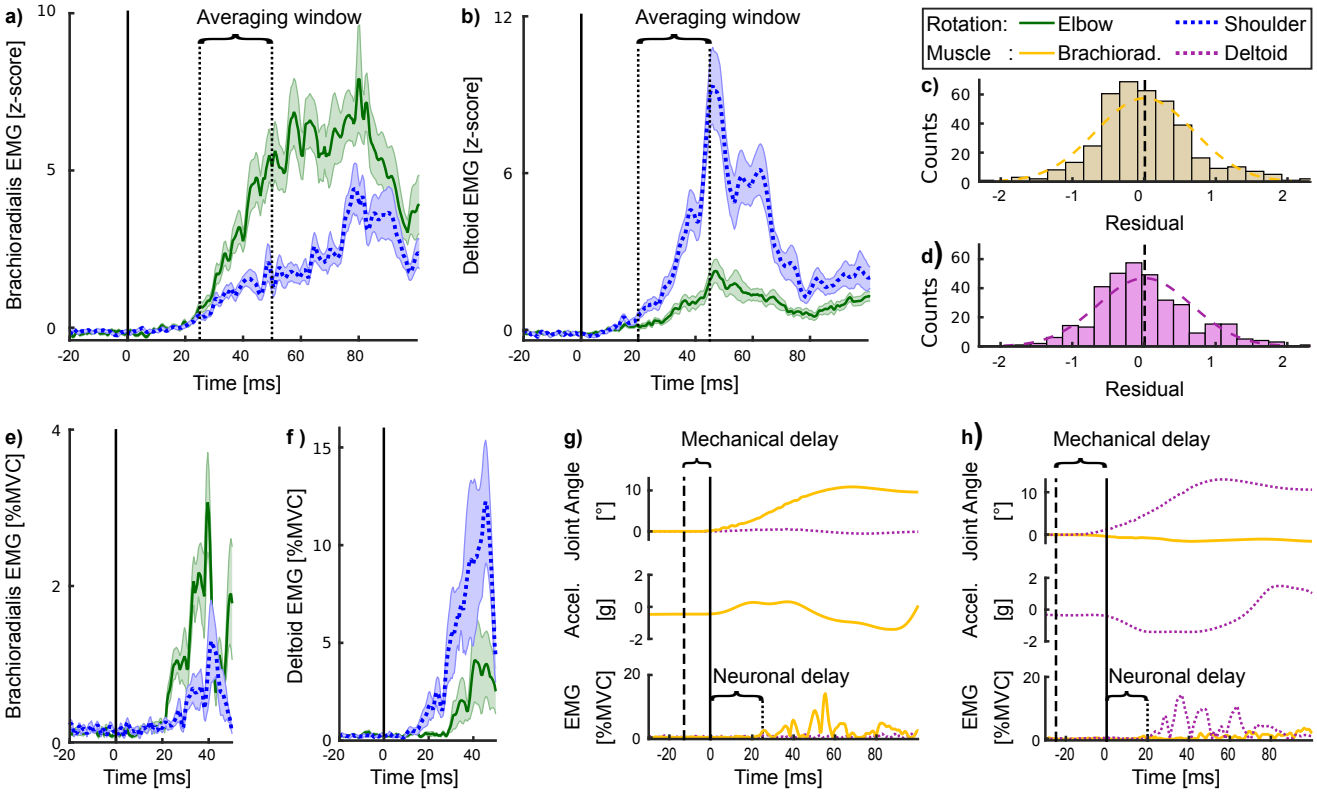

Figure 3: Monosynaptic reflex responses after movement of the shoulder or elbow joint. **a)** Averaged over all subjects, the right brachioradialis showed a higher monosynaptic EMG response to stretching after rotating the right elbow than after rotating the right shoulder. **b)** The opposite effect was observed for the right posterior deltoid. Vertical solid lines indicate the onset of the joint perturbation. The shaded areas indicate the standard errors in the EMG signals at each time step. Statistical significance was determined by fitting a linear mixed-effects model to the reflex response, averaged over the indicated window, of the respective muscle. As required for linear mixed-effects models, the residuals for both **c)** the brachioradialis and **d)** the posterior deltoid were well fitted by a normal distribution (dashed curves). Reflex responses of **e)** the right brachioradialis and **f)** the posterior deltoid of an individual subject resembled the subject-averaged responses. Individual reflex responses in **g)** the brachioradialis or **h)** the deltoid were elicited by mechanically perturbing the subject's hand along the elbow or shoulder joint, respectively. The angle of the other joint remained comparatively constant. After a mechanical delay, the perturbation accelerated the lower arm for the brachioradialis or the upper arm for the deltoid, as measured by accelerometers that recorded the horizontal movement of the respective arm segment. Following a neuronal transduction delay, the EMG electrodes recorded the monosynaptic reflex response in the perturbed muscle, while the other muscle remained silent.

the EMG responses were averaged over the time window from 25 ms to 50 ms and from 20 ms to 45 ms after onset of the joint stretch for the brachioradialis and the deltoid, respectively. These time windows are known to start after the neuronal transduction delays and end before onset of the polysynaptic reflex responses [24, 25].

Verifying the assumptions on the joint movement

The study design imposes two assumptions on the rotatory movement that triggered the gain scaling: First, the two movement conditions were assumed to be clearly divisible into rotation of the elbow and rotation of the shoulder joint, respectively. Second, the subjects were assumed to perform strong and fast movements, which are known to be shaped by compliant elements in the body. As the original robotic controller was designed to minimize the high metabolic demands of these specific movements, its neuroscientific predictions must be tested in such highly dynamic movement scenarios. The above assumptions were verified by recording rotatory movements of all subjects.

In agreement with the first assumption, the differentiation between elbow and shoulder rotation is evident from the angular trajectory of the elbow and the shoulder joint, measured by goniometers, and from the EMG of the bradioradialis and posterior deltoid. For one exemplary subject, these measures are presented in panel a and b of

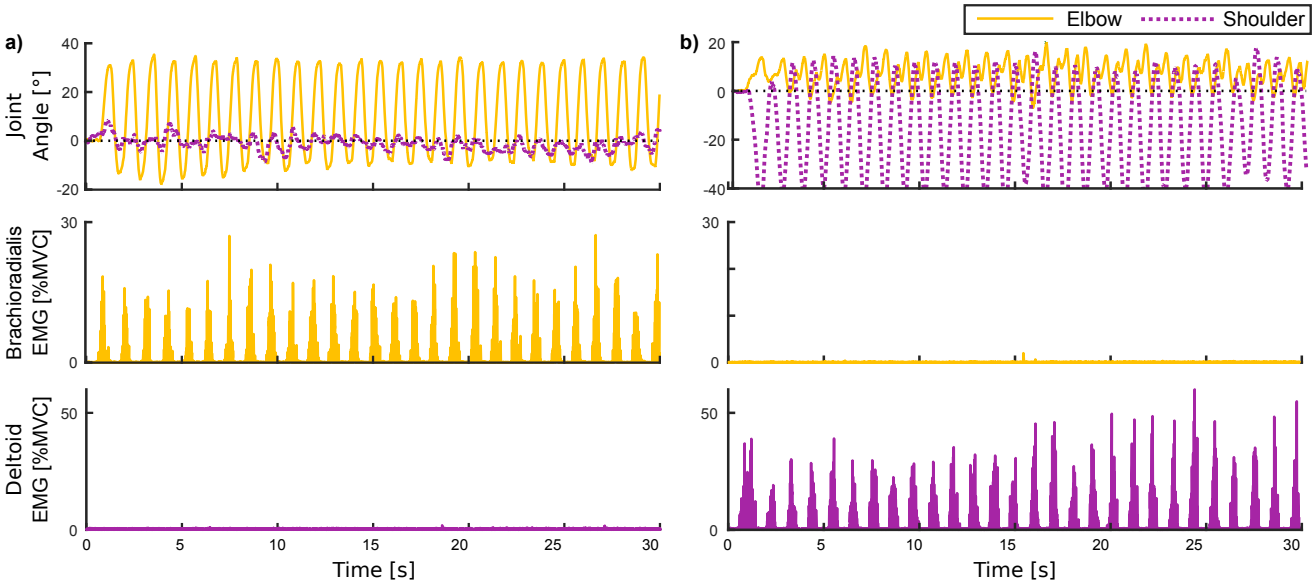

Figure 4: Quality of manipulandum-guided movement for one exemplary subject. Depending on the trial, the subject was guided to perform a rotation involving either the **a)** elbow or **b)** shoulder. The angles of the joints, as measured by goniometers, confirm that the two conditions could be clearly differentiated. The difference between the two conditions is also evident from the EMG of the brachioradialis, which actuates the elbow, and the posterior deltoid, which actuates the shoulder.

Figure 4 for elbow and shoulder rotation, respectively. When the subjects were guided to perform elbow rotations, the peak angles were on average 7.0 ± 2.8 (s.d.) times higher in the elbow than in the shoulder trajectory. Conversely, when the subjects were guided to perform shoulder rotations, the peak angles were on average 3.5 ± 0.9 (s.d.) times higher in the shoulder than in the elbow trajectory. The EMG traces of the observed muscles further support that subjects performed clean movements of individual joints. For each subject, both the peak and the average brachioradialis EMG were higher during elbow than during shoulder movement and vice versa for the deltoid.

In agreement with the second assumption, all subjects performed strong and fast movements. In each movement cycle, the peak forces exciting the elbow and shoulder rotation were $(19 \pm 2)\,\mathrm{N}$ and $(22 \pm 6)\,\mathrm{N}$ (s.d.), respectively. This resulted in peak velocities of $(74 \pm 8)\,\mathrm{cm\,s^{-1}}$ and $(72 \pm 9)\,\mathrm{cm\,s^{-1}}$ (s.d.), respectively.

Excluding diffuse neuromodulation as cause of observed gain scaling

According to the study hypothesis, the different motoneuron excitabilities of the brachioradialis and deltoid arise from topographically precise neuromodulation. The differences may, in principle, also arise from the time delay between each rotation and the subsequent excitability measurement. Over the delay interval, the effect underlying increased motoneuron excitability potentially decayed. The delay, which accounted for the time that motoneuron activity required to return to rest, varied from trial to trial. In this alternative scenario, gain scaling is caused by purely diffuse neuromodulation, and lower observed motoneuron excitability was caused by a higher delay before the excitability measurement. However, under conditions of higher motoneuron excitability, the delay was lengthened. Averaged over all trials of all subjects, the brachioradialis perturbations were delayed by $(0.35 \pm 0.68)\,\mathrm{s}$ (s.d.) after an elbow rotation, longer than the delay of $(0.23 \pm 0.69)\,\mathrm{s}$ after a shoulder rotation. This relationship was statistically significant at $p = 2.3 \times 10^{-7}$ across all subjects (linear mixed-effects model and two-tailed t-test; $df = 379$, $t = 5.3$) and was observed in 15 out of 16 individual subjects. Meanwhile, the perturbations of the deltoid were delayed by $(0.33 \pm 0.26)\,\mathrm{s}$ (s.d.) after a shoulder rotation and by $(0.22 \pm 0.69)\,\mathrm{s}$ after an elbow rotation. This relationship was also statistically significant at $p = 3.9 \times 10^{-6}$ across all subjects (linear mixed-effects model and two-tailed t-test; $df = 338$, $t = 4.7$) and was observed in 15 out of 16 subjects. Thus, the observed differences in motoneuron excitability cannot be explained by the different delays between the rotations and the excitability measurements.

During the trials, the proprioceptive input that triggered the raphe nuclei and the resulting motoneuron gains were quantified by indirect recording methods. Indirect measurements provide only relative statements on these two parameters and prevent determination of their precise units or amplitudes. Furthermore, the proprioceptive inputs to the raphe neurons originating from the elbow and shoulder muscles cannot be compared. Despite these

limitations, the following analysis demonstrates that diffuse neuromodulation cannot explain the different motoneuron excitabilities after elbow and shoulder motions. The only reasonable explanation is topographical precision in the serotonergic system. Here, diffuse neuromodulation means that the raphe nuclei behave as a single pool of neurons, where all neurons in the pool receive the same combination of proprioceptive input characterizing the movement of individual joints and form the same projection pattern to the motorpools innervating the brachioradialis and the deltoid.

This analysis requires two assumptions that are supported by previous studies. First, during the present experiments, the sensory input sens_e of the elbow muscles to the raphe nuclei was higher during an elbow rotation, denoted $\hat{\alpha}_e$, than during shoulder rotation, denoted $\hat{\alpha}_s$ (the major symbols are also explained in Figure 1). The opposite was true for the shoulder muscles, whose sensory input is denoted by sens_s [26, 27, 28]. That means,

$$\text{sens}_\text{e}(\hat{\alpha}_\text{e}) > \text{sens}_\text{e}(\hat{\alpha}_\text{s}) \ , \tag{1}$$
$$\text{sens}_\text{s}(\hat{\alpha}_\text{s}) > \text{sens}_\text{s}(\hat{\alpha}_\text{e}) \ . \tag{2}$$

Second, the serotonin released by the raphe nuclei onto motoneurons monotonically increases with increasing proprioceptive input [10, 29]. The release multiplicatively scales the gain of motoneurons driving elbow flexors, w_e, and shoulder extensors, w_s, from their initial gain $w_{\text{e}0}$ and $w_{\text{s}0}$, respectively [16]. This process can be modeled as

$$w_\text{e} = w_{\text{e}0} \cdot (m_{\text{ee}}\text{sens}_\text{e} + m_{\text{se}}\text{sens}_\text{s}) \ , \tag{3}$$
$$w_\text{s} = w_{\text{s}0} \cdot (m_{\text{es}}\text{sens}_\text{e} + m_{\text{ss}}\text{sens}_\text{s}) \ . \tag{4}$$

Here, the constant of proportionality m_{ij} quantifies how the raphe nuclei affect the gain of motoneuron pool j when they receive proprioceptive input sens_i. Both i and j can refer to the elbow, e, or the shoulder, s. The higher-order interaction terms of sens_e and sens_s are likely to be negligible, because the raphe feedback loop receives proprioceptive inputs by a mono- or at most a disynaptic pathway [10] and monosynaptically releases serotonin into the motoneuron pools [30]. Importantly, the two stated assumptions are independent of the precise amplitude of the sensory input and of the ratio of the input from different muscles.

As illustrated in Figure 1, the raphe neurons are predicted to provide topographically precise neuromodulation that predominantly amplifies the actuators of the joints delivering a large proprioceptive input. Topographic precision means that at least one of the following holds:

$$m_{\text{ee}} > m_{\text{se}} \ , \tag{5}$$
$$m_{\text{ss}} > m_{\text{es}} \ . \tag{6}$$

In contrast, the current literature suggests that the raphe nuclei act on the motoneurons by diffuse neuromodulation alone, implying that

$$m_{\text{ee}} = m_{\text{se}} \ , \tag{7}$$
$$m_{\text{ss}} = m_{\text{es}} \ . \tag{8}$$

To decide between these two options, recall that the measured gain of the elbow muscle was significantly higher after an elbow movement than after a shoulder movement, and vice versa for the shoulder muscle. That is,

$$w_\text{e}(\hat{\alpha}_\text{e}) > w_\text{e}(\hat{\alpha}_\text{s}) \ , \tag{9}$$
$$w_\text{s}(\hat{\alpha}_\text{s}) > w_\text{s}(\hat{\alpha}_\text{e}) \ . \tag{10}$$

Equations (3) to (10) can be rearranged to show that

$$\frac{1}{\gamma} m_{\text{ee}} > m_{\text{se}} \ , \tag{11}$$
$$\gamma m_{\text{ss}} \ > m_{\text{es}} \ . \tag{12}$$

The factor γ, obtained as

$$\gamma := \frac{\text{sens}_\text{s}(\hat{\alpha}_\text{s}) - \text{sens}_\text{s}(\hat{\alpha}_\text{e})}{\text{sens}_\text{e}(\hat{\alpha}_\text{e}) - \text{sens}_\text{e}(\hat{\alpha}_\text{s})} \ , \tag{13}$$

must be positive according to equations (1) and (2). Depending on how the proprioceptive input is quantified, equations (11) and (12) distinguish the following three cases:

$$0 < \gamma < 1 \implies m_{\mathrm{ss}} > m_{\mathrm{es}} \ , \tag{14}$$

$$\gamma = 1 \implies m_{\mathrm{ee}} > m_{\mathrm{se}} \wedge m_{\mathrm{s}} > m_{\mathrm{es}} \ , \tag{15}$$

$$\gamma > 1 \implies m_{\mathrm{ee}} > m_{\mathrm{se}} \ . \tag{16}$$

When $\gamma > 1$, it is not logically necessary that also $m_{\mathrm{ss}} > m_{\mathrm{es}}$, but possible depending on the unknown absolute amplitude of the proprioceptive input. The same reasoning applies to $\gamma < 1$ and the statement $m_{\mathrm{ee}} > m_{\mathrm{se}}$. In conclusion, equations (14) to (16) prove that, regardless of how the proprioceptive input is quantified, the serotonergic feedback loop affects the motorpools not by a diffuse mechanism, but by topographically precise neuromodulation.

Discussion

The present study argues that serotonin amplifies the gain of motorpools with high topographical precision after persistent motion of individual joints. This finding contradicts the widely held assumption that the serotonergic system acts purely by diffuse neuromodulation in the spinal cord [9, 16]. More specifically, the motoneuron excitability was increased for motorpools that innervate a moving joint, while motorpools of resting joints showed a smaller excitability. To verify this, human subjects performed strong and fast periodic rotations primarily moving either their elbow or their shoulder joint. After repeated rotations, a monosynaptic stretch reflex was elicited and its EMG response quantified the motoneuron excitability. Rotation conditions that caused a higher motoneuron excitability were thereby found to be associated with longer time delays between the end of the rotation and the excitability measurements. As this delay gave the underlying effect time to decay, it can be expected that the observed difference in motoneuron excitability was even more pronounced directly after a rotation than observed here. The increased motoneuron excitability was observed several hundred milliseconds after cessation of the rotatory movement and the corresponding muscle activity, meaning that the excitability change outlasted the action that triggered it.

According to wide-ranging evidence, the motoneuron gain is scaled by the raphe nucleus obscurus and pallidus, as they receive proprioceptive input [10, 11, 12] and accordingly release serotonin into the spinal cord [13, 14]. This motor feedback loop is responsible for approximately 90 % of the serotonin in this region of the central nervous system [13]. In a recent review, Stratmann et al. [23] demonstrated that neither ionotropic nor non-serotonergic metabotropic circuitry provides an alternative explanation for the observed spinal excitability and its time scale. The protocol of the present study suppressed non-serotonergic effects that are known to change motoneuron gain, namely, different joint positions [31], pre-activation of motoneurons [32], and synaptic plasticity [33]. For this purpose, the perturbation parameters, such as the initial position as well as the stretch duration and distance, were kept constant. Additionally, the muscles were at rest prior to perturbation, and the trials under the different conditions were equally distributed over time. Wei et al. [9] reported that the reflex amplification observed several hundred milliseconds after strong proprioceptive input is elevated by serotonin agonists and blocked by its antagonists. Thus, it must be governed by serotonergic neuromodulation.

The present study was designed to non-invasively prove the topographic precision of gain scaling. It overcomes the limitations inherent in non-invasive recordings, namely, that the joint movement and muscle EMG is only an indirect measure of the proprioceptive information during rotatory movements, and that the EMG response to a stretch reflex is an indirect measure of the motorpool gain. These measures yielded only relative values for individual joints or muscles. In particular, the movement and the EMG of the muscles were substantially more pronounced during rotation than during quiescence of the associated muscle. As both parameters are known to monotonically increase the proprioceptive signals [26, 27, 28], it can be deduced that the raphe nuclei received more input from elbow proprioceptors during elbow rotation than during shoulder movement, and vice versa for the shoulder. The resulting excitability of the brachioradialis was higher after elbow movement than after shoulder movement, and vice versa for the deltoid. Mathematically, these findings were sufficient to prove the topographic precision of both the proprioceptive input to the raphe neurons and their projections to motorpools.

Topographically precise signal processing is compatible with previous anatomical studies on the individual steps along the serotonergic motor feedback loop. Proprioceptive signals are forwarded to the raphe pallidus and obscurus with a delay of 20 ms, implying a monosynaptic or a strong disynaptic transduction [10]. In turn, the nuclei project exclusively to the spinal cord [34, 35], and release serotonin through well-defined synaptic connections [15]. The collateralization degree of these projections [36] are comparable to that of pyramidal neurons, which induce joint-specific effects [37].

Although the present study focuses on arm movement, topographically precise neuromodulation is also expected during leg movement, because the raphe feedback loop acts similarly across limbs and conditions. Scaling of motorpool gains has been observed in the upper limbs during movement [7] and static force exertion [9, 38], and in the legs

during jumping [8], walking, and running [39]. In the lobster, it is even known that serotonin disparately increases the firing of different muscles in the same leg [40]. In the phylogeny, the serotonergic motor feedback loop is in general well-conserved from invertebrates to mammals [41], and also its topographic precision is still observable in the human arm according to the present results. Thus, it is likely that the topographic precision of the serotonergic system is also conserved in mammalian locomotion control.

The evolutionary advantage of topographically precise neuromodulation is revealed in the robotic control algorithm that predicted it. Owing to its unique properties, precise serotonergic neuromodulation is ideally suited to simplify the control of fast periodic movement and to minimize its energy consumption. This inference is supported by our previous analytic derivations and computational simulations based on previous serotonin dynamics models [42]. In functional resemblance to the robotic controller [43], the topographically focused serotonergic neuromodulation amplifies the motor signals along the optimal, local, linear approximation of the resonance mode of the mechanical system in a least-squared sense [21]. Experiments in biomimetic robots demonstrated what this phenomenon implies: It exploits the compliant properties of a locomotor system. Under mechanical conditions that are typical for biological motions, such as nonlinear dynamics, physical noise, and damping [44], the energy efficiency of the resulting motion matches the performance of computationally intense optimal controllers. To achieve the high motor performance, a common motor signal was sufficient to drive all actuators involved in the movement simultaneously. Such a signal can be created by a simple neuronal synergy, such as a single pool of excitatory reflex neurons, a central pattern generator, or a pool of M1 neurons [21]. The serotonergic feedback loop parallels this ionotropic synergy circuitry and can adjust the ionotropic signals by non-local learning, i.e., learning based on information that is not processed by the premotor interneuron or the motorneuron. The raphe nuclei can thus adapt the ionotropic control, for example, as a runner steps from a stiff to a compliant ground. To counteract the decreasing ground stiffness, the runner increases his leg stiffness and thereby straightens his knee [45]. Still, he exerts the same ground contact force to maintain his energy-efficient stride frequency [45]. For this purpose, the CNS scales up the activation of ankle muscles relative to that of the knee muscles [46]. Serotonergic neuromodulation is the ideal candidate for this task, because it acts sufficiently slow to adjust the motoneuron gain to information accumulated across the movement cycle, while it decays quickly enough to react to the changing tracks [23, 43]. .

In addition to the neuroscientific findings, the present study reveals a new methodology for neuroscience to generate promising research hypotheses. As exemplified in Figure 1, neuroscientists can apply the large set of algorithms developed for the control of biomimetic robots as blueprints to identify functionally analogous neuronal circuitry. This type of knowledge transfer fundamentally differs from the previous contributions of robotics to neuroscience. According to recent reviews [47, 48], neuroscientists have used robotics analysis tools only for analyzing biological motor control and for replicating their obtained principles on biomimetic robotic systems in order to expose incomplete knowledge. The newly proposed methodology fully reverses the existing bionic knowledge transfer, which seeks engineering solutions from biological knowledge. Instead, the proposed *enginic* knowledge transfer seeks to understand biological motor circuits from engineering solutions.

Enginics is a new avenue that is promising because of a recent fundamental change in the field of robotics. Although many of the first robots already mimicked animals, the various mechanical features underlying the remarkable biological movement performance, such as passive compliance, are only now being mimicked by robotics engineers [49, 50]. This trend has markedly aligned robotic control theory with neuroscience. Conventionally, robotic control enforces the desired dynamics on a given mechanical system by mechanisms such as feedback linearization [51], virtual model control [52], or artificial damping [53]. Modern roboticists are increasingly designing control algorithms that exploit the beneficial natural dynamics of novel biomimetic robots. Thereby, they can produce movement that is stable [54] and minimizes the energy consumption in quickly changing environments [44]. These design principles have such substantial benefits that neuronal structures in the CNS have likely evolved an analogous functionality [55, 56]. Roboticists typically characterize the function of their algorithms in detail, but without considering their biological plausibility. Therefore, the source of algorithms suitable for future enginic projects is large. Especially, these algorithms can help to elucidate the neuronal control of highly dynamic movements, since traditional invasive analysis methods are obstructed by the pronounced movement of the spinal cord in vivo [19].

In summary, the results of this study demonstrate that the serotonergic innervation of spinal circuitry provides not merely the diffuse modulation of ionotropic circuitry, as is widely assumed. Rather, it forms a computationally substantial network within the network of the ionotropic motor circuitry. By virtue of its topographic and temporal precision, serotonin sustains metabolically efficient motions in changing environments. Future work should test whether the serotonergic circuitry is similarly involved in higher brain functions requiring topographic precision, which may mistakenly be attributed to ionotropic effects [23]. In addition, the present results demonstrate that robotic control algorithms have become an efficient source of models that identify the unknown characteristics of neuronal motor circuitry and challenge misconceptions about them. These algorithms can diminish the common problem that neuroscience is data rich and theory poor [57].

Methods

Subjects

Sixteen healthy, right-handed subjects (aged 17–30 years, mean 26 ± 4 (s.d.); 12 male) participated in the experiments. All subjects were naive to the purpose of the study and provided informed consent prior to participating. The study was approved by the Ethics Committee of the Medical Faculty of the Technical University of Munich.

Experimental apparatus

Throughout the experiments, subjects wore a stiff splint on their right arm, which prevented wrist movement. The subjects' hands were firmly attached to the endpoint of a manipulandum by a magnetic clutch with their palms facing downwards. The safety clutch allowed detachment when a predefined maximal force was exceeded. Subjects were seated in an adjustable chair facing the manipulandum, with their trunk tightly restrained by seat belts. Their lower and upper arm were supported against gravity by the manipulandum handle and an arm rest that hung freely from the ceiling, respectively. The manipulandum is a custom-built apparatus that controls the arm movement in a horizontal plane. Being particularly stiff, fast, and strong, it delivers a high force and precise movement [58]. The endpoint position was calculated from the positions of the motors (*Linmot PS01-48x360F-C*, *NTI AG*, Switzerland) and the endpoint forces were measured by a six-axis force-torque sensor (*mini45*, *ATI Industrial Automation*, USA). As the position sensors and the force-torque sensor have a very small relative delay, a force exerted on the end effector causes a change in the position readings less than 1 ms after being detected by the force–torque sensor. To record the surface EMG, wireless electrodes (*Trigno Avanti*, *Delsys*, USA) were attached to the skin above the brachioradialis and posterior deltoid muscle according to the recommendations by the *SENIAM* project [59]. The electrode attached to the brachioradialis, and a further electrode attached to the upper arm, also recorded their horizontal acceleration and thus the acceleration of the lower and upper arm, respectively. The movement of the elbow and shoulder joints were recorded by wireless goniometers (*SG110* and *SG150B*, *Biometrics*, USA). The intrinsic recording delay was 48 ms in the EMG electrodes and 96 ms in the accelerometers and goniometers. All delays were considered in the following analysis. All signals were sampled at 2 kHz. A computer screen was placed in front of the subjects. It signaled the beginning of an individual trial and provided visual feedback on the movement.

Experimental design

Each subject underwent a set of preliminary recordings and the main experiment, lasting approximately 4.5 h in total.

The experiment was subdivided into a sequence of individual trials. In each trial, the subject first performed a rotatory movement of either the elbow or shoulder joint, which was predicted to increase predominantly the excitability of motoneurons driving either elbow or shoulder muscles, respectively. After movement cessation, the motoneuron excitability was measured using a perturbation for a muscle driving the target joint. Between trials, a delay of 30 s allowed restoration of motoneuron excitability.

During the rotation tasks, the manipulandum exerted forces that guaranteed the desired rotation, as verified in preliminary recordings described below. From the subjects' point of view, the controlled mechanical system resembled a point mass acted on by two springs: an almost rigid spring which pushed the handle back to its rotatory trajectory in case of deviations, and a slack spring which pushed the handle back to its predefined equilibrium position along the rotatory trajectory. The underlying controller of the manipulandum is detailed in the *Supplementary Methods*. Based on theoretical work by De Luca et al. [60], the controller was developed to ensure a well-defined environment for the subjects. In particular, it prevented interference from the mechanical manipulandum design, as verified in Supplementary Figure 1.

The subjects were requested to produce an oscillatory rotation around the equilibrium position. Visual feedback stipulated an amplitude of $0.105\,\mathrm{rad\,m^{-1}}/r_0$ and $0.15\,\mathrm{rad\,m^{-1}}/r_0$ for elbow and shoulder rotation, respectively, where r_0 is the circle radius. After 30 s, the controller smoothly stopped the handle at the equilibrium point by exponentially increasing the virtual damping.

Once the rotation had stopped, the motoneuron excitability of the brachioradialis or posterior deltoid muscle, which drive elbow flexion or shoulder extension, respectively, was measured. The controller waited until the EMG of the respective muscle had remained below its resting value, measured prior to the rotation, for 100 ms. Once this condition was fulfilled, the manipulandum either extended the elbow or horizontally flexed the shoulder by 10° within 60 ms. This perturbation excited a monosynaptic stretch reflex in the respective muscle. The reflex EMG was measured and quantified the motoneuron excitability as described below.

Trials were divided into four groups, defined by four combinations of rotation direction and subsequent perturbation direction. Every subject completed a randomized sequence of 120 trials, consisting of 15 trials of each trial group and 50 % catch trials without perturbations. Across subjects, trials were distributed to exclude training- or time-dependent effects on the measured motoneuron excitability. Accordingly, the sequence of trials was constrained such that at every of the 120 steps, exactly two subjects completed a trial from each of the four groups. Therefore, at each step, eight subjects performed a trial while another eight subjects performed a catch trial. This design determined the chosen number of 16 subjects. Apart from this constraint, trials from the four groups were equally distributed along the sequence for each subject. Subjects received no prior information about the perturbation direction or the occurrence of catch trials.

Prior to the experiment, each subject underwent four sets of preliminary recordings. First, the subject's arm was characterized to allow manipulandum guidance of the pure elbow and shoulder rotations. Starting from a predetermined zero position, the subject was requested to rotate either the elbow or shoulder joint for 30 s while the other joint was fixed by a mechanical splint. This task was completed 10 times. The handle position was recorded and circles were fitted [61] to the trials as shown in Figure 2. The crossing position of the circles around the elbow and the shoulder was defined as both the equilibrium position of the rotation and the initial position of the perturbations. The rotation trajectory of both the shoulder and elbow movements could be fully defined by the equilibrium position, the radii of the lower and upper arm, and the position of the shoulder-joint axis. As the trunk of the subject was fixed, the center of the shoulder joint was assumed constant. For each subject, the standard error in the center position of the shoulder joint was below 5 mm, and the standard error in the lower and upper arm radii were less than 4 mm and 6 mm, respectively.

Second, the rotatory movement was characterized, i.e., the quality of the controller and the arm characterization. The subjects performed two trials with no perturbation: a rotatory movement of the elbow and a rotatory movement of the shoulder. These measurements were used to test whether subjects performed joint-specific rotations and to evaluate their occurring peak forces and velocities.

Third, subjects were habituated to perturbations. For this purpose, the manipulandum alternately perturbed the brachioradialis and the deltoid 15 times each. Between two successive perturbations, the manipulandum moved the arm back to the equilibrium position and waited for a random duration between 5 s and 10 s.

Fourth, the EMG signals of the brachioradialis and posterior deltoid were measured at maximum voluntary contraction (MVC). This measurement was repeated after the main experiment to ensure that the electrodes had remained properly attached.

Analysis of EMG data

All data were analyzed in *Matlab 2017*. The EMG electrodes outputted signals with a bandwidth of 20 Hz–450 Hz. The signals were demeaned, rectified, and normalized to the MVC measurement. The EMG data were further processed first to determine the monosynaptic reflex response to mechanical perturbations, and second to ensure that the EMG of the observed muscle was at rest prior to this response.

The monosynaptic reflex responses of the brachioradialis and deltoid muscles were quantified based on their EMG signals after perturbing the corresponding joint. The reflex response occurred after a time delay composed of the mechanical delay between the movement of the manipulandum handle and the movement of the joint, and of the neuronal transduction delay, which is illustrated in Figure 3g and 3h for two exemplary reflex responses. The neuronal transduction delays of the brachioradialis and deltoid were set to 25 ms and 20 ms [24, 25], respectively. The mechanical delays were determined from the accelerometers attached to the lower and upper arm for the elbow and shoulder perturbations, respectively. The onset of a joint perturbation was detected when the accelerometer readings had exceeded their resting value by three standard deviations. To account for interfering oscillations of the accelerometers after movement of the corresponding joint, the mechanical delays for each subject were averaged over all trials where perturbation and rotation direction differed. After the reflex delay, the EMG response was averaged over a time window of 25 ms and normalized by subtracting its resting EMG as averaged over the 25 ms preceding the perturbation. As EMG signals were restricted to positive values, the reflex response was defined as the natural logarithm of the EMG response in the statistical analysis.

Prior to perturbations, muscles were ensured to be delaying the perturbations until the EMG signal of the considered muscle had decayed to its resting value and remained there for 100 ms, as mentioned before. If the muscle remained active within 3 s after movement cessation, the perturbation was omitted and the respective trial was repeated. Any information that distinguished trials with omitted perturbation from the catch trials was withheld from the subjects. The resting detection was based on 3 recordings of the mean and maximum unprocessed EMG signals, termed $\mathrm{EMG}_{\mathrm{mean}}$ and $\mathrm{EMG}_{\mathrm{max}}$, respectively, over a 1 s period before an individual trial. The recording with the smallest $\mathrm{EMG}_{\mathrm{max}}$ was chosen to prevent any measurement artifacts resulting from brief unintended muscle

contractions. The EMG recordings within the range $\mathrm{EMG_{max}} - \mathrm{EMG_{mean}}$ around $\mathrm{EMG_{mean}}$ were defined as the resting EMG. In addition to the actions taken during measurements, trials were neglected in the data analysis if the EMG exceeded its resting value by more than 20 % over a time period which could not be checked during the trials. This period started 48 ms prior to a perturbation, corresponding to the delay of the EMG electrodes. It ended 10 ms after the perturbation, since this is the minimal possible neuronal transduction delay of monosynaptic stretch reflexes [62].

A further analysis step ensured that any observed changes in the motoneuron gain could not arise from a muscle activation remaining after a movement. For this purpose, the pre-reflex activity was matched between the different rotation conditions for each subject. Accordingly, the EMG signal of the brachioradialis was averaged within the first 10 ms after the onset of elbow perturbations, as determined by the accelerometer. Elbow-rotation trials were sorted from highest to lowest remaining muscle activation and iteratively excluded until the average muscle activation equaled at most the average muscle activation of shoulder-rotation trials. The converse procedure was applied to the recordings of deltoid perturbations.

Panels a and b of Figure 3 illustrate the reflex responses of the brachioradialis and deltoid, respectively, after both rotation types. The responses were averaged over all trials of all subjects. To make the EMG responses comparable across subjects for these plots, the muscular responses of the individual subjects were first normalized to a z-score. The z-scores for the brachioradialis and deltoid muscles were calculated from the EMG recordings over the first 50 ms and 45 ms after perturbation onset, respectively. The different durations account for the different neuronal transduction delays between the two muscles. The normalized values were averaged across all subjects during each 0.5 ms time step.

Statistical analysis

The present study examined whether the increased gain of the motoneurons after limb movement is topographically precise. The gain increase of motoneurons was predicted to be higher after the movement of a joint actuated by muscles innervated by the motorneurons than after movement of other joints. For the brachioradialis, this hypothesis was tested on $n_\mathrm{e} = 172$ trials with prior elbow rotation and $n_\mathrm{s} = 209$ trials with prior shoulder rotation which had passed the exclusion criteria stated in the previous section. For the deltoid, the respective number of trials amounted to $n_\mathrm{e} = 203$ and $n_\mathrm{s} = 137$. The hypothesis was tested by fitting a linear mixed-effects model to the observed reflex responses r_i of the brachioradialis and deltoid muscles. The model is given by

$$r_i = \beta_0 + \beta_1 \cdot \mathrm{rot_i} + b_{0,\mathrm{m}} + b_{1,\mathrm{m}} \cdot \mathrm{rot_i} + \epsilon_\mathrm{im} \ . \tag{17}$$

Here, β_0 and β_1 denote the fixed-effect regression coefficients, $b_{0,\mathrm{m}}$ and $b_{1,\mathrm{m}}$ are the random-effect regression coefficients, and ϵ_im denotes the residuals. The subjects were denoted by m and differences between them were considered as random effects. The fixed effect $\mathrm{rot_i}$ describes whether in trial number i the rotating movement recruited mainly the subsequently perturbed or the non-perturbed joint,

$$\mathrm{rot_i} = \begin{cases} +1 & \text{if rotation and perturbation involved same joint ,} \\ -1 & \text{if rotation and perturbation involved different joints .} \end{cases} \tag{18}$$

The assumption states that the reflex response in either of the two muscles is higher after its innervated joint has moved. This implies that $\beta_1 > 0$. The corresponding null hypothesis $\beta_1 = 0$ was tested by a two-tailed t-test. Since the hypothesis predicts that the effect must be significant in both muscles simultaneously, the linear fixed-effects model described in equation (17) was individually fitted to the brachioradialis and deltoid measurements, and no correction for multiple comparisons was required. The linear mixed-effects model assumes that the residuals ϵ_im are normally distributed, consistent with the histograms in Figure 3c and Figure 3d.

To test whether the perturbation delays after an elbow and shoulder rotation were significantly different, the same linear mixed-effects model described in equation (17) was applied. Here, the dependent response variable r_i was chosen as the natural logarithm of the delay between the movement cessation and the perturbation onset. The logarithm accounts for the fact that the delay is restricted to positive values. The linear mixed-effects model was fitted to the measured delays of the above-described trials.

Data Availability Statement

The authors declare that the recorded data that support the results of this study are available on *figshare* under the private link `https://figshare.com/s/2a2633641854d2ffb21b`. After publication, it will be available under `https://doi.org/10.6084/m9.figshare.7467023`. A brief description of the provided data files is provided in the supplementary information.

References

1 Sawicki, G. S., Lewis, C. L. & Ferris, D. P. It pays to have a spring in your step. *Exerc Sport Sci Rev* **37**, 130–138 (2009).

2 Cavagna, G. A., Heglund, N. C. & Taylor, C. R. Mechanical work in terrestrial locomotion: two basic mechanisms for minimizing energy expenditure. *American Journal of Physiology-Regulatory, Integrative and Comparative Physiology* **233**, R243–R261 (1977). URL `https://doi.org/10.1152/ajpregu.1977.233.5.R243`. PMID: 411381, `https://doi.org/10.1152/ajpregu.1977.233.5.R243`.

3 Roberts, T. J. & Azizi, E. Flexible mechanisms: the diverse roles of biological springs in vertebrate movement. *Journal of Experimental Biology* **214**, 353–361 (2011). URL `http://jeb.biologists.org/content/214/3/353`. `http://jeb.biologists.org/content/214/3/353.full.pdf`.

4 Shemmell, J., An, J. H. & Perreault, E. J. The differential role of motor cortex in stretch reflex modulation induced by changes in environmental mechanics and verbal instruction. *J. Neurosci.* **29**, 13255–13263 (2009).

5 Franklin, S., Wolpert, D. M. & Franklin, D. W. Visuomotor feedback gains upregulate during the learning of novel dynamics. *Journal of Neurophysiology* **108**, 467–478 (2012). URL `https://doi.org/10.1152/jn.01123.2011`. PMID: 22539828, `https://doi.org/10.1152/jn.01123.2011`.

6 Cluff, T. & Scott, S. H. Rapid feedback responses correlate with reach adaptation and properties of novel upper limb loads. *Journal of Neuroscience* **33**, 15903–15914 (2013). URL `http://www.jneurosci.org/content/33/40/15903`. `http://www.jneurosci.org/content/33/40/15903.full.pdf`.

7 Damm, L. & McIntyre, J. Physiological basis of limb-impedance modulation during free and constrained movements. *Journal of Neurophysiology* **100**, 2577–2588 (2008).

8 Taube, W. *et al.* Differential modulation of spinal and corticospinal excitability during drop jumps. *Journal of Neurophysiology* **99**, 1243–1252 (2008).

9 Wei, K. *et al.* Serotonin affects movement gain control in the spinal cord. *Journal of Neuroscience* **34**, 12690–12700 (2014).

10 Springfield, S. A. & Moolenaar, G.-M. Differences in the responses of raphe nuclei to repetitive somatosensory stimulation. *Experimental Neurology* **79**, 360–370 (1983). URL `http://www.sciencedirect.com/science/article/pii/0014488683902194`.

11 Veasey, S. C., Fornal, C. A., Metzler, C. W. & Jacobs, B. L. Response of serotonergic caudal raphe neurons in relation to specific motor activities in freely moving cats. *Journal of Neuroscience* **15**, 5346–5359 (1995).

12 Fornal, C. A. *et al.* A subgroup of dorsal raphe serotonergic neurons in the cat is strongly activated during oral-buccal movements. *Brain Research* **716**, 123–133 (1996). URL `http://www.sciencedirect.com/science/article/pii/0006899396000066`.

13 ElBasiouny, S. M., Schuster, J. E. & Heckman, C. J. Persistent inward currents in spinal motoneurons: Important for normal function but potentially harmful after spinal cord injury and in amyotrophic lateral sclerosis. *Clinical Neurophysiology* 1669–1679 (2010).

14 Watson, C., Paxinos, G. & Puelles, L. *The Mouse Nervous System.* Academic Press (Elsevier Academic Press, 2012).

15 Perrier, J. F., Rasmussen, H. B., Christensen, R. K. & Petersen, A. V. Modulation of the intrinsic properties of motoneurons by serotonin. *Curr. Pharm. Des.* **19**, 4371–4384 (2013).

16 Heckman, C. J., Hyngstrom, A. S. & Johnson, M. D. Active properties of motoneurone dendrites: diffuse descending neuromodulation, focused local inhibition. *Journal of Physiology (Lond.)* **586**, 1225–1231 (2008).

17 Cope, T. *Motor Neurobiology of the Spinal Cord.* Frontiers in Neuroscience (CRC Press, 2001).

18 Franklin, D. W. & Wolpert, D. M. Computational mechanisms of sensorimotor control. *Neuron* **72**, 425–442 (2011).

19 Sekiguchi, K. J. *et al.* Imaging large-scale cellular activity in spinal cord of freely behaving mice. *Nat Commun* **7**, 11450 (2016).

20 Fuxe, K. *et al.* The discovery of central monoamine neurons gave volume transmission to the wired brain. *Progress in Neurobiology* **90**, 82–100 (2010). URL http://www.sciencedirect.com/science/article/pii/S0301008209001634.

21 Stratmann, P., Lakatos, D. & Albu-Schäffer, A. Neuromodulation and synaptic plasticity for the control of fast periodic movement: Energy efficiency in coupled compliant joints via pca. *Frontiers in Neurorobotics* **10**, 2 (2016). URL https://www.frontiersin.org/article/10.3389/fnbot.2016.00002.

22 Stratmann, P., Lakatos, D., Özparpucu, M. C. & Albu-Schäffer, A. Legged elastic multibody systems: Adjusting limit cycles to close-to-optimal energy efficiency. *Robotics and Automation Letters* **2**, 436–443 (2016).

23 Stratmann, P., Albu-Schäffer, A. & Jörntell, H. Scaling our world view: How monoamines can put context into brain circuitry. *Frontiers in Cellular Neuroscience* **12**, 506 (2018). URL https://doi.org/10.3389/fncel.2018.00506.

24 Kurtzer, I. L., Pruszynski, J. A. & Scott, S. H. Long-latency reflexes of the human arm reflect an internal model of limb dynamics. *Current Biology* **18**, 449–453 (2008). URL http://www.sciencedirect.com/science/article/pii/S0960982208002406.

25 Forgaard, C. J., Franks, I. M., Maslovat, D. & Chua, R. Perturbation predictability can influence the long-latency stretch response. *PLoS ONE* **11**, e0163854 (2016).

26 Rothwell, J. C. Proprioceptors in muscle, joint and skin. In *Control of Human Voluntary Movement*, 74–104 (Springer US, Boston, MA, 1987). URL https://doi.org/10.1007/978-1-4684-7688-0_4.

27 Muniak, M. A., Ray, S., Hsiao, S. S., Dammann, J. F. & Bensmaia, S. J. The neural coding of stimulus intensity: Linking the population response of mechanoreceptive afferents with psychophysical behavior. *The Journal of Neuroscience* **27**, 11687–11699 (2007). URL http://www.jneurosci.org/content/27/43/11687.abstract.

28 Bensmaia, S. J. Tactile intensity and population codes. *Behavioural Brain Research* **190**, 165–173 (2008).

29 Charnay, Y. & Leger, L. Brain serotonergic circuitries. *Dialogues Clin Neurosci* **12**, 471–487 (2010).

30 Perrier, J.-F. & Cotel, F. Serotonergic modulation of spinal motor control. *Current Opinion in Neurobiology* **33**, 1–7 (2015). URL http://www.sciencedirect.com/science/article/pii/S095943881400244X. Motor circuits and action.

31 Weiler, J., Gribble, P. L. & Pruszynski, J. A. Spinal stretch reflexes support efficient hand control. *Nat. Neurosci.* **22**, 529–533 (2019).

32 Pruszynski, J. A., Kurtzer, I., Lillicrap, T. P. & Scott, S. H. Temporal evolution of automatic gain scaling. *J. Neurophysiol.* **102**, 992–1003 (2009).

33 Thompson, A. K. & Wolpaw, J. R. The simplest motor skill: mechanisms and applications of reflex operant conditioning. *Exerc Sport Sci Rev* **42**, 82–90 (2014).

34 Jacobs, B. L., Martin-Cora, F. J. & Fornal, C. A. Activity of medullary serotonergic neurons in freely moving animals. *Brain Research Reviews* **40**, 45–52 (2002). The Segerfalk symposium on Principles of Spinal Cord Function, Plasticity and Repair.

35 Nieuwenhuys, R., Voogd, J. & van Huijzen, C. *The Human Central Nervous System: A Synopsis and Atlas* (Steinkopff, 2007).

36 Cavada, C., Huisman, A. M. & Kuypers, H. G. Retrograde double labeling of neurons: the combined use of horseradish peroxidase and diamidino yellow dihydrochloride (dy 2hcl) compared with true blue and dy 2hcl in rat descending brainstem pathways. *Brain Research* **308**, 123–136 (1984).

37 Shinoda, Y., Zarzecki, P. & Asanuma, H. Spinal branching of pyramidal tract neurons in the monkey. *Experimental Brain Research* **34**, 59–72 (1979).

38 Krutky, M. A., Ravichandran, V. J., Trumbower, R. D. & Perreault, E. J. Interactions between limb and environmental mechanics influence stretch reflex sensitivity in the human arm. *Journal of Neurophysiology* **103**, 429–440 (2010).

39 Ferris, D. P., Aagaard, P., Simonsen, E. B., Farley, C. T. & Dyhre-Poulsen, P. Soleus h-reflex gain in humans walking and running under simulated reduced gravity. *The Journal of Physiology* **530**, 167–180 (2001). URL https://physoc.onlinelibrary.wiley.com/doi/abs/10.1111/j.1469-7793.2001.0167m.x. https://physoc.onlinelibrary.wiley.com/doi/pdf/10.1111/j.1469-7793.2001.0167m.x.

40 Kravitz, E. A. Serotonin and aggression: insights gained from a lobster model system and speculations on the role of amine neurons in a complex behavior. *Journal of Comparative Physiology A* **186**, 221–238 (2000). URL https://doi.org/10.1007/s003590050423.

41 Gillette, R. Evolution and function in serotonergic systems. *Integrative and Comparative Biology* **46**, 838–846 (2006). URL http://dx.doi.org/10.1093/icb/icl024. /oup/backfile/content_public/journal/icb/46/6/10.1093/icb/icl024/2/icl024.pdf.

42 Best, J., Nijhout, H. F. & Reed, M. Serotonin synthesis, release and reuptake in terminals: a mathematical model. *Theor Biol Med Model* **7**, 34 (2010).

43 Lakatos, D., Görner, M., Petit, F., Dietrich, A. & Albu-Schäffer, A. A modally adaptive control for multi-contact cyclic motions in compliantly actuated robotic systems. In *Intelligent Robots and Systems, Intl Conf on*, 5388–5395 (2013).

44 Stratmann, P., Lakatos, D., Özparpucu, M. C. & Albu-Schäffer, A. Legged elastic multibody systems: Adjusting limit cycles to close-to-optimal energy efficiency. *IEEE Robotics and Automation Letters* **2**, 436–443 (2017).

45 Ferris, D. P., Louie, M. & Farley, C. T. Running in the real world: adjusting leg stiffness for different surfaces. *Proceedings of the Royal Society of London B: Biological Sciences* **265**, 989–994 (1998).

46 Farley, C. T., Houdijk, H. H. P., Van Strien, C. & Louie, M. Mechanism of leg stiffness adjustment for hopping on surfaces of different stiffnesses. *Journal of Applied Physiology* **85**, 1044–1055 (1998). URL https://doi.org/10.1152/jappl.1998.85.3.1044. PMID: 9729582, https://doi.org/10.1152/jappl.1998.85.3.1044.

47 Ijspeert, A. J. Biorobotics: Using robots to emulate and investigate agile locomotion. *Science* **346**, 196–203 (2014). URL https://science.sciencemag.org/content/346/6206/196. https://science.sciencemag.org/content/346/6206/196.full.pdf.

48 Gravish, N. & Lauder, G. V. Robotics-inspired biology. *Journal of Experimental Biology* **221** (2018). URL http://jeb.biologists.org/content/221/7/jeb138438. http://jeb.biologists.org/content/221/7/jeb138438.full.pdf.

49 Rus, D. & Tolley, M. T. Design, fabrication and control of soft robots. *Nature* **521**, 467–475 (2015).

50 Wolf, S. *et al.* Variable stiffness actuators: Review on design and components. *IEEE/ASME Transactions on Mechatronics* **21**, 2418–2430 (2016).

51 Sreenath, K., Park, H.-W., Poulakakis, I. & Grizzle, J. Embedding active force control within the compliant hybrid zero dynamics to achieve stable, fast running on mabel. *The International Journal of Robotics Research* **32**, 324–345 (2013). URL https://doi.org/10.1177/0278364912473344. https://doi.org/10.1177/0278364912473344.

52 Hutter, M., Remy, C. D., Höpflinger, M. A. & Siegwart, R. Slip running with an articulated robotic leg. In *2010 IEEE/RSJ International Conference on Intelligent Robots and Systems*, 4934–4939 (2010).

53 Stramigioli, S. & van Dijk, M. Energy conservative limit cycle oscillations. *IFAC Proceedings Volumes* **41**, 15666–15671 (2008). URL http://www.sciencedirect.com/science/article/pii/S1474667016415144. 17th IFAC World Congress.

54 Lakatos, D. & Albu-Schäffer, A. Switching based limit cycle control for compliantly actuated second-order systems. In *Proceedings of the IFAC World Congress*, vol. 19, 6392–6399 (2014).

55 Wise, S. P. & Shadmehr, R. Motor control. In Ramachandran, V. S. (ed.) *Encyclopedia of the Human Brain*, vol. 3 (Academic Press, 2002).

56 Babič, J., Oztop, E. & Kawato, M. Human motor adaptation in whole body motion. *Sci Rep* **6**, 32868 (2016).

57 Churchland, P. S. & Sejnowski, T. J. Blending computational and experimental neuroscience. *Nat. Rev. Neurosci.* **17**, 667–668 (2016).

58 Höppner, H., Grebenstein, M. & van der Smagt, P. Two-dimensional orthoglide mechanism for revealing areflexive human arm mechanical properties. In *2015 IEEE/RSJ International Conference on Intelligent Robots and Systems (IROS)*, 1178–1185 (2015).

59 Hermens, H. J., Freriks, B., Disselhorst-Klug, C. & Rau, G. Development of recommendations for semg sensors and sensor placement procedures. *Journal of Electromyography and Kinesiology* **10**, 361–374 (2000). URL `http://www.sciencedirect.com/science/article/pii/S1050641100000274`.

60 De Luca, A., Albu-Schäffer, A., Haddadin, S. & Hirzinger, G. Collision detection and safe reaction with the dlr-iii lightweight manipulator arm. In *2006 IEEE/RSJ International Conference on Intelligent Robots and Systems*, 1623–1630 (2006).

61 Taubin, G. Estimation of planar curves, surfaces, and nonplanar space curves defined by implicit equations with applications to edge and range image segmentation. *IEEE Transactions on Pattern Analysis and Machine Intelligence* **13**, 1115–1138 (1991).

62 Leinonen, V. Sensory-motor posture control in lumbar disorders. In Hanninen, O. O. P. *et al.* (eds.) *Medical and health sciences - Volume IV* (Eolss Publishers Co. Ltd., 2010).

Acknowledgments

The authors are indebt to Florian Schmidt and Robert Burger for restructuring the electronic recording and control modules of the manipulandum. The authors are further grateful to Tilo Wüsthoff for designing Figure 1. Thanks also go to Manuel Keppler and Dominic Lakatos for their advice on control theory. The authors also thank Daniel Seidel and Georg Stillfried for their help on the fine-tuning of the experimental setup and to all participants of the experiments. They further thankfully acknowledge the stimulating discussions with their colleagues in the Human Brain Project, funded by the European Union's Horizon 2020 Framework Programme for Research and Innovation under the Specific Grant Agreement No. 785907 (Human Brain Project SGA2).

Author Contributions

All authors designed the study. H.H. and P.S. restructured the mechanical setup. P.S. developed the robotic controller, performed the experiments, analyzed the data, and wrote the manuscript. A.A.-S., D.F., H.H., and P.v.d.S. discussed the results and critically revised the manuscript.

Competing Interests

The authors declare no competing financial interests.

COMMUNICATIONS BIOLOGY

Supplementary Information
Focused neuromodulation of individual motorpools: confirmation of predictions from the efficient control of biomimetic robots.

Philipp Stratmann[1,2,*], Hannes Höppner[2,3], David Franklin[4], Patrick van der Smagt[5], Alin Albu-Schäffer[1,2]

[1] Department of Informatics, Technical University of Munich, 85748 Garching, Germany.
[2] Institute of Robotics and Mechatronics, German Aerospace Center (DLR), Münchener Straße 20, 82234 Weßling, Germany.
[3] Institute for Applied Training Science, Marschnerstraße 29, 04109 Leipzig, Germany.
[4] Department of Sport and Health Sciences, Georg-Brauchle-Ring 60-62/II, 80992 Munich, Germany.
[5] Data Lab, Volkswagen Group, Ungererstraße 69, 80805 Munich, Germany.

Corresponding author: Philipp Stratmann
philipp.stratmann@tum.de
Chair for Sensor Based Robotic Systems and Intelligent Assistance Systems
Department of Informatics
Technical University of Munich
DE-85748 Garching

Supplementary Methods

The *Methods* section describes the virtual mechanical environment of the subject's arm. This environment enforced the subject to move along a circular trajectory that involved either pure elbow or shoulder rotation. The following two sections describe the controller of the manipulandum that guaranteed this well-defined environment.

Friction compensation, decoupling of the mass matrix, and mass scaling

The controller artificially compensated three interfering effects originating from the mechanical manipulandum design: the high friction that typifies strong linear motors, the high mass $m = 12.9\,\mathrm{kg}$ of the manipulandum arms and motors which must be moved by the participants, and the coupled dynamics of the manipulandum arms. After reducing the friction, scaling down the mass, and decoupling the manipulandum dynamics, the handle attached to the subject reacted like a frictionless point mass to the forces exerted by the virtual environment and by the subject, denoted by $\boldsymbol{F}_e$ and $\boldsymbol{F}_s$, respectively,

$$s \cdot m \cdot \boldsymbol{I}\ddot{\boldsymbol{x}} = \boldsymbol{F}_\mathrm{e} + \boldsymbol{F}_\mathrm{s} \ . \tag{S1}$$

In equation (S1), $\boldsymbol{I}$ denotes the 2×2 identity matrix and $\boldsymbol{x} \in \mathbb{R}^2$ is the handle position in the subject's coordinate system. The mass was artificially scaled down by a factor of $s = 0.4$.

The dynamics of the manipulandum, which experiences a friction force $\boldsymbol{\tau}_\mathrm{f}$ and reacts to the motor force $\boldsymbol{\tau}_m$ as well as the force $\boldsymbol{F}_s$ exerted by the subject on the handle, are given by

$$\boldsymbol{M}(\boldsymbol{q})\ddot{\boldsymbol{q}} + \boldsymbol{C}(\boldsymbol{q}, \dot{\boldsymbol{q}})\dot{\boldsymbol{q}} = \boldsymbol{\tau}_\mathrm{m} + \boldsymbol{J}^T(\boldsymbol{q})\boldsymbol{F}_\mathrm{s} + \boldsymbol{\tau}_\mathrm{f} \ . \tag{S2}$$

For convenience, this equation of motion is stated in the coordinate system spanned by the motor positions $\boldsymbol{q}$,

$$\boldsymbol{q} = \begin{pmatrix} \sqrt{l^2 - x_1^2} - x_2 \\ \sqrt{l^2 - x_2^2} - x_1 \end{pmatrix} \ , \tag{S3}$$

where $l = 1.0\,\mathrm{m}$ is the length of the manipulandum arms. The Jacobian

$$\boldsymbol{J}_\mathrm{ij}(\boldsymbol{q}) = \frac{\partial x_\mathrm{i}}{\partial q_\mathrm{j}} \tag{S4}$$

transforms the positions and forces from the subject coordinate system into the motor coordinate system, in which the forces are denoted by $\boldsymbol{\tau}$. Note that $\boldsymbol{J}(\boldsymbol{q})$ is a square matrix which is non-singular within the coordinate range allowed by the motor end stops and is hence invertible. The off-diagonal entries in the symmetric, positive-definite inertia matrix $\boldsymbol{M}(\boldsymbol{q})$, along with the generalized Coriolis plus centrifugal matrix $\boldsymbol{C}(\boldsymbol{q}, \dot{\boldsymbol{q}})$, imply a mechanical system with coupled dynamics. For control purposes, these matrices were derived by approximating the manipulandum as five point masses: one for each of the two motors moving along its slider, one at the center of each arm, and one at the center of the handle. The mass distributions of the individual modules were neglected because the modules were barely rotated throughout the experiments.

Without compensating for the interfering effects of the manipulandum mechanics, the commanded motor force would amount to $\boldsymbol{J}^T(\boldsymbol{q})\boldsymbol{F}_\mathrm{e}$. In the mechanical system with decoupled dynamics and a scaled mass, the commanded motor force was instead adjusted to

$$\tilde{\boldsymbol{\tau}}_m \quad = \frac{1}{s \cdot m} \cdot \boldsymbol{J}^T \boldsymbol{\Lambda}(\boldsymbol{x}) \left[\boldsymbol{F}_\mathrm{e} + \boldsymbol{F}_s\right] - \boldsymbol{J}^T(\boldsymbol{q})\boldsymbol{F}_s + \boldsymbol{\mu}(\boldsymbol{x}, \dot{\boldsymbol{x}})\dot{\boldsymbol{x}} \ , \tag{S5}$$

where

$$\begin{aligned} \boldsymbol{\Lambda}(\boldsymbol{x}) \quad &= \boldsymbol{J}^{-T}\boldsymbol{M}(\boldsymbol{q})\boldsymbol{J}^{-1}(\boldsymbol{q}) \ , \\ \boldsymbol{\mu}(\boldsymbol{x}, \dot{\boldsymbol{x}}) &= \boldsymbol{C}(\boldsymbol{q}, \dot{\boldsymbol{q}})\boldsymbol{J}^{-1}(\boldsymbol{q}) - \boldsymbol{M}(\boldsymbol{q})\boldsymbol{J}^{-1}(\boldsymbol{q})\dot{\boldsymbol{J}}(\boldsymbol{q}, \dot{\boldsymbol{q}})\boldsymbol{J}^{-1}(\boldsymbol{q}) \ . \end{aligned} \tag{S6}$$

For motors exerting a force $\tilde{\boldsymbol{\tau}}_m$, the manipulandum dynamics in equation (S2) can be reformulated as

$$s \cdot m \cdot \boldsymbol{I}\ddot{\boldsymbol{x}} = \boldsymbol{F}_\mathrm{e} + \boldsymbol{F}_\mathrm{s} + s \cdot m \cdot \boldsymbol{J}^T \boldsymbol{\Lambda}(\boldsymbol{x})\boldsymbol{\tau}_f \ . \tag{S7}$$

Under the adjusted motor force, the manipulandum behaves like a point mass that is downscaled by a factor of s. As a beneficial side effect, also the effective friction experienced by the subject was downscaled by the same factor.

The remaining uncompensated friction $\boldsymbol{\tau}_\mathrm{f}$ of the device was compensated by a friction observer. The manipulandum observes the commanded motor force $\tilde{\boldsymbol{\tau}}_m$ and measures the force exerted by the subject $\boldsymbol{F}_\mathrm{s}$ at the handle. To compensate the remaining friction, the expected movement of a frictionless manipulandum was compared to the actual movement observed by the position sensors in the motors. Any deviation between these two movements was ascribed to friction. Mathematically, the friction was estimated by the time integral

$$\boldsymbol{r}(t) = \boldsymbol{K}_I \left[\boldsymbol{p}(t) - \boldsymbol{p}(0) - \int_0^t \left(\boldsymbol{C}^{\boldsymbol{T}} \dot{\boldsymbol{q}} + \tilde{\boldsymbol{\tau}}_\mathrm{m} + \boldsymbol{J}^T(\boldsymbol{q}) \boldsymbol{F}_\mathrm{s} \right) ds \right], \tag{S8}$$

where the initial condition is $\boldsymbol{r}(0) = 0$, the gain $\boldsymbol{K}_I = \frac{1}{0.01\,\mathrm{s}} \boldsymbol{I}$, and the generalized momentum is given by

$$\boldsymbol{p}(t) = \boldsymbol{M}(\boldsymbol{q}) \dot{\boldsymbol{q}} \ . \tag{S9}$$

The time integral approximates the friction of the system,

$$\lim_{\boldsymbol{K}_I \to \infty} \boldsymbol{r}(t) = \boldsymbol{\tau}_\mathrm{f}(t) \ . \tag{S10}$$

To show this, equation (S2) can be combined with equation (S8) and with the fact that $\dot{\boldsymbol{M}}(\boldsymbol{q}) - 2\boldsymbol{C}(\boldsymbol{q}, \dot{\boldsymbol{q}})$ is skew-symmetric, resulting in

$$\dot{\boldsymbol{M}}(\boldsymbol{q}) = \boldsymbol{C}^{\boldsymbol{T}}(\boldsymbol{q}, \dot{\boldsymbol{q}}) \dot{\boldsymbol{q}} + \boldsymbol{C}(\boldsymbol{q}, \dot{\boldsymbol{q}}) \dot{\boldsymbol{q}} \ . \tag{S11}$$

The time integral is then given by

$$\dot{\boldsymbol{r}}(t) = \boldsymbol{K}_I \cdot (\boldsymbol{\tau}_\mathrm{f} - \boldsymbol{r}) \ . \tag{S12}$$

To compensate for the observed friction, the commanded motor force must be reduced by $\boldsymbol{r}(t)$. Therefore, the motor force commanded throughout the experiments was

$$\boldsymbol{\tau}_\mathrm{m} = \tilde{\boldsymbol{\tau}}_m - \boldsymbol{r}(t) \ . \tag{S13}$$

The resulting manipulandum dynamics are then described by plugging $\boldsymbol{\tau}_m$, computed by equation (S13), into the general equation of motion (S2):

$$s \cdot m \cdot \boldsymbol{I} \ddot{\boldsymbol{x}} = \boldsymbol{F}_\mathrm{e} + \boldsymbol{F}_\mathrm{s} + s \cdot m \cdot \boldsymbol{J}^T \boldsymbol{\Lambda}(\boldsymbol{x}) \left[\boldsymbol{\tau}_f - \boldsymbol{r} \right] \ . \tag{S14}$$

From the subject's viewpoint, this compensated mechanical system resembled a point mass $s \cdot m = 5.2\,\mathrm{kg}$ acted upon by forces from the virtual environment, the subject, and the scaled-down friction of the manipulandum dynamics.

To evaluate the controller performance, the manipulandum trajectory was recorded while pulling the handle under a constant force $\boldsymbol{F}_\mathrm{s}$ in the absence of an environmental force, i.e., $\boldsymbol{F}_\mathrm{e} = \boldsymbol{0}$. In successive trials, the pull force was increased from 1 N to 10 N by attaching different weights via a deflection pulley. Under gravity, the handle was accelerated in the direction characterized by the equal movement of both motors. Since the effective sticking friction is at a maximum along this direction, the controller will show even better performance along the other directions. Without friction compensation, the friction of the manipulandum required forces higher than 20 N to initiate a movement. Under ideal friction compensation, the total distance traveled in time t, predicted by equation (S1), is given by

$$\mathrm{Distance}^{\frac{1}{2}}(t) = \sqrt{\frac{|\boldsymbol{F}_\mathrm{s}|}{s \cdot m}} \cdot (t - t_0) = \mathrm{slope} \cdot (t - t_0) \ . \tag{S15}$$

Supplementary Figure 1a illustrates this linear behavior. The repeatability was checked in 10 trials under a 5 N pulling force. The standard deviation of the resulting movement (shaded regions in the figure) is barely visible. Between trials, the distance traveled within the first second differed by less than 1.3%. In linear fits to trials with different $|\boldsymbol{F}_\mathrm{s}|$, the adjusted R^2 was consistently above 0.994 and converged towards 1.0 with increasing weight (Supplementary Figure 1c). As predicted by equation (S15), the slope^2 was proportional to $|\boldsymbol{F}_\mathrm{s}|$ (Supplementary Figure 1c). The delay t_0, defined as the time required for the friction observer to overcome the sticking friction, decreased with $|\boldsymbol{F}_\mathrm{s}|$ and eventually fell below 30 ms (Supplementary Figure 1e). As the subjects performed particularly strong movements throughout the experiments, the manipulandum rapidly behaved like a frictionless system.

When the mass matrix was fully decoupled, the handle was expected to move along the pulling-force direction, i.e., along a straight line in the subject coordinate system. This behavior is shown in Supplementary Figure 1b. The slope differed from the pulling direction only under very low forces (Supplementary Figure 1c). The adjusted R^2 values were above 0.996, indicating good fitting of the linear model (Supplementary Figure 1d).

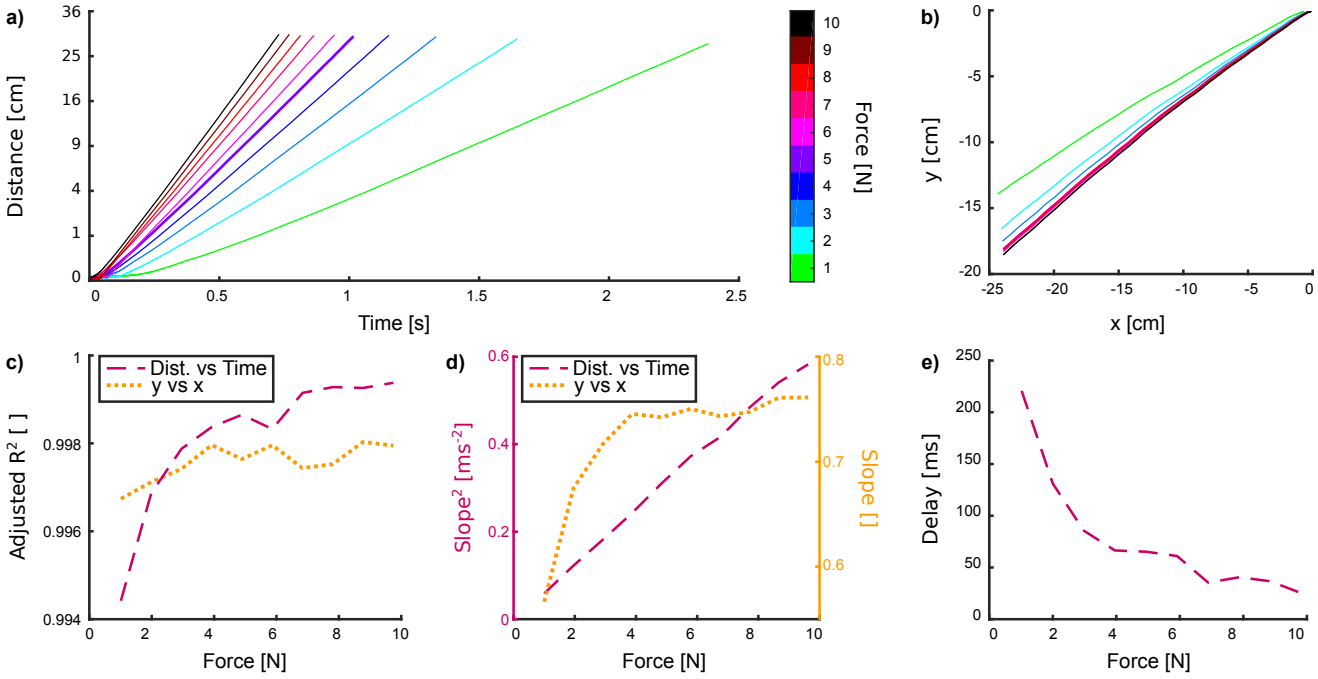

Supplementary Figure 1: Evaluation of friction compensation and decoupling of the mass matrix of the manipulandum. **a)** When varying the force on the manipulandum handle, the distance traveled by the handle should increase proportionally to the second power of time. Here, the y-axis is accordingly scaled quadratically, so that the plotted distance is expected to trace a straight line. The standard deviation of 10 trials under a pulling force of 5 N is indicated as the shaded area around the purple line. **b)** As the mass matrix is decoupled, the corresponding handle trajectories should trace a straight line in the subject coordinate space x–y. **c)** Adjusted R^2 values of the linear fits to the graphs in the previous subfigures. **d)** The squared slope of the linear fit of the traveled distance versus time plots was expected to increase proportionally to the pulling force. The slope of the straight line in the x–y coordinate space should be constant, and indeed converged already under low forces. **e)** The delay between controller onset and movement of the manipulandum quantifies the sticking friction felt by the subjects. The delay was obtained by linearly fitting the distance versus time plot and defines the parameter t_0 in the main text.

Enforcing circular trajectory

The simulated environment of the trials enforced a circular movement around the subject's elbow or shoulder joint. For this purpose, the controller exerted the sum of two forces on the subject's arm:

$$\boldsymbol{F}_\mathrm{e} = \boldsymbol{F}_\mathrm{rad} + \boldsymbol{F}_\mathrm{ang} \ . \tag{S16}$$

The first force simulated an almost rigid spring which pushed the handle back to its circular trajectory when its current distance r from the joint center deviated from the desired radius r_0. This force was given by

$$\boldsymbol{F}_\mathrm{rad} = -(k_\mathrm{rad} \cdot (r - r_0) + d_\mathrm{rad} \cdot r_0 * \dot{r}) \cdot \boldsymbol{e}_\mathrm{rad} \ . \tag{S17}$$

The stiffness and damping constant of the near-rigid spring were $k_\mathrm{rad} = 4000\,\mathrm{N\,m^{-1}}$ and $d_\mathrm{rad} = 300\,\mathrm{Ns/m^2}$, respectively. The force acted along the radial unit vector $\boldsymbol{e}_\mathrm{rad}$ pointing from the handle position to the joint. The radial velocity $\dot{r}$ was derived from r and filtered through a discrete 2nd-order Butterworth lowpass filter with a cutoff frequency of 50 Hz.
The second force simulated a slack spring which pushed the handle back to its equilibrium position along the circular trajectory:

$$\boldsymbol{F}_\mathrm{ang} = -r_0 \cdot (k_\mathrm{ang} \cdot \alpha + d_\mathrm{ang} \cdot \dot{\alpha}) \cdot \boldsymbol{e}_\mathrm{ang} \ . \tag{S18}$$

The angular stiffness of the slack spring was $k_\mathrm{ang} = 250\,\mathrm{N\,rad^{-1}\,m^{-1}}$, and its angular damping constant was $d_\mathrm{ang} = 32\,\mathrm{N\,s\,rad^{-1}\,m^{-1}}$ and $d_\mathrm{ang} = 35\,\mathrm{N\,s\,rad^{-1}\,m^{-1}}$ for the shoulder and elbow movements, respectively. Under the damping effect, the subjects needed to repeatedly push the system to sustain the movement, thus preventing friction overcompensation. The force $\boldsymbol{F}_\mathrm{ang}$ acted along the clockwise tangential unit vector $\boldsymbol{e}_\mathrm{ang}$ and increased with the angular deviation from the equilibrium position, $\alpha \in [-\pi, \pi]$.

Description of the Supplementary Data

For researchers wishing to reproduce the study findings, the data are available on *figshare* under the link `https://doi.org/10.6084/m9.figshare.7467023`. The data include the preliminary recordings and the main experimental recordings for each subject, as described in the *Methods* section. The MVC recordings taken before and after the main experiments are denoted as *prior* and *post*, respectively. The main experimental data of each subject are provided in separate files. Each file also summarizes the general information of the preliminary experiments and states the order of the individual trials performed by the subject. The four trial conditions are denoted by integers as follows:

1: Rotation of the shoulder, followed by a perturbation of the shoulder.
2: Rotation of the elbow, followed by a perturbation of the shoulder.
3: Rotation of the shoulder, followed by a perturbation of the elbow.
4: Rotation of the elbow, followed by a perturbation of the elbow.

A minus sign denotes no perturbation, implying that the EMG of the respective muscle remained above its resting level and the trial was repeated. A single data file is provided for each trial where a perturbation was applied. Two additional files describe the resting EMG directly before and after each of these trials.

Bibliography

[1] Richard Feyman. 1988. eprint: http://archives.caltech.edu/pictures/1.10-29.jpg.

[2] Auke J. Ijspeert. "Biorobotics: Using robots to emulate and investigate agile locomotion". *Science* 346.6206 (2014), pp. 196–203. ISSN: 0036-8075. DOI: 10.1126/science.1254486. eprint: https://science.sciencemag.org/content/346/6206/196.full.pdf.

[3] Dario Floreano, Auke Jan Ijspeert, and Stefan Schaal. "Robotics and Neuroscience". *Current Biology* 24.18 (2014), R910–R920. ISSN: 0960-9822. DOI: 10.1016/j.cub.2014.07.058.

[4] Nick Gravish and George V. Lauder. "Robotics-inspired biology". *Journal of Experimental Biology* 221.7 (2018). ISSN: 0022-0949. DOI: 10.1242/jeb.138438. eprint: http://jeb.biologists.org/content/221/7/jeb138438.full.pdf.

[5] Steven P. Wise and Reza Shadmehr. "Motor Control". *Encyclopedia of the Human Brain*. Ed. by Vilayanur S. Ramachandran. Vol. 3. Academic Press, 2002.

[6] J. Babič, E. Oztop, and M. Kawato. "Human motor adaptation in whole body motion". *Sci Rep* 6 (Sept. 2016), p. 32868.

[7] D. W. Franklin and D. M. Wolpert. "Computational Mechanisms of Sensorimotor Control". *Neuron* 72.3 (2011), pp. 425–442. ISSN: 0896-6273.

[8] J. Shemmell, J. H. An, and E. J. Perreault. "The differential role of motor cortex in stretch reflex modulation induced by changes in environmental mechanics and verbal instruction". *J. Neurosci.* 29.42 (Oct. 2009), pp. 13255–13263.

[9] M. Jetté, K. Sidney, and G. Blümchen. "Metabolic equivalents (METS) in exercise testing, exercise prescription, and evaluation of functional capacity". *Clinical Cardiology* 13.8 (1990), pp. 555–565. DOI: 10.1002/clc.4960130809. eprint: https://onlinelibrary.wiley.com/doi/pdf/10.1002/clc.4960130809.

[10] Gregory S. Sawicki and Daniel P. Ferris. "Mechanics and energetics of level walking with powered ankle exoskeletons". *Journal of Experimental Biology* 211.9 (2008), pp. 1402–1413. ISSN: 0022-0949. DOI: 10.1242/jeb.009241. eprint: http://jeb.biologists.org/content/211/9/1402.full.pdf.

[11] G. S. Sawicki, C. L. Lewis, and D. P. Ferris. "It pays to have a spring in your step". *Exerc Sport Sci Rev* 37.3 (July 2009), pp. 130–138.

[12] G. A. Cavagna, N. C. Heglund, and C. R. Taylor. "Mechanical work in terrestrial locomotion: two basic mechanisms for minimizing energy expenditure". *American Journal of Physiology-Regulatory, Integrative and Comparative Physiology* 233.5 (1977). PMID: 411381, R243–R261. DOI: 10.1152/ajpregu.1977.233.5.R243. eprint: https://doi.org/10.1152/ajpregu.1977.233.5.R243.

[13] Thomas J. Roberts and Emanuel Azizi. "Flexible mechanisms: the diverse roles of biological springs in vertebrate movement". *Journal of Experimental Biology* 214.3 (2011), pp. 353–361. ISSN: 0022-0949. DOI: 10.1242/jeb.038588. eprint: http://jeb.biologists.org/content/214/3/353.full.pdf.

[14] Marc Raibert, Kevin Blankespoor, Gabriel Nelson, Rob Playter, et al. "Bigdog, the rough-terrain quadruped robot". *Proceedings of the 17th World Congress*. Vol. 17. 2008, pp. 10822–10825.

[15] Alexander Spröwitz, Alexandre Tuleu, Massimo Vespignani, Mostafa Ajallooeian, Emilie Badri, and Auke Jan Ijspeert. "Towards Dynamic Trot Gait Locomotion: Design, Control, and Experiments with Cheetah-cub, a Compliant Quadruped Robot". *The International Journal of Robotics Research* (2013).

[16] D. Lakatos, K. Ploeger, F. Löffl, D. Seidel, F. Schmidt, T. Gumpert, F. John, T. Bertram, and A. Albu-Schäffer. "Dynamic Locomotion Gaits of a Compliantly Actuated Quadruped With SLIP-Like Articulated Legs Embodied in the Mechanical Design". *IEEE Robotics and Automation Letters* 3.4 (Oct. 2018), pp. 3908–3915. ISSN: 2377-3766. DOI: 10.1109/LRA.2018.2857511.

[17] D. Lakatos, M. Görner, F. Petit, A. Dietrich, and A. Albu-Schäffer. "A modally adaptive control for multi-contact cyclic motions in compliantly actuated robotic systems". *Intelligent Robots and Systems, Intl Conf on*. 2013, pp. 5388–5395.

[18] D. Lakatos, F. Petit, and A. Albu-Schäffer. "Nonlinear Oscillations for Cyclic Movements in Human and Robotic Arms". *Robotics, Transactions on* 30.4 (Aug. 2014), pp. 865–879. ISSN: 1552-3098.

[19] D. Lakatos and A. Albu-Schäffer. "Neuron model interpretation of a cyclic motion control concept". *Intl Conf on Biomedical Robotics and Biomechatronics*. Aug. 2014, pp. 905–910.

[20] Wulfram Gerstner. "Hebbian Learning and Plasticity". *From Neuron to Cognition Via Computational Neuroscience*. Computational Neuroscience Series. MIT Press, 2016. Chap. 6, pp. 199–218. ISBN: 9780262034968.

[21] Guo-qiang Bi and Mu-ming Poo. "Synaptic Modifications in Cultured Hippocampal Neurons: Dependence on Spike Timing, Synaptic Strength, and Postsynaptic Cell Type". *Journal of Neuroscience* 18.24 (1998), pp. 10464–10472. ISSN: 0270-6474. DOI: 10.1523/JNEUROSCI.18-24-10464.1998. eprint: https://www.jneurosci.org/content/18/24/10464.full.pdf.

[22] Demis Hassabis, Dharshan Kumaran, Christopher Summerfield, and Matthew Botvinick. "Neuroscience-Inspired Artificial Intelligence". *Neuron* 95.2 (2017), pp. 245–258. ISSN: 0896-6273. DOI: 10.1016/j.neuron.2017.06.011.

[23] Daniela Rus and Michael Thomas Tolley. "Design, fabrication and control of soft robots". *Nature* 521 (2015), pp. 467–475.

[24] S. Wolf et al. “Variable Stiffness Actuators: Review on Design and Components”. *IEEE/ASME Transactions on Mechatronics* 21.5 (Oct. 2016), pp. 2418–2430. ISSN: 1083-4435. DOI: 10.1109/TMECH.2015.2501019.

[25] Diego Torricelli, Jose Gonzalez, Maarten Weckx, René Jiménez-Fabián, Bram Vanderborght, Massimo Sartori, Strahinja Dosen, Dario Farina, Dirk Lefeber, and Jose L Pons. “Human-like compliant locomotion: state of the art of robotic implementations”. *Bioinspiration & Biomimetics* 11.5 (Aug. 2016), p. 051002. DOI: 10.1088/1748-3190/11/5/051002.

[26] D. Lakatos, W. Friedl, and A. Albu-Schäffer. “Eigenmodes of Nonlinear Dynamics: Definition, Existence, and Embodiment into Legged Robots With Elastic Elements”. *IEEE Robotics and Automation Letters* 2.2 (Apr. 2017), pp. 1062–1069. ISSN: 2377-3766. DOI: 10.1109/LRA.2017.2658018.

[27] Philipp Stratmann, Alin Albu-Schäffer, and Henrik Jörntell. “Scaling Our World View: How Monoamines Can Put Context Into Brain Circuitry”. *Frontiers in Cellular Neuroscience* 12 (2018), p. 506. ISSN: 1662-5102. DOI: 10.3389/fncel.2018.00506.

[28] T. Buschmann, A. Ewald, A. von Twickel, and A. Buschges. “Controlling legs for locomotion-insights from robotics and neurobiology”. *Bioinspir Biomim* 10.4 (Aug. 2015), p. 041001.

[29] Koushil Sreenath, Hae-Won Park, Ioannis Poulakakis, and JW Grizzle. “A Compliant Hybrid Zero Dynamics Controller for Stable, Efficient and Fast Bipedal Walking on MABEL”. *Int J Robot Res* (2010).

[30] A.S. Shiriaev, L.B. Freidovich, and I.R. Manchester. “Can we make a robot ballerina perform a pirouette? Orbital stabilization of periodic motions of underactuated mechanical systems”. *Annu Rev Control* 32 (July 2008), pp. 200–211.

[31] David J. Braun, Matthew Howard, and Sethu Vijayakumar. “Exploiting Variable Stiffness in Explosive Movement Tasks”. *Robotics: Science and Systems VII*. Los Angeles, CA, USA, June 2011.

[32] Tobias Siebert and Christian Rode. “Computational modeling of muscle biomechanics”. *Computational Modelling of Biomechanics and Biotribology in the Musculoskeletal System*. Ed. by Z Jin. 1st ed. Woodhead Publishing - Elsevier, 2014, pp. 173–204. ISBN: 9780857096616.

[33] Stefano Stramigioli and Michel van Dijk. “Energy Conservation Limit Cycle Oscillations”. *International Federation Of Automatic Control, Proceedings Of The 17th World Congress*. 2008, pp. 15666–15671.

[34] Dominic Lakatos and Alin Albu-Schäffer. “Switching Based Limit Cycle Control for Compliantly Actuated Second-Order Systems”. *Proceedings of the IFAC World Congress*. Vol. 19. 1. 2014, pp. 6392–6399.

[35] Kenneth D. Miller and David J. C. MacKay. “The Role of Constraints in Hebbian Learning”. *Neural Computation* 6 (1994), pp. 100–126.

[36] Philipp Stratmann, Dominic Lakatos, and Alin Albu-Schäffer. “Neuromodulation and Synaptic Plasticity for the Control of Fast Periodic Movement: Energy Efficiency in Coupled Compliant Joints via PCA”. *Frontiers in Neurorobotics* 10 (2016), p. 2. ISSN: 1662-5218. DOI: 10.3389/fnbot.2016.00002.

[37] P. J. Whelan, G. W. Hiebert, and K. G. Pearson. "Plasticity of the extensor group I pathway controlling the stance to swing transition in the cat". *J. Neurophysiol.* 74.6 (Dec. 1995), pp. 2782–2787.

[38] Erkki Oja. "Simplified neuron model as a principal component analyzer". *Journal of Mathematical Biology* 15.3 (Nov. 1982), pp. 267–273. ISSN: 0303-6812.

[39] E. Jankowska. "Interneuronal relay in spinal pathways from proprioceptors". *Progress in Neurobiology* 38.4 (1992), pp. 335–378.

[40] Marco Santello and Catherine E. Lang. "Are Movement Disorders and Sensorimotor Injuries Pathologic Synergies? When Normal Multi-Joint Movement Synergies Become Pathologic". *Frontiers in Human Neuroscience* 8 (2015), p. 1050. ISSN: 1662-5161. DOI: 10.3389/fnhum.2014.01050.

[41] P. J. Whelan, G. W. Hiebert, and K. G. Pearson. "Stimulation of the group I extensor afferents prolongs the stance phase in walking cats". *Exp Brain Res* 103.1 (1995), pp. 20–30.

[42] G. W. Hiebert, P. J. Whelan, A. Prochazka, and K. G. Pearson. "Contribution of hind limb flexor muscle afferents to the timing of phase transitions in the cat step cycle". *J. Neurophysiol.* 75.3 (Mar. 1996), pp. 1126–1137.

[43] F. Lacquaniti, Y. P. Ivanenko, and M. Zago. "Patterned control of human locomotion". *Journal of Physiology (Lond.)* 590.10 (May 2012), pp. 2189–2199.

[44] Cristiano Alessandro, Ioannis Delis, Francesco Nori, Stefano Panzeri, and Bastien Berret. "Muscle synergies in neuroscience and robotics: from input-space to task-space perspectives". *Frontiers in Computational Neuroscience* 7 (2013), p. 43. ISSN: 1662-5188. DOI: 10.3389/fncom.2013.00043.

[45] Marco Santello et al. "Hand synergies: Integration of robotics and neuroscience for understanding the control of biological and artificial hands". *Physics of Life Reviews* 17 (2016), pp. 1–23. ISSN: 1571-0645.

[46] Marco Santello, Gabriel Baud-Bovy, and Henrik Jörntell. "Neural bases of hand synergies". *Frontiers in Computational Neuroscience* 7 (2013), p. 23. ISSN: 1662-5188. DOI: 10.3389/fncom.2013.00023.

[47] Henrik Jörntell. "Synergy Control in Subcortical Circuitry: Insights from Neurophysiology". *Human and Robot Hands: Sensorimotor Synergies to Bridge the Gap Between Neuroscience and Robotics*. Ed. by Alessandro Bianchi Matteoand Moscatelli. Cham: Springer International Publishing, 2016, pp. 61–68. ISBN: 978-3-319-26706-7. DOI: 10.1007/978-3-319-26706-7_5.

[48] O. Kiehn. "Decoding the organization of spinal circuits that control locomotion". *Nature Reviews Neuroscience* 17.4 (Apr. 2016), pp. 224–238.

[49] Nikolai Aleksandrevich Bernstein. *The co-ordination and regulation of movements*. 1st English ed. Oxford: Pergamon Press, 1967.

[50] D. J. Clark, L. H. Ting, F. E. Zajac, R. R. Neptune, and S. A. Kautz. "Merging of healthy motor modules predicts reduced locomotor performance and muscle coordination complexity post-stroke". *Journal of Neurophysiology* 103.2 (Feb. 2010), pp. 844–857.

[51] A. J. Levine, C. A. Hinckley, K. L. Hilde, S. P. Driscoll, T. H. Poon, J. M. Montgomery, and S. L. Pfaff. "Identification of a cellular node for motor control pathways". *Nature Neuroscience* 17.4 (Apr. 2014), pp. 586–593.

[52] S. M. Danner, U. S. Hofstoetter, B. Freundl, H. Binder, W. Mayr, F. Rattay, and K. Minassian. “Human spinal locomotor control is based on flexibly organized burst generators”. *Brain* 138.Pt 3 (Mar. 2015), pp. 577–588.

[53] S. Perez-Nombela, F. Barroso, D. Torricelli, A. de Los Reyes-Guzman, A. J. Del-Ama, J. Gomez-Soriano, J. L. Pons, and A. Gil-Agudo. “Modular control of gait after incomplete spinal cord injury: differences between sides”. *Spinal Cord* 55.1 (Jan. 2017), pp. 79–86.

[54] Tomohiko Takei, Joachim Confais, Saeka Tomatsu, Tomomichi Oya, and Kazuhiko Seki. “Neural basis for hand muscle synergies in the primate spinal cord”. *Proceedings of the National Academy of Sciences* 114.32 (2017), pp. 8643–8648.

[55] Michael Graziano. “The Organization of Behavioral Repertoire in Motor Cortex”. *Annual Review of Neuroscience* 29.1 (2006). PMID: 16776581, pp. 105–134. DOI: 10.1146/annurev.neuro.29.051605.112924.

[56] S. A. Overduin, A. d’Avella, J. M. Carmena, and E. Bizzi. “Microstimulation activates a handful of muscle synergies”. *Neuron* 76.6 (Dec. 2012), pp. 1071–1077.

[57] Juan A. Gallego, Matthew G. Perich, Lee E. Miller, and Sara A. Solla. “Neural Manifolds for the Control of Movement”. *Neuron* 94.5 (2017), pp. 978–984. ISSN: 0896-6273. DOI: 10.1016/j.neuron.2017.05.025.

[58] Fredrik Bengtsson and Henrik Jörntell. “Specific Relationship between Excitatory Inputs and Climbing Fiber Receptive Fields in Deep Cerebellar Nuclear Neurons”. *PLOS ONE* 9.1 (Jan. 2014), pp. 1–9. DOI: 10.1371/journal.pone.0084616.

[59] Henrik Jörntell. “Cerebellar physiology: links between microcircuitry properties and sensorimotor functions”. *The Journal of Physiology* 595.1 (2017), pp. 11–27. ISSN: 1469-7793. DOI: 10.1113/JP272769.

[60] Subhi Shaker Barikhan, Florentin Wörgötter, and Poramate Manoonpong. “Multiple Decoupled CPGs with Local Sensory Feedback for Adaptive Locomotion Behaviors of Bio-inspired Walking Robots”. *From Animals to Animats 13*. Ed. by AngelP. del Pobil, Eris Chinellato, Ester Martinez-Martin, John Hallam, Enric Cervera, and Antonio Morales. Vol. 8575. Lecture Notes in Computer Science. Springer International Publishing, 2014, pp. 65–75. ISBN: 978-3-319-08863-1.

[61] B.W. Verdaasdonk, H.F.J.M. Koopman, and F.C.T. Van Der Helm. “Energy efficient and robust rhythmic limb movement by central pattern generators”. *Neural Networks* 19.4 (2006), pp. 388–400. ISSN: 0893-6080.

[62] Timo Nachstedt, Florentin Wörgötter, and Poramate Manoonpong. “Adaptive Neural Oscillator with Synaptic Plasticity Enabling Fast Resonance Tuning”. *Artificial Neural Networks and Machine Learning at ICANN 2012*. Ed. by Alessandro Villa, Wlodzislaw Duch, Peter Erdi, Francesco Masulli, and Günther Palm. Vol. 7552. Lecture Notes in Computer Science. Springer Berlin Heidelberg, 2012, pp. 451–458. ISBN: 978-3-642-33268-5.

[63] X. Xiong, F. Wörgötter, and P. Manoonpong. “Adaptive and Energy Efficient Walking in a Hexapod Robot Under Neuromechanical Control and Sensorimotor Learning”. *Cybernetics, Transactions on* PP.99 (2015), pp. 1–1. ISSN: 2168-2267.

[64] Jonas Buchli and Auke Jan Ijspeert. “Self-organized adaptive legged locomotion in a compliant quadruped robot”. *Autonomous Robots* 25.4 (2008), pp. 331–347. ISSN: 0929-5593.

[65] Yuval Yanai, Nofya Adamit, Zvi Israel, Ran Harel, and Yifat Prut. "Coordinate Transformation is First Completed Downstream of Primary Motor Cortex". *Journal of Neuroscience* 28.7 (2008), pp. 1728–1732. ISSN: 0270-6474. DOI: 10.1523/JNEUROSCI.4662-07.2008.

[66] W. Roozing, Z. Li, D. G. Caldwell, and N. G. Tsagarakis. "Design Optimisation and Control of Compliant Actuation Arrangements in Articulated Robots for Improved Energy Efficiency". *IEEE Robotics and Automation Letters* 1.2 (July 2016), pp. 1110–1117. ISSN: 2377-3766. DOI: 10.1109/LRA.2016.2521926.

[67] Navvab Kashiri et al. "An Overview on Principles for Energy Efficient Robot Locomotion". *Frontiers in Robotics and AI* 5 (2018), p. 129. ISSN: 2296-9144. DOI: 10.3389/frobt.2018.00129.

[68] A. J. Young and D. P. Ferris. "State of the Art and Future Directions for Lower Limb Robotic Exoskeletons". *IEEE Transactions on Neural Systems and Rehabilitation Engineering* 25.2 (Feb. 2017), pp. 171–182. ISSN: 1534-4320. DOI: 10.1109/TNSRE.2016.2521160.

[69] Hans Moravec. *Mind Children: The Future of Robot and Human Intelligence*. Cambridge, MA, USA: Harvard University Press, 1988. ISBN: 0-674-57616-0.

[70] Frederico A.C. Azevedo, Ludmila R.B. Carvalho, Lea T. Grinberg, José Marcelo Farfel, Renata E.L. Ferretti, Renata E.P. Leite, Wilson Jacob Filho, Roberto Lent, and Suzana Herculano-Houzel. "Equal numbers of neuronal and nonneuronal cells make the human brain an isometrically scaled-up primate brain". *Journal of Comparative Neurology* 513.5 (2009), pp. 532–541. DOI: 10.1002/cne.21974. eprint: https://onlinelibrary.wiley.com/doi/pdf/10.1002/cne.21974.

[71] Sjoerd J. Finnema et al. "Imaging synaptic density in the living human brain". *Science Translational Medicine* 8.348 (2016), 348ra96–348ra96. ISSN: 1946-6234. DOI: 10.1126/scitranslmed.aaf6667. eprint: https://stm.sciencemag.org/content/8/348/348ra96.full.pdf.

[72] D. Purves, G.J. Augustine, R.D. Mooney, M.L. Platt, D. Fitzpatrick, W.C. Hall, A.S. LaMantia, and L.E. White. "Neuroscience". Ed. by George J. Augustine, David Fitzpatrick, William C. Hall, Anthony-Samuel LaMantia, and Dale Purves. Oxford University Press Incorporated, 2018. Chap. Neurotransmitters, Receptors, and Their Effects. ISBN: 9781605357416.

[73] W.J. Savitch. *Pascal, an introduction to the art and science of programming*. Benjamin/Cummings series in structured programming. Benjamin/Cummings Pub. Co., 1984.

[74] Robert Ajemian and Neville Hogan. "Experimenting with Theoretical Motor Neuroscience". *Journal of Motor Behavior* 42.6 (2010). PMID: 21184350, pp. 333–342. DOI: 10.1080/00222895.2010.529332. eprint: https://doi.org/10.1080/00222895.2010.529332.

[75] K. J. Sekiguchi, P. Shekhtmeyster, K. Merten, A. Arena, D. Cook, E. Hoffman, A. Ngo, and A. Nimmerjahn. "Imaging large-scale cellular activity in spinal cord of freely behaving mice". *Nat Commun* 7 (Apr. 2016), p. 11450.

[76] T. W. Fawcett and A. D. Higginson. "Heavy use of equations impedes communication among biologists". *Proc. Natl. Acad. Sci. U.S.A.* 109.29 (July 2012), pp. 11735–11739.

[77] NN. “The practice of theoretical neuroscience”. *Nat. Neurosci.* 8.12 (Dec. 2005), p. 1627.

[78] Kunlin Wei, Joshua I. Glaser, Linna Deng, Christopher K. Thompson, Ian H. Stevenson, Qining Wang, Thomas George Hornby, Charles J. Heckman, and Konrad P. Kording. “Serotonin Affects Movement Gain Control in the Spinal Cord”. *Journal of Neuroscience* 34.38 (2014), pp. 12690–12700. ISSN: 0270-6474.

[79] C. J. Heckman, A. S. Hyngstrom, and M. D. Johnson. “Active properties of motoneurone dendrites: diffuse descending neuromodulation, focused local inhibition”. *Journal of Physiology (Lond.)* 586.5 (Mar. 2008), pp. 1225–1231.

[80] H. Höppner, M. Grebenstein, and P. van der Smagt. “Two-dimensional orthoglide mechanism for revealing areflexive human arm mechanical properties”. *2015 IEEE/RSJ International Conference on Intelligent Robots and Systems (IROS)*. Sept. 2015, pp. 1178–1185. DOI: 10.1109/IROS.2015.7353519.

[81] Manju A Kurian, Paul Gissen, Martin Smith, Simon JR Heales, and Peter T Clayton. “The monoamine neurotransmitter disorders: an expanding range of neurological syndromes”. *The Lancet Neurology* 10.8 (2011), pp. 721–733. ISSN: 1474-4422. DOI: 10.1016/S1474-4422(11)70141-7.

[82] Philipp Stratmann, Dominic Lakatos, Mehmet Can Özparpucu, and Alin Albu-Schäffer. “Legged Elastic Multibody Systems: Adjusting Limit Cycles to Close-to-Optimal Energy Efficiency”. *IEEE Robotics and Automation Letters* 2.2 (Apr. 2017), pp. 436–443. DOI: 10.1109/LRA.2016.2633580.

[83] B.F. Feeny and R. Kappagantu. “On The Physical Interpretation Of Proper Orthogonal Modes In Vibrations”. *J. Sound Vibration* 211.4 (1998), pp. 607–616. ISSN: 0022-460X.

[84] D. Lakatos, D. Seidel, W. Friedl, and A. Albu-Schäffer. “Targeted jumping of compliantly actuated hoppers based on discrete planning and switching control”. *Intelligent Robots and Systems, Intl Conf on*. Sept. 2015, pp. 5802–5808.

[85] D. J. Farris and G. S. Sawicki. “The mechanics and energetics of human walking and running: a joint level perspective”. *J R Soc Interface* 9.66 (Jan. 2012), pp. 110–118.

[86] Michael A. Patterson and Anil V. Rao. “GPOPS-II: A MATLAB Software for Solving Multiple-Phase Optimal Control Problems Using hp-Adaptive Gaussian Quadrature Collocation Methods and Sparse Nonlinear Programming”. *ACM Trans. Math. Softw.* 41.1 (Oct. 2014), 1:1–1:37. ISSN: 0098-3500. DOI: 10.1145/2558904.

[87] T. Lorenz Wächter Andreasand Biegler. “On the implementation of an interior-point filter line-search algorithm for large-scale nonlinear programming”. *Math Program* 106.1 (2005), pp. 25–57. ISSN: 1436-4646. DOI: 10.1007/s10107-004-0559-y.

[88] Philip Holmes, Robert J. Full, Dan Koditschek, and John Guckenheimer. “The Dynamics of Legged Locomotion: Models, Analyses, and Challenges”. *SIAM Review* 48.2 (2006), pp. 207–304.

[89] Adrian Lai, Anthony G. Schache, Yi-Chung Lin, and Marcus G. Pandy. “Tendon elastic strain energy in the human ankle plantar-flexors and its role with increased running speed”. *Journal of Experimental Biology* 217.17 (2014), pp. 3159–3168. ISSN: 0022-0949.

[90] S. M. ElBasiouny, J. E. Schuster, and C. J. Heckman. "Persistent inward currents in spinal motoneurons: Important for normal function but potentially harmful after spinal cord injury and in amyotrophic lateral sclerosis". *Clinical Neurophysiology* (2010), pp. 1669–1679. DOI: 10.1016/j.clinph.2009.12.041.

[91] R. F. Martin, L. M. Jordan, and W. D. Willis. "Differential projections of cat medullary raphe neurons demonstrated by retrograde labelling following spinal cord lesions". *The Journal of Comparative Neurology* 182.1 (1978), pp. 77–88. ISSN: 1096-9861. DOI: 10.1002/cne.901820106.

[92] A.D. Loewy. "Raphe pallidus and raphe obscurus projections to the intermediolateral cell column in the rat". *Brain Research* 222.1 (1981), pp. 129–133. ISSN: 0006-8993. DOI: 10.1016/0006-8993(81)90946-X.

[93] R. Nieuwenhuys, J. Voogd, and C. van Huijzen. "The Reticular Formation and the Monoaminergic and Cholinergic Cell Groups". *The Human Central Nervous System*. Berlin, Heidelberg: Springer Berlin Heidelberg, 2008, pp. 889–916. ISBN: 978-3-540-34686-9. DOI: 10.1007/978-3-540-34686-9_22.

[94] C. Watson, G. Paxinos, and L. Puelles. *The Mouse Nervous System*. Academic Press. Elsevier Academic Press, 2012. ISBN: 9780123694973.

[95] Sanya A. Springfield and Gwen-Marie Moolenaar. "Differences in the responses of raphe nuclei to repetitive somatosensory stimulation". *Experimental Neurology* 79.2 (1983), pp. 360–370. ISSN: 0014-4886. DOI: 10.1016/0014-4886(83)90219-4.

[96] S. C. Veasey, C. A. Fornal, C. W. Metzler, and B. L. Jacobs. "Response of serotonergic caudal raphe neurons in relation to specific motor activities in freely moving cats". *Journal of Neuroscience* 15.7 Pt 2 (July 1995), pp. 5346–5359.

[97] Casimir A. Fornal, Christine W. Metzler, Franco Marrosu, Luiz E. Ribiero-do-Valle, and Barry L. Jacobs. "A subgroup of dorsal raphe serotonergic neurons in the cat is strongly activated during oral-buccal movements". *Brain Research* 716.1-2 (1996), pp. 123–133. ISSN: 0006-8993. DOI: 10.1016/0006-8993(96)00006-6.

[98] J. F. Perrier, H. B. Rasmussen, R. K. Christensen, and A. V. Petersen. "Modulation of the intrinsic properties of motoneurons by serotonin". *Curr. Pharm. Des.* 19.24 (2013), pp. 4371–4384.

[99] Matthew D. Abbinanti and Ronald M. Harris-Warrick. "Serotonin modulates multiple calcium current subtypes in commissural interneurons of the neonatal mouse". *Journal of Neurophysiology* 107.8 (2012), pp. 2212–2219. ISSN: 0022-3077. DOI: 10.1152/jn.00768.2011.

[100] T.C. Cope. *Motor Neurobiology of the Spinal Cord*. Frontiers in Neuroscience. CRC Press, 2001. ISBN: 9781420042641.

[101] Jean-François Perrier and Rodolfo Delgado-Lezama. "Synaptic Release of Serotonin Induced by Stimulation of the Raphe Nucleus Promotes Plateau Potentials in Spinal Motoneurons of the Adult Turtle". *The Journal of Neuroscience* 25.35 (2005), pp. 7993–7999. DOI: 10.1523/JNEUROSCI.1957-05.2005.

[102] I.D. Hentall, A. Pinzon, and B.R. Noga. "Spatial and temporal patterns of serotonin release in the rat's lumbar spinal cord following electrical stimulation of the nucleus raphe magnus". *Neuroscience* 142.3 (2006), pp. 893–903. ISSN: 0306-4522. DOI: 10.1016/j.neuroscience.2006.06.038.

[103] C. Crone, H. Hultborn, O. Kiehn, L. Mazieres, and H. Wigstrom. "Maintained changes in motoneuronal excitability by short-lasting synaptic inputs in the decerebrate cat". *Journal of Physiology (Lond.)* 405 (Nov. 1988), pp. 321–343.

[104] J. Best, H. F. Nijhout, and M. Reed. "Serotonin synthesis, release and reuptake in terminals: a mathematical model". *Theor Biol Med Model* 7 (2010), p. 34.

[105] M. R. Brumley, I. D. Hentall, A. Pinzon, B. H. Kadam, A. Blythe, F. J. Sanchez, A. M. Taberner, and B. R. Noga. "Serotonin concentrations in the lumbosacral spinal cord of the adult rat following microinjection or dorsal surface application". *J. Neurophysiol.* 98.3 (Sept. 2007), pp. 1440–1450.

[106] S. Verleysdonk, B. Hamprecht, M. Rapp, and J. Wellard. "Uptake and metabolism of serotonin by ependymal primary cultures". *Neurochem. Res.* 29.9 (Sept. 2004), pp. 1739–1747.

[107] G. F. Molodtsova. "[Effect of prolonged cold exposure on monoamine oxidase activity and kinetics and on serotonin metabolism in the rat brain]". *Biull Eksp Biol Med* 96.9 (Sept. 1983), pp. 16–18.

[108] D. M. Katz and H. K. Kimelberg. "Kinetics and autoradiography of high affinity uptake of serotonin by primary astrocyte cultures". *J. Neurosci.* 5.7 (July 1985), pp. 1901–1908.

[109] Bernard Widrow and Marcian E. Hoff. "Adaptive Switching Circuits". *1960 IRE WESCON Convention Record, Part 4*. New York: IRE, 1960, pp. 96–104.

[110] Stephen José Hanson. "A stochastic version of the delta rule". *Physica D: Nonlinear Phenomena* 42.1 (1990), pp. 265–272. ISSN: 0167-2789. DOI: https://doi.org/10.1016/0167-2789(90)90081-Y.

[111] M. Azad and R. Featherstone. "Modelling the Contact between a Rolling Sphere and a Compliant Ground Plane". *Australasian Conf. Robotics and Automation* (2010).

[112] Herbert Hensel. "Cutaneous Thermoreceptors". *Somatosensory System*. Ed. by Ainsley Iggo. Berlin, Heidelberg: Springer Berlin Heidelberg, 1973, pp. 79–110. ISBN: 978-3-642-65438-1. DOI: 10.1007/978-3-642-65438-1_4.

[113] J. N. Davis. "The response to stretch of human intercostal muscle spindles studied in vitro". *Journal of Physiology (Lond.)* 249.3 (Aug. 1975), pp. 561–579.

[114] John C. Rothwell. "Proprioceptors in Muscle, Joint and Skin". *Control of Human Voluntary Movement*. Boston, MA: Springer US, 1987, pp. 74–104. ISBN: 978-1-4684-7688-0. DOI: 10.1007/978-1-4684-7688-0_4.

[115] Michael A. Muniak, Supratim Ray, Steven S. Hsiao, J. Frank Dammann, and Sliman J. Bensmaia. "The Neural Coding of Stimulus Intensity: Linking the Population Response of Mechanoreceptive Afferents with Psychophysical Behavior". *The Journal of Neuroscience* 27.43 (2007), pp. 11687–11699. DOI: 10.1523/JNEUROSCI.1486-07.2007.

[116] S. J. Bensmaia. "Tactile intensity and population codes". *Behavioural Brain Research* 190.2 (July 2008), pp. 165–173.

[117] Friedemann Zenke, Guillaume Hennequin, and Wulfram Gerstner. "Synaptic plasticity in neural networks needs homeostasis with a fast rate detector." *PLoS computational biology* 9.11 (Nov. 2013).

[118] Jean-Pascal Pfister and Wulfram Gerstner. "Triplets of Spikes in a Model of Spike Timing-Dependent Plasticity". *The Journal of Neuroscience* 26.38 (Sept. 2006), pp. 9673–9682. ISSN: 1529-2401.

[119] M. C. van Rossum, G. Q. Bi, and G. G. Turrigiano. "Stable Hebbian learning from spike timing-dependent plasticity". *J. Neurosci.* 20.23 (Dec. 2000), pp. 8812–8821.

[120] Y. Nishimura, S. I. Perlmutter, R. W. Eaton, and E. E. Fetz. "Spike-timing-dependent plasticity in primate corticospinal connections induced during free behavior". *Neuron* 80.5 (Dec. 2013), pp. 1301–1309.

[121] C.J. Heckman, Robert H. Lee, and Robert M. Brownstone. "Hyperexcitable dendrites in motoneurons and their neuromodulatory control during motor behavior". *Trends in Neurosciences* 26.12 (2003), pp. 688–695. ISSN: 0166-2236.

[122] K.G. Pearson. "Role of sensory feedback in the control of stance duration in walking cats". *Brain Research Reviews* 57.1 (2008). Networks in Motion, pp. 222–227. ISSN: 0165-0173.

[123] A. T. DeLeo, T. A. Dierks, R. Ferber, and I. S. Davis. "Lower extremity joint coupling during running: a current update". *Clin Biomech (Bristol, Avon)* 19.10 (Dec. 2004), pp. 983–991.

[124] N. Chen, J. Bayer, S. Urban, and P. van der Smagt. "Efficient movement representation by embedding Dynamic Movement Primitives in deep autoencoders". *2015 IEEE-RAS 15th International Conference on Humanoid Robots (Humanoids)*. Nov. 2015, pp. 434–440. DOI: 10.1109/HUMANOIDS.2015.7363570.

[125] G. Cybenko. "Approximation by superpositions of a sigmoidal function". *Mathematics of Control, Signals and Systems* 2.4 (1989), pp. 303–314. ISSN: 1435-568X. DOI: 10.1007/BF02551274.

[126] Kurt Hornik. "Approximation capabilities of multilayer feedforward networks". *Neural Networks* 4.2 (1991), pp. 251–257. ISSN: 0893-6080. DOI: 10.1016/0893-6080(91)90009-T.

[127] Kjell Fuxe, Annica B. Dahlström, Gösta Jonsson, Daniel Marcellino, Michele Guescini, Mauro Dam, Paul Manger, and Luigi Agnati. "The discovery of central monoamine neurons gave volume transmission to the wired brain". *Progress in Neurobiology* 90.2 (2010), pp. 82–100. ISSN: 0301-0082. DOI: 10.1016/j.pneurobio.2009.10.012.

[128] H. Johansson and H. Silfvenius. "Connexions from large, ipsilateral hind limb muscle and skin afferents to the rostral main cuneate nucleus and to the nucleus X region in the cat". *Journal of Physiology (Lond.)* 265.2 (Feb. 1977), pp. 395–428.

[129] Jean-Pierre Hornung. "The human raphe nuclei and the serotonergic system". *Journal of Chemical Neuroanatomy* 26.4 (2003). Special Issue on the Human Brain - The Structural Basis for understanding Human Brain function and dysfunction, pp. 331–343. ISSN: 0891-0618. DOI: 10.1016/j.jchemneu.2003.10.002.

[130] Y. Shinoda, P. Zarzecki, and H. Asanuma. "Spinal branching of pyramidal tract neurons in the monkey". *Experimental Brain Research* 34.1 (1979), pp. 59–72. ISSN: 1432-1106.

[131] G. Skagerberg and A. Bjorklund. "Topographic principles in the spinal projections of serotonergic and non-serotonergic brainstem neurons in the rat". *Neuroscience* 15.2 (June 1985), pp. 445–480.

[132] Carmen Cavada, A. Margriet Huisman, and Henricus G.J.M. Kuypers. “Retrograde double labeling of neurons: the combined use of horseradish peroxidase and diamidino yellow dihydrochloride (DY 2HCl) compared with true blue and DY 2HCl in rat descending brainstem pathways”. *Brain Research* 308.1 (1984), pp. 123–136. ISSN: 0006-8993.

[133] Florence Cotel, Richard Exley, Stephanie J. Cragg, and Jean-François Perrier. “Serotonin spillover onto the axon initial segment of motoneurons induces central fatigue by inhibiting action potential initiation”. *Proceedings of the National Academy of Sciences* 110.12 (2013), pp. 4774–4779. DOI: 10.1073/pnas.1216150110.

[134] Hideaki Myoga, Satoshi Nonaka, Kiyoji Matsuyama, and Shigemi Mori. “Postnatal development of locomotor movements in normal and para-chlorophenylalanine-treated newborn rats”. *Neuroscience Research* 21.3 (1995), pp. 211–221. ISSN: 0168-0102. DOI: 10.1016/0168-0102(94)00857-C.

[135] Jean-François Pflieger, François Clarac, and Laurent Vinay. “Postural Modifications and Neuronal Excitability Changes Induced by a Short-Term Serotonin Depletion during Neonatal Development in the Rat”. *Journal of Neuroscience* 22.12 (2002), pp. 5108–5117. ISSN: 0270-6474.

[136] E. Pearlstein, F. Ben Mabrouk, J. F. Pflieger, and L. Vinay. “Serotonin refines the locomotor-related alternations in the in vitro neonatal rat spinal cord”. *Eur. J. Neurosci.* 21.5 (Mar. 2005), pp. 1338–1346.

[137] N. C. Heglund and C. R. Taylor. “Speed, stride frequency and energy cost per stride: how do they change with body size and gait?” *Journal of Experimental Biology* 138.1 (1988), pp. 301–318. ISSN: 0022-0949.

[138] Daniel P. Ferris, Micky Louie, and Claire T. Farley. “Running in the real world: adjusting leg stiffness for different surfaces”. *Proceedings of the Royal Society of London B: Biological Sciences* 265.1400 (1998), pp. 989–994. ISSN: 0962-8452.

[139] Johannes Mathis, Victor Gurfinkel, and A Struppler. “Facilitation of motor evoked potentials by postcontraction response (Kohnstamm phenomenon)”. *Electroencephalography and Clinical Neurophysiology/Electromyography and Motor Control* 101 (Sept. 1996), pp. 289–97.

[140] Arko Ghosh, John Rothwell, and Patrick Haggard. “Using voluntary motor commands to inhibit involuntary arm movements”. *Proceedings of the Royal Society of London B: Biological Sciences* 281.1794 (2014). ISSN: 0962-8452. DOI: 10.1098/rspb.2014.1139. eprint: http://rspb.royalsocietypublishing.org/content/281/1794/20141139.full.pdf.

[141] R. A. Silver. “Neuronal arithmetic”. *Nat. Rev. Neurosci.* 11.7 (July 2010), pp. 474–489.

[142] M. Carandini and D. J. Heeger. “Normalization as a canonical neural computation”. *Nat. Rev. Neurosci.* 13.1 (Jan. 2012), pp. 51–62.

[143] Rita Bardoni, Pier Cosimo Magherini, and Amy B. MacDermott. “NMDA EPSCs at Glutamatergic Synapses in the Spinal Cord Dorsal Horn of the Postnatal Rat”. *Journal of Neuroscience* 18.16 (1998), pp. 6558–6567. ISSN: 0270-6474. DOI: 10.1523/JNEUROSCI.18-16-06558.1998. eprint: https://www.jneurosci.org/content/18/16/6558.full.pdf.

[144] A. Konnerth, B. U. Keller, and A. Lev-Tov. "Patch clamp analysis of excitatory synapses in mammalian spinal cord slices". *Pflügers Archiv* 417.3 (Nov. 1990), pp. 285–290. ISSN: 1432-2013. DOI: 10.1007/BF00370994.

[145] Jeremy S. Dittman and Joshua M. Kaplan. "Behavioral Impact of Neurotransmitter-Activated G-Protein-Coupled Receptors: Muscarinic and GABAB Receptors Regulate Caenorhabditis elegans Locomotion". *Journal of Neuroscience* 28.28 (2008), pp. 7104–7112. ISSN: 0270-6474. DOI: 10.1523/JNEUROSCI.0378-08.2008. eprint: https://www.jneurosci.org/content/28/28/7104.full.pdf.

[146] Y. Prut and S. I. Perlmutter. "Firing properties of spinal interneurons during voluntary movement. I. State-dependent regularity of firing". *Journal of Neuroscience* 23.29 (Oct. 2003), pp. 9600–9610.

[147] Uri Shalit, Nofya Zinger, Mati Joshua, and Yifat Prut. "Descending Systems Translate Transient Cortical Commands into a Sustained Muscle Activation Signal". *Cerebral Cortex* 22.8 (2012), pp. 1904–1914. DOI: 10.1093/cercor/bhr267.

[148] Anton Spanne, Pontus Geborek, Fredrik Bengtsson, and Henrik Jörntell. "Spike generation estimated from stationary spike trains in a variety of neurons in vivo". *Frontiers in Cellular Neuroscience* 8.199 (2014). ISSN: 1662-5102.

[149] P. V. Zelenin, L. J. Hsu, V. F. Lyalka, G. N. Orlovsky, and T. G. Deliagina. "Putative spinal interneurons mediating postural limb reflexes provide a basis for postural control in different planes". *European Journal of Neuroscience* 41.2 (Jan. 2015), pp. 168–181.

[150] R. K. Powers and M. D. Binder. "Effective synaptic current and motoneuron firing rate modulation". *Journal of Neurophysiology* 74.2 (1995), pp. 793–801. ISSN: 0022-3077.

[151] Randall K. Powers and Marc D. Binder. "Summation of Effective Synaptic Currents and Firing Rate Modulation in Cat Spinal Motoneurons". *Journal of Neurophysiology* 83.1 (2000), pp. 483–500. ISSN: 0022-3077.

[152] H. Hultborn, M. E. Denton, J. Wienecke, and J. B. Nielsen. "Variable amplification of synaptic input to cat spinal motoneurones by dendritic persistent inward current". *Journal of Physiology (Lond.)* 552.Pt 3 (Nov. 2003), pp. 945–952.

[153] S. Cushing, T. Bui, and P. K. Rose. "Effect of Nonlinear Summation of Synaptic Currents on the Input–Output Properties of Spinal Motoneurons". *Journal of Neurophysiology* 94.5 (2005), pp. 3465–3478. ISSN: 0022-3077.

[154] Allison S. Hyngstrom, Michael D. Johnson, and C. J. Heckman. "Summation of Excitatory and Inhibitory Synaptic Inputs by Motoneurons With Highly Active Dendrites". *Journal of Neurophysiology* 99.4 (2008), pp. 1643–1652. ISSN: 0022-3077. DOI: 10.1152/jn.01253.2007. eprint: http://jn.physiology.org/content/99/4/1643.full.pdf.

[155] P. Dayan and L.F. Abbott. *Theoretical Neuroscience: Computational and Mathematical Modeling of Neural Systems*. Computational Neuroscience Series. Massachusetts Institute of Technology Press, 2001. ISBN: 9780262041997.

[156] Cornelia I. Bargmann. "Beyond the connectome: How neuromodulators shape neural circuits". *BioEssays* 34.6 (2012), pp. 458–465. ISSN: 1521-1878. DOI: 10.1002/bies.201100185.

[157] R. W. Berg, A. Alaburda, and J. Hounsgaard. “Balanced inhibition and excitation drive spike activity in spinal half-centers”. *Science* 315.5810 (Jan. 2007), pp. 390–393.

[158] F. S. Chance, L. F. Abbott, and A. D. Reyes. “Gain modulation from background synaptic input”. *Neuron* 35.4 (Aug. 2002), pp. 773–782.

[159] Simon J. Mitchell and R. Angus Silver. “Shunting Inhibition Modulates Neuronal Gain during Synaptic Excitation”. *Neuron* 38.3 (2003), pp. 433–445. ISSN: 0896-6273. DOI: 10.1016/S0896-6273(03)00200-9.

[160] Matthew H. Higgs, Sean J. Slee, and William J. Spain. “Diversity of Gain Modulation by Noise in Neocortical Neurons: Regulation by the Slow Afterhyperpolarization Conductance”. *The Journal of Neuroscience* 26.34 (2006), pp. 8787–8799. DOI: 10.1523/JNEUROSCI.1792-06.2006.

[161] S. M. Sherman and C Koch. “The Control of Retinogeniculate Transmission in the Mammalian Lateral Geniculate Nucleus”. *Experimental Brain Research* 63 (1986), pp. 1–20.

[162] Jeffry S. Isaacson and Massimo Scanziani. “How Inhibition Shapes Cortical Activity”. *Neuron* 72.2 (2011), pp. 231–243. ISSN: 0896-6273. DOI: 10.1016/j.neuron.2011.09.027.

[163] Marc A. Maier Perlmutter Steve I. and and Eberhard E. Fetz. “Activity of Spinal Interneurons and Their Effects on Forearm Muscles During Voluntary Wrist Movements in the Monkey”. *Journal of Neurophysiology* 80.5 (1998). PMID: 9819257, pp. 2475–2494. DOI: 10.1152/jn.1998.80.5.2475. eprint: https://doi.org/10.1152/jn.1998.80.5.2475.

[164] Marc A. Maier, Steve I. Perlmutter, and Eberhard E. Fetz. “Response Patterns and Force Relations of Monkey Spinal Interneurons During Active Wrist Movement”. *Journal of Neurophysiology* 80.5 (1998). PMID: 9819258, pp. 2495–2513. DOI: 10.1152/jn.1998.80.5.2495. eprint: https://doi.org/10.1152/jn.1998.80.5.2495.

[165] E. Ahissar. “Temporal-code to rate-code conversion by neuronal phase-locked loops”. *Neural Computation* 10.3 (Apr. 1998), pp. 597–650.

[166] Mark C. W. van Rossum, Gina G. Turrigiano, and Sacha B. Nelson. “Fast Propagation of Firing Rates through Layered Networks of Noisy Neurons”. *The Journal of Neuroscience* 22.5 (2002), pp. 1956–1966.

[167] Richard B. Stein, E. Roderich Gossen, and Kelvin E. Jones. “Neuronal variability: noise or part of the signal?” *Nature Reviews Neuroscience* 6 (2005), pp. 389–397.

[168] M. Carandini, D. J. Heeger, and W. Senn. “A synaptic explanation of suppression in visual cortex”. *Journal of Neuroscience* 22.22 (Nov. 2002), pp. 10053–10065.

[169] H. Ozeki, I. M. Finn, E. S. Schaffer, K. D. Miller, and D. Ferster. “Inhibitory stabilization of the cortical network underlies visual surround suppression”. *Neuron* 62.4 (May 2009), pp. 578–592.

[170] J. S. Rothman, L. Cathala, V. Steuber, and R. A. Silver. “Synaptic depression enables neuronal gain control”. *Nature* 457.7232 (Feb. 2009), pp. 1015–1018.

[171] P. J. Magistretti and I. Allaman. “A cellular perspective on brain energy metabolism and functional imaging”. *Neuron* 86.4 (May 2015), pp. 883–901.

[172] Lauren E. McElvain, Michael Faulstich, James M. Jeanne, Jeffrey D. Moore, and Sascha du Lac. "Implementation of Linear Sensory Signaling via Multiple Coordinated Mechanisms at Central Vestibular Nerve Synapses". *Neuron* 85.5 (2015), pp. 1132–1144. ISSN: 0896-6273. DOI: 10.1016/j.neuron.2015.01.017.

[173] P. W. Jones and F. Gabbiani. "Logarithmic compression of sensory signals within the dendritic tree of a collision-sensitive neuron". *Journal of Neuroscience* 32.14 (Apr. 2012), pp. 4923–4934.

[174] Fabrizio Gabbiani, Holger G. Krapp, Christof Koch, and Gilles Laurent. "Multiplicative computation in a visual neuron sensitive to looming". *Nature* 420.6913 (2002), pp. 320–324.

[175] I Segev, John Rinzel, and GM Shepherd. *The theoretical foundation of dendritic function: Selected papers of Wilfrid Rall with commentaries*. MIT Press, 1994.

[176] Hysell Oviedo and Alex D. Reyes. "Boosting of neuronal firing evoked with asynchronous and synchronous inputs to the dendrite". *Nature Neuroscience* 5.3 (2002), pp. 261–266. ISSN: 1097-6256. DOI: 10.1038/nn807.

[177] Stephen R. Williams and Greg J. Stuart. "Dependence of EPSP Efficacy on Synapse Location in Neocortical Pyramidal Neurons". *Science* 295.5561 (2002), pp. 1907–1910. ISSN: 0036-8075. DOI: 10.1126/science.1067903. eprint: http://science.sciencemag.org/content/295/5561/1907.full.pdf.

[178] W. Hamish Mehaffey, Brent Doiron, Leonard Maler, and Ray W. Turner. "Deterministic Multiplicative Gain Control with Active Dendrites". *Journal of Neuroscience* 25.43 (2005), pp. 9968–9977. ISSN: 0270-6474. DOI: 10.1523/JNEUROSCI.2682-05.2005. eprint: http://www.jneurosci.org/content/25/43/9968.full.pdf.

[179] Paul Rhodes. "The Properties and Implications of NMDA Spikes in Neocortical Pyramidal Cells". *Journal of Neuroscience* 26.25 (2006), pp. 6704–6715. ISSN: 0270-6474. DOI: 10.1523/JNEUROSCI.3791-05.2006. eprint: http://www.jneurosci.org/content/26/25/6704.full.pdf.

[180] Attila Losonczy and Jeffrey C. Magee. "Integrative Properties of Radial Oblique Dendrites in Hippocampal CA1 Pyramidal Neurons". *Neuron* 50.2 (2006), pp. 291–307. ISSN: 0896-6273. DOI: 10.1016/j.neuron.2006.03.016.

[181] S. Remy, J. Csicsvari, and H. Beck. "Activity-dependent control of neuronal output by local and global dendritic spike attenuation". *Neuron* 61.6 (Mar. 2009), pp. 906–916.

[182] G. Major, M. E. Larkum, and J. Schiller. "Active properties of neocortical pyramidal neuron dendrites". *Annuual Review of Neuroscience* 36 (July 2013), pp. 1–24.

[183] Zsuzsanna Varga, Hongbo Jia, Bert Sakmann, and Arthur Konnerth. "Dendritic coding of multiple sensory inputs in single cortical neurons in vivo". *Proceedings of the National Academy of Sciences* 108.37 (2011), pp. 15420–15425. DOI: 10.1073/pnas.1112355108. eprint: http://www.pnas.org/content/108/37/15420.full.pdf.

[184] H. Jia, N. L. Rochefort, X. Chen, and A. Konnerth. "Dendritic organization of sensory input to cortical neurons in vivo". *Nature* 464.7293 (Apr. 2010), pp. 1307–1312.

[185] N. J. Priebe and D. Ferster. “Neuroscience: Each synapse to its own”. *Nature* 464.7293 (Apr. 2010), pp. 1290–1291.

[186] Sydney Cash and Rafael Yuste. “Input Summation by Cultured Pyramidal Neurons Is Linear and Position-Independent”. *Journal of Neuroscience* 18.1 (1998), pp. 10–15. ISSN: 0270-6474. eprint: http://www.jneurosci.org/content/18/1/10.full.pdf.

[187] Sydney Cash and Rafael Yuste. “Linear Summation of Excitatory Inputs by CA1 Pyramidal Neurons”. *Neuron* 22.2 (1999), pp. 383–394. ISSN: 0896-6273. DOI: 10.1016/S0896-6273(00)81098-3.

[188] F. Longordo, M. S. To, K. Ikeda, and G. J. Stuart. “Sublinear integration underlies binocular processing in primary visual cortex”. *Nature Neuroscience* 16.6 (June 2013), pp. 714–723.

[189] Philipp Stratmann, Hannes Höppner, David Franklin, Patrick van der Smagt, and Alin Albu-Schäffer. “Focused neuromodulation of individual motorpools: confirmation of predictions from the efficient control of biomimetic robots”. *Nature Communications Biology* (2020, to be submitted).

[190] G. Taubin. “Estimation of planar curves, surfaces, and nonplanar space curves defined by implicit equations with applications to edge and range image segmentation”. *IEEE Transactions on Pattern Analysis and Machine Intelligence* 13.11 (Nov. 1991), pp. 1115–1138. ISSN: 0162-8828. DOI: 10.1109/34.103273.

[191] A. D. Luca, A. Albu-Schäffer, S. Haddadin, and G. Hirzinger. “Collision Detection and Safe Reaction with the DLR-III Lightweight Manipulator Arm”. *2006 IEEE/RSJ International Conference on Intelligent Robots and Systems*. Oct. 2006, pp. 1623–1630. DOI: 10.1109/IROS.2006.282053.

[192] Isaac L. Kurtzer, J. Andrew Pruszynski, and Stephen H. Scott. “Long-Latency Reflexes of the Human Arm Reflect an Internal Model of Limb Dynamics”. *Current Biology* 18.6 (2008), pp. 449–453. ISSN: 0960-9822. DOI: 10.1016/j.cub.2008.02.053.

[193] C. J. Forgaard, I. M. Franks, D. Maslovat, and R. Chua. “Perturbation predictability can influence the long-latency stretch response”. *PLoS ONE* 11.10 (2016), e0163854.

[194] Y. Charnay and L. Leger. “Brain serotonergic circuitries”. *Dialogues Clin Neurosci* 12.4 (2010), pp. 471–487.

[195] J. Weiler, P. L. Gribble, and J. A. Pruszynski. “Spinal stretch reflexes support efficient hand control”. *Nat. Neurosci.* 22.4 (Apr. 2019), pp. 529–533.

[196] J. A. Pruszynski, I. Kurtzer, T. P. Lillicrap, and S. H. Scott. “Temporal evolution of gain scaling”. *J. Neurophysiol.* 102.2 (Aug. 2009), pp. 992–1003.

[197] A. K. Thompson and J. R. Wolpaw. “The simplest motor skill: mechanisms and applications of reflex operant conditioning”. *Exerc Sport Sci Rev* 42.2 (Apr. 2014), pp. 82–90.

[198] Guang-Zhong Yang et al. “The grand challenges of Science Robotics”. *Science Robotics* 3.14 (2018). DOI: 10.1126/scirobotics.aar7650. eprint: https://robotics.sciencemag.org/content/3/14/eaar7650.full.pdf.

[199] Yoshua Bengio, Dong-Hyun Lee, Jorg Bornschein, Thomas Mesnard, and Zhouhan Lin. "Towards Biologically Plausible Deep Learning". *arXiv* (2015). arXiv: 1502.04156 [cs.LG].

[200] Sophie Denève, Alireza Alemi, and Ralph Bourdoukan. "The Brain as an Efficient and Robust Adaptive Learner". *Neuron* 94.5 (2017), pp. 969–977. ISSN: 0896-6273. DOI: https://doi.org/10.1016/j.neuron.2017.05.016.

[201] Giuseppe Di Giovanni et al. "Monoaminergic and Histaminergic Strategies and Treatments in Brain Diseases". *Frontiers in Neuroscience* 10 (2016), p. 541. ISSN: 1662-453X. DOI: 10.3389/fnins.2016.00541.

[202] H. Markram. "Seven challenges for neuroscience". *Funct. Neurol.* 28.3 (2013), pp. 145–151.

[203] Reinhardt Rosenberg. "The Normal Modes of Nonlinear n-Degree-of-Freedom Systems". *Journal of Applied Mechanics* 29.1 (1962), pp. 7–14. DOI: 10.1115/1.3636501.

[204] A.M. Lyapunov. *General Problem of the Stability Of Motion*. Control Theory and Applications Series. Taylor & Francis, 1992. ISBN: 9780748400621.

[205] Alan Weinstein. "Normal modes for nonlinear hamiltonian systems". *Inventiones mathematicae* 20.1 (Mar. 1973), pp. 47–57. ISSN: 1432-1297. DOI: 10.1007/BF01405263.

[206] Eric D.B. Wendel and Aaron D. Ames. "Rank Properties of Poincare Maps for Hybrid Systems with Applications to Bipedal Walking". *Proceedings of the 13th ACM International Conference on Hybrid Systems: Computation and Control*. HSCC '10. Stockholm, Sweden: ACM, 2010, pp. 151–160. ISBN: 978-1-60558-955-8. DOI: 10.1145/1755952.1755975.

[207] Robert Shorten, Fabian Wirth, Oliver Mason, Kai Wulff, and Christopher King. "Stability Criteria for Switched and Hybrid Systems". *SIAM Review* 49.4 (2007), pp. 545–592. DOI: 10.1137/05063516X. eprint: https://doi.org/10.1137/05063516X.

[208] Peter Giesl and Sigurdur Hafstein. "Review on computational methods for Lyapunov functions". *Discrete & Continuous Dynamical Systems - B* 20 (2015), p. 2291. ISSN: 1531-3492. DOI: 10.3934/dcdsb.2015.20.2291.

[209] W. P. M. H. Heemels, B. De Schutter, J. Lunze, and M. Lazar. "Stability analysis and controller synthesis for hybrid dynamical systems". *Philosophical Transactions of the Royal Society A: Mathematical, Physical and Engineering Sciences* 368.1930 (2010), pp. 4937–4960. DOI: 10.1098/rsta.2010.0187.

[210] Hai Lin and Panos J. Antsaklis. "Hybrid Dynamical Systems: An Introduction to Control and Verification". *Foundations and Trends® in Systems and Control* 1.1 (2014), pp. 1–172. ISSN: 2325-6818. DOI: 10.1561/2600000001.

[211] G. Courtine et al. "Transformation of nonfunctional spinal circuits into functional states after the loss of brain input". *Nat. Neurosci.* 12.10 (Oct. 2009), pp. 1333–1342.

[212] Rubia van den Brand et al. "Restoring Voluntary Control of Locomotion after Paralyzing Spinal Cord Injury". *Science* 336.6085 (2012), pp. 1182–1185. ISSN: 0036-8075. DOI: 10.1126/science.1217416. eprint: https://science.sciencemag.org/content/336/6085/1182.full.pdf.

[213] E. M. Moraud, M. Capogrosso, E. Formento, N. Wenger, J. DiGiovanna, G. Courtine, and S. Micera. “Mechanisms Underlying the Neuromodulation of Spinal Circuits for Correcting Gait and Balance Deficits after Spinal Cord Injury”. *Neuron* 89.4 (Feb. 2016), pp. 814–828.

[214] M. Bonizzato, G. Pidpruzhnykova, J. DiGiovanna, P. Shkorbatova, N. Pavlova, S. Micera, and G. Courtine. “Brain-controlled modulation of spinal circuits improves recovery from spinal cord injury”. *Nat Commun* 9.1 (Aug. 2018), p. 3015.

[215] F. B. Wagner et al. “Targeted neurotechnology restores walking in humans with spinal cord injury”. *Nature* 563.7729 (Nov. 2018), pp. 65–71.

[216] Loïc Damm and Joseph McIntyre. “Physiological Basis of Limb-Impedance Modulation During Free and Constrained Movements”. *Journal of Neurophysiology* 100.5 (2008), pp. 2577–2588. ISSN: 0022-3077.

[217] Matthew A. Krutky, Vengateswaran J. Ravichandran, Randy D. Trumbower, and Eric J. Perreault. “Interactions Between Limb and Environmental Mechanics Influence Stretch Reflex Sensitivity in the Human Arm”. *Journal of Neurophysiology* 103.1 (2010), pp. 429–440. ISSN: 0022-3077.

[218] Wolfgang Taube, Christian Leukel, Martin Schubert, Markus Gruber, Timo Rantalainen, and Albert Gollhofer. “Differential Modulation of Spinal and Corticospinal Excitability During Drop Jumps”. *Journal of Neurophysiology* 99.3 (2008), pp. 1243–1252. ISSN: 0022-3077.

[219] Daniel P. Ferris, Per Aagaard, Erik B. Simonsen, Claire T. Farley, and Poul Dyhre-Poulsen. “Soleus H-reflex gain in humans walking and running under simulated reduced gravity”. *The Journal of Physiology* 530.1 (2001), pp. 167–180. DOI: 10.1111/j.1469-7793.2001.0167m.x. eprint: https://physoc.onlinelibrary.wiley.com/doi/pdf/10.1111/j.1469-7793.2001.0167m.x.

[220] E. A. Kravitz. “Serotonin and aggression: insights gained from a lobster model system and speculations on the role of amine neurons in a complex behavior”. *Journal of Comparative Physiology A* 186.3 (Mar. 2000), pp. 221–238. ISSN: 1432-1351. DOI: 10.1007/s003590050423.

[221] SL Mackey, ER Kandel, and RD Hawkins. “Identified serotonergic neurons LCB1 and RCB1 in the cerebral ganglia of Aplysia produce presynaptic facilitation of siphon sensory neurons”. *Journal of Neuroscience* 9.12 (1989), pp. 4227–4235. ISSN: 0270-6474. DOI: 10.1523/JNEUROSCI.09-12-04227.1989. eprint: http://www.jneurosci.org/content/9/12/4227.full.pdf.

[222] Rhanor Gillette. “Evolution and Function in Serotonergic Systems”. *Integrative and Comparative Biology* 46.6 (2006), pp. 838–846. DOI: 10.1093/icb/icl024. eprint: /oup/backfile/content_public/journal/icb/46/6/10.1093/icb/icl024/2/icl024.pdf.

[223] J. C. R. Whittington and R. Bogacz. “Theories of Error Back-Propagation in the Brain”. *Trends Cogn. Sci. (Regul. Ed.)* 23.3 (Mar. 2019), pp. 235–250.

[224] Bernd Illing, Wulfram Gerstner, and Johanni Brea. “Biologically plausible deep learning—But how far can we go with shallow networks?” *Neural Networks* 118 (2019), pp. 90–101. ISSN: 0893-6080. DOI: https://doi.org/10.1016/j.neunet.2019.06.001.

[225] Paul J. Werbos. "Generalization of backpropagation with application to a recurrent gas market model". *Neural Networks* 1.4 (1988), pp. 339–356. ISSN: 0893-6080. DOI: https://doi.org/10.1016/0893-6080(88)90007-X.

[226] R. Urbanczik and W. Senn. "Learning by the dendritic prediction of somatic spiking". *Neuron* 81.3 (Feb. 2014), pp. 521–528.

[227] Paul W. Glimcher. "Understanding dopamine and reinforcement learning: The dopamine reward prediction error hypothesis". *Proceedings of the National Academy of Sciences* 108.Supplement 3 (2011), pp. 15647–15654. ISSN: 0027-8424. DOI: 10.1073/pnas.1014269108. eprint: https://www.pnas.org/content/108/Supplement_3/15647.full.pdf.

[228] David W. Franklin, Alexandra V. Batchelor, and Daniel M. Wolpert. "The Sensorimotor System Can Sculpt Behaviorally Relevant Representations for Motor Learning". *eNeuro* 3.4 (2016). DOI: 10.1523/ENEURO.0070-16.2016. eprint: http://www.eneuro.org/content/3/4/ENEURO.0070-16.2016.full.pdf.

[229] Frederic Libersat and Hans-Joachim Pflueger. "Monoamines and the Orchestration of Behavior". *BioScience* 54.1 (Jan. 2004), pp. 17–25. ISSN: 0006-3568. DOI: 10.1641/0006-3568(2004)054[0017:MATOOB]2.0.CO;2. eprint: http://oup.prod.sis.lan/bioscience/article-pdf/54/1/17/26894837/54-1-17.pdf.

[230] Magor L. Lőrincz and Antoine R. Adamantidis. "Monoaminergic control of brain states and sensory processing: Existing knowledge and recent insights obtained with optogenetics". *Progress in Neurobiology* 151 (2017). Neurobiology and Neuropharmacology of Monoaminergic systems, pp. 237–253. ISSN: 0301-0082. DOI: https://doi.org/10.1016/j.pneurobio.2016.09.003.

[231] Paul Witkovsky and Allen Dearry. "Chapter 10 Functional roles of dopamine in the vertebrate retina". *Progress in Retinal Research* 11 (1991), pp. 247–292. ISSN: 0278-4327. DOI: https://doi.org/10.1016/0278-4327(91)90031-V.

[232] George C. Brainard and William W. Morgan. "Light-induced stimulation of retinal dopamine: a dose-response relationship". *Brain Research* 424.1 (1987), pp. 199–203. ISSN: 0006-8993. DOI: 10.1016/0006-8993(87)91211-X.

[233] Xiao-Bo Xia and Stephen L. Mills. "Gap junctional regulatory mechanisms in the AII amacrine cell of the rabbit retina". *Visual Neuroscience* 21.5 (2004), pp. 791–805. DOI: 10.1017/S0952523804215127.

[234] S. L. Mills and S. C. Massey. "Differential properties of two gap junctional pathways made by AII amacrine cells". *Nature* 377.6551 (Oct. 1995), pp. 734–737.

[235] W.-C. Li and J. C. Rekling. "Electrical Coupling in the Generation of Vertebrate Motor Rhythms". *Network Functions and Plasticity: Perspectives from Studying Neuronal Electrical Coupling in Microcircuits*. Ed. by J. Jing. Elsevier Science, 2017, pp. 243–264. ISBN: 9780128034996.

[236] S. A. Bloomfield and B. Volgyi. "The diverse functional roles and regulation of neuronal gap junctions in the retina". *Nat. Rev. Neurosci.* 10.7 (July 2009), pp. 495–506.

[237] R. C. Foehring, P. C. Schwindt, and W. E. Crill. "Norepinephrine selectively reduces slow Ca2+- and Na+-mediated K+ currents in cat neocortical neurons". *Journal of Neurophysiology* 61.2 (1989). PMID: 2918353, pp. 245–256. DOI: 10.1152/jn.1989.61.2.245. eprint: https://doi.org/10.1152/jn.1989.61.2.245.

[238] Yan Dong and Francis J. White. “Dopamine D1-Class Receptors Selectively Modulate a Slowly Inactivating Potassium Current in Rat Medial Prefrontal Cortex Pyramidal Neurons”. *Journal of Neuroscience* 23.7 (2003), pp. 2686–2695. ISSN: 0270-6474. eprint: http://www.jneurosci.org/content/23/7/2686.full.pdf.

[239] Z. W. Zhang and D. Arsenault. “Gain modulation by serotonin in pyramidal neurones of the rat prefrontal cortex”. *Journal of Physiology (Lond.)* 566.Pt 2 (July 2005), pp. 379–394.

[240] D. J. Surmeier, J. Ding, M. Day, Z. Wang, and W. Shen. “D1 and D2 dopamine-receptor modulation of striatal glutamatergic signaling in striatal medium spiny neurons”. *Trends in Neuroscience* 30.5 (May 2007), pp. 228–235.

[241] X Yu et al. “Wakefulness Is Governed by GABA and Histamine Cotransmission”. *Neuron* 87 (2015), pp. 164–178. DOI: 10.1016/j.neuron.2015.06.003.

[242] Michael P. Jankowski and Susan R. Sesack. “Prefrontal cortical projections to the rat dorsal raphe nucleus: Ultrastructural features and associations with serotonin and gamma-aminobutyric acid neurons”. *The Journal of Comparative Neurology* 468.4 (2004), pp. 518–529. ISSN: 1096-9861. DOI: 10.1002/cne.10976.

[243] Patrizio Blandina, Gustavo Provensi, Leonardo Munari, and Maria Beatrice Passani. “Histamine neurons in the tuberomamillary nucleus: a whole center or distinct subpopulations?” *Frontiers in Systems Neuroscience* 6 (2012), p. 33. ISSN: 1662-5137. DOI: 10.3389/fnsys.2012.00033.

[244] Stephanie B. Vertes Robert P.and Linley. “Efferent and afferent connections of the dorsal and median raphe nuclei in the rat”. *Serotonin and Sleep: Molecular, Functional and Clinical Aspects*. Basel: Birkhäuser Basel, 2008, pp. 69–102. ISBN: 978-3-7643-8561-3. DOI: 10.1007/978-3-7643-8561-3_3.

[245] E. R. Samuels and E. Szabadi. “Functional neuroanatomy of the noradrenergic locus coeruleus: its roles in the regulation of arousal and autonomic function part I: principles of functional organisation”. *Current Neuropharmacology* 6.3 (Sept. 2008), pp. 235–253.

[246] Eric J. Nestler, Steven E. Hyman, David M. Holtzman, and Robert C. Malenka. “Widely Projecting Systems: Monoamines, Acetylcholine, and Orexin”. *Molecular Neuropharmacology: A Foundation for Clinical Neuroscience, 3e*. New York, NY: McGraw-Hill Education, 2015. Chap. 6.

[247] A. John Rush et al. “Acute and Longer-Term Outcomes in Depressed Outpatients Requiring One or Several Treatment Steps: A STAR*D Report”. *American Journal of Psychiatry* 163.11 (2006). PMID: 17074942, pp. 1905–1917. DOI: 10.1176/ajp.2006.163.11.1905. eprint: https://ajp.psychiatryonline.org/doi/pdf/10.1176/ajp.2006.163.11.1905.

[248] Madhukar H. Trivedi et al. “Evaluation of Outcomes With Citalopram for Depression Using Measurement-Based Care in STAR*D: Implications for Clinical Practice”. *American Journal of Psychiatry* 163.1 (2006). PMID: 16390886, pp. 28–40. DOI: 10.1176/appi.ajp.163.1.28. eprint: https://doi.org/10.1176/appi.ajp.163.1.28.

[249] David A. Mrazek, John C. Hornberger, C. Anthony Altar, and Irina Degtiar. "A Review of the Clinical, Economic, and Societal Burden of Treatment-Resistant Depression: 1996–2013". *Psychiatric Services* 65.8 (2014). PMID: 24789696, pp. 977–987. DOI: 10.1176/appi.ps.201300059. eprint: https://doi.org/10.1176/appi.ps.201300059.

[250] Evan Mayo-Wilson, Sofia Dias, Ifigeneia Mavranezouli, Kayleigh Kew, David M Clark, A E Ades, and Stephen Pilling. "Psychological and pharmacological interventions for social anxiety disorder in adults: a systematic review and network meta-analysis". *The Lancet Psychiatry* 1.5 (2014), pp. 368–376. ISSN: 2215-0366. DOI: https://doi.org/10.1016/S2215-0366(14)70329-3.

[251] P.E. Nathan and J.M. Gorman. *A Guide to Treatments That Work*. Oxford University Press, 2015. ISBN: 9780199342228.

[252] Andrea Cipriani et al. "Comparative Efficacy and Acceptability of 21 Antidepressant Drugs for the Acute Treatment of Adults With Major Depressive Disorder: A Systematic Review and Network Meta-Analysis". *FOCUS* 16.4 (2018), pp. 420–429. DOI: 10.1176/appi.focus.16407. eprint: https://doi.org/10.1176/appi.focus.16407.

[253] D. Lakatos, W. Friedl, and A. Albu-Schäffer. "Eigenmodes of Nonlinear Dynamics: Definition, Existence, and Embodiment into Legged Robots With Elastic Elements". *IEEE Robotics and Automation Letters* 2.2 (Apr. 2017), pp. 1062–1069. ISSN: 2377-3774. DOI: 10.1109/LRA.2017.2658018.

[254] Zhenyu Gan, Yevgeniy Yesilevskiy, Petr Zaytsev, and C. David Remy. "All common bipedal gaits emerge from a single passive model". *Journal of The Royal Society Interface* 15.146 (2018), p. 20180455. DOI: 10.1098/rsif.2018.0455. eprint: https://royalsocietypublishing.org/doi/pdf/10.1098/rsif.2018.0455.

[255] Koushil Sreenath, Hae-Won Park, Ioannis Poulakakis, and JW Grizzle. "Embedding active force control within the compliant hybrid zero dynamics to achieve stable, fast running on MABEL". *The International Journal of Robotics Research* 32.3 (2013), pp. 324–345. DOI: 10.1177/0278364912473344. eprint: https://doi.org/10.1177/0278364912473344.

[256] M. Hutter, C. D. Remy, M. A. Höpflinger, and R. Siegwart. "SLIP running with an articulated robotic leg". *2010 IEEE/RSJ International Conference on Intelligent Robots and Systems*. Oct. 2010, pp. 4934–4939. DOI: 10.1109/IROS.2010.5651461.

[257] Stefano Stramigioli and Michel van Dijk. "Energy Conservative Limit Cycle Oscillations". *IFAC Proceedings Volumes* 41.2 (2008). 17th IFAC World Congress, pp. 15666–15671. ISSN: 1474-6670. DOI: https://doi.org/10.3182/20080706-5-KR-1001.02649.

[258] G. M. Gasparri, S. Manara, D. Caporale, G. Averta, M. Bonilla, H. Marino, M. Catalano, G. Grioli, M. Bianchi, A. Bicchi, and M. Garabini. "Efficient Walking Gait Generation via Principal Component Representation of Optimal Trajectories: Application to a Planar Biped Robot With Elastic Joints". *IEEE Robotics and Automation Letters* 3.3 (July 2018), pp. 2299–2306. ISSN: 2377-3774. DOI: 10.1109/LRA.2018.2807578.

[259] Weitao Xi, Yevgeniy Yesilevskiy, and C. David Remy. "Selecting gaits for economical locomotion of legged robots". *The International Journal of Robotics Research* 35.9 (2016), pp. 1140–1154. DOI: 10.1177/0278364915612572. eprint: https://doi.org/10.1177/0278364915612572.

[260] N. Smit-Anseeuw, R. Gleason, R. Vasudevan, and C. D. Remy. "The Energetic Benefit of Robotic Gait Selection—A Case Study on the Robot RAMone". *IEEE Robotics and Automation Letters* 2.2 (Apr. 2017), pp. 1124–1131. ISSN: 2377-3774. DOI: 10.1109/LRA.2017.2661801.

[261] C. Della Santina, R. K. Katzschmann, A. Biechi, and D. Rus. "Dynamic control of soft robots interacting with the environment". *2018 IEEE International Conference on Soft Robotics (RoboSoft)*. Apr. 2018, pp. 46–53. DOI: 10.1109/ROBOSOFT.2018.8404895.

[262] P. S. Churchland and T. J. Sejnowski. "Blending computational and experimental neuroscience". *Nat. Rev. Neurosci.* 17.11 (Nov. 2016), pp. 667–668.